

---

RELATIONSHIPS BETWEEN MAS NMR  
AND MINERAL STRUCTURE

By

© BARBARA LUCY SHERRIFF, B.A., B.Sc., M.Sc.

A Thesis

Submitted to the school of Graduate Studies  
In Partial Fulfilment of the Requirements  
for the Degree  
Doctor of Philosophy

McMaster University

September 1988

---

✓

MAS NMR AND MINERAL STRUCTURE

DOCTOR OF PHILOSOPHY (1988) MCMASTER UNIVERSITY.

(Geology) Hamilton, Ontario.

TITLE: Relationships between MAS NMR and Mineral Structure

AUTHOR: Barbara Lucy Sherriff, B.A. (The Open University)

B.Sc. (Leicester University)

M.Sc. (Brock University)

SUPERVISOR: Professor H. D. Grundy

NUMBER OF PAGES: xv, 214

### ABSTRACT

$^{29}\text{Si}$  magic angle spinning nuclear magnetic resonance (MAS nmr) has been used extensively to study the structure, properties, and reactions of silicate minerals, ceramics and glasses. Despite many attempts to relate chemical shift with crystal structure the factors governing  $^{29}\text{Si}$  chemical shift are not well understood.

This study investigates the effect of local structural environment of the silicate tetrahedron on  $^{29}\text{Si}$  chemical shift. A simple relationship is found between the atomic positions of the cations bonded to the terminal oxygens of the tetrahedron and  $^{29}\text{Si}$  chemical shift, which can be used to calculate chemical shift from atomic positions. A plot of calculated against experimental chemical shift has a correlation coefficient of 0.986 for 124 sets of data from all groups of silicates.

$^{29}\text{Si}$  chemical shifts calculated from diffraction data, are used to interpret MAS nmr spectra of scapolite, a partially disordered mineral system. Models are devised for cation ordering throughout the solid solution series, in which the charge on the cavities are balanced locally by the requisite number of  $\text{AlO}_4$  tetrahedra.

$^{29}\text{Si}$ ,  $^{27}\text{Al}$ ,  $^{23}\text{Na}$ ,  $^7\text{Li}$  and  $^9\text{Be}$  MAS nmr spectroscopy is used to investigate the difference in atomic sites

between beryls with slightly different compositions.  $^9\text{Be}$  and  $^{29}\text{Si}$  MAS nmr results agree with the presence of domains in the Li-Cs beryls with the structure of low-alkali beryls. Lack of a tetrahedral peak in the  $^{27}\text{Al}$  spectra of Li-Cs beryls eliminates the coupled substitution of Li for Al and Al for Be. Peaks in the  $^{23}\text{Na}$  spectra of Li-Cs beryls from NaCl in solution in fluid inclusions show the potential of nmr to study fluid inclusions.

Models of theoretical structures based on a symmetrical  $\text{SiO}_4$  tetrahedron with Al or Si ligands show that chemical shift is linearly proportional to cation-oxygen distance ( $r$ ) and exponentially proportional to silicon-oxygen-cation angle ( $\alpha$ ). The possible ranges of chemical shift for each type of silicate are more extensive than those of Lippmaa et al. (1980).

## ACKNOWLEDGEMENTS

I would like to thank my supervisor Dr. H. D. Grundy for instructing me in the art of carrying out scientific research and for his help with computing. Thanks also go to Dr. I. D. Brown, Dr. M. J. McGlinchey, Dr. A. D. Bain, Dr. F. C. Hawthorne, Dr. J. R. Kramer, Dr. J. S. Hartman and Dr. D. M. Shaw for helpful discussions. Dr. D. M. Shaw is especially thanked for constructive criticism and reading of the manuscript and Dr. J. S. Hartman for providing the MAS nmr probes from the design of Dr. C. A. Fyfe.

I am grateful to Dr. R. E. Lenkinski, W. Klimstra, Dr. C. A. Fyfe, and Dr. S. Johnson at Guelph University and B. Sayer of McMaster University for help with nmr instrumentation.

This project was supported by NSERC funding and also by Hooker and Sherman scholarships from McMaster University. The time on the nmr spectrometers at the South Western Ontario Nmr Centre was paid for by Brock University through Dr. J. S. Hartman.

Finally I would like to thank all my friends at McMaster University especially Kathy Teeter, Jill Gleed and Dr. Marilyn Truscott and my children Barry and Jackie for their friendship and support.

## CONTENTS

	Page
Abstract	iii
Acknowledgements	v
Chapter 1. Introduction to nuclear magnetic resonance of silicate minerals	1
1.1 Introduction	1
1.2 Nuclear Magnetic Resonance	2
1.3 $^{29}\text{Si}$ MAS nmr	3
1.4 Previous work on the relationship of $^{29}\text{Si}$ MAS nmr chemical shift with mineral structure	4
Chapter 2 Correlation between atomic structure and $^{29}\text{Si}$ MAS nmr chemical shift	20
2.1 Introduction	20
2.2 Nmr and diffraction data	21
2.2.1 Disorder of cations in a crystallographic site	22
2.2.2 Difference in composition or ordering between mineral samples	24
2.2.3 Inaccurate structural data	26
2.2.4 Errors in nmr data	27
2.3 Calculations	32
2.3.1 The first term; magnetic anisotropy	34
2.3.2 Second term; bond valence	38
2.3.3 Third term; Si-O-X angle	44
2.3.4 Resultant equation	46

	Page
2.4 A discussion of the relationship between calculated and experimental values of chemical shift	49
2.4.1 Orthosilicates	50
2.4.2 Sorosilicates	53
2.4.3 Inosilicates	56
2.4.4 Phyllosilicates	57
2.4.5 Tectosilicates	59
2.5 Conclusions	70
Chapter 3 Cation ordering in the scapolite mineral system	73
3.1 Introduction	73
3.2 The structure of scapolite	75
3.3 Experimental	78
3.4 Results and discussion	82
3.4.1 $^{29}\text{Si}$ MAS nmr spectra	82
3.4.2 $^{27}\text{Al}$ MAS nmr spectra	95
3.4.3 Sodium-23 MAS nmr	99
3.4.4 Carbon-13 MAS nmr	105
3.4.5 A model for cation ordering	105
3.5 Conclusion	116
Chapter 4 A multinuclear nmr study of beryls	118
4.1 Introduction	118
4.2 Structure of beryl	119
4.3 Experimental	121
4.4 Results and Discussion	123
4.4.1 Silicon-29	123



	Page
4.4.2 Aluminum-27	127
4.4.3 Sodium-23	129
4.4.4 Beryllium-9	136
4.4.5 Lithium-7	140
4.5 Conclusions	143
Chapter 5 Modelling theoretical silicate structures and thoughts for the future	145
5.1 Introduction	145
5.2 SiO <sub>4</sub> tetrahedral model	146
5.3 Results and discussion	149
5.4 Present state of chemical shift calculations	153
5.5 Ideas for the future	153
References	157
Appendix I The theory of nuclear magnetic resonance	172
1.1 General theory of nmr spectroscopy	172
1.2 Pulse Fourier Transform	176
1.3 Chemical shift	178
1.4 High Resolution nmr of solids	180
1.5 MAS nmr spectra of quadrupolar nuclei	184
1.6 Relaxation times	188
Appendix II Mineral samples	190
Appendix III Dum.For	191
Appendix IV Len.For	194
Appendix V Chisi.For	197

	Page
Appendix VI Values of $\Omega$ for $\text{SiO}_2$ polymorphs summed at 1/2 Å intervals to 10 Å	202
Appendix VII Summations of geometric terms for $\text{SiO}_2$ polymorphs averaged from 6 - 10 Å	203
Appendix VIII $^{29}\text{Si}$ chemical shift of silicate minerals, experimental values, and values calculated from equations 3, and 4.	204
Appendix IX Calculated chemical shifts from theoretical models (angle $\alpha$ varied between 125 and 180°)	209
Appendix X Calculated chemical shifts from theoretical models (distance $r$ varied between 1.75 and 1.55 Å)	210
Appendix XI The relationship between the McConnell equation and equations 3 and 4	212

## FIGURES

	Page
1.1 Ranges of $^{29}\text{Si}$ MAS nmr chemical shift for silicates and framework aluminosilicates	6
1.2 $^{29}\text{Si}$ isotropic chemical shift plotted against the mean number of silicon atoms for (a) for 52 zeolites with faujasitic framework (b) for 26 Zeolite-A framework materials	7
1.3 $^{29}\text{Si}$ chemical shift versus (a) average Si-O bond length (b) total cation-oxygen bond strength for the four oxygen atoms surrounding each Si site	9
1.4 Relation between chemical shift and structural parameters	10
1.5 Bond direction related shielding versus Si-O bond distances for silica polymorphs	11
1.6 Relationship between $^{29}\text{Si}$ chemical shift and mean oxygen s character of silica polymorphs and zeolites	13
1.7 Experimental $^{29}\text{Si}$ nmr chemical shift of zeolites and silica polymorphs plotted against calculated chemical shifts.	15
1.8 Graph showing correlation between $^{29}\text{Si}$ MASS nmr chemical shift and chemical shift predicted on the basis of the group electronegativity sum.	17
2.1 Diagram showing the definitions of angles $\theta$ and $\alpha$ and the lengths $r$ and $R$ .	33
2.2 Summations of $\Omega$ , using equation (1), at 1/2 Å intervals from Si, plotted against distance from Si for the $\text{SiO}_2$ polymorphs	36
2.3 The mean of summations, at 1/2 Å intervals, from 6 to 10 Å, for the geometric term $\Sigma((1-3\cos^2\theta_i)/3R_i^3)$ plotted against experimental $\delta$ for the silica polymorphs.	38
2.4 Experimental $^{29}\text{Si}$ MAS nmr chemical shift plotted against chemical shift calculated from equations 3 and 4.	47
2.5 $^{29}\text{Si}$ MAS nmr spectrum of white kyanite	51

	Page
2.6 $^{29}\text{Si}$ MAS nmr spectrum of piemontite	54
2.7 $^{29}\text{Si}$ MAS nmr spectrum of wollastonite	58
2.8 $^{29}\text{Si}$ MAS nmr spectra of albite/microcline perthites	61
2.9 $^{29}\text{Si}$ MAS nmr spectra of the plagioclase feldspar series.	64
2.10 $^{29}\text{Si}$ MAS nmr spectrum of nepheline	66
3.1 The structure of scapolite viewed along the c-axis	76
3.2 The structure of scapolite viewed along the a-axis	77
3.3 $^{29}\text{Si}$ MAS nmr spectra of scapolite samples	84
3.4 Peak fitting to the $^{29}\text{Si}$ MAS nmr spectrum of GL (34.1% Me)	86
3.5 $^{27}\text{Al}$ MAS nmr spectra of scapolite samples	96
3.6 A graph of $^{27}\text{Al}$ peak width plotted against meionite content	98
3.7 Configuration of the Na-O polyhedron.	100
3.8 A plot of (Na,Ca)-O distances as a function of meionite content	101
3.9 $^{23}\text{Na}$ MAS nmr spectra of scapolite samples	103
3.10 $^{13}\text{C}$ MAS nmr spectrum of scapolite sample Q13	107
3.11 Model of cation ordering in 37% Me scapolite	109
3.12 Model of cation ordering in 20% Me scapolite	112
3.13 Model of cation ordering in 75% Me scapolite	114
4.1 Photographs of computer simulated models of the structure of Li-Cs beryl viewed along (a) the c-axis; (b) the a-axis.	120
4.2 $^{29}\text{Si}$ MAS nmr spectra of (a) T-24 Li-Cs beryl (b) SHEE-1-6 low alkali beryl	124

	Page
4.3 $^{27}\text{Al}$ MAS nmr spectra of (a) SHEE-1-6 low alkali beryl (b) T-24 Li-Cs beryl (c) Columbian emeralds	128
4.4 $^{23}\text{Na}$ MAS nmr spectra of (a) SHEE-1-6 low alkali beryl (b) T-24 Li-Cs beryl (c) T-24 Li-Cs beryl spinning at an angle of approximately $65^\circ$ to the applied magnetic field	132
4.5 $^{23}\text{Na}$ static nmr spectrum of T-24 Li-Cs beryl.	134
4.6 (a) $^{23}\text{Na}$ nmr spectrum of 1 molar aqueous solution of NaCl (b) $^{23}\text{Na}$ MAS nmr spectrum of solid NaCl (c) $^{23}\text{Na}$ MAS nmr spectrum of T-24 Li-Cs beryl	135
4.7 $^9\text{Be}$ MAS nmr spectra of (a) SHEE-1-6 low alkali beryl (b) T-24 Li-Cs beryl	138
4.8 $^7\text{Li}$ MAS nmr spectra of (a) SHEE-1-6 low alkali beryl (b) T-24 Li-Cs beryl	142
5.1 Cation-oxygen distance (r) plotted against calculated chemical shift for one Si or Al ligand on a terminal oxygen of a symmetrical $\text{SiO}_4$ tetrahedron.	147
5.2 A plot of angle ( $\alpha$ ) against calculated chemical shift for: (a) Si-O (r = 1.59 Å) and (b) Al-O (r = 1.76 Å).	148
5.3 Theoretical ranges of $^{29}\text{Si}$ MAS nmr chemical shift for the five groups of silicates;	151
1.1 The 2I+1 orientations with respect to $B_0$ and the quantization of $\mu$ on $B_0$ .	174
1.2 Vectorial representation of Larmor precession.	175
1.3 (a) A $90^\circ$ pulse along $x'$ rotates the magnetization from the equilibrium position to the $y'$ axis. (b) The magnetization decreases as the magnetic moments dephase (c) The input signal, a $90^\circ$ pulse (d) Free induction decay output signal	177
1.4 $^{29}\text{Si}$ nmr spectra of BLS036 oligoclase feldspar (a) static sample (b) sample spinning at an angle of $54.7^\circ$ to the applied magnetic field at 3200 Hz	182

	Page
I.5 Magic Angle Spinning vectors	183
I.6 Computer simulated variable angle sample spinning lineshapes for the central ( $m = 1/2$ ) to ( $m = -1/2$ ) transition of $^{23}\text{Na}$ ( $I = 3/2$ )	185
I.7 Energy level diagram for a spin 5/2 nucleus showing the effect of first order quadrupolar interaction on Zeeman energy levels.	187

## TABLES

	Page
2.1 Correlation coefficients between calculated and measured values of $^{29}\text{Si}$ chemical shift, for differing values of $r_0$ for Al-O and Si-O, and different functions of angle Si-O-X	42
2.2 $^{29}\text{Si}$ peak allocation for feldspar minerals	62
2.3 $^{29}\text{Si}$ peak allocation for nepheline	68
3.1 Scapolite samples used for nmr analyses	79
3.2 $^{29}\text{Si}$ MAS nmr parameters	83
3.3 $^{29}\text{Si}$ MAS nmr chemical shift calculations for 34% meionite scapolite	87
3.4 Calculated $^{29}\text{Si}$ chemical shift for ON8 (21.3% Me)	91
3.5 $^{29}\text{Si}$ MAS nmr chemical shift calculated for Q13 (51.3% Me)	92
3.6 $^{29}\text{Si}$ MAS nmr chemical shift calculated for 70% meionite scapolite	93
3.7 $^{29}\text{Si}$ MAS nmr chemical shift calculated for 91.0% meionite scapolite (MONTE)	94
3.8 $^{27}\text{Al}$ MAS nmr parameters	97
3.9 $^{23}\text{Na}$ MAS nmr parameters	104
3.10 $^{13}\text{C}$ MAS nmr parameters of scapolite	106
3.11 Calculated cation populations of scapolite cavities	110
3.12 Number of silicon atoms in T configurations	115
4.1 Chemical analyses of alkali beryls	122
4.2 $^{29}\text{Si}$ MAS nmr parameters of beryl	125
4.3 $^{27}\text{Al}$ MAS nmr parameters of beryl	130
4.4 $^9\text{Be}$ MAS nmr parameters of beryl.	137

	Page
4.5 $^7\text{Li}$ MAS nmr parameters of beryl.	141
5.1 Possible ranges of $^{29}\text{Si}$ chemical shift	152



## CHAPTER 1

### INTRODUCTION TO NUCLEAR MAGNETIC RESONANCE OF SILICATE MINERALS

#### 1.1 INTRODUCTION

This study set out to investigate the effect of local structural environment of the silicate tetrahedron on  $^{29}\text{Si}$  chemical shift and in doing so found a simple relationship between structure and chemical shift. The relationship can be used to calculate chemical shift from atomic positions and with structural modelling techniques to examine the environment of silicon in a structure.

The thesis is divided into three parts; chapter 1, chapter 2, and a third section comprising chapters 3, 4, and 5.

Chapter 1 explains the reasons for studying the relationship between  $^{29}\text{Si}$  MAS nmr chemical shift and silicate mineral structure.

In Chapter 2 this relationship is explored by relating atomic positions found from diffraction methods with  $^{29}\text{Si}$  nmr data using a computer crystal structure modelling program.

Chapters 3, 4 and 5 show how this new understanding

of the factors affecting  $^{29}\text{Si}$  MAS nmr chemical shift can be used together with information from MAS nmr spectroscopy of other isotopes to study the structure of silicate minerals and glasses. In Chapter 3, MAS nmr of  $^{29}\text{Si}$ ,  $^{27}\text{Al}$ ,  $^{23}\text{Na}$ , and  $^{13}\text{C}$  are used to devise an ordering scheme for the scapolite series of minerals for both Al-Si order in the tetrahedral (T) sites and for the ordering of cations and anions in the cavities. The changes occurring in the structure of beryl with the introduction of alkali cations in the channel sites is investigated in Chapter 4, using  $^{29}\text{Si}$ ,  $^{27}\text{Al}$ ,  $^{23}\text{Na}$ ,  $^7\text{Li}$  and  $^9\text{Be}$  MAS nmr. In Chapter 5 theoretical structures are simulated to examine the relationship between nmr chemical shift and both cation-oxygen distance and Si-O-cation angle and to show that the relationship can be used to study amorphous material with only short range order.

## 1.2 NUCLEAR MAGNETIC RESONANCE

When a nucleus is placed in a magnetic field it attains a series of energy levels. Nuclear magnetic resonance spectroscopy (nmr) measures the frequency of transition between these nuclear energy levels. These radio frequency transitions, which are measured as parts per million of the magnetic field (ppm), are affected by the size of the applied magnetic field, the nature of the magnetic isotope and by the surrounding electronic

environment. Therefore nmr provides information about the local chemical environment of an atom. X-ray and neutron diffraction techniques, on the other hand, give an average position and occupancy for a particular crystallographic site across a crystal.

Magic angle spinning (MAS) (Lippmaa et al. 1980) has enabled nmr spectroscopy to be applied to solids and to study the chemical environment of atoms in crystalline and amorphous structures. The primary use of MAS nmr for geologists has been the study of the crystal chemistry of silicate minerals and glasses.

The theory of nmr is well documented (Becker 1980; Gunther 1980; Paudler 1987) and a detailed description of the application of nmr to solids can be found in Fyfe (1983). Therefore, in this thesis, only a brief description of the main features of nmr is given in Appendix I.

### 1.3 $^{29}\text{Si}$ MAS NMR

$^{29}\text{Si}$  magic angle spinning nuclear magnetic resonance (MAS nmr) has been used extensively for the past eight years to study the structure, properties and reactions of silicate minerals (Sanz and Seratosa 1984; Stebbins et al. 1986; Kirkpatrick et al. 1985), ceramics (Carduner et al. 1987; Barnes et al. 1985) and glasses (Dupree et al. 1986; Kirkpatrick et al. 1986).

As it has a nuclear spin of  $1/2$ ,  $^{29}\text{Si}$  gives simple spectra without quadrupolar broadening or shift (Appendix I, section 1.5). In the MAS nmr spectra of quadrupolar nuclei, such as  $^{27}\text{Al}$  and  $^{23}\text{Na}$ , quadrupolar interactions are superimposed on chemical shift making the chemical shift information difficult to extract.

$^{29}\text{Si}$  is a dilute nucleus (4.6% abundant) which eliminates  $^{29}\text{Si}$ - $^{29}\text{Si}$  dipolar interactions (Appendix I, section 1.4). The range of chemical shift for 4-coordinate silicon is about 60 ppm from -60 to -120 ppm from the reference tetramethylsilane (TMS). Therefore the differences in  $^{29}\text{Si}$  chemical shift between different silicate environments are greater than the error of measurement ( $\pm 0.1$  ppm), but not so large as to cause instrumental problems, as is found for the wide range of chemical shifts of a large isotope such as  $^{207}\text{Pb}$ .

Despite many attempts to correlate chemical shift or peak position with crystal structure the factors which govern  $^{29}\text{Si}$  chemical shift are not well understood and this is the subject of this thesis.

#### 1.4 PREVIOUS WORK ON THE RELATIONSHIP OF $^{29}\text{Si}$ MAS NMR CHEMICAL SHIFT WITH MINERAL STRUCTURE

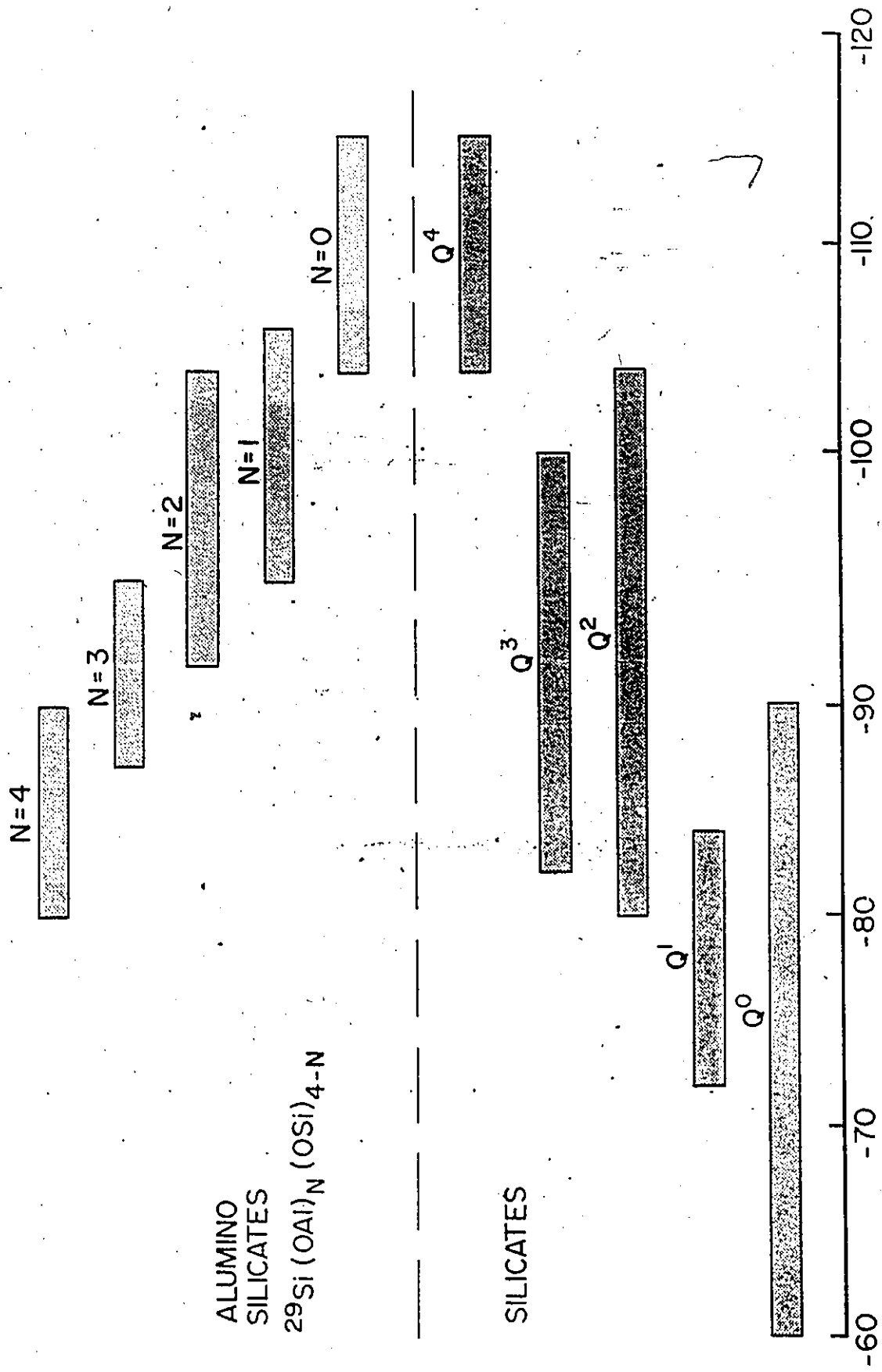
Since the first data were published on  $^{29}\text{Si}$  MAS nmr of minerals (Lippmaa et al. 1978, 1980, 1981) there have

been many attempts to relate chemical shift ( $\delta$ ) to mineral structure.

Lippmaa et al. (1980, 1981) and Mägi et al. (1984) divided the 60 ppm range of  $^{29}\text{Si}$  silicate chemical shifts into 5 separate ranges depending on the number of bridging oxygens ( $Q^0$ ,  $Q^1$ ,  $Q^2$ ,  $Q^3$ ,  $Q^4$  Engelhardt et al. 1973) and also subdivided the  $Q^3$  and  $Q^4$  ranges depending on the number of aluminum next-nearest-neighbours (Fig. 1.1). The overall trend is a shift to high field (higher negative values of  $\delta$  in ppm) for increasing degree of condensation (higher Q number) and to lower field for increased substitution of silicon next-nearest-neighbour by aluminum. Newsom (1985) using two zeolite structural types, faujasite and zeolite-A, found five correlations between the ratio of silicon to aluminum in the unit cell and  $\delta$  (Fig. 1.2a; 1.2b). He interpreted the separate trends as relating to the number of aluminum atoms in the first coordination sphere and the slope of the linear regressions as being indicative of the number of aluminum atoms in the second coordination sphere.

Higgins and Woessner (1982) published the first attempt to relate mean Si-O distances to  $\delta$  using quartz, cristobalite, albite and natrolite. They found a correlation coefficient of 0.992 for their linear regression but had few data. Smith and Blackwell (1983) found a correlation coefficient of 0.84 for a similar plot

Figure 1.1 Ranges of  $^{29}\text{Si}$  MAS nmr chemical shift for  
silicates and framework aluminosilicates  
(Williams (Sherriff) 1984).



ALUMINO  
SILICATES

SILICATES

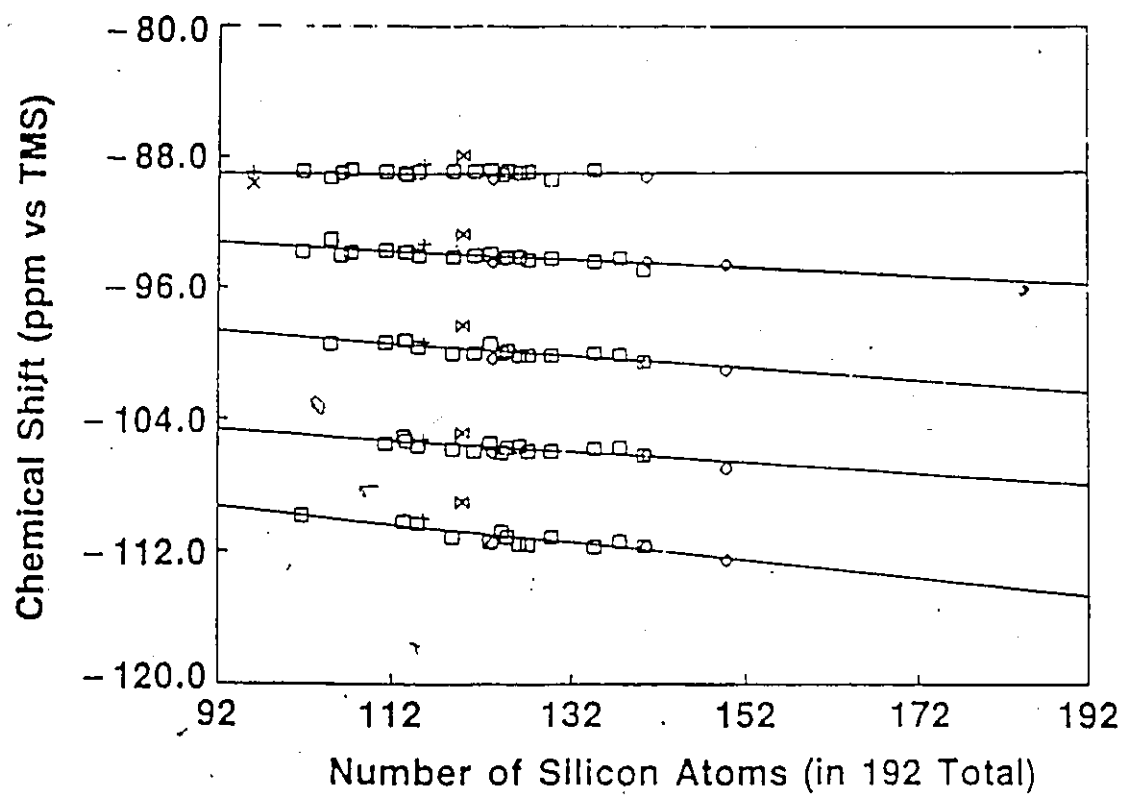
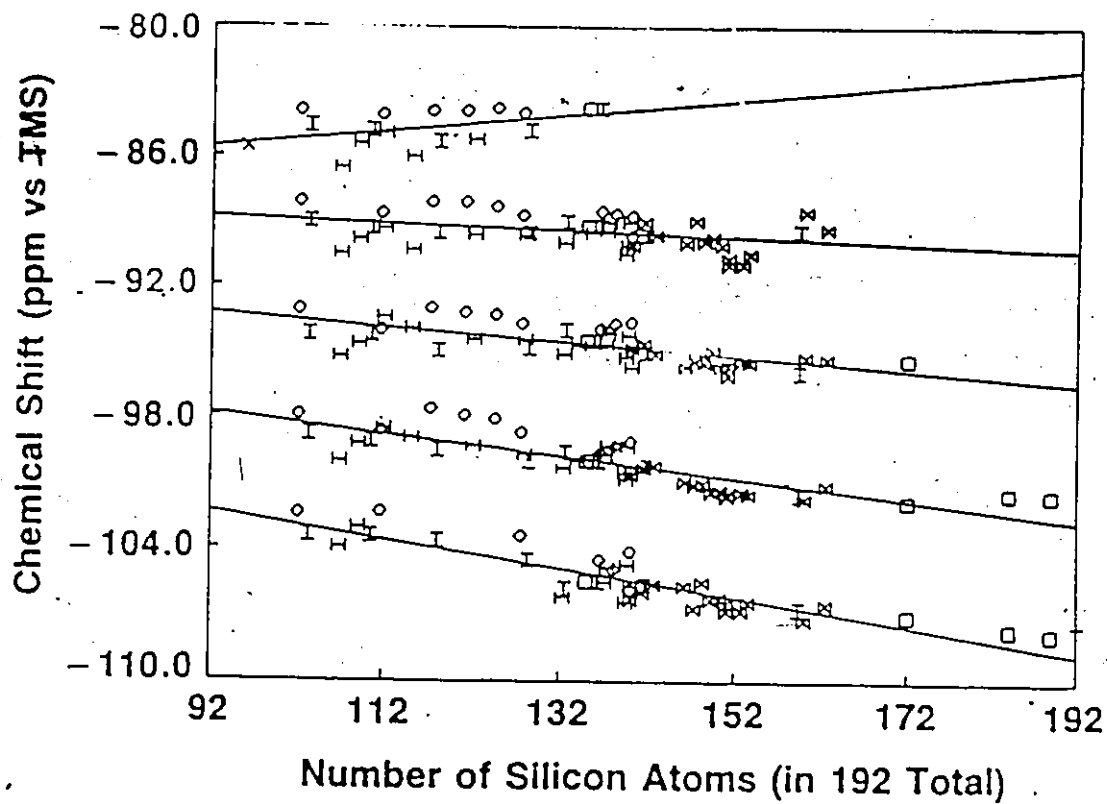
PPM FROM TMS

7

Figure 1.2a:  $^{29}\text{Si}$  isotropic chemical shift data for 52 synthetic materials with the faujasitic framework plotted against the mean number of silicon atoms in the unit cell. The five separate groups of data correspond, from top to bottom, to the different silicon environments  $\text{Si-nAl}$  ( $n = 4, 3, 2, 1,$  and  $0$ ) (Newsam 1985).

Figure 1.2b  $^{29}\text{Si}$  isotropic chemical shift data for 26 Zeolite-A framework materials plotted against the mean number of silicon atoms in the unit cell. The five separate groups of data correspond, from top to bottom, to the different silicon environments  $\text{Si-nAl}$  ( $n = 4, 3, 2, 1,$  and  $0$ ) (Newsam 1985).





using ortho-, soro-, ino-, phyllo- and tectosilicates (Fig. 1.3a). They improved the correlation coefficient to 0.93 by converting Si-O distances to Si-O bond strengths using the formula of Brown and Shannon (1973) (Fig. 1.3b). Smith and Blackwell (1983) tried various correlations of structural parameters and chemical shift for the silica polymorphs, and found a very poor relationship between mean Si-O bond length and chemical shift (Fig 1.4). A theoretical relationship produced by Grimmer and Radeaglia (1984) for silicate and aluminosilicate minerals

$$\delta = 1.187 \times 10^4 d(\text{Si-O})$$

was used to calculate the chemical shift of rankinite, hemimorphite and kaolinite although the results are not listed in the publication. Grimmer (1985) showed the directional nature of chemical shift with the relationships between the magnetic shielding tensor  $\sigma$  perpendicular and parallel to the Si-O bond direction and mean Si-O distance (Fig 1.5).  $\sigma$  is the magnetic shielding which is related to  $\delta$  by  $\sigma = -\delta$ .

$$\sigma_{\text{parallel}}(\text{Si-O}) = 2070 - 1.222 \times 10^4 d(\text{Si-O})$$

$$\sigma_{\text{perpendicular}}(\text{Si-O}) = 2250 - 1.334 \times 10^4 d(\text{Si-O})$$

Figure 1.3a  $^{29}\text{Si}$  solid state chemical shift versus average Si-O bond length. (Smith et al. 1983)

Figure 1.3b  $^{29}\text{Si}$  isotropic chemical shift versus total cation-oxygen bond strength for the four oxygen atoms surrounding each Si site. (Smith et al. 1983).

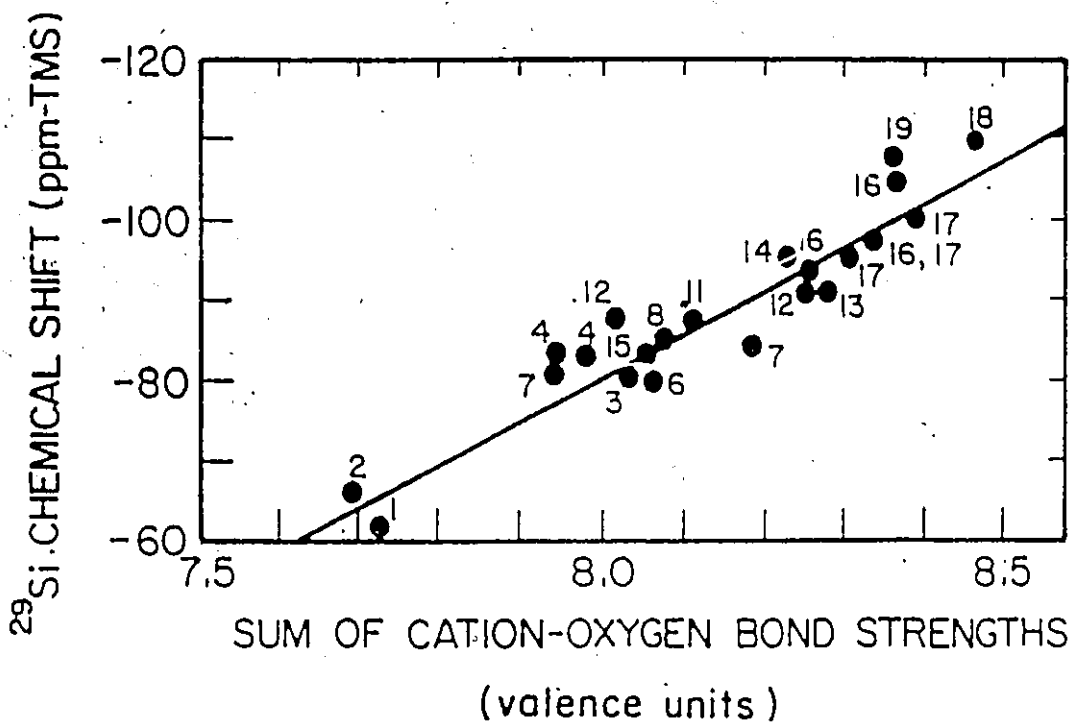
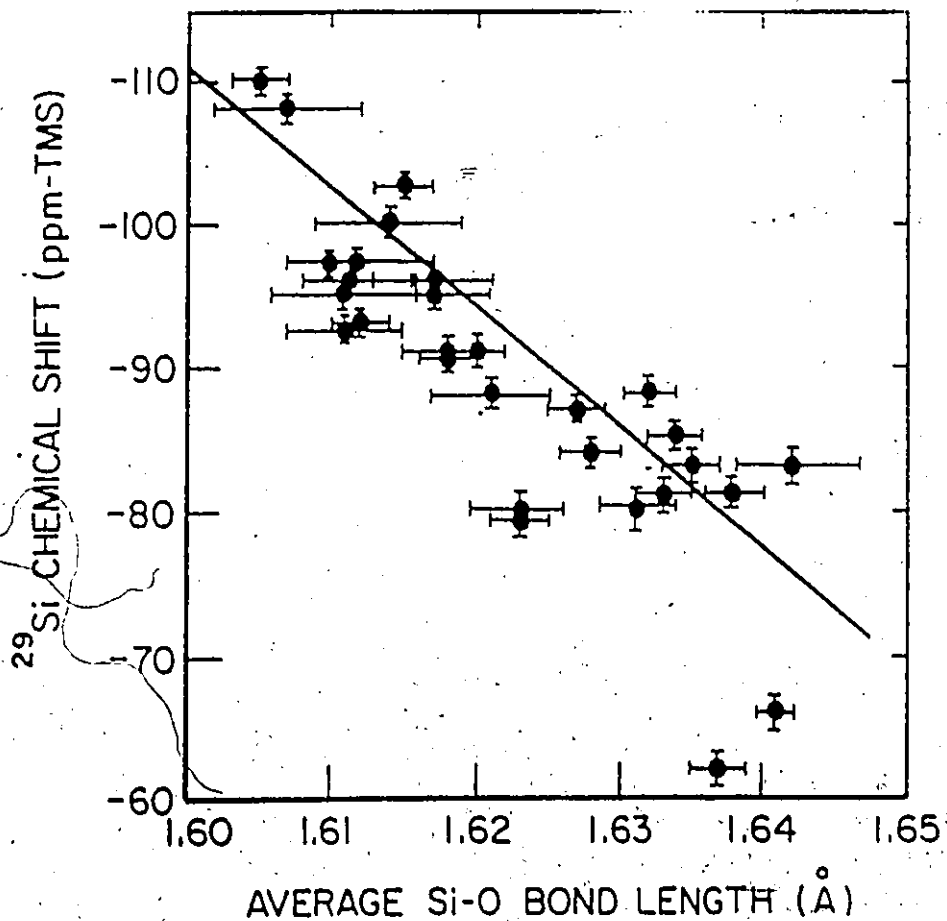


Figure 1.4 Relation between chemical shift for  $^{29}\text{Si}$  and structural parameters. CO, coesite; CR, cristobalite; H, holdstite; Q, quartz; TR, tridymite; UFS, uncalcined fluoride-silicalite. Solid symbols Smith & Blackwell 1983; open symbols Lippmaa et al. 1980 (Smith & Blackwell, 1983).

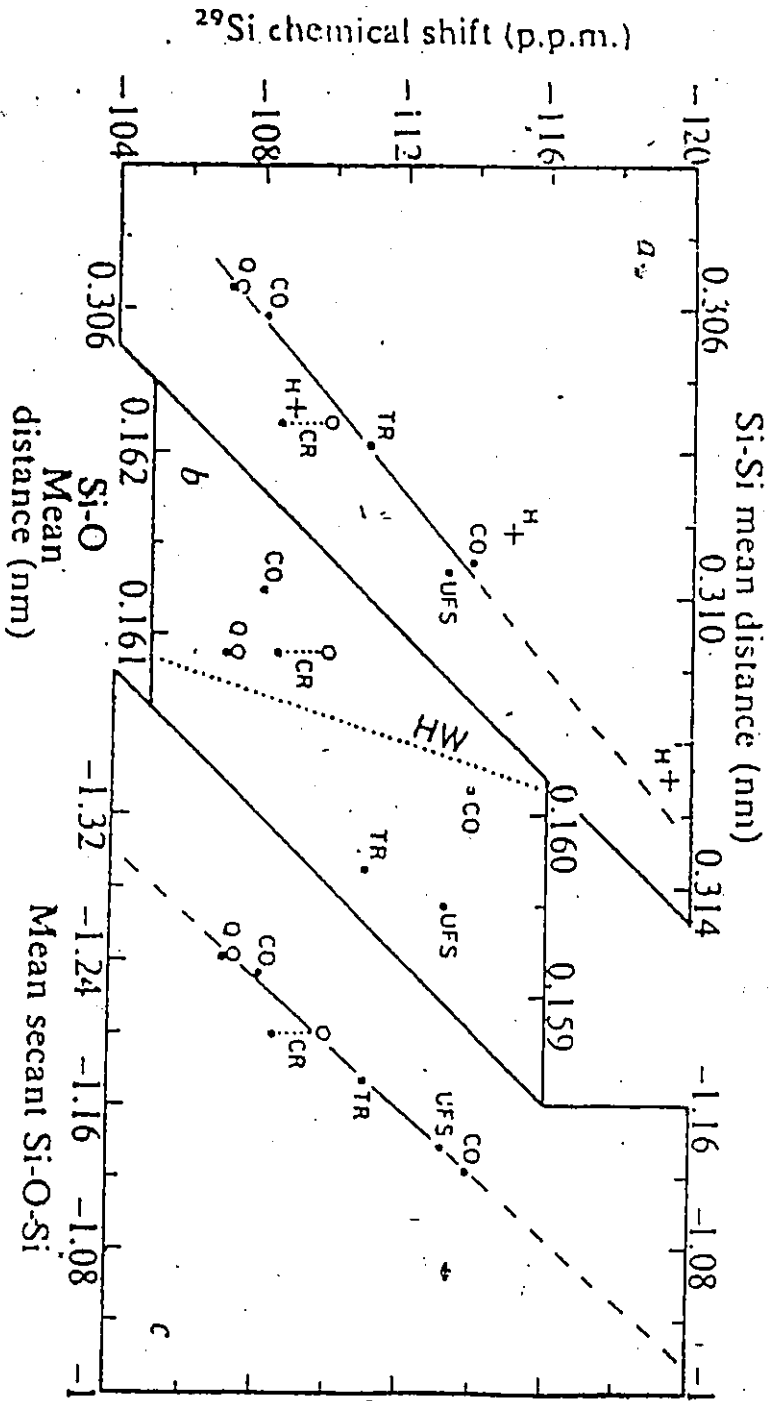
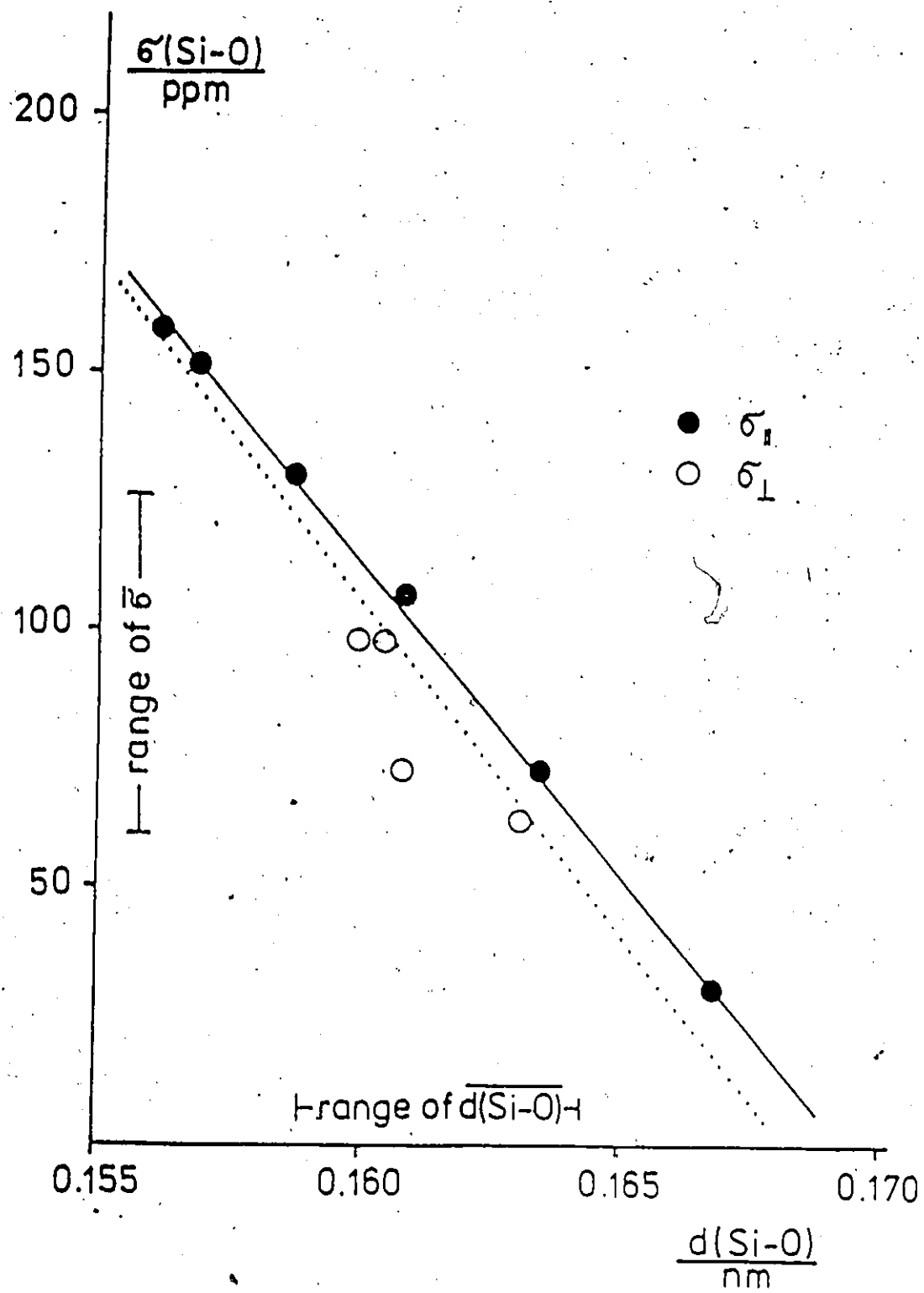


Figure 1.5 Bond direction related shielding  $\sigma(\text{Si-O})$  versus bond lengths  $d(\text{Si-O})$  for silica polymorphs (Grimmer 1985).





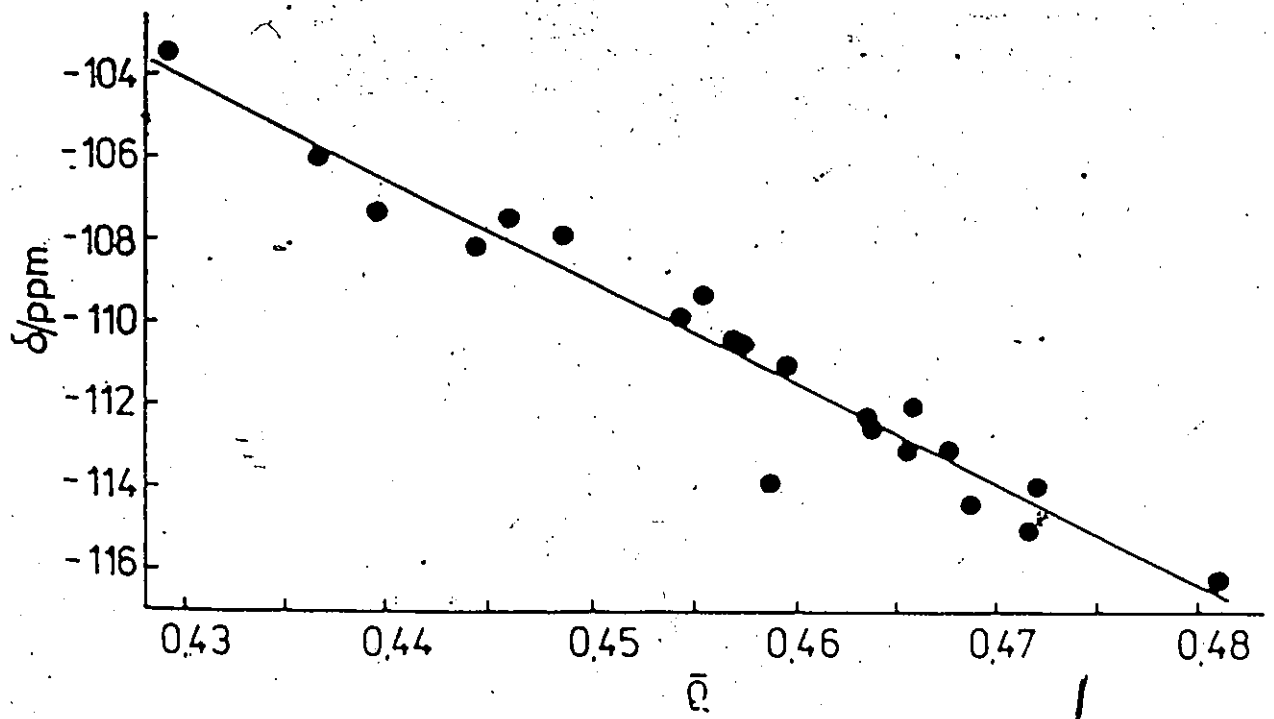
However, only 6 data points were used to obtain the relationship.

There have been other attempts to relate Si-O-Si angle to nmr chemical shift with variable success. Ernst et al. (1974) and Hoebbel et al. (1976) were two of the first to show a relationship between size of ring and  $^{29}\text{Si}$  chemical shift in solution of siloxanes. Smaller rings give less negative values of  $\delta$  indicating a shift to low field with tighter Si-O-Si angles. Grimmer and coworkers (1983, 1984) showed for MAS nmr of lanthanide series disilicates that straight Si-O-Si angles produce a shift to high field. Smith and Blackwell (1983) obtained correlation coefficients of over 0.99 for plots between  $\delta$  and mean secant Si-O-Si or mean Si-Si distance (Fig. 1.4). They used only silica polymorphs, however, discounted cristobalite, as their value for chemical shift did not fit their trend, and averaged twelve tridymite silicon sites and peaks. Engelhardt and Radeaglia (1984) used  $\cos\alpha/\cos\alpha-1$  ( $\alpha$  = Si-O-Si) from the d-p  $\pi$ -bonding hybridization factor of Gibbs (1982) as a basis of the following regression for silica polymorphs and zeolites:

$$\delta = 247.05 (\cos\alpha/\cos\alpha-1) + 2.19$$

They found a correlation coefficient of 0.987 for 21 points (Fig 1.6). They later extended their relationship (Radeaglia

Figure 1.6 Relationship between  $^{29}\text{Si}$  chemical shift  $\delta$  and mean oxygen  $s$  character  $\rho$  of the silica polymorphs and zeolitic aluminosilicates. The line is obtained from regression analysis. (Englehardt & Radeglia 1984).



and Engelhardt, 1985) to aluminosilicate structures by including a shift to low field of 5 ppm for each aluminum next-nearest-neighbour(n).

$$\delta = -7.2 + 5n - 223.9 (\cos\alpha/\cos\alpha-1)$$

This increased their correlation coefficient to 0.988 for 49 data points (Fig 1.7).

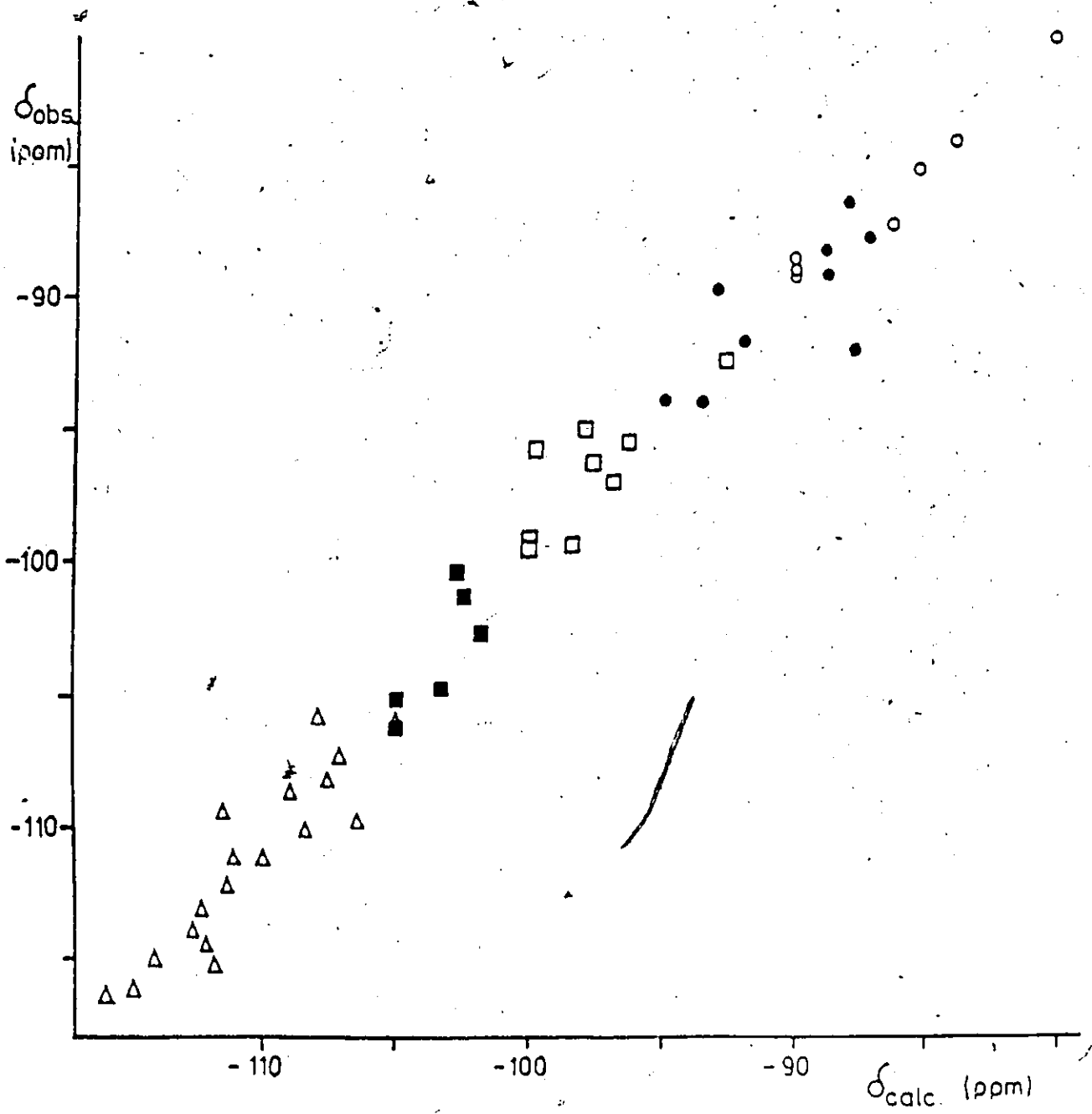
The effect of electronegativity of adjacent cations on chemical shift was used by Ernst *et al.* (1974) to relate the downfield shift of solution  $^{29}\text{Si}$  nmr peaks with electron donating groups. Magi *et al.* (1984) showed a trend in  $\delta$  with electrostatic bond strength and also with electronegativity. Grimmer and Radeglia (1984) used a shielding factor related to electronegativity in finding a relationship with chemical shift. Janes and Oldfield (1985) calculated an electronegativity factor (EN) from  $^{29}\text{Si}$  MAS nmr data for various cation-oxygen pairs of atoms and used this to predict the chemical shift of other aluminosilicate minerals from

$$\delta = - 24.336 \Sigma \text{EN} + 279.27$$

Allowance was made for variation in EN (O-Si) due to different Si-O-Si angles.

$$\text{EN}(\text{OSi}) = (\text{angle Si-O-Si}/136.79) + 2.734$$

Figure 1.7 . The experimental  $^{29}\text{Si}$  nmr chemical shifts,  $\delta_{\text{obs}}$  of zeolites and silica polymorphs plotted against the shifts  $\delta_{\text{calc}}$ . The various  $\text{Si}(\text{OSi})_{4-n}(\text{OAl})_n$  units are designated by: open circle,  $n = 4$ ; closed circle,  $n = 3$ ; open square,  $n = 2$ ; closed square,  $n = 1$ ; triangle,  $n = 0$  (Radeglia & Englehardt 1985).



They had a correlation coefficient of 0.979 for 99 data points (Fig 1.8).

Sherriff et. al. (1987a) modified the formula of Janes and Oldfield to allow for the variation in EN (O-Al) with Al-O-Si angle in their interpretation of the scapolite series of minerals.

$$EN(OAl) = (\text{angle Si-O-Al}/138.41) + 2.734$$

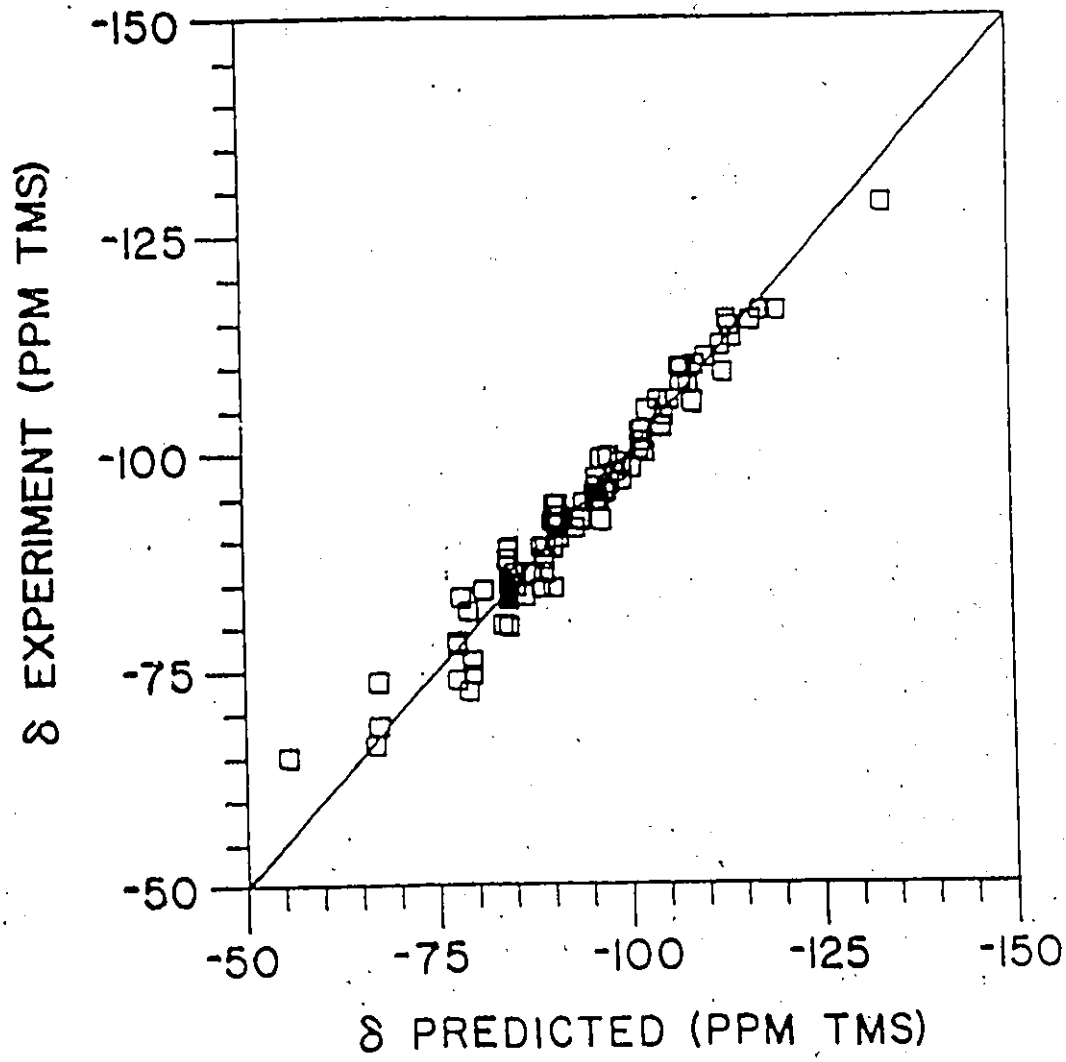
Another structural factor that has been considered related to chemical shift, is the symmetry of the SiO<sub>4</sub> tetrahedron. However Smith and Blackwell (1983) found no significant correlation between ((angle O-Si-O)-109.47) and  $\delta$  for the silica polymorphs (Fig. 1.4).

Ab initio calculations of <sup>29</sup>Si chemical shift were carried out by Tossel (1984) and Tossel and Lazzeretti, (1986, 1987) on the apparently simple systems quartz, olivine, SiF<sub>4</sub>, (Si(OH)<sub>4</sub>, H<sub>3</sub>SiOSiH<sub>3</sub> and (OH)<sub>3</sub>SiOSi(OH)<sub>3</sub>. They related chemical shift to changes in occupied to unoccupied orbital energy gaps and found that as variations in  $\sigma$ -diamagnetic (Appendix I section I.3) covered less than 1 ppm,  $\sigma$ -paramagnetic was the dominant factor in determining chemical shift. They also calculated that while  $\delta$  showed some correlation with Si-O-Si it was only weakly dependent on Si-O bond-length, thus corroborating the findings of the experimentalists.

Figure 1-8 Graph showing correlation between experimentally determined silicon-29 MASS NMR chemical shift and chemical shift predicted on the basis of the group electronegativity sum. Correlation coefficient = 0.979. Solid line represents  $\delta(\text{experimental}) = \delta(\text{predicted})$ . The mean absolute deviation between experimental and prediction is 1.96 ppm (Janes and Oldfield 1985).



2



From all of the above studies, it appears that there are relationships between  $\delta$  and Si-O bond length, Si-O-Si angle, number of bridging oxygens and type of next-nearest-neighbour and other adjacent cations. Published plots usually have good values of the correlation coefficient but they often refer to only a limited type of silicate structure (e.g. Smith and Blackwell 1983). There is also no indication of the sphere of influence for MAS nmr, i.e. how far away a cation must be to cease to perturb the magnetic field at the silicon.

In  $^{29}\text{Si}$  MAS nmr studies of silicate minerals there has often been considerable debate, as to which of the variables to use in the calculation of chemical shift. Weiss et al. (1987) in their study of 2:1 layer silicates decided to use the electronegativity of cations rather than a function for the T-O-T angle, as this produced better correlations between calculated and experimental spectra.

In the study of glasses using  $^{29}\text{Si}$  MAS nmr the only way to assign peaks fitted to the broad envelopes of resonances has been by comparison with the spectra of crystalline material. Schramm et al. (1984) tried using the chemical shifts of sodium and potassium silicates to assign the peaks fitted to spectra of lithium silicate glasses. They obtained closer agreement between predicted and measured chemical shift by using the data from lithium silicate crystal structures but as there was no  $Q^1$

(sorosilicate) type crystal structure available, that value had to be extrapolated from other data.

$^{29}\text{Si}$  MAS nmr spectroscopy of glasses has been used to determine the distribution of Si-O-Si angles in silica glasses (Gladden et al. 1986; De Jong et al. 1987). However the distribution found is dependent on the equation used to relate chemical shift to bond angle. Different empirical correlations (e.g Dupree and Pettifer 1984; Smith and Blackwell 1984) give very different results for angular distribution:

The factors affecting  $^{29}\text{Si}$  MAS nmr chemical shift also need to be understood for the correct interpretation of studies of dynamic systems such as high temperature melting of albite glass (Liu et al. 1987).

These are just a few examples of the difficulties experienced in the interpretation of  $^{29}\text{Si}$  MAS nmr spectra due to the problem of not understanding the factors affecting chemical shift. Apart from the theoretical calculations of Tossel, the studies of  $^{29}\text{Si}$  chemical shift consisted of taking average structural parameters and correlating them empirically with nmr peak position.

In the experiment described in the next chapter, a mathematical function is devised, which relates to the actual electronic environment surrounding a particular  $^{29}\text{Si}$  atom. This is then compared with the measured  $^{29}\text{Si}$  chemical shift to investigate the factors affecting chemical shift.

CHAPTER 2  
CORRELATION BETWEEN ATOMIC STRUCTURE AND  
<sup>29</sup>Si MAS NMR CHEMICAL SHIFT

2.1 INTRODUCTION

Nmr chemical shift is dependent on the type of isotope and the electronic environment surrounding the magnetic nucleus. Therefore the difference between <sup>29</sup>Si MAS nmr chemical shift of SiO<sub>4</sub> groups in silicate structures should be related in some way to the position and chemical state of the surrounding atoms.

In the experiment to be described in the following pages the relationship between the positions of the surrounding atoms and <sup>29</sup>Si chemical shift was studied in order to obtain a greater understanding of this relationship and if possible to find some way of calculating nmr chemical shift from atomic structure.

It has been established that the position and orientation of the electronic density along surrounding bonds affects chemical shift (McGlinchey, et al. 1986). Therefore an experiment was devised to determine geometric functions for each bond surrounding a particular silicon atom and study the effect of this electronic density on

$^{29}\text{Si}$  chemical shift. The bond anisotropy term of McConnell (1957) forms a basis for the calculations and this is modified by the bond valence function (Altermatt & Brown 1985) to allow for different types of cations in the structure. A third refinement to the function allows for the effect on chemical shift, of tight ring structures producing delocalised electron density.

## 2.2 NMR AND DIFFRACTION DATA

The measured nmr chemical shifts of 132 Si atoms in a wide range of silicates with known crystal structures were taken from various compilations (Lippmaa et al. 1980; 1981; Smith and Blackwell 1983; Engelhardt and Radeglia 1984; Radeglia and Engelhardt 1985; Janes and Oldfield 1985; Smith et al. 1983; Grimmer and Radeglia 1984; Newsam 1985; Williams (Sherriff) 1984; Sherriff and Hartman 1984; Sherriff et al. 1987a; Kinsey et al. 1985; Sanz and Serratosa 1984) and from data from samples listed in Appendix II. The data were sorted using the DBase III data processing computer program.

X-ray and neutron diffraction crystal structural data of the corresponding silicates were retrieved from the Inorganic Crystal Structure Database (ICSD) at CISTI in Ottawa (Bergerhoff et al. 1983).

The nmr and diffraction data were screened for

errors and inaccuracies. Five minerals, for which nmr data were available, were not used in the final correlation, leaving 124 pairs of data. Discussion about the specific mineral data used or rejected is given in Section 2.4.

### 2.2.1 DISORDER OF CATIONS IN A CRYSTALLOGRAPHIC SITE

X-ray or neutron diffraction data for a particular site in a mineral are averages for all the atoms located on that site in the structure regardless of type of atom. If there is cation substitutional disorder the diffraction data contain information from sites containing different cations. Nuclear magnetic resonance, on the other hand, is specific to each chemical environment of one type of atom in that site.

The best example, indeed the worst problem, of cation disorder is Al-Si ordering in tetrahedral sites. Conventional X-ray diffraction data do not discriminate between tetrahedral (T) sites containing Si or Al because they have similar scattering factors. However aluminum is a larger cation than silicon, so alumina tetrahedra are larger than silica tetrahedra and therefore have longer T-O bond distances. The amount of Al in a T site is calculated from the T-O bondlength, assuming the pure Si-O bondlength to be about 1.60 Å and the pure Al-O bondlength to be about 1.75 Å. Other structural parameters such as T-O-T angle and

O-O distances also vary depending on whether Al or Si occupies the site.

The occupancy of other sites around the tetrahedral site can be dependent on the nature of the tetrahedral cation. Diffraction data for a particular T-site therefore can be averages not only of sites containing both Si and Al, but also with differing next nearest neighbour cations and hence a variety of structural and chemical environments. Atomic positions calculated from diffraction data of the tetrahedral cation, the surrounding oxygens, and of other cations are, therefore, average positions over the whole crystal.

Nmr data, on the other hand, are specific to either Si- or Al- containing sites. In this study  $^{29}\text{Si}$  MAS nmr is used to study just the Si containing sites. Nmr is also very sensitive to the nature of the next-nearest neighbour tetrahedral cation, giving a difference in chemical shift of approximately 5 ppm for each substitution of Si by Al. Substitution of other neighbouring cations also causes a change in chemical shift. Therefore each different chemical environment gives a different peak position. These peaks might, however, not all be individually resolvable.

In order to obtain a meaningful relationship between structure and chemical shift it was necessary to eliminate all structures with a large degree of Si-Al disorder, such as some zeolites, disordered scapolites and

high temperature feldspars. Unfortunately if all structures, with a possibility of Al-Si disorder are removed there would be very little data left.

For some disordered minerals, such as muscovite, where the  $^{29}\text{Si}$  MAS nmr spectrum consists of separately resolved peaks relating to different next-nearest neighbour configurations of one T-site (Sanz and Serratosa 1984), it is possible to assign the main peak to the dominant configuration and use this value of chemical shift in the calculation.

#### 2.2.2 DIFFERENCE IN COMPOSITION OR ORDERING BETWEEN MINERAL SAMPLES.

Another problem encountered when relating between diffraction and nmr data from the literature is the difference between samples used to obtain each type of data. There can be differences in composition, ordering or state of minerals which have the same name.

Wherever possible nmr and diffraction data were obtained on minerals from the same source. This was achieved in the case of albite from the Amelia Courthouse locality (nmr data: Sherriff and Hartman 1985; structural data: Harlow and Brown 1980), and of the scapolite samples from the McMaster collection (Shaw 1960a and 1960b; nmr data: Sherriff et al. 1987a; structural data: Levien &



Papike 1976). In some compilations of nmr data, the source of the material was not listed and in most cases it proved impossible to find nmr and structural data on the same material.

Differences in composition were unavoidable in minerals with variable chemical composition, such as amphiboles. Where possible, the chemistry of the diffraction structure was matched to that of the nmr sample. For minerals with variations in cation compositions, such as tourmaline (Donnay & Buerger 1950), structures were selected which had the lowest possible content of iron and other transition metals. Nmr spectroscopists can only study minerals with a low content of iron or other transition metals because of the effect of paramagnetic atoms in broadening signals and reducing signal to noise ratio (Sherriff and Hartman 1985).

If the nmr data were reported on synthetic samples, such as for tridymite (Smith & Blackwell 1983), diffraction data of synthetic minerals (Baur 1977) were used to eliminate any difference in ordering between synthetic and natural minerals.

It was sometimes difficult to determine as to which polymorphic form of a mineral the nmr data referred. In the case of low temperature stable versus high temperature unstable forms, the low temperature form such as alpha-quartz was the obvious choice. In the case of cristobalite,

Lippmaa et al. (1980) report a value of -109.9 ppm for the chemical shift but Smith and Blackwell (1983) report -108.5 ppm. Smith and Blackwell had analyzed their sample by powder X-ray diffraction and suggest that the discrepancy between the two values may be due to polytypic disorder in the stacking sequence in the sample, used by Lippmaa. The chemical shift of Smith and Blackwell (1983) was used for correlation with the calculated value for cristobalite.

### 2.2.3 INACCURATE STRUCTURAL DATA

In some cases there were errors in the numbers obtained from the data base. These were found by initially carrying out the calculations using at least two different structures for each mineral. In the case of disagreement between the answers a check of calculated against reported bondlengths or angles often revealed a mistake in the original paper such as the transposition of two figures. In the structure of anorthite (Wainwright and Starkey 1971) the x coordinate of the T2(0000) site published as 0.6485, gives bond distances that do not agree with those quoted in the paper but 0.6845 produced the correct results. All errors found in this way have been reported back to the database for correction. For simplicity, only the one structure used for the final calculation is reported for each mineral.

Accuracy of the diffraction data was also a factor to be considered, so recent structures from renowned authors or laboratories were used whenever possible and the calculations checked with second structures.

#### 2.2.4 ERRORS IN NMR DATA

Purity of mineral specimens and correct identification of mineral phases has been a problem in the reporting of nmr data. Lippmaa et al. (1980) reported two peaks in the  $^{29}\text{Si}$  MAS nmr spectrum of pyrophyllite at -91.5 and -95.0 ppm. Later authors (Barron et al. 1983; Sanz and Serratosa 1984), in trying to duplicate these chemical shifts of Lippmaa, found only one peak at -95.0 ppm and decided that the peak at -91.5 was due to kaolinite intergrown with pyrophyllite.

To reduce the possibility of misnamed minerals I tried to obtain nmr data from at least two different sources giving more credence to data where it is specified that the mineral has been checked by X-ray diffraction. This was carried out on all the samples reported in Williams (Sherriff) (1984). The samples listed in Appendix II had all been characterized by the donors.

Assessing the quality of the published nmr data can be difficult as often only the chemical shift is quoted and sometimes to few significant figures (Smith et al. 1983).

If the spectrum was figured in the publication, or the peak width at half height reported, the accuracy of the data could be estimated, e.g. chondrodite reported to be 5 ppm wide (Mägi et al., 1984).

It is difficult to establish the position of the top of the peak for broad peaks especially if there is difficulty in phasing the spectrum because the baseline is not completely flat. Broad peaks can be due to poor instrumentation, a slow spin rate or to paramagnetic elements in the sample. They can also be due to overlapping unresolved peaks in a spectrum due to different sites in the structure, different chemical environments for each site and intergrowths, inclusions of other minerals or alteration products e.g. perthitic intergrowths of plagioclase and alkali feldspar often contained inclusions of quartz, and showed sericitization.

In multipeak spectra peaks must be allocated to specific crystal structure sites. This has been done previously on the grounds of number and type of next nearest neighbour and also by using the various empirical calculations. Previous interpretations have usually been found to coincide with peak allocation based on the predictive method developed in this study; e.g. feldspars (Janes and Oldfield 1985; Sherriff and Hartman 1985). However in the case of tridymite where 5 peaks represent 12 sites (Smith and Blackwell 1983), and of anorthite where

3 peaks represent 8 Si containing sites (Sherriff & Hartman 1984), the spectra have been reinterpreted and the peaks were assigned to sites on the basis of the calculated chemical shift (Appendix VIII).

Differences in spin relaxation times between sites can often aid in spectral interpretation. In the case of intergrown minerals different delays between pulses can be used to enhance or suppress peaks from a secondary mineral. Quartz intergrowths are rarely seen in spectra of feldspars run with a relaxation delay of less than 30 s because pure quartz has a  $T_1$  of several hours (Sherriff and Hartman 1985). Broad peaks from sites close to paramagnetic elements are not seen with relaxation delays of greater than 1 s as these have very short relaxation times. Differences in relaxation rates of individual sites in a mineral can lead to peaks being missed during standard runs of the spectra. Certain peaks with initially long  $T_1$ 's can be enhanced by relaxation techniques, such as cross polarization (Fyfe 1983). This is evident in the case of clinoptilolite where the peaks due to sites close to hydrogen atoms are enhanced with  $^1\text{H}$  cross polarization (Lippmaa et al. 1981).

Discrepancies can also occur during integration of spectra in relative areas of peaks not being representative of the number of atoms in each environment. This can be checked by carrying out all peak integrations on duplicate

spectra collected with a range of delays between pulses.

Another possible source of error, when using data from different laboratories, lies in the use of secondary standards. All  $^{29}\text{Si}$  chemical shifts are reported with respect to tetramethylsilane (TMS). However, without proton decoupling, the  $^{29}\text{Si}$  peak of TMS is split by  $^{29}\text{Si}$ - $^1\text{H}$  spin-spin coupling to the 12 protons of the methyl groups giving a very broad signal, not suitable as a standard. TMS is also a very volatile toxic liquid and while a few drops added to a sealed sample for solution nmr is not hazardous, spiking poorly sealed powder samples with TMS is a health hazard. All solid state  $^{29}\text{Si}$  spectra are therefore measured with reference to a secondary standard, which is different in each laboratory. The peak, at -104.6 ppm, of a spectrum of sample BLS036 oligoclase is used as a standard for the collection of data in Williams (Sherriff) (1984) and Appendix II. This has been cross referenced to a proton spin decoupled spectrum of TMS. It is not always possible in the literature to determine whether secondary references are accurate. The best check is duplicate results from different laboratories.

Differences among instrumentation can lead to discrepancies between reported spectra. There can be differences in size and homogeneity of magnetic field, and in sample spinning rate. In the case of a discrepancy, greater weight has been given to spectra obtained at higher

magnetic field and faster spinning rate. It is also important to note the conditions of FID acquisition including the use of cross polarization, decoupling, or any non standard pulse sequence. The data should also be examined for digital manipulation during Fourier transform operations such as the application of line broadening or Gaussian enhancement of the peaks.

The matrix effect, which causes differences in chemical shift in solution nmr depending on the composition of the solvent, could potentially have an effect on solid state nmr but this has not yet been found. It is unlikely to cause a problem within a system such as silicate minerals where the structures are similar.

As most MAS nmr peaks have widths at half height greater than 80 Hz (1 ppm at 79.46 MHz), the accuracy of measurement of solid state nmr chemical shift is, at best,  $\pm 0.1$  ppm. Therefore errors of measurements less than this are not significant and can be ignored. Spectral resolution can be improved for very pure synthetic materials with improved instrumentation, with higher, more homogeneous magnetic fields and with a faster spin rate (Fyfe et al. 1987) but the inherent disorder and chemical variability prevents much improvement in the spectra of natural minerals.

### 2.3 CALCULATIONS

Crystal models, centred on each nonequivalent crystallographic silicon site, were simulated from diffraction data on the VAX 8600 computer using the Chem-X crystal structure modelling package (developed and distributed by Chemical Design Ltd, Oxford, England). Atoms were connected automatically by Chem-X if the spheres representing the atoms overlapped using standard atomic radii. Dummy atoms were inserted to mark the midpoint of all cation-oxygen bonds (Appendix III).

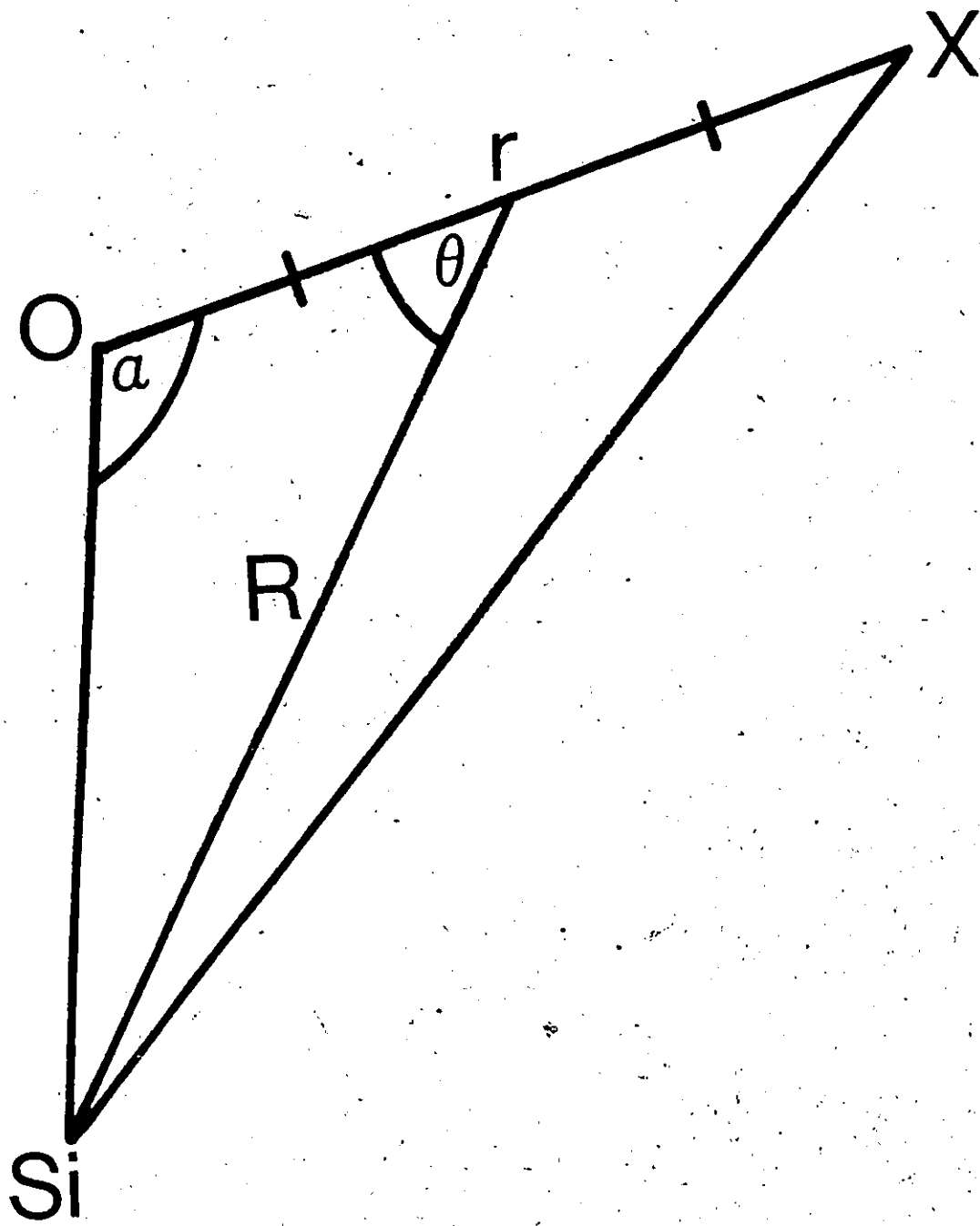
One problem with this computer modelling technique lies in deciding which atoms should be joined so that their bonds are included in the calculations. The Chem-X program was allowed to join any overlapping atoms using standard atomic radii thus eliminating human bias.

Atomic coordinates of these structures were used to calculate the distance ( $R$ ) between each silicon atom and the midpoint of the oxygen-second neighbour cation bonds, the length ( $r$ ) of these bonds, the distance ( $S$ ) of the cation from the silicon atom, the angle ( $\theta$ ) between  $R$  and  $r$ , and the Si-O-cation angle ( $\alpha$ ) (Fig 2.1; Appendix IV).

Other Fortran computer programs (e.g. Appendix V) were written to calculate geometric functions for atoms surrounding the silicon from these bond distances and angles. The sums of these geometric functions were plotted



Figure 2.1 : Diagram showing the definitions of angles  $\theta$  and  $\alpha$  and the lengths  $r$  and  $R$ .  $X$  is any second-neighbour cation (Including Si or Al) (Sherriff and Grundy 1988).



against  $^{29}\text{Si}$  MAS nmr chemical shift firstly for the silica polymorphs and then for all silicate minerals.

The Mihitab statistics computer program was used on a VAX 8600 to calculate chemical shift, plot the results and to carry out regression analyses.

Errors are caused by rounding of figures to 5 decimal places, at each stage of the calculations. Calculated chemical shifts are given to  $\pm 0.1$  ppm as this is the accuracy of the measured chemical shifts.

### 2.3.1 THE FIRST TERM; MAGNETIC ANISOTROPY

The term  $((3\cos^2\theta-1)/3R^3)$  was applied by McConnell (1957) to investigate proton chemical shift in solution spectra of organic compounds. McGlinchey *et al.* (1986) adapted the equation to provide a geometric term that could be used to study the effect of orientation on the shielding caused by a metal-metal bond (see Appendix XI).

The assumption is made that the electron density of the bond is evenly distributed along the length of the bond and can therefore be represented by the midpoint of the bond in the determination of length  $R$  and angle  $\theta$ . This generalization is only correct if both atoms are the same, as for the metal-metal bonds of McGlinchey and coworkers (1986). For cation-oxygen bonds the electron density across the bond will not be evenly distributed across the bond and

using the midpoint is an oversimplification. The correlation might be improved by taking another point, rather than the midpoint, as the average electronic density or perhaps by having a movable point dependent on the electronegativity of the cation. The error introduced by the midpoint approximation will be in the same direction but by varying amounts for all cation-oxygen bonds.

The summation  $\Omega$  of bond anisotropies provides a means of calculating the effect of the position and orientation of the electron quadrupole moments between atoms with respect to the silicon nucleus being studied.

$$\Omega = \Sigma((1-3\cos^2\theta_i)/3R_i^3) \quad (1)$$

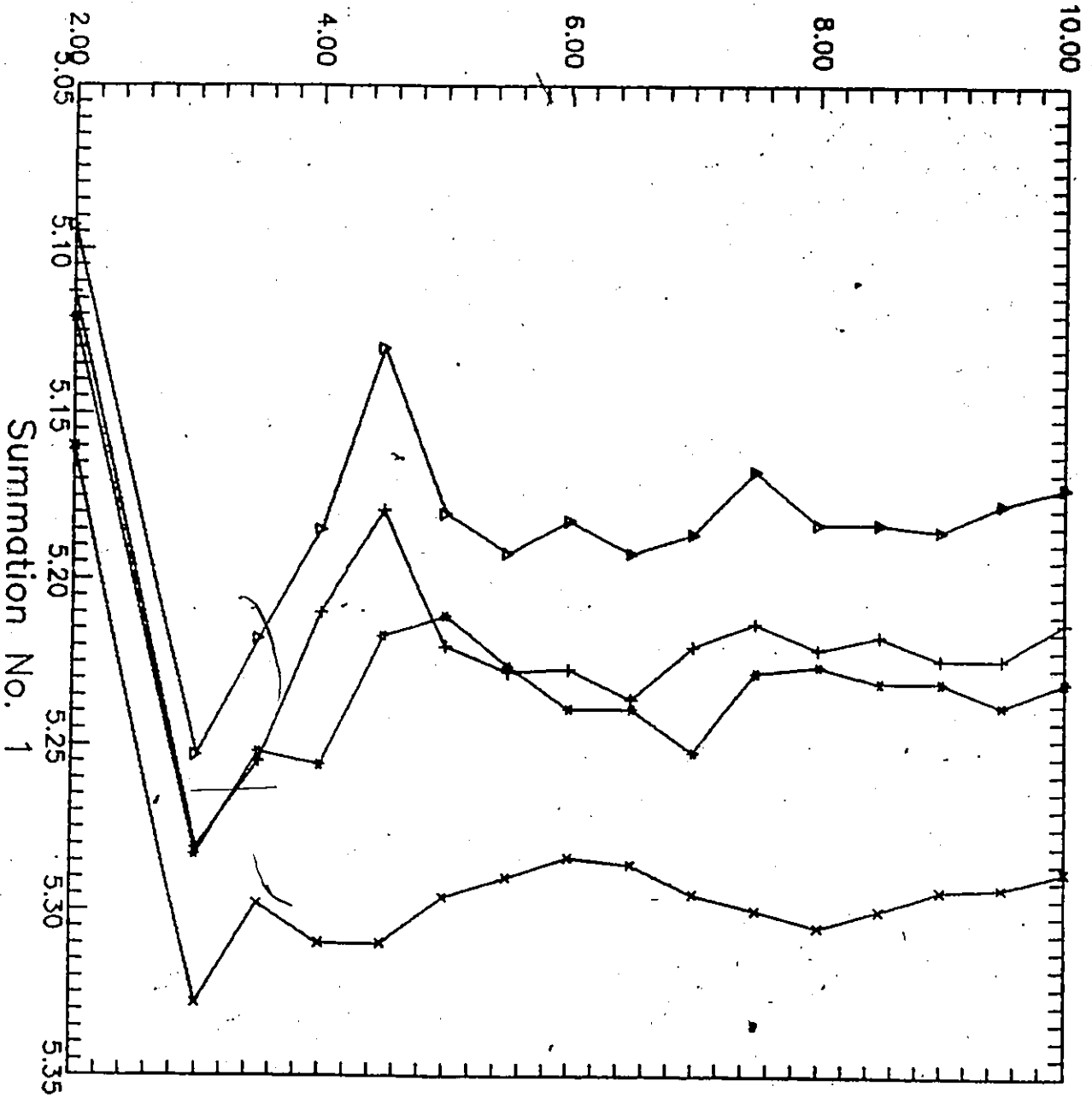
Initially this factor was summed over all silicon-oxygen bonds contained in a surrounding sphere for the silica polymorphs. These summations were made at 1/2 Å intervals out to a radius of 20 Å. A relationship was found between chemical shift and  $\Omega$  at each interval.

As the summations became less erratic after 5 Å (Fig 2.2; Appendix VI), a mean of the values of summations at 1/2 Å intervals from 6 to 10 Å was taken to represent the steady state of the bond anisotropy factor around the silicon.

The bond anisotropy term  $(1-3\cos^2\theta_i)/3R_i^3$  was then multiplied by different terms for angle  $\alpha$  (the Si-O-Si

Figure 2.2 Summations of  $\Omega$ , using equation (1), made at  $1/2 \text{ \AA}$  intervals spherically out from Si, plotted against distance from Si for the silica polymorphs. \* = quartz; x = cristobalite; + = coesite T1;  $\Delta$  = coesite T2.

Distance from Si (angstroms)



angle) in an attempt to find a optimum correlation between the "steady state bond anisotropy factor" and chemical shift for the silica polymorphs. The term  $(\cos\alpha/\cos\alpha-1)$  used for angle  $\alpha$  was taken from Gibbs (1982).

Calculations were carried out at 1/2 Å intervals from Si spherically out to 10 Å using the three following summations.

$$(1) \quad \Sigma((1-3\cos^2\theta_i)/3R_i^3)$$

$$(2) \quad \Sigma((1-3\cos^2\theta_i)/3R_i^3)(\cos\alpha/\cos\alpha-1)$$

$$(3) \quad \Sigma((1-3\cos^2\theta_i)/3R_i^3)(1/\cos\alpha)$$

The mean of the summations from 6 to 10 Å for each of these geometric terms (Appendix VII) were plotted against measured chemical shift for the 16 Si sites. In these plots the chemical shift values of tridymite were ordered according to the summation from geometric term (1). The calculated sum of bonds using the first term plotted against experimental chemical shift is given in figure 2.3.

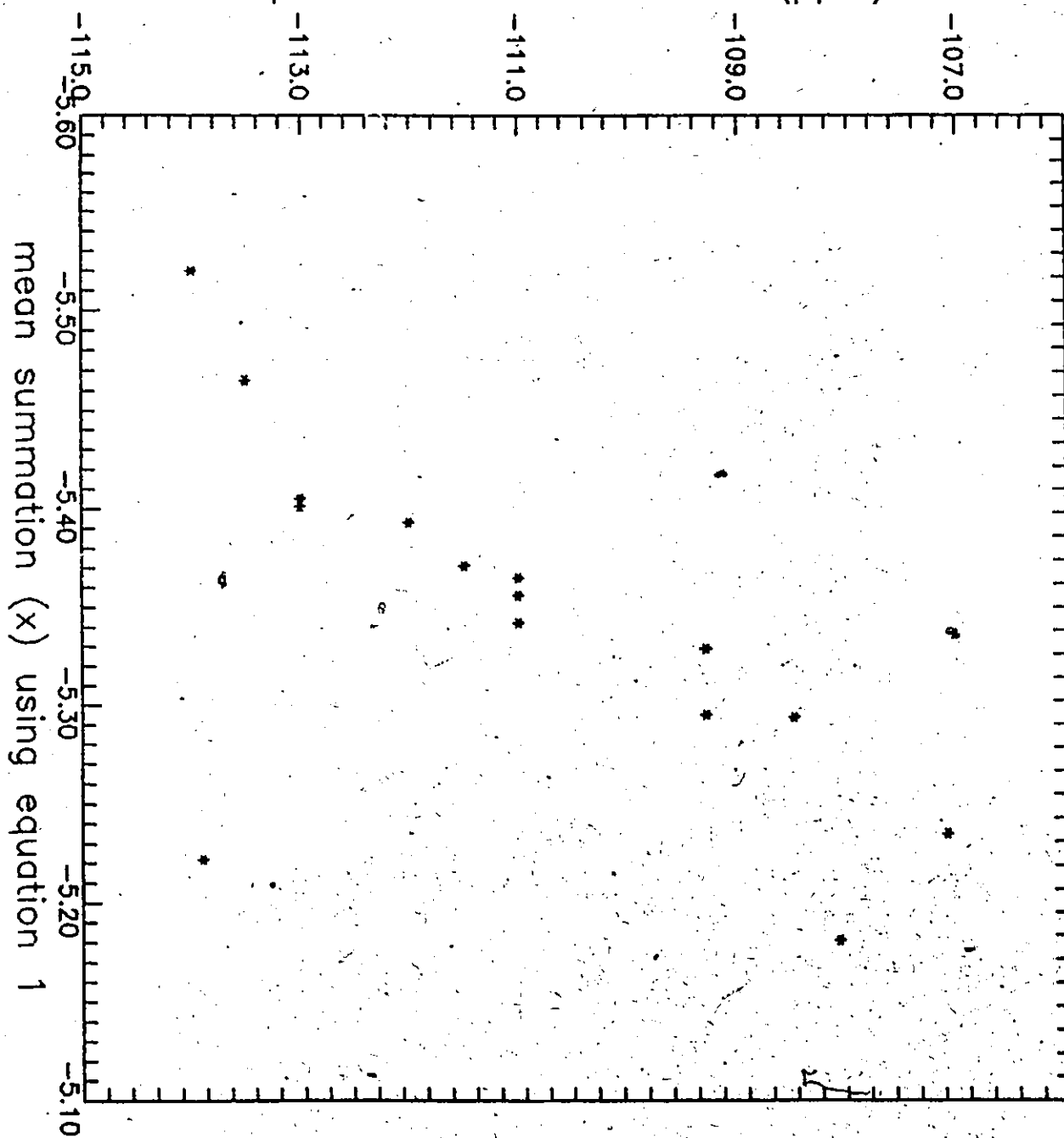
### 2.3.2 SECOND TERM; BOND VALENCE

To extend the calculation to other minerals, it was necessary to include a factor for the type of cation such

Figure 2.3 The mean of summations, at 1/2 Å intervals, from 6 to 10 Å, for the geometric term  $\Sigma((1-3\cos^2\theta_i)/3R_i^3)$  plotted against experimental chemical shift for the silica polymorphs, quartz, cristobalite, coesite and tridymite.



Experimental chemical shift (ppm)



as the electronegativity values of Pauling (1967). The bond valence equation of Altermatt and Brown (1985)

$$s_i = (\exp[(r_0 - r_i)/0.37])$$

allows for variations in both type of cation and cation-oxygen distance. In this expression  $r_i$  is the length of the cation-oxygen bond and  $r_0$  is a value for unit valence.

This term is an empirical correlation between bond length and bond valence for bonds between different atoms. It was found by plotting bond length against valence for a particular bond in many different structures. Brown and Shannon (1973) first derived the equation

$$s = (R/R_0)^{-N}$$

where  $s$  is the bond strength,  $R$  bond length and  $R_0$  and  $N$  fitted parameters for each type of bond. This gave different curves for each type of bond.

The equation was later rewritten as

$$s = \exp[(r_0 - r_i)/B]$$

and values of  $r_0$  and  $B$  calculated (Brown 1981) for many types of bonds.

Later calculations, using a much larger data set,

simplified the application of the equation by constraining all bonds to lie along the same curve. This gives a value for  $B$  of 0.37, for all type of bonds (Altermatt and Brown 1985) and leaves only one variable,  $r_0$  the unit bond valence term, to be input. Values of  $r_0$  for different bonds are listed in Brown and Altermatt (1985).

The accuracy of bond valence values calculated using these equations depends on the accuracy of the values taken for  $r_0$  and  $B$  which in turn depend on the accuracy of the bond distances in the original data from which  $r_0$  and  $B$  were calculated.

The data used for the calculation of the values of  $r_0$ , contained silicate structures which possibly showed Al-Si disorder in the tetrahedral sites, such as zeolites (I. D. Brown, McMaster University, personal communication). This would lead to errors in the Si-O and Al-O distances and hence inaccurate values for  $r_0$  for Al-O and Si-O. Several different values of  $r_0$  were used in the calculations to try to improve the correlation between calculated and measured chemical shift. These were taken initially for all cation-oxygen bonds from Brown and Altermatt (1985), secondly from Brown (1981) and finally with the values for all other cation-oxygen bonds from Brown and Altermatt (1985) and those of Si-O and Al-O changed incrementally.  $\Omega'$  was calculated for the 124 Si sites for each set of values. The correlation coefficients

of these plots are given in the third column of Table 2.1.

The values for  $r_0$  of 1.64 for Si-O and 1.62 for Al-O consistently were found to give the best correlation coefficients for calculations using  $\Omega'$  and also when terms for angle  $\alpha$  were included. These values were therefore used in the final calculations of chemical shift given in Appendix VIII.

Obtaining accurate values for Al-O and Si-O distances was considered to be of paramount importance as these occur in all calculations except for some orthosilicates. The effect of changing  $r_0$  for Al-O and Si-O was greatest for tectosilicates, where the four short T-O bonds dominate the calculation. As the values for Si-O and Al-O were changed in the opposite direction, to allow for Al in Si sites and vice versa, the effect was to change the slope of the functional line. The values of calculated chemical shift for high field sites with four Si next nearest neighbours increased, and for sites with four Al next nearest neighbours decreased.

The differences between calculated and measured chemical shift for minerals which have Si sites surrounded by four silicon or by four aluminum atoms may be indicative that the values of  $r_0$ , for Si-O and Al-O require further fine adjustments.

There is also the possibility of errors in the values of  $r_0$  for other cation-oxygen bonds. This could

TABLE 2.1

Correlation coefficients between calculated and measured values of  $^{29}\text{Si}$  chemical shift, for differing values of  $r_0$  for Al-O and Si-O, and different functions of angle Si-O-X

Values of unit valence		Si-O-X angle function			
$r_0/B$		no term	$\cos\alpha/\cos\alpha-1$	$\log(\text{Si-X})$	$\cos\alpha$
Si-O	Al-O				
*1.624/0.37	1.651/0.37	0.973	0.975	0.976	0.974
**1.63/0.36	1.63/0.36	0.972	0.975	0.976	0.973
***1.64/0.36	1.62/0.36	0.981	0.981	0.986	0.977
***1.65/0.36	1.61/0.36	0.975	0.979	0.980	0.977

\* Values for  $r_0$  for all cation-oxygen bonds from Brown and Altermatt (1985),  $B = 0.37$ .

\*\* Values of  $r_0$  and  $B$  for all cation-oxygen bonds from Brown (1981).

\*\*\* Values of  $r_0$  for all other cation-oxygen bonds from Brown and Altermatt (1985),  $B = 0.37$ .

cause the greatest discrepancy for minerals with only one type of cation other than silicon involved in the calculation, such as hemimorphite  $Zn_4(Si_2O_7)(OH)_2 \cdot H_2O$ . Unfortunately there were insufficient nmr data to investigate this problem and separate the effect of inaccurate values for other cations from that for Si and Al.

The bond valence equation was combined with the anisotropy equation to form the summation in equation 2.

$$\Omega' = \sum (\exp[(r_0 - r_i)/0.37]) ((1 - 3\cos^2\theta_i)/3R_i^3) \quad (2)$$

$\Omega'$  was then calculated for the silica polymorphs and the aluminum silicate polymorphs again with summations out to 10 Å.

The only summation found to give a reasonable correlation with measured chemical shift  $\delta$  was obtained using just the cations bonded to the terminal oxygens of the silicate tetrahedron. Equation (2) was then used to calculate  $\Omega'$  for all other silicate minerals for which reliable nmr and diffraction data were available.  $\Omega'$  was compared with  $\delta$  and gave a correlation coefficient of 0.973, which was an encouraging result.

### 2.3.3 THIRD TERM; SI-O-X ANGLE

The third term in the equation is to allow for the effect on chemical shift of the geometric distortions introduced by tight rings in the structure (Hoebbel et al. 1976).

There is a good correlation between calculated and experimental chemical shift without introducing a third term (column 3, Table 2.1). However it was noted that some structures with either very small or very large values for angle  $\alpha$  showed a large discrepancy between calculated and experimental values of chemical shift.

Three modifications of equation 2 were tried to include a factor for the cation-oxygen-silicon angle ( $\alpha$ ). The first modification was with Gibbs (1982) "hybridization index" for the bridging oxygen.

$$(\cos\alpha/(\cos\alpha-1))$$

The second was  $\log (Si-X)$  where Si-X is the cation-silicon distance (Hill and Gibbs 1979) from

$$\log d(Si..X) = \log 2d(Si-O) + b \log \sin(1/2(\text{angle}(Si-O-X)))$$

The third function tried was simply  $\cos(\alpha)$ .

The first two of these modifications were factors

used in equations to relate Si-O bond distance with Si-O-Si angle in silica polymorphs and explain the relationship in the terms of d-p  $\pi$ -bonding as this has been considered to be important to chemical shift determinations (James & Oldfield 1986).

The three different terms tried are not necessarily the best functions to use but were chosen because they had been used previously to investigate the relationship between Si-O bond distance and Si-O-Si angle. All these angular functions gave larger effects at smaller angles, which was the type of correction needed to produce a linear correlation between geometric summation and measured chemical shift.

The correlation coefficients for the relationship between measured chemical shift and calculations of  $\Omega'$  using each of these modifications are given in columns 4, 5 and 6, of Appendix VI. As the best correlation was found when using the term  $\log(\text{Si-X})$  this was used in the final equation.

Even with this modification benitoite, which has tight  $\text{Si}_3\text{O}_9$  rings in the structure, is anomalous with a calculated chemical shift of -88.9 and a measured value of -94.2 ppm.



#### 2.3.4 RESULTANT EQUATION

The three terms for bond anisotropy, bond valence and angle  $\alpha$  are combined together to give the resultant equation:

$$\Omega'' = \sum [((1-3\cos^2\theta_i)/3R_i^3) (\exp[(r_0-r_i)/0.37]) (\log(Si-X_i))] (3)$$

The linear regression of  $\Omega''$  plotted against measured chemical shift  $\delta$  for 124 Si sites is:

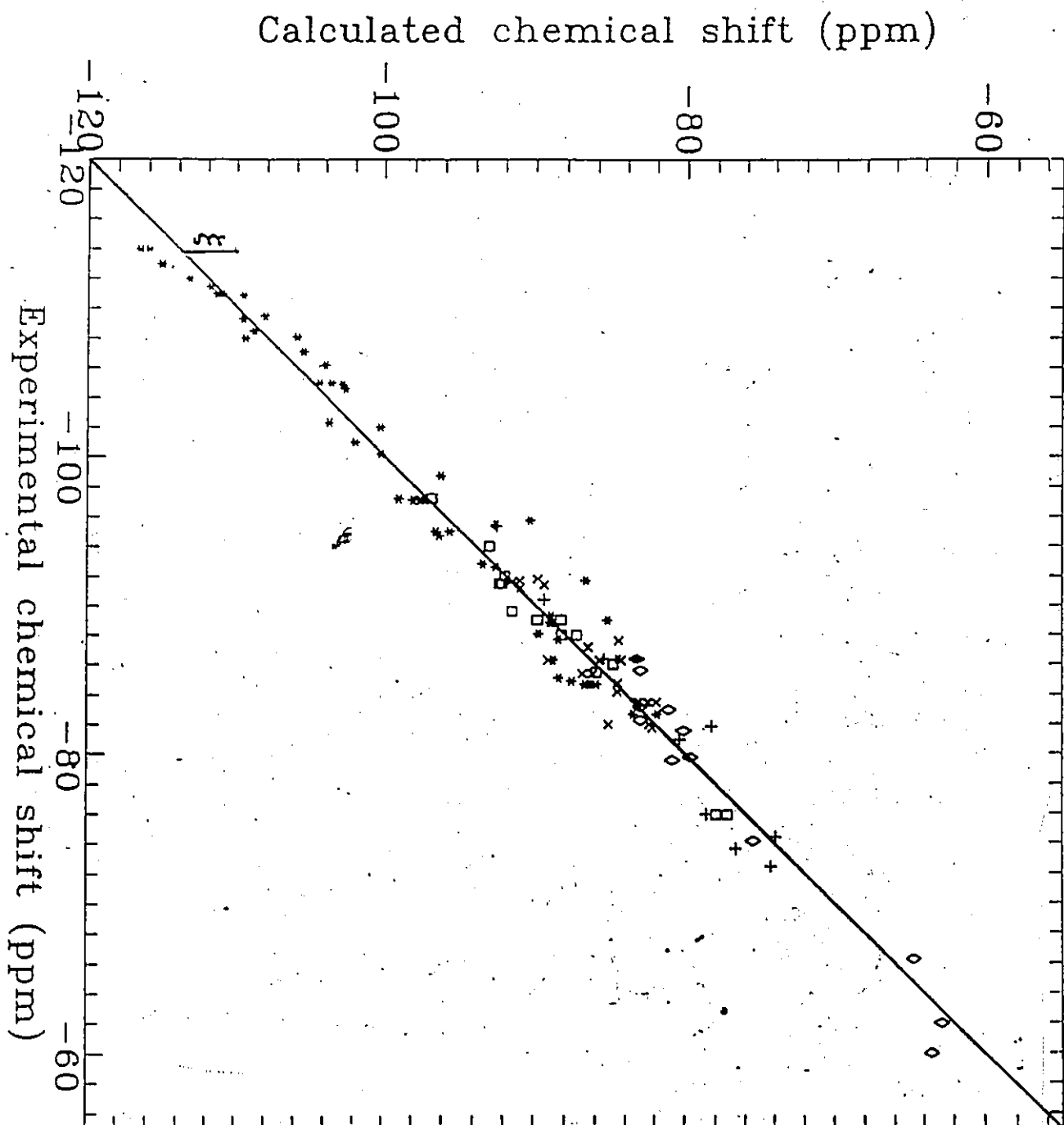
$$\delta = 701.6 \Omega'' - 45.7 \quad (4)$$

This can be used to calculate the expected chemical shift, to compare with measured values.

Figure 2.4 shows experimental chemical shift plotted against values calculated using equations 3 and 4 for 124 Si sites; 12 from orthosilicates (diamonds), 9 from sorosilicates (+), 23 from inosilicates (squares), 19 from phyllosilicates (x) and 61 from tectosilicates (\*). The plot has a correlation coefficient of .986 and a standard deviation of 0.66 ppm. The results of the calculations and the difference between calculated and experimental values of chemical shift are given in Appendix VIII.

O-H bonds were initially included in the equation but found to have a disproportionate effect on the

Figure 2.4 Experimental  $^{29}\text{Si}$  MAS nmr chemical shift plotted against chemical shift calculated from equations 3 and 4 for orthosilicates (diamonds), sorosilicates (+), inosilicates (squares), phyllosilicates (x), and tectosilicates (\*).  $\xi$  is the deviation of calculated from experimental chemical shift.



summations producing a calculated chemical shift which was displaced by several ppm. Minerals such as micas and clays give a better correlation between experimental and calculated values when hydrogen is excluded from the calculations. This indicates that the single electron of the hydrogen atom has very little effect on the chemical shift of  $^{29}\text{Si}$  in the form of  $\text{SiO}_4^{4-}$ , where the Si nucleus is surrounded by 97 electrons in bonding and non-bonding orbitals, without considering the influence of other cations outside the silicate tetrahedron.

The rapidly diminishing effect of bonds with increased distance is allowed for in the equation by the factor of  $3R^3$  in the denominator of the equation. As  $R$  is geometrically related to Si-O bonds of the silicate, the correlation found between mean Si-O distance and chemical shift (Smith and Blackwell 1983, Smith et al. 1983, Grimmer and Radeglia 1984, Grimmer 1985, Higgins and Woessner 1982) can be explained.

Changes in size of the Si tetrahedra are incorporated into the calculation of  $R$  (Fig 2.1). Distortions of the silicate tetrahedron do not appear to be significant, which agrees with the findings of Smith and Blackwell (1983) that there is little relationship between O-Si-O angle and chemical shift.

The orientation of the cation-oxygen bond with respect to the central silicon is calculated by the term

$(1-3\cos^2\theta)$  which has a minimum value of  $-2$  for  $\theta$  of  $180^\circ$  and a maximum of  $+1$  for  $\theta$  of  $90^\circ$ . When  $\theta$  is  $125.26^\circ$ , or  $(180 - 54.74^\circ)$ , the term  $(1-3\cos^2\theta)$  becomes zero and the bond has no influence on chemical shift. As the angle  $\theta$  is dependent on the Si-O-cation angle ( $\alpha$ ) the effect of orientation on chemical shift anisotropy is an alternative explanation to p-d  $\pi$ -bonding for the correlation of chemical shift with Si-O-T angle (Smith and Blackwell 1983, Janes and Oldfield 1985, Engelhardt and Radeaglia 1984, Radeaglia and Engelhardt 1985, Ramdas and Klinowski 1984, Sherriff et al. 1987a).

#### 2.4 A DISCUSSION OF THE RELATIONSHIP BETWEEN CALCULATED AND EXPERIMENTAL VALUES OF CHEMICAL SHIFT.

The relationships between calculated and experimental chemical shifts shown in Fig. 2.4 will now be discussed group by group: the minerals are listed in Appendix VIII.  $\xi$  is the deviation of the calculated from the experimental chemical shift. To a degree this analysis at first sight appears to be a circular discussion but is nevertheless legitimate. Ortho, soro, ino, phyllo and tecto silicates are considered separately but the different mineral groups are treated the same in all of the calculations.

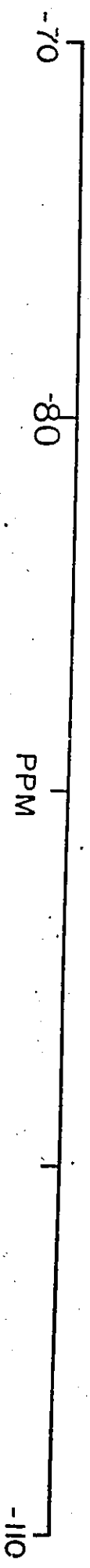
#### 2.4.1 ORTHOSILICATES

Orthosilicates have isolated silicate tetrahedra, therefore the contributions to calculated chemical shift are from bonds between oxygen and cations, which usually have a higher coordination number than four. The orthosilicates in this study, with the exception of kyanite, have only one silicon site eliminating dispute about the allocation of peaks in the spectra.

The calculated chemical shift values for the aluminosilicate polymorphs agree within one standard deviation (0.7 ppm) with the measured values, indicating a lack of Al-Si disorder in the tetrahedral sites.

The spectrum of white kyanite from Pfitschthal, Tyrol (Fig. 2.5) (R.O.M. specimen M22990) has two narrow peaks at -83.2 and -82.3 ppm (Williams (Sherriff) 1984). All other nmr spectra of kyanite report one peak at -83.2 ppm (Janes & Oldfield 1985), -82.9 ppm (Mägi et al. 1984), -83.0 ppm (Williams (Sherriff) 1984). Janes and Oldfield (1985) calculated one value of chemical shift of -84.2 ppm for kyanite although it had been speculated that there should be two different shifts for the sites (Mägi et al. 1984). The calculated chemical shifts for the two sites, from the diffraction data of a specimen from Celo Mines, Burnsville, North Carolina (Burnham 1963a), have similar shifts of -83.0 and -83.1 ppm (Appendix VIII), as the two

Figure 2.5  $^{29}\text{Si}$  MAS nmr spectrum of white kyanite  
from the Tyrol (Williams (Sherriff)  
1984).



White Kyanite  
Pfitschithal, Tyrol





sites have similar Si-O, Al-O distances and Si-O-Al angles. These peaks would not be resolved and would give the sole peak usually seen in the spectrum of kyanite. The two separated peaks for white kyanite indicate a different structural environment for silicon in this sample from that in the more usual blue kyanite.

Minerals with an olivine type structure, olivine, monticellite and chondrodite resonate 10 ppm to lower field than all other minerals including other orthosilicates (Appendix VIII). Although there are nine Mg atoms surrounding Si in olivine, six of the twelve Mg-O bonds involved in the calculation have values of  $\theta$  of about  $125.3^\circ$ . The magnetic anisotropy term  $(1-3\cos^2\theta)$  becomes zero at this angle and therefore the magnetic dipole of these bonds provide little contribution towards chemical shift. The chemical shift is therefore determined by the remaining six Mg-O bonds, which accounts for the small value of  $\Omega'$  and the low field shift of olivine type minerals.

The humite group of minerals consist of layers of olivine structure ( $Mg_2SiO_4$ ) interspersed with layers of brucite structure ( $Mg(OH,F)_2$ ) (Gibbs et al. 1970). Chondrodite, the only humite mineral for which nmr data were available, has a ratio of olivine to brucite layers of 1:2. The 5ppm width at half height of the  $^{29}Si$  MAS nmr peak (Mägi et al. 1984), could be due to polytypical disorder in

the layer structure of chondrodite and explain the  $\xi$  value of 2.5 ppm.

Garnet was excluded from the final correlation. Williams (Sherriff) (1984) found it very difficult to determine an accurate chemical shift for garnet because of broad weak signals. There is no indication of quality of signal for value of shift in Appendix VIII, (Mägi *et al.* 1984). The large number of substitutions cations possible in garnets, including paramagnetic cations, such as  $\text{Fe}^{2+}$ ,  $\text{Fe}^{3+}$ , Mn, Ti, Cr can explain the broad weak signals (Sherriff & Hartman 1984) and perhaps the  $\xi$  value of 6.3 ppm. Janes and Oldfield (1985) also report a value for  $\xi$  of 5.4 ppm for grossular garnet.

#### 2.4.2. SOROSILICATES

Piemontite ( $\text{Ca}_2(\text{Mn}, \text{Fe}^{2+}, \text{Al})_2\text{AlO} \cdot \text{OH}[\text{Si}_2\text{O}_7][\text{SiO}_4]$ ) has three crystallographically nonequivalent silicon sites which give calculated  $^{29}\text{Si}$  chemical shifts of -85.6, -89.4 and -78.3 ppm. The experimental spectrum (Williams (Sherriff) 1984) is very poorly resolved consisting of a broad centre peak at -86.4 with two shoulders at -90.4 and -81.9 ppm (Fig. 2.6). The width of the peaks can possibly be attributed to cation disorder and to the proximity of  $\text{Mn}^{2+}$  and  $\text{Fe}^{3+}$  paramagnetic centres (Sherriff and Hartman 1985). The low field peak at -81.9 ppm is allocated to the

Figure 2.6  $^{29}\text{Si}$  MAS nmr spectrum of piemontite  
(Williams (Sherriff) 1984).

-80

ppm

-100



isolated  $\text{SiO}_4$  site which has a calculated shift of  $-78.3$  ppm. Large values of  $\xi$  also be reconciled with varying substitution of Mn and Fe for Al in octahedral sites giving the possibility of differences in structure between the samples used for the collection of diffraction and nmr data.

In the melilite group of minerals there are two tetrahedral sites. In the magnesium end member akermanite  $\text{Ca}_2\text{MgSi}_2\text{O}_7$ , Mg is supposedly ordered into the T2 site and Si into the T1 site (Kimata and Li 1981) whereas the aluminum end member gehlenite  $\text{Ca}_2\text{Al}_2\text{Si}_2\text{O}_7$  has disorder of Al and Si between the two tetrahedral sites (Kimata and Li 1982).

Both the nmr and diffraction data for gehlenite and akermanite were measured on synthetic samples (nmr data: Janes & Oldfield 1985; structural data: Kimata & Li 1981; 1982). Disorder of the tetrahedral cations between the two sites in both minerals would lead to Si-O bond distances, calculated from diffraction data, being too long, thus explaining the calculated chemical shift being 3.0 and 1.8 ppm to higher field than that measured. Janes and Oldfield (1985) also had higher field values for calculated than experimental shift; their values of  $\xi$  were 6.4 and 3.8 ppm respectively.

Hemimorphite ( $\text{Zn}_4\text{Si}_2\text{O}_7$ ) was excluded from the final correlation due to the value for  $\xi$  of 7.9 ppm being more

than 10 times the standard deviation. A very narrow peak with 30 Hz linewidth (Mägi et al. 1984) indicates that the nmr data are accurate but does not rule out a wrongly identified specimen. The neutron diffraction refinement (Hill et al. 1977) is similar to previous X-ray studies (McDonald & Cruikshank 1967) and therefore considered to be reliable. The major contribution to the summation is from Zn-O bonds, so inaccuracy of the  $r_0$  value for Zn-O could explain the difference between calculated and experimental values of chemical shift. Optimization of the value of  $r_0$  for Zn-O, as for Al-O and Si-O, was not possible because of the small nmr data set for Zn containing minerals.

#### 2.4.3 INOSILICATES

The large amount of cation substitution, including paramagnetic ions, causes very poor resolution in many of the MAS nmr spectra of pyroxenes and amphiboles.

in the inosilicates there are several examples of one broad experimental peak corresponding to the calculated values for two or more Si-sites. Pseudowollastonite has one peak at -83.5 ppm (Mägi et al. 1984; Janes & Oldfield 1985) for five tetrahedral silicon sites which have calculated shifts ranging from -82.0 to -83.3 ppm. In the spectrum of the three Si sites of wollastonite, however, although two peaks overlap, one peak at lower field can be separately

resolved (Fig. 2.7).

The  $^{29}\text{Si}$  spectrum of clinoenstatite has two separate peaks at -84.2 ppm and -81.8 ppm corresponding to the calculated values of -84.6 and -82.2 ppm. However for orthoenstatite one broad experimental peak at -82.0 apparently conceals two peaks with calculated values of -85.2 ppm and -82.5 ppm.

The 0.6 ppm difference between the calculated shifts for the two T-sites of omphacite would be unlikely to produce separately resolved peaks. There is only one peak in the experimental spectrum at -85.4 ppm.

Benitoite ( $\text{BaTiSi}_3\text{O}_9$ ) is listed with inosilicates because it has two bridging oxygens between silicate groups although it has a tight  $\text{Si}_3\text{O}_9$  ring. It behaves anomalously when studied by other spectroscopic techniques and has an unexplained brilliant blue colour (Dr. Glen Waychunas, Stanford University, personal communication). The value of  $\xi$  of 5.3 ppm could be due to an unusual electronic state caused by the tight  $\text{Si}_3\text{O}_9$  rings in the structure.

#### 2.4.4 PHYLLOSILICATES

As with inosilicates, phyllosilicates are subject to considerable cation substitution producing broad nmr peaks for most naturally occurring minerals.

Separately resolved peaks (Sanz & Serratosa 1984)


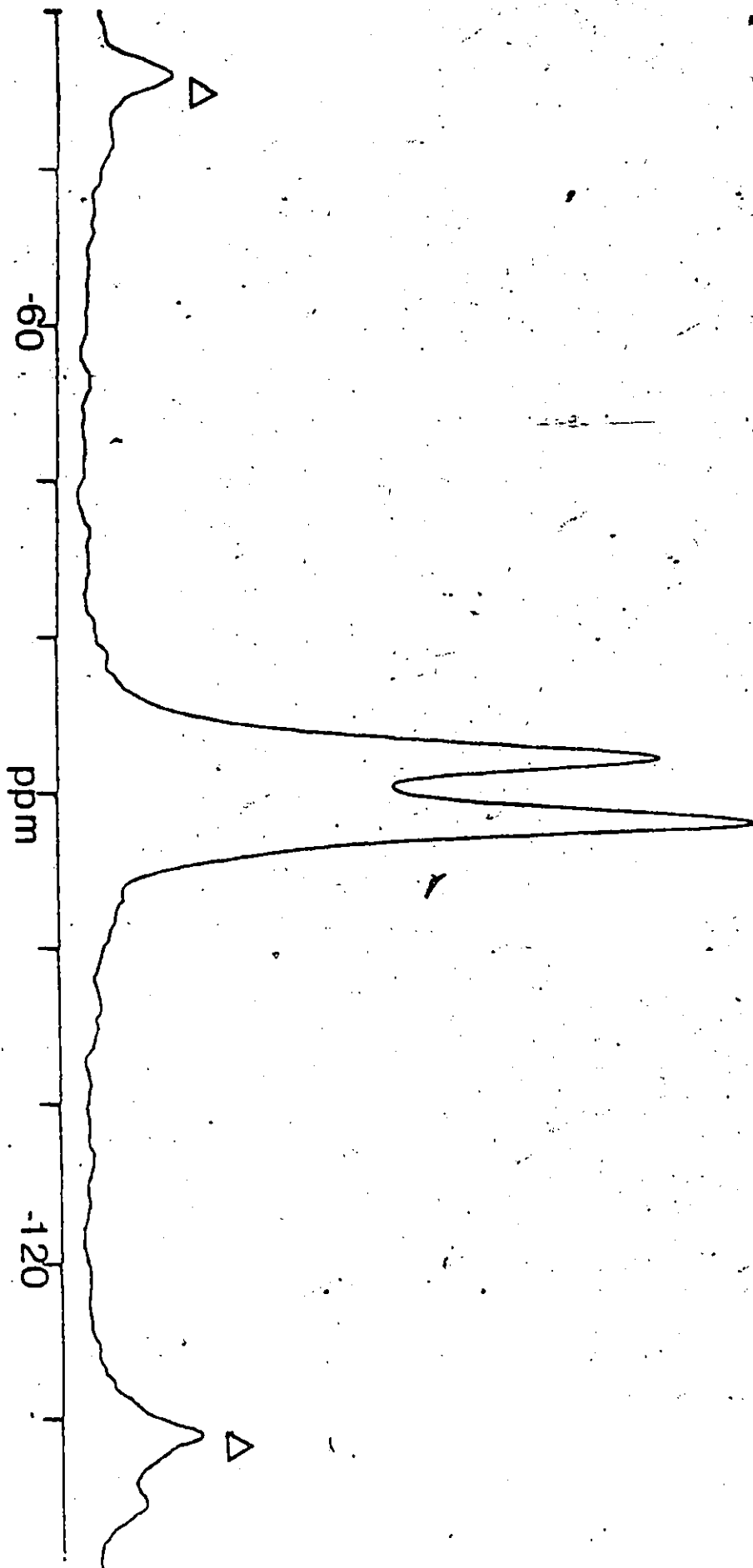


Figure 2.7  $^{29}\text{Si}$  MAS nmr spectrum of wollastonite  
(Williams (Sherriff) 1984).  
( $\Delta$  mark spinning sidebands)





could be correlated with calculations from different T-sites only for muscovite (Appendix VIII). There was only one peak in each  $^{29}\text{Si}$  nmr spectrum for all other phyllosilicates. The differences in environment between tetrahedral sites in each mineral are very small, producing differences between calculated values of chemical shift that would not be resolvable in MAS spectra.

#### 2.4.5 TECTOSILICATES

Most tectosilicates have the possibility of Al-Si disorder in tetrahedral sites, as well as disorder among cations in other sites. Only structures with little or no Al-Si disorder reported in the structure determinations were used in the production of the correlation because the calculations are extremely sensitive to T-O distances.

The nmr data for all the silica polymorphs are from Smith and Blackwell (1983), in which all the spectra are figured, so that an estimation of spectral resolution could be made.

The spectrum of tridymite consists of a broad envelope of peaks with three maxima at -109.3, -111.0 and -114.0 ppm and shoulders at -112 and -113 ppm. The calculated values of chemical shifts for the twelve T-sites in tridymite (Baur 1977) lie between -109.5 and -116.6 ppm. The twelve sites are assigned to the five experimental peak

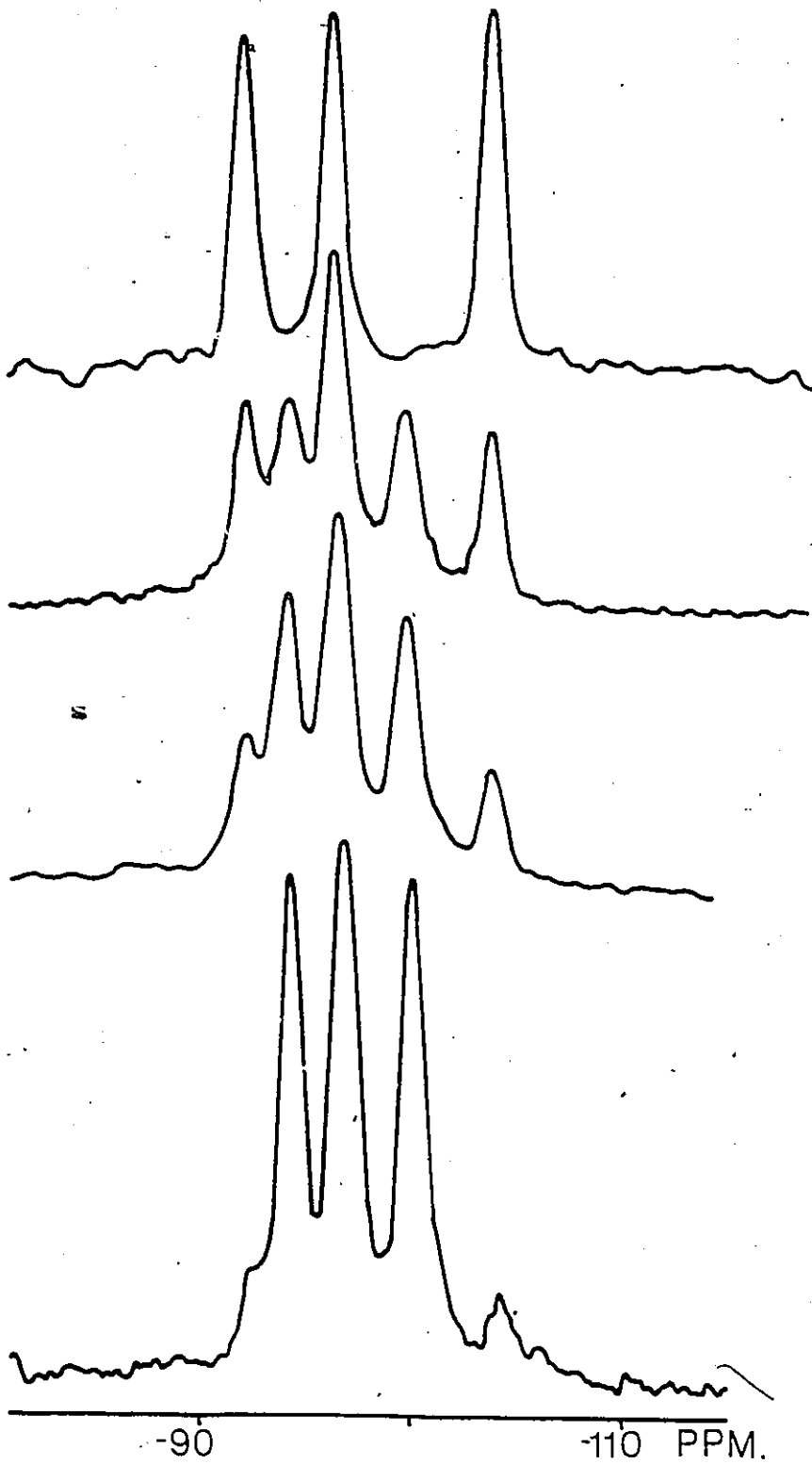
positions by ordering the calculated values (Appendix VIII).

Quartz and coesite have  $\xi$  values between 1.6 and 3.8 ppm to low field (Appendix VIII). Janes and Oldfield (1985) used quartz, cristobalite and the T1 site of coesite to calculate their EN value for SiO. Their  $\xi$  value for the T2 site of coesite was only 0.7 ppm to low field.

There are several reported values of  $^{29}\text{Si}$  nmr chemical shift for quartz, including one measured on a synthetic sample, which all give results within 0.3 ppm of -107.1 ppm. Wright and Lehman (1981) published structural refinements from neutron diffraction data of a synthetic quartz crystal at 25 and 590°C. Calculations of chemical shift using these structures give values of -104.8 and -110.3 ppm for the low and high temperature structures.

The low temperature ordered end members of the alkali feldspar series, albite and microcline, both give three peaks relating to the three silicon containing tetrahedral sites in the minerals (Fig. 2.8). The central spectra of figure 2.8 are of perthitic intergrowths of the two minerals and show very clearly the difference in chemical shift of the outer two peaks of albite and microcline. These differences between the experimental spectra of albite and microcline are reflected in the calculated peak positions (Table 2.2). The values of  $\xi$  for alkali feldspars are under 2 ppm compared with those of

Figure 2.8  $^{29}\text{Si}$  MAS nmr spectra of albite/microcline  
perthites (Sherriff & Hartman 1984).



ALBITE MICROCLINE

100% 0%

30% 70%

20% 80%

10% 90%

-90

-110 PPM.

TABLE 2.2

<sup>29</sup>Si peak allocation for feldspar minerals

Si site	Chemical shift (ppm)		
	Measured	Calculated	
albite NaAlSi <sub>3</sub> O <sub>8</sub>			
T <sub>2m</sub>	-92.8	-93.5	-96.6*
T <sub>20</sub>	-97.1	-97.3	-99.3*
T <sub>1m</sub>	-104.9	-102.9	-104.8*
oligoclase (Na,Ca)[(Al,Si)AlSi <sub>2</sub> O <sub>8</sub> ]			
T <sub>2m</sub>	-92.8	-93.5	
T <sub>20</sub>	-97.1	-98.1	
T <sub>1m</sub>	-104.6	-102.6	
microcline KAlSi <sub>3</sub> O <sub>8</sub>			
T <sub>2m</sub>	-100.2	-100.2	-101.5*
T <sub>20</sub>	-97.1	-97.6	-98.4*
T <sub>1m</sub>	-94.7	-96.3	-97.1*
anorthite Ca[Al <sub>2</sub> Si <sub>2</sub> O <sub>8</sub> ]			
T <sub>1</sub> (0000)	-82.7	-81.9	-81.7**
T <sub>1</sub> (00i0)	-82.7	-81.9	-83.0**
T <sub>1</sub> (mz00)	-89.3	-89.0	-91.1**
T <sub>1</sub> (mzi0)	-84.7	-86.8	-89.6**
T <sub>2</sub> (0z00)	-82.7	-83.6	-83.0**
T <sub>2</sub> (0zi0)	-84.7	-86.4	-85.5**
T <sub>2</sub> (m000)	-84.7	-86.1	-84.8**
T <sub>2</sub> (m0i0)	-84.7	-86.5	-86.3**

\* Values of chemical shift calculated by Janes and Oldfield (1985)

\*\* Values of chemical shift from simulated spectrum of An<sub>100</sub> from Val Pasmada (Kirkpatrick et al. 1988).

Janes and Oldfield (1985) which are up to 4.3 ppm.

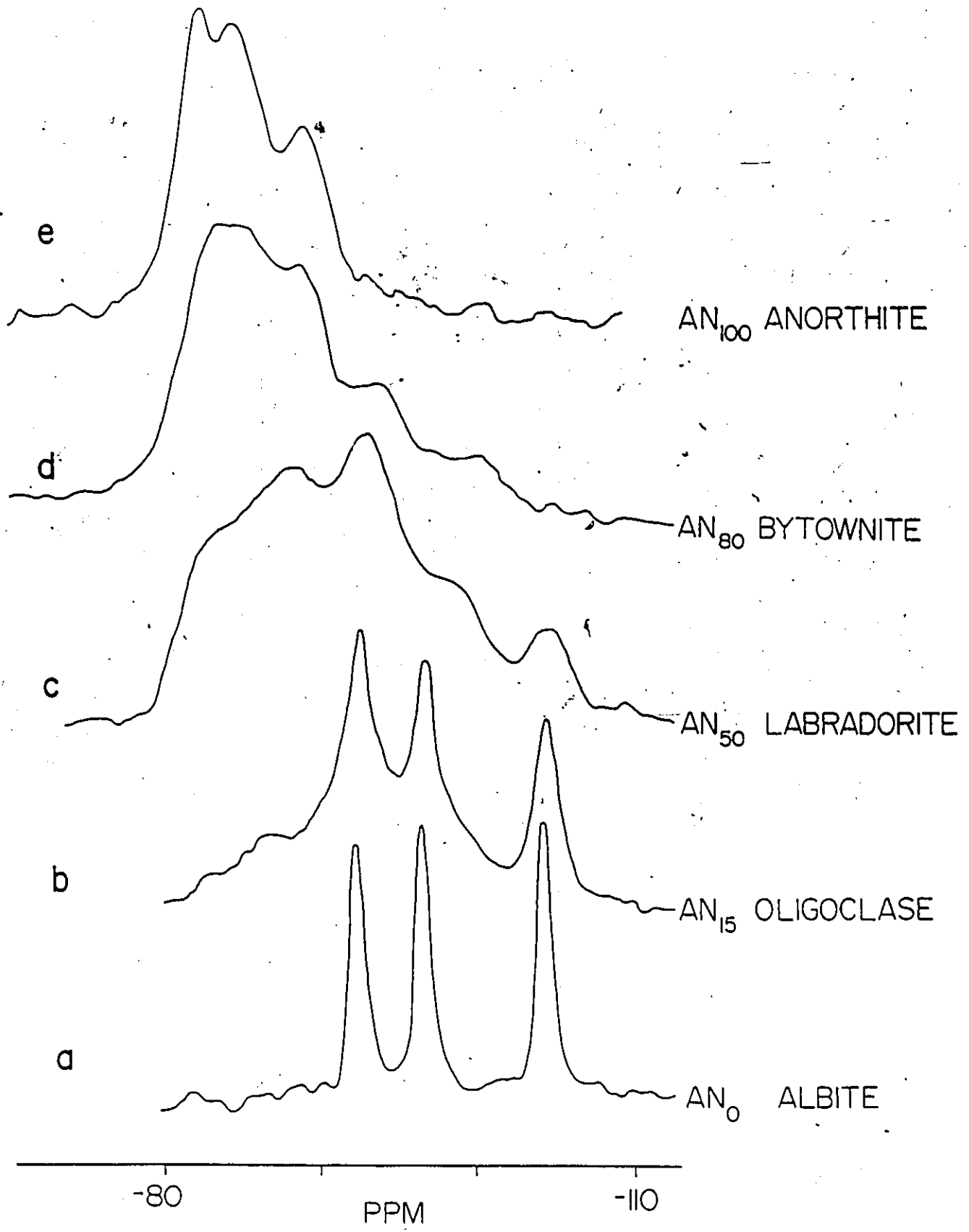
The allocation of the three peaks in the spectrum of albite to silicon sites agrees with previous ones. The peak at -104.9 is due to the  $T_{1m}$  site, that at -97.1 to the  $T_{20}$  site and at -92.8 to the  $T_{2m}$  site. The difference between the chemical shift of the  $T_{1m}$  peak in the pure endmember albite from Amelia courthouse locality (Royal Ontario Museum number M13943) at -104.9 ppm and the value of -104.6 from a slightly less pure sample of oligoclase (BLS036) is reflected in the 0.3 ppm difference between calculations of chemical shift from the diffraction structures of Amelia albite and oligoclase (Harlow & Brown 1980; Ribbe et al. 1969).

$^{29}\text{Si}$  MAS nmr spectra of the plagioclase feldspar solid solution series show considerable variation (Fig. 2.9). The ordered end members albite and anorthite both have three distinct peaks but intermediate compositions show a combination of these six peaks plus many other overlapping peaks giving broad envelopes of peaks with very little fine structure. This is due to the complex system of intergrowths, exsolution textures, twinning and disorder present in feldspars with compositions between albite and anorthite.

The spectrum of ordered anorthite, from Miakejima, Japan, has three peaks at -82.7, -84.7 and -89.3 ppm with relative peak intensities in the ratio of 2:5:1 (Fig.

Figure 2.9  $^{29}\text{Si}$  MAS nmr spectra of the plagioclase feldspar series (Sherriff and Hartman 1984).





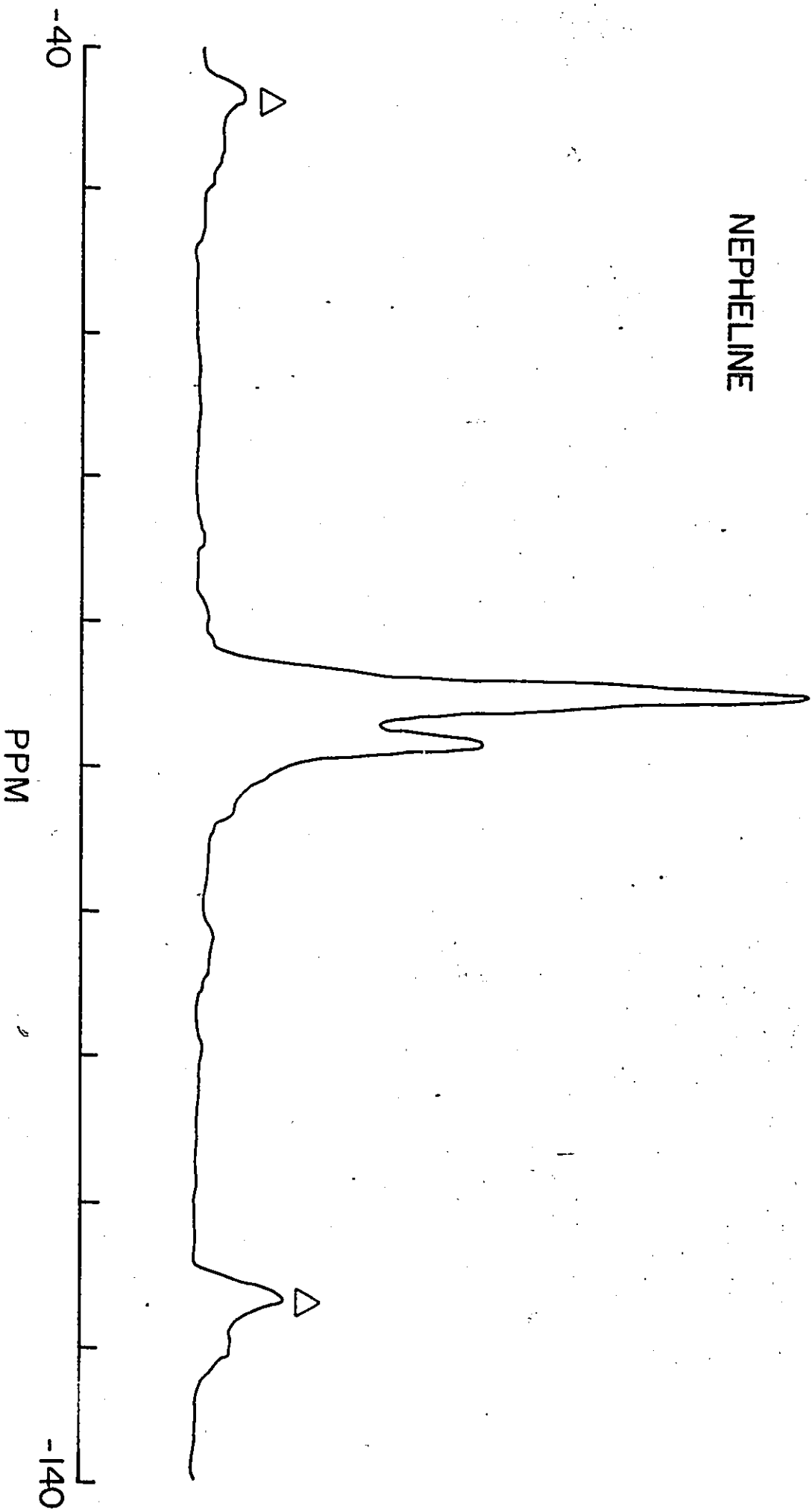
2.9e). In the structural refinement of Wainwright and Starkey (1971), carried out on  $An_{100}$  anorthite from Val Paseda, there are 16 crystallographically nonequivalent sites; eight containing silicon surrounded by four aluminum next nearest neighbours. The early techniques of assigning peaks on the grounds of number of aluminum next nearest neighbours would be useless in interpreting this spectrum (Lippmaa et al. 1980, 1981). Calculations of the eight possible  $^{29}\text{Si}$  chemical shifts (Table 2.2) give two values of -81.9 and one of -89.0 ppm which correspond very well to the outer peaks in the experimental spectrum. The four calculated shifts of about -86 ppm and the one of -83.6 ppm have been allocated to the broad resonance with a maximum at -84.7 ppm.

Kirkpatrick et al. (1988) resolved six peaks in the  $^{29}\text{Si}$  MAS nmr spectrum of a sample of anorthite from Val Paseda. They simulated the spectrum with 7 peaks which have been assigned to the calculated values (column 3, Table 2.2) and give  $\xi$  values of up to 2.1 ppm.

There are two peaks, at -88.1 and -85.1 ppm in the  $^{29}\text{Si}$  MAS nmr spectrum of nepheline (Fig 2.10). The initial interpretation of the spectrum (Lippmaa et al. 1980; Williams (Sherriff) 1984) was that the two peaks were due to silicons with either  $\text{Si}(4\text{Al})$  or  $\text{Si}(3\text{Al } 1\text{Si})$  configurations. Stebbins et al. (1986), on the contrary, allocated these peaks to the  $T_S$  and  $T_G$  sites respectively

Figure 2.10  $^{29}\text{Si}$  MAS nmr spectrum of nepheline  
(Williams (Sherriff) 1984).

NEPHELINE



both with four aluminum next nearest neighbours. As  $T_S$  is on a special site and  $T_G$  is on a general site the ratio of the two sites is 1:2. The ratio of integrals of the two nmr peaks is approximately 1:3.

The structure of nepheline is supposedly ordered (Simmons et al. 1972) with each silicon site surrounded by four aluminum next nearest neighbours. The two Si sites are very similar, except that one site is close to three sodium atoms and the other to two sodiums and one potassium.

Calculations of chemical shift of the two sites give equal values of -88.5 ppm. If about 25% Al-Si disorder is allowed for, by increasing all the Al-O distances by 0.05 Å and decreasing all the Si-O distances by 0.05 Å, the calculated value of chemical shift for both silicon sites with four aluminum next nearest neighbours is -85.8 ppm. If the chemical shifts are recalculated with one of the aluminum neighbours replaced by silicon and the bond distances changed accordingly, the results are -89.2 and -89.8 ppm (Table 2.3). These changes in bond lengths result in mean Si-O distances of 1.605 and 1.581 Å and mean Al-O distances of 1.765 and 1.770 Å, which are not abnormal Si-O and Al-O distances.

There is usually an excess of silicon over aluminum in the stoichiometry of nepheline (Merlino 1984). Each excess silicon in an aluminum site would create four silicons with three instead of four aluminum next nearest

TABLE 2.3

<sup>29</sup>Si peak allocation for nepheline

Si site	Chemical shift (ppm)	
	Measured	Calculated
T <sub>G</sub> (4Al)	-84.9	-88.5
T <sub>S</sub> (4Al)	-88.3	-88.5
(Si-O - 0.05 Å, Al-O + 0.05 Å)		
T <sub>G</sub> (4Al)	-84.9	-85.8
T <sub>S</sub> (4Al)	-84.9	-85.8
T <sub>G</sub> (3Al1Si)	-88.3	-89.2
T <sub>G</sub> (3Al1Si)	-88.3	-89.8

neighbours. Stoichiometric amounts of 8.5 silicon atoms and 7.5 aluminum atoms would mean that 25% of the Si sites would have Si(3Al 1Si) configuration. Very little additional disorder is necessary to produce the 3:1 ratio of peaks observed in the nmr spectrum.

Natural zeolites tend to give extremely poorly resolved  $^{29}\text{Si}$  MAS nmr spectra due to the amount of disorder possible in the zeolite structure. There can be Al-Si disorder in the tetrahedral sites, cation disorder in other sites and variation in position of cations which are loosely bonded in the cavities. There is also the possibility of dipolar interactions with  $^1\text{H}$  in  $\text{H}_2\text{O}$  molecules in the cavities which could cause splitting of peaks and hence many overlapping resonances.

The zeolites used for the correlation; scolecite, chabazite, gmelinite, thomsonite and heulandite, are all supposed to have aluminum and silicon ordered into different T-sites (Faeth & Hansen 1979; Smith & Rinaldi 1963; Galli et al. 1982; Albert et al. 1981; Merkle & Slaughter 1968). However the values of  $\xi$  from 0.03 to 5.3 ppm reflect both disorder in the minerals used for the diffraction data and also the poor quality of the nmr data due to broad overlapping peaks. Janes and Oldfield (1985) also found values of  $\xi$  of up to 4.9 ppm for a range of natural and synthetic zeolites.

## 2.5 CONCLUSIONS

As a result of this study an excellent predictor of  $^{29}\text{Si}$  MAS nmr has been constructed which can now be used together with structure modelling to study the atomic structure of minerals, even if they contain cation disorder.

There is a very strong relationship between  $^{29}\text{Si}$  chemical shift calculated from equations 3 and 4 and experimental values.

Some differences between calculated and experimental values of chemical shift can be reconciled with differences between chemistry and structure of samples used for structural and nmr data. The values of  $\xi$  in these calculations are less than those of Janes and Oldfield (1985).

Calculated chemical shifts for Si(4Si) environments are often to low magnetic field of the experimental values and those for Si(4Al) sites to high magnetic field of the experimental values. This could be rectified by changing the values of  $r_0$  for Si-O and Al-O and hence changing the slope of the correlation line. However ortho and sorosilicates would then no longer lie along the same straight line. It is possible that the correlation is not a straight line but a curve. Calculating the equation for such a curve would introduce a much greater level of



complexity into a beautifully simple correlation.

A plot of  $\chi'$  (from equation 2) against experimental chemical shift  $\delta$  gave a correlation coefficient of 0.973. Extensive calculations resulting in changes in values of  $r_0$  and terms for angle  $\alpha$  gave a better relationship with a correlation coefficient of 0.986. Further changes in  $r_0$  and terms for angle  $\alpha$  may result in marginal improvements but give diminishing returns for the amount of time and money used for calculations.

One important aspect of this study is the information about the size of the sphere of atoms influencing chemical shift. Summations of geometric functions were calculated at 0.5 Å intervals to 10 Å. Although this gave some correlation within a small group of minerals, the silica polymorphs, it vanished when other silicate structures were added. The only correlation found, common to all silicate minerals, was between the cations bonded to the terminal oxygens of the silicate group and the chemical shift of the central silicon. Therefore the sphere of influence is very local, between 2 and 4 Å. If other cation-oxygen bonds within this zone were included the discrepancy between calculated and measured chemical shift increased.

The approach to the interpretation of MAS nmr spectra developed in this study; that of simulating the crystal structure with a computer graphics program and

examining the immediate environment of an atom, can be applied to other  $^{29}\text{Si}$  structures and used to investigate MAS nmr of other magnetic nuclei.

## CHAPTER 3

### CATION ORDERING IN THE SCAPOLITE MINERAL SERIES

#### 3.1 INTRODUCTION

MAS nmr is here used to study cation ordering in scapolite, a partially disordered mineral system.  $^{29}\text{Si}$ ,  $^{27}\text{Al}$ ,  $^{23}\text{Na}$ , and  $^{13}\text{C}$  MAS nmr spectra are measured and  $^{29}\text{Si}$  chemical shifts are calculated from equations 3 and 4 in chapter 2. An ordering system is developed for both Al-Si and for the alkali cations and anions by taking into consideration both X-ray and nmr data. A comparison of the relative intensities of the  $^{29}\text{Si}$  peaks anticipated from the ordering model with the intensities of peaks fitted to the experimental data is used to estimate the validity of the structural model.

Considerable interest in scapolite has been generated by the proposal that meionite scapolite is a reservoir for  $\text{CO}_2$  in the lower crust (Newton & Goldsmith 1975) and also by the recent discovery of scapolite in a chondritic meteorite (Alexander et al. 1987).

A number of crystal structure refinements have been reported on scapolite, covering a range of meionite contents. Those refined with the  $I4/m$  space group are 21.3%

Me (Papike & Zoltai 1965), 70.1% Me (Papike & Stephenson 1966), 77% Me (Peterson et al. 1979), and a synthetic sulfate free sample with a composition of 84% Me (Aitkin et al. 1984). Lin & Burley used  $P4_2/n$  space group for the refinement of samples containing 21.3% Me (1973a), 52% Me (1975) and 92.7% Me (1973b) as did Levien & Papike (1976) for a 33.5% Me sample (ON6A). Levien & Papike also studied thermal effects on ON6A up to 1000C.

Duplicate analyses of scapolite samples from the same locality can cause some confusion. The analysis of ON8 in Shaw (1960a) gives a composition of 19.4% Me compared to 21.3% Me produced by a later analysis by Evans et al. (1969). Papike & Zoltai (1965) and Lin & Burley (1973) both refer to the earlier analysis of 19.4% Me. To simplify matters in this thesis, the later analysis of 21.3% Me is used even in reference to papers which quote 19.4% Me. A similar problem occurs in the analyses of scapolite from Monte Somma. The analysis of Evans et al. 1969 gives a meionite content of 92.7%. Both Lin & Burley (1973b) and Ulbrich (1973) round this figure to 93.0% Me. The sample of MONTE scapolite provided for the nmr analyses has been found by D. Moecher (University of Michigan, personal communication) to have a meionite content of 91.0%. In this case the meionite content of 91.0% is used for the nmr data and calculations and 92.7% for the diffraction data of Lin & Burley (1973b).

### 3.2 THE STRUCTURE OF SCAPOLITE

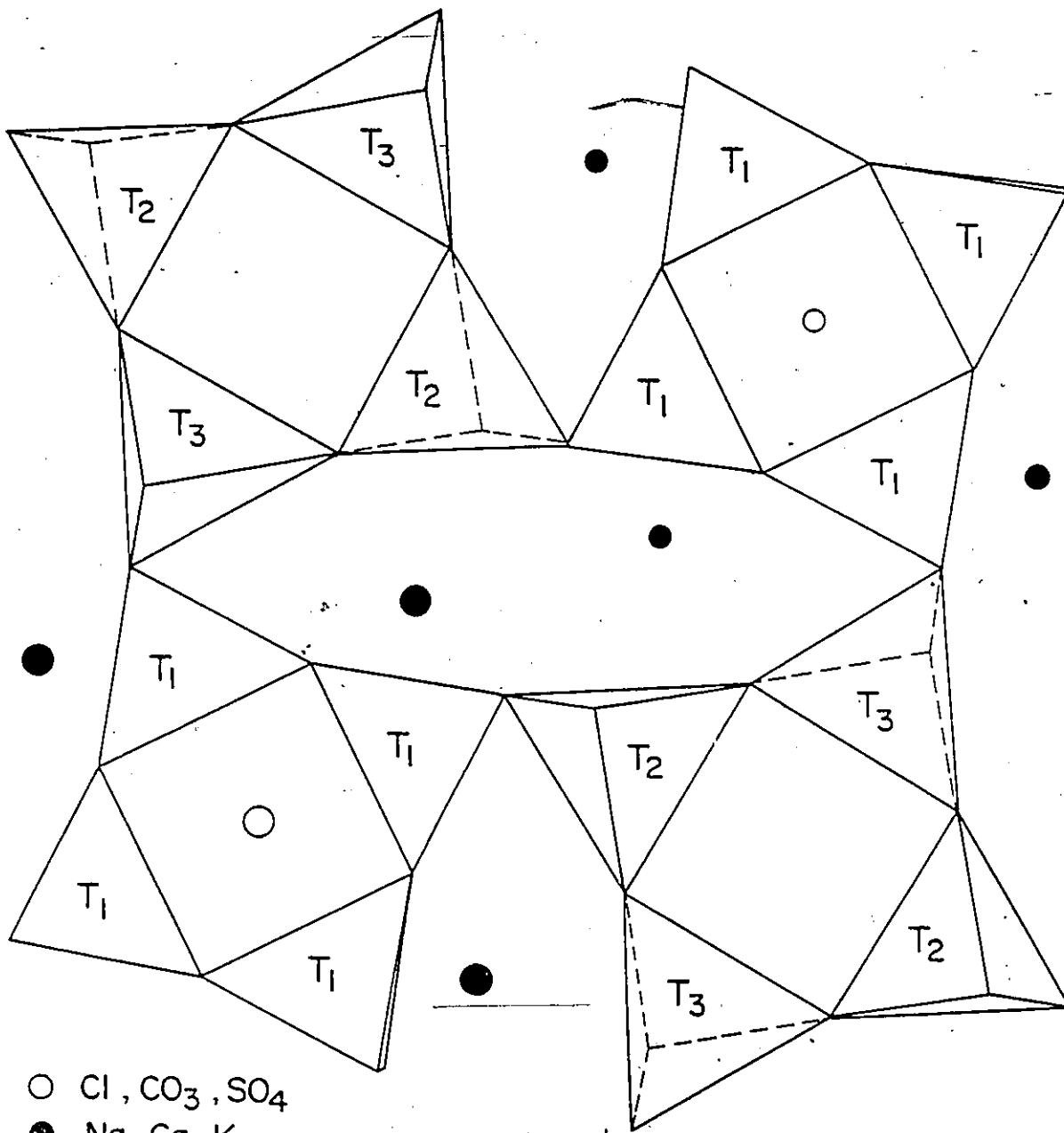
Scapolite is a framework aluminosilicate; compositions define a solid solution series with end members marialite,  $\text{Na}_4\text{Al}_3\text{Si}_9\text{O}_{24}\text{Cl}$ , and meionite,  $\text{Ca}_4\text{Al}_6\text{Si}_6\text{O}_{24}\text{CO}_3$ . Between 0 and 75% meionite, the substitution is between  $\text{Ca}_3\text{Al}_2\text{CO}_3$  and  $\text{Na}_3\text{Si}_2\text{Cl}$ , but from 75% to 100% meionite it only involves CaAl and NaSi (Lin 1971).

There are three tetrahedral (T) sites in the scapolite structure containing silicon or aluminum. The T2 and T3 sites are geometrically identical in the  $I4/m$  space group but differ slightly in position in the  $P4_2/n$  space group.

The tetrahedral sites form four-membered rings, either consisting of T1 sites or of alternating T2 and T3 sites perpendicular to the  $c$  axis (Fig. 3.1). The T2-T3 four-membered rings are joined parallel to the  $c$  axis to form chains that are linked to the T1 rings and form a series of five membered rings (Fig. 3.2). This rigid framework has large cavities, which each contain four sodium or calcium cations and one chloride, carbonate or sulfate anion.

Perfect Al-Si ordering has been inferred, from X-ray data, for scapolites with a composition of 37% Me

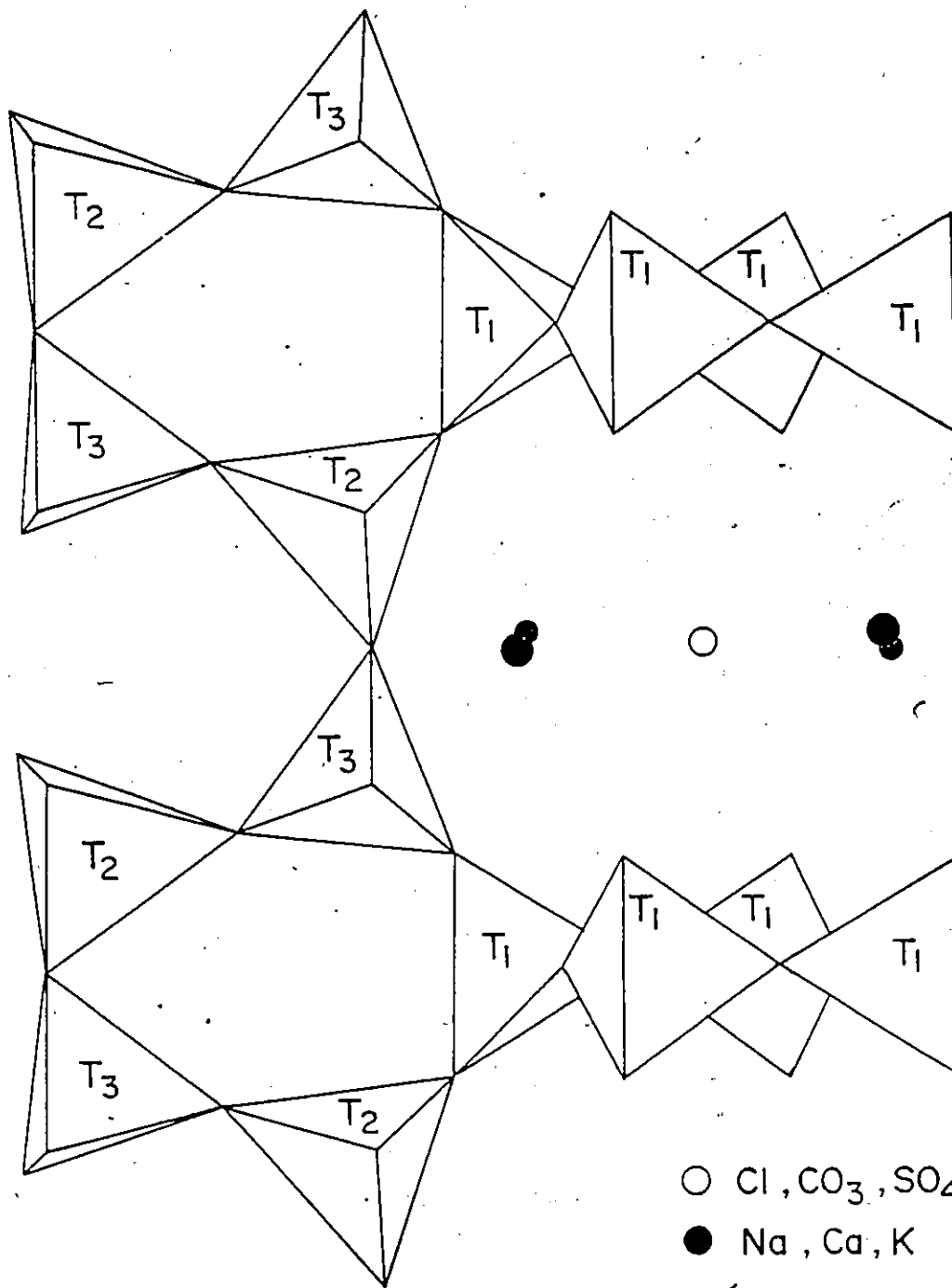
Figure 3.1 The structure of scapolite viewed along the c-axis (Sherriff et al. 1987a).



58

Figure 3.2 The structure of scapolite viewed along  
the a-axis (Sherriff et al. 1987a)





(Lin 1971, Levien & Papike 1976). In this mineral, which has a ratio of Si:Al of 2:1, the T2 site contains only aluminum and the T1 and T3 sites silicon. With less aluminum (0-37% Me), aluminum and silicon become disordered between T2 and T3 sites, but the T1 site contains only silicon. In the more aluminous compositions (37-100% Me), aluminum and silicon become progressively distributed over all three T sites with a theoretical 50% aluminum occupancy of each site in end-member meionite (Lin 1971).

Lowenstein's rule (1954) that Al-O-Al linkages are unstable in aluminosilicates cannot be obeyed in scapolite with greater than 37% Me as the five-membered rings do not allow for complete alternation of aluminum and silicon (Lin 1971).

### 3.3 EXPERIMENTAL

MAS nmr spectra were obtained on a series of powdered scapolite samples with compositions between 21.3 and 91.0% Me, covering the entire range of naturally occurring compositions (Table 3.1). A magic angle spinning probe (Fyfe et al. 1982) with Delrin rotors was used with (i) a Bruker WH-400 multinuclear Fourier Transform nmr spectrometer equipped with a 9.4 Tesla superconducting magnet and (ii) a Bruker CXP-200 spectrometer with a 4.7 Tesla superconducting magnet at the South Western Ontario

TABLE 3.1

## Scapolite samples used for nmr analyses

Sample#	%Meionite	Rock Type	Locality	
ON8	21.3	syenite pegmatite	Gooderham, Glamorgan Twp. Ont.	*
TANZ	29.5	hbl.px.granulite	Morongoro, Tanzania.	**
ON7	33.3	calcareous gneiss	Monmouth Twp, Ontario.	*
GL	34.1	marble	Gib Lake, Pontiac Twp, Ontario	*
ON70	39.5	-	MpWapwa, Tanzania.	*
CA63A	44.5	Pegmatitic skarn	Grand Calumet Twp., Quebec.	*
MAD	45.2	-	Madagascar.	**
Q26	48.2	Pegmatitic skarn	Clapham Twp, Quebec	*
Q13	51.3	Px. gneiss	Huddersfield Twp., Ontario	*
MIN	56.8	Skarn	Minden, Ontario.	**
ON27	59.3	Pegmatitic skarn	Olmsteadville, New York, U.S.A	*
Q85	65.2	Pegmatitic skarn	Huddersfield Twp., Quebec	*
BOLT	69.5	Marble pegmatite	Bolton, Mass., U.S.A.	**
ON47	79.6	Calc.silicate schist	Slyudyanka, Siberia, U.S.S.R	*
MONT	91.0	Vugs in limestone	Mount Vesuvius, Naples, Italy	**

\* Donated by D. M. Shaw, McMaster University.

Chemical analyses from Evans et al. 1969.

Localities from Shaw 1960a

\*\* Donated by D Moecher, University of Michigan.

Analyses from D Moecher (personal communication).

NMR Centre at Guelph University. The samples were spun at approximately 3500 Hz at the Magic Angle of  $54.7^\circ$  to the magnetic field.

$^{29}\text{Si}$  MAS nmr spectra were recorded at a frequency of 79.46 MHz on the Bruker WH-400 instrument, with 8192 data points using a spectral width of 25000 Hz,  $30^\circ$  pulses and a 5 seconds relaxation delay between pulses. A range of relaxation delays from 0.1 to 30 s were tried on three samples ON7, ON70 and ON47, but no difference in resolution with relaxation delay was observed, in contrast to the findings of Sherriff & Hartman (1985) on certain samples of feldspar.  $^{29}\text{Si}$  MAS nmr spectra were also recorded on the Bruker CXP-200 instrument at 38.73 MHz with  $30^\circ$  pulses and a 5 seconds delay between scans. Chemical shifts were found to be reproducible to  $\pm 0.1$  ppm on both instruments and are reported in parts per million of the magnetic field with reference to tetramethylsilane (TMS).

$^{27}\text{Al}$  and  $^{23}\text{Na}$  MAS nmr spectra were recorded on the Bruker WH-400 instrument at 104.23 and 105.80 MHz respectively, with  $15^\circ$  pulses and a 0.3 seconds relaxation delay between pulses. The chemical shifts of  $^{23}\text{Na}$  were measured with reference to 0.1M aqueous solution of NaCl, and those of  $^{27}\text{Al}$ , with reference to  $[\text{Al}(\text{H}_2\text{O})_6]^{3+}$  in a saturated aqueous solution of  $\text{Al}(\text{ClO}_4)_3$ .

$^{13}\text{C}$  MAS nmr spectra were recorded on the Bruker CXP200 instrument at 50.32 MHz, with  $30^\circ$  pulses and

relaxation delays between pulses ranging from 5 to 60 seconds to achieve optimum strength of the signal.

Peaks were fitted to the complex  $^{29}\text{Si}$  spectra, using a least-squares iterative curve-fitting program written for the deconvolution of Lorentzian peaks. The width of the peaks at half height was constrained to be the same within each spectrum, although they were allowed to vary between spectra, as the factors which affect width of peaks would be expected to be constant for all sites within one sample.

MAS nmr peaks actually have both Lorentzian and Gaussian components and the fitting procedure could be improved by including a function which fitted an experimental peak shape. However it is extremely difficult to find a MAS nmr peak which is definitely from only one environment to provide the initial peak shape. It was decided that the error in fitting peaks to the broad MAS nmr resonances was so large that using an experimentally derived peak shape would give minimal improvement in the accuracy.

Relative intensities of the  $^{29}\text{Si}$  peaks were found from the curve-fitting program and also by cutting out individual peaks from the plot and weighing them. Both methods gave similar accuracy and reproducibility for the simple spectra, but the weighing technique was judged to be less accurate for spectra with many overlapping peaks.

$^{29}\text{Si}$  chemical shifts were calculated using the correlation for all possible Al-Si next nearest neighbour configurations for the three tetrahedral sites of scapolite with 21.3% Me (Lin & Burley 1973a), 33.5% Me (Levien & Papike 1976), 52% Me (Lin & Burley 1975) 70.1% Me (Papike & Stephenson 1966) and 92.7% Me (Lin & Burley 1973b). Calculations for 21.3% Me, 33.5% Me and 52% Me also allowed for the adjacent alkali cations being either Na or Ca. These calculated peak positions were used to allocate peaks fitted to the experimental  $^{29}\text{Si}$  MAS nmr of scapolites with similar chemical composition.

### 3.4 RESULTS AND DISCUSSION

#### 3.4.1 $^{29}\text{Si}$ MAS NMR SPECTRA

$^{29}\text{Si}$  MAS nmr spectra of scapolite vary considerably with meionite content. The peak positions for each sample, measured directly from the spectra, are listed in Table 3.2 and representative spectra throughout the series are shown in figure 3.3. For samples ON7 (33.3% Me) and GL (34.1% Me; Fig. 3.3d) there are only two peaks, at -106 and -92 ppm. ON8 (21.3% Me; Fig 3.3e) has the same two peaks plus poorly resolved peaks between -95 and -100 ppm and at -110 ppm. As the meionite content increases beyond 40% Me the high field peak at -106 ppm diminishes in size, and that at

TABLE 3.2  
<sup>29</sup>Si MAS nmr parameters

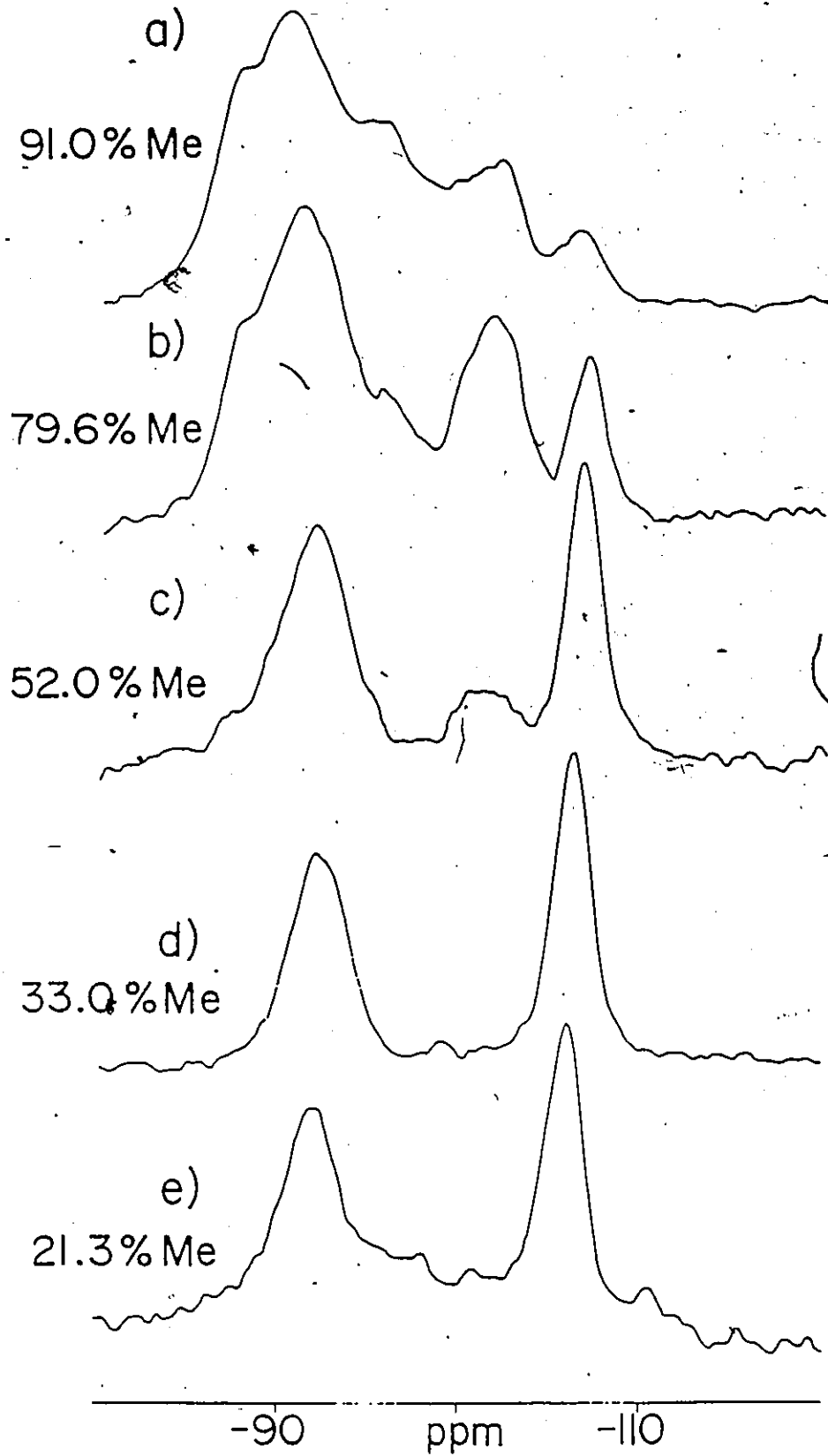
Sample	%Meionite	Peak Positions (ppm)*							
ON8	21.3	-88.9	-91.8	-95.4	-98.0	-100.8		-105.8	-110.6
TANZ	29.5	-91.4	-91.9	-92.5	-97.7	-102.4	-105.8	-106.1	-110.5
ON7	33.3		-92.0					-106.2	
GL	34.1		-92.1					-106.2	
ON70	39.5		-92.1			-100.8		-106.3	
CA63A	44.5	-87.9	-92.0	-92.4				-106.2	
MAD	45.2	-90.9	-91.6	-92.4		-101.0	-105.7	-106.1	-106.6
Q26	48.2	-88.1	-91.9	-92.3		-100.2		-106.4	
Q13	51.3	-87.3	-91.6	-95.3		-101.0	-102.6	-106.4	
MIN	56.8	-91.1	-92.8	-95.5		-101.5		-106.1	-106.4
ON27	59.3	-89.0	-91.7		-98.9	-101.0	-102.8	-106.8	
Q85	65.2	-87.6	-91.5		-99.2	-101.2	-102.7	-106.5	
BOLT	69.5	-86.6	-90.9	-92.7		-100.5	-102.3	-106.1	-106.9
ON47	79.6	-87.6	-90.8		-99.6	-101.6	-102.7	-106.7	
MONT	91.0	-87.2	-90.5	-95.6		-101.9		-106.7	

\*Peak position measured directly from spectra

Figure 3.3  $^{29}\text{Si}$  MAS nmr spectra of scapolite samples: (a) MONT (91.0% Me)  
(b) ON47 (79.6% Me)  
(c) Q13 (52% Me)  
(d) ON7 (33.3% Me)  
(e) ON8 (21.3% Me)  
(Sherriff et al. 1987a)



$^{29}\text{Si}$



approximately -100 ppm increases. This is shown in the spectrum of Q13 (51.3% Me; Fig 3.3c). At the higher meionite content [79.6% (ON47) and 91.0% Me (MONTE); Fig 3.3b and 3.3a] a low field peak appears at -88 ppm, and those at -106 and -100 ppm diminish in size relative to the peak at -96 ppm.

Fitting peaks to the  $^{29}\text{Si}$  spectra of GL (34.1% Me), using calculations based on the structure of ON6A (33.5% Me) (Levien & Papike 1976) shows that even the simple two-peak spectrum of this ordered structure contains at least two absorptions giving rise to each peak (Fig. 3.4). Since there are only two major Si-Al configurations possible in this structure; T1(3Si1Al) and T3(1Si3Al), the division into further peaks must be the effect of having either Na or Ca as adjacent cations. Magi et al. (1984) reported that replacing sodium by calcium produces shift to high field in the adjacent silicon atoms. In some structures this effect could be considerable, e.g. 8.8 ppm for dehydrated Ca-Y zeolite (Grobet et al. 1985) although it appears to be much less in the case of scapolites.

The values of chemical shift were calculated for Si1(3Si1Al) and Si3(1Si3Al) configurations, for 33.5% Me, in which all the surrounding cations were either Ca or Na. In the calculations only the type of cation was changed as from the X-ray data there is no indication of different positions for Na or Ca.

Figure 3.4 Peak fitting to the  $^{29}\text{Si}$  MAS nmr spectrum of GL (34.1% Me) using a least squares iterative program. (Sherriff et al. 1987a)

SPECTRAL INTENSITY

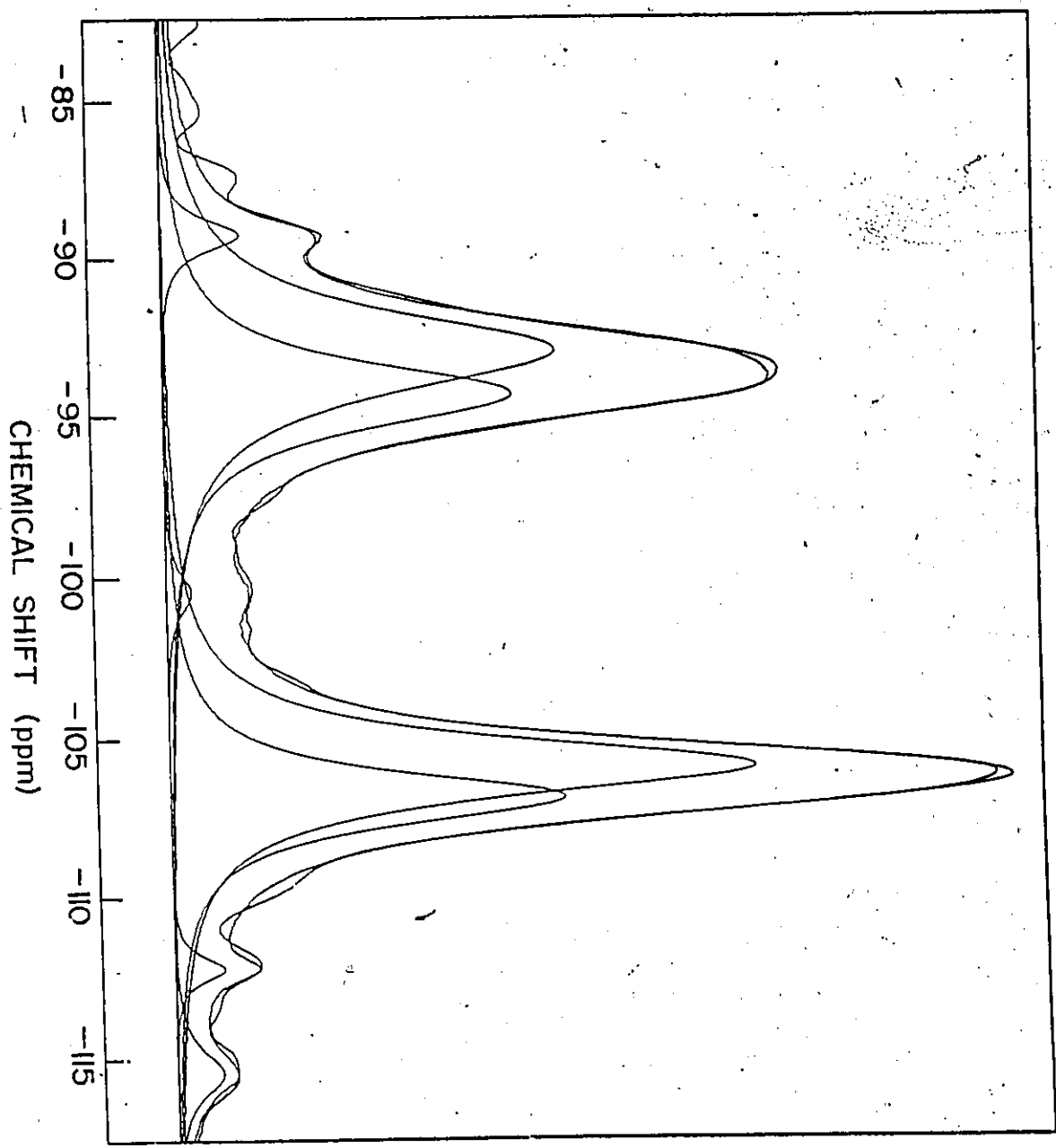


TABLE 3.3

<sup>29</sup>Si MAS nmr chemical shift calculations for  
34% meionite scapolite

Si site	Chemical shift (ppm)			# of Si
	Measured*	Calculated**	Calculated***	
T1(1Al 3Si Na)	-105.5	-104.1	-105.9	1.9
T1(1Al 3Si Ca)	-106.4	-104.8	-106.7	1.9
Difference	0.9	0.7	0.8	
T3(3Al 1Si Na)	-91.4	-92.7	-92.8	1.8
T3(3Al 1Si Ca)	-93.9	-95.1	-95.2	1.1
Difference	2.5	2.4	2.4	
T3(4Al Na)	-86.4		-87.4	0.3
T3(4Al Ca)	-89.4		-89.9	0.6
Difference	3.0		2.5	

\* Values of chemical shift from peaks fitted to the spectrum of GL (34.1% Me) (Fig. 3.8).

\*\* Calculated using equations 3 and 4 and atomic positions given in Levien and Papike (1976) for sample of 33.5 %Me.

\*\*\* 5% Al estimated in all T sites: Si-O - 0.01 Å, Al-O + 0.01 Å, structure of Levian and Papike (1976) for 33.5 %Me.

For the T1 site the calculated difference between the calcic and sodic peaks is 0.7 ppm and the measured value from the fitted spectrum is 0.9 ppm. For the T2 site this calculated difference is 2.4 ppm and the measured difference is 2.5 ppm (Table 3.3). The T3 site is closer to the alkali cations than the T1 and therefore changing from Na to Ca has more effect on the chemical shift of the T3 site than of the T1.

There is a change in the position of the T1(3Si1Al) peak across the series from -105.8 ppm for ON8, the most sodic scapolite, to -106.7 ppm for MONTE the most calcic one. This variation in chemical shift can be correlated with an increase in number of Si sites adjacent to calcium and hence in the relative intensity of the high-field peak with increasing meionite content.

In view of these results for GL,  $^{29}\text{Si}$  MAS nmr chemical shifts were calculated for environments with either all Na or all Ca adjacent for compositions of 21.3% Me and 52% Me. In scapolites with compositions more calcic than 70% Me there are only insignificant amounts of Na and so the calculations from the structures of 70% Me and 91.0% Me were carried out only for calcic environments.

X-ray diffraction techniques cannot easily differentiate between Al and Si as they have similar scattering factors. Therefore T-O distances for any tetrahedral site containing both Al and Si are averages of

Al-O and Si-O values. In these cases Si-O distances found from X-ray data are longer than the true value and Al-O distances shorter.

The T1(3Si1Al) site in all scapolite spectra can be allocated to a peak at about -106 ppm by comparison with the spectrum of the ordered 34.1% Me scapolite. T-O bond distances were changed during calculations of chemical shift, initially in accordance with the Al-Si ordering estimated by Lin (1971). Other minor adjustments to the T-O distances were then made, allowing for differing amounts of Al-Si disorder, until the calculated value for this peak was within 1 ppm of the experimental value. The difference between the pure Si-O and Al-O distances, taken from Lin (1971) to be 0.16 Å, could then be used to estimate the amount of Al-Si disorder in any T-site.

Calculations of chemical shift for the T1(3Si 1Al) configuration of the supposedly ordered structure at 33.5% Me gave values of -104 ppm instead of -106 ppm. (Table 3.3). The T3 site calculations agreed with the measured value at -92 ppm.

If 0.01 Å is added to all the Al-O bondlengths and subtracted from the Si-O lengths, allowing about 5% Al-Si disorder in all three tetrahedral sites, then the calculated value for T1 becomes -106 ppm but the T3 calculation remains the same at -92 ppm. The calculation for the T3 site remains the same because the increase in

the length of three Al-O bonds is cancelled by shortening the five Si-O bonds in the calculation. In the case of the T1 site there are seven Si-O bonds and only one Al-O bond involved in the calculation. Thus 5% disorder in all sites gives calculated results that fit the measured ones.

This disorder can also be seen by examination of the structure from the X-ray data, as the mean T-O bondlengths for the T1 site are 0.0015 Å longer for 33.5% Me than for the structure of 21.3% Me, indicating that the decrease in the amount of Al in the T1 site continues past 33.5% Me to at least 21.3% Me. This is contrary to the ordering scheme proposed by Lin (1971) in which there is no Al in the T1 site at compositions more marialitic than 37% Me.

Calculated chemical shifts for 21.3% Me, 51.3% Me, 70.1% Me and 91.0% Me were used to allocate the peaks fitted to each spectrum and estimate the number of Si atoms in each environment from the relative intensities of the peaks and the chemical analyses. The calculated and corresponding experimental values of chemical shift are given in Tables 3.4, 3.5, 3.6 and 3.7 which also include an estimation of the silicon content of each site and the changes in T-O distances used in the calculations. The correlation between experimental and calculated values is very good especially when the type of adjacent alkali cation is taken into consideration.



TABLE 3.4

Calculated  $^{29}\text{Si}$  chemical shift for ON8 (21.3% Me)

Si site	Chemical shift (ppm)		# of Si atoms
	Measured*	Calculated**	
T1(4Si 0Al Na)	-111.0	-110.6	0.26
T1(4Si 0Al Ca)	-111.0	-111.0	0.26
T1(3Si 1Al Na)	-105.2	-105.1	1.34
T1(3Si 1Al Ca)	-106.4	-105.5	1.93
T2(2Si 2Al Na)	-98.4	-99.3	0.61
T2(2Si 2Al Ca)	-101.5	-101.5	0.17
T3(2Si 2Al Na)	-95.8	-98.7	0.74
T3(2Si 2Al Ca)	-101.5	-101.5	0.17
T2(1Si 3Al Na)	-91.4	-92.4	0.61
T2(1Si 3Al Ca)	-93.4	-94.6	0.58
T3(1Si 3Al Na)	-90.3	-91.9	0.56
T3(1Si 3Al Ca)	-92.4	-94.2	1.06

\* From peaks fitted to the spectrum of ON8

\*\* From structure of ON8 (Lin &amp; Burley 1973a) with

5% Al estimated in T1: Si1-O - 0.01 Å, Al-O + 0.01 Å

60% Al estimated in T2 : Si2-O - 0.095 Å, Al-O + 0.065 Å

30% Al estimated in T3 : Si3-O - 0.05 Å, Al-O + 0.11 Å

TABLE 3.5

<sup>29</sup>Si MAS nmr chemical shift calculated for Q13

51.3% meionite scapolite

Si site	Chemical shift (ppm)		
	- Measured*	Calculated**	# of Si atoms
T1(3Si 1Al Na)	-106.0	-105.5	1.2
T1(3Si 1Al Ca)	-106.7	-106.3	1.3
T1(2Si 2Al Na)	-100.2	-100.2	0.5
T1(2Si 2Al Ca)	-101.8	-101.0	0.3
T2(2Si 2Al Na)	-103.8	-100.3	1.4
T2(2Si 2Al Ca)	-103.8	-102.8	1.4
T2(1Si 3Al Na)	-94.1	-93.8	0.2
T2(1Si 3Al Ca)	-94.1	-96.3	0.2
T3(1Si 3Al Na)	-90.8	-91.0	1.0
T3(1Si 3Al Ca)	-92.2	-93.4	1.5
T2(0Si 4Al Na)	-86.9	-87.0	0.2
T2(0Si 4Al Ca)	-86.9	-89.5	0.2
T3(0Si 4Al Na)	-84.0	-85.8	0.2
T3(0Si 4Al Ca)	-88.8	-88.2	0.5

\* Measured from the peaks fitted to the spectrum of Q13

\*\* Calculated from atomic positions of Q13 (Lin &amp; Burley 1975) with:

10% Al estimated in T1 site: Si-O - 0.02 Å, Al-O + 0.14 Å;

80% Al estimated in T2 site: Si-O - 0.12 Å, Al-O + 0.04 Å;

15% Al estimated in T3 site: Si-O - 0.03 Å, Al-O + 0.12 Å

TABLE 3.6

$^{29}\text{Si}$  MAS nmr chemical shift calculated for  
70% meionite scapolite

Si site	Chemical shift (ppm)		# of Si atoms
	Measured*	Calculated**	
T1(3Si 1Al)	-106.0	-105.3	1.6
T1(2Si 2Al)	-101.6	-100.2	1.0
T1(1Si 3Al)	-93.4	-92.5	0.5
T2(2Si 2Al)	-97.9	-99.2	0.3
T3(2Si 2Al)	-98.6	-99.2	0.1
T2(1Si 3Al)	-90.7	-92.7	1.2
T3(1Si 3Al)	-92.4	-92.7	1.2
T2(0Si 4Al)	-86.4	-87.7	0.4
T3(0Si 4Al)	-88.3	-87.7	0.4

\* Measured from peaks fitted to spectrum of BOLT 69.5% Me.

\*\* Structure of 70.1% Me refined in the  $I4/m$  space group (Papike & Stephenson 1966); there is no crystallographic difference between T2 and T3, therefore the calculations of chemical shift are identical. Calculations carried out with 25% Al estimated in T1 site: Si-O - 0.04 Å, Al-O + 0.12 Å; 50% Al in both T2 and T3 sites: Si-O - 0.08 Å, Al-O + 0.08 Å.

TABLE 3.7

<sup>29</sup>Si MAS nmr chemical shift calculated for  
91.0% Meionite Scapolite (Monte Somma)

Si site	Chemical shift (ppm)		# of Si atoms
	Calculated**	Experimental*	
Si1(3Si,1Al)	-106.5	-106.5	0.3
Si1(2Si,2Al)	-101.2	-102.0	0.4
Si1(1Si,3Al)	-95.5	-96.3	0.6
Si1(4Al)	-89.9	-90.7	0.7
Si2(1Si,3Al)	-92.7	-92.3	0.6
Si2(4Al)	-89.1	-87.3	0.8
Si3(2Si,2Al)	-99.6	-100.3	0.7
Si3(1Si,3Al)	-93.2	-95.0	0.7

\* From peaks fitted to the spectrum of MONTE 91.3% Me

\*\* 30% Al estimated in T1 and 50% in T2 and T3 sites:

Si-O distances of T1 sites -0.05 Å

Al-O distances of T1 sites +0.05 Å

Si-O distances of T2 and T3 sites -0.08 Å

Al-O distances of T2 and T3 sites +0.08 Å

### 3.4.2 $^{27}\text{Al}$ MAS NMR SPECTRA

The  $^{27}\text{Al}$  MAS nmr spectra of scapolite consist of one broad asymmetric peak at  $57.8 \pm 0.5$  ppm (Fig. 3.5, Table 3.8). This is in the range of chemical shifts for Al in tetrahedral configuration (Fyfe 1983). There is a steady increase in peak width with increasing content of aluminum through the solid solution series (Fig. 3.6). There is also a discontinuity of approximately 200 Hz between 45.2% Me and 48.2% Me.

In scapolites with meionite content less than 37% there is insufficient Al, for Al-O-Al linkages to occur. Therefore the only possible Al configurations are with four Si next nearest neighbours.  $^{29}\text{Si}$  chemical shifts calculated for T2 and T3 sites are similar, and so these sites would be expected to give very similar  $^{27}\text{Al}$  spectra. The variation in the widths of  $^{27}\text{Al}$  peaks is therefore related to the relative intensities of overlapping peaks from T1(4Si) with T2/T3(4Si) peaks.

If there were no Al in the T1 site below 37% Me there would be a minimum in the graph of peakwidth against meionite content (Fig. 3.6) at 37% Me. The decrease in peakwidth with decreasing meionite continues beyond 37% Me to 21.3% Me, implying that there is still some Al in the T1 site in scapolites with compositions below 37% Me and that

Figure 3.5  $^{27}\text{Al}$  MAS nmr spectra of scapolite samples:

- (a) ON47 (79.6% Me)
- (b) Q26 (48.2% Me)
- (c) CA63A (44.5% Me)
- (d) ON8 (21.3% Me)

(Sherriff et al. 1987a)

$^{27}\text{Al}$

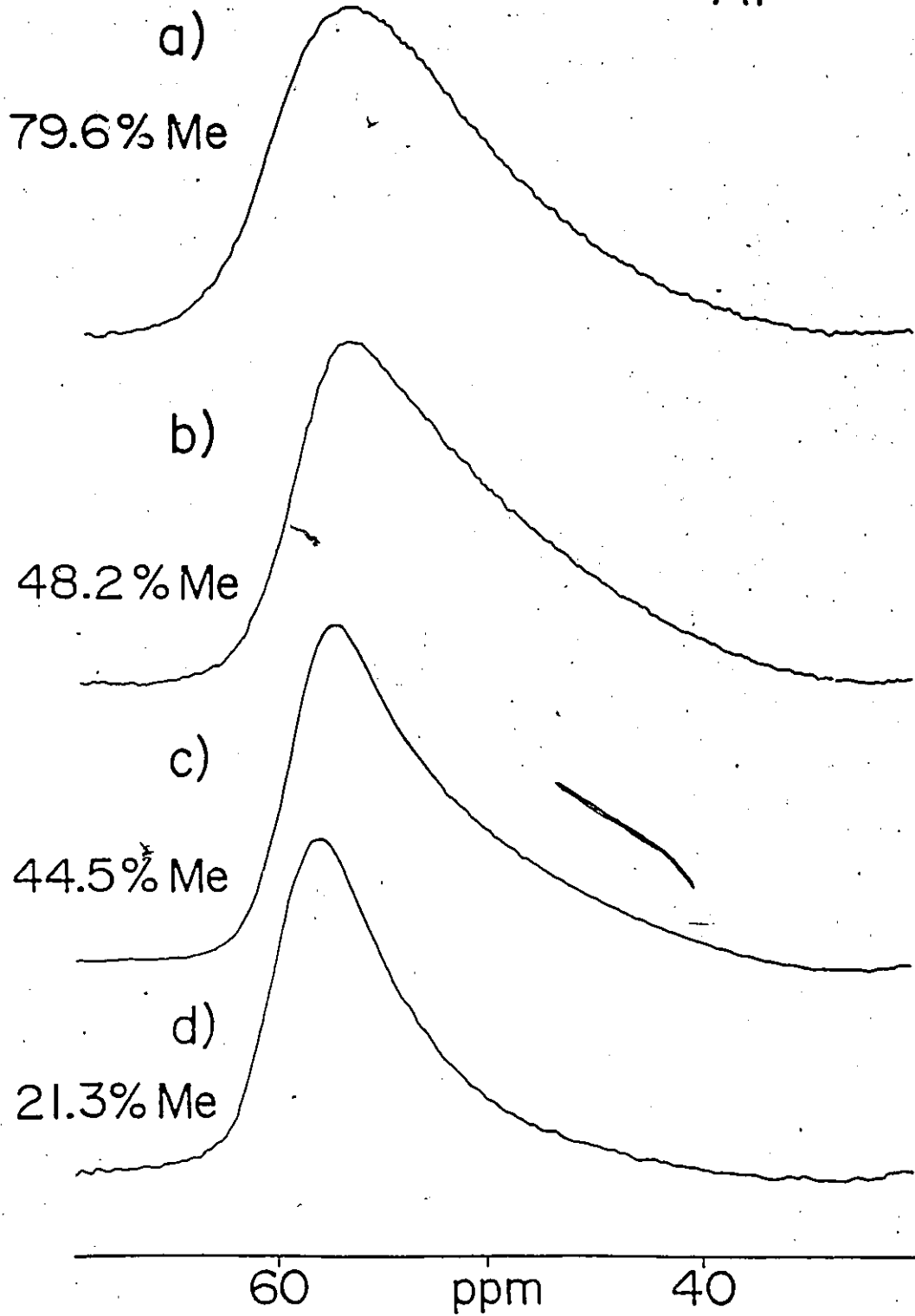
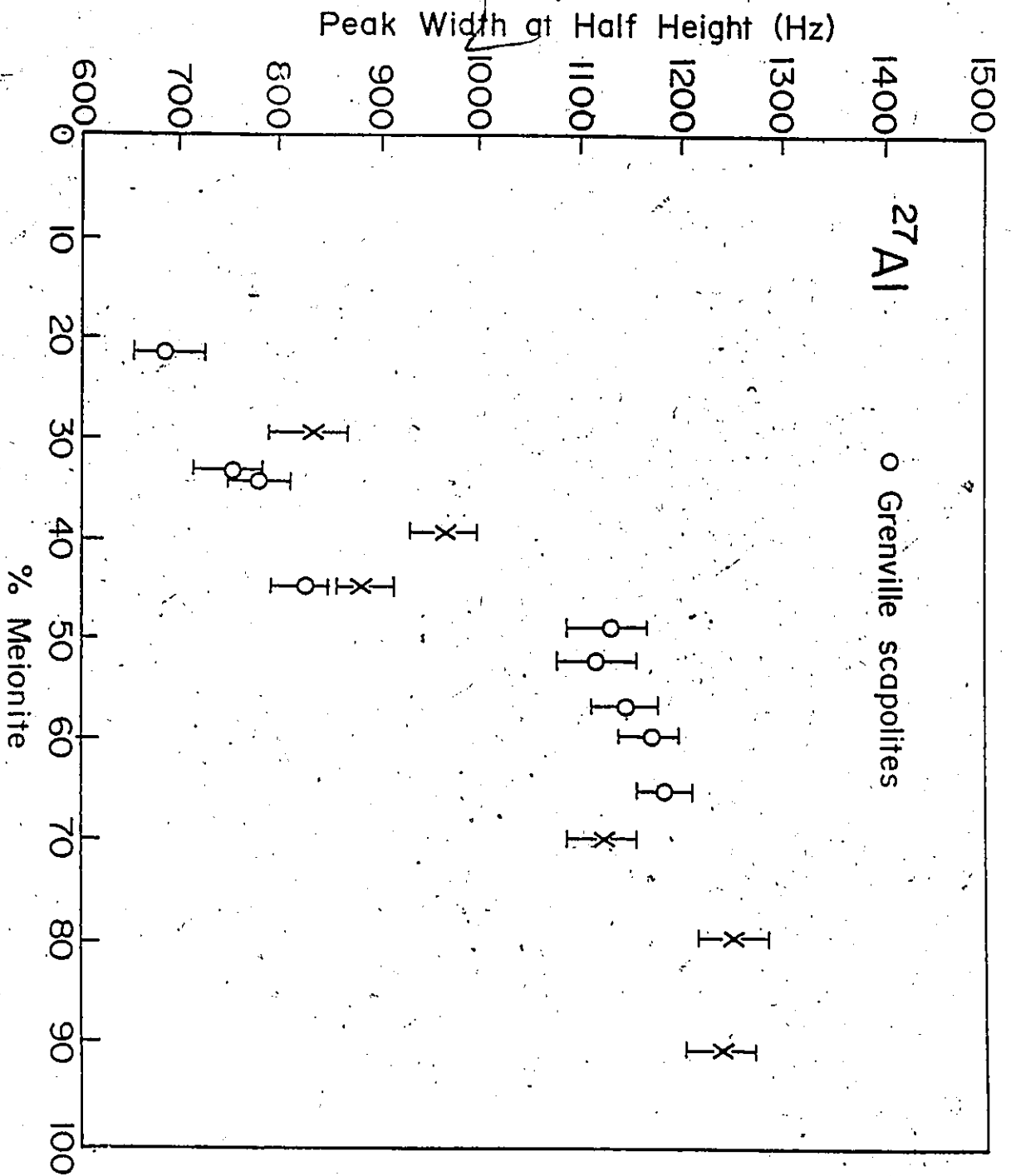


TABLE 3.8  
<sup>27</sup>Al MAS nmr parameters

Sample	%Meionite	Peak Position (ppm)	Peakwidth at half height (Hz)
ON8	21.3	58.2	680
TANZ	29.5	57.9	830
ON7	33.3	57.9	780
GL	34.1	57.9	880
ON70	39.5	57.7	970
CA63A	44.5	57.9	820
MAD	45.2	58.0	880
Q26	48.2	57.6	1110
Q13	51.3	57.5	1120
MIN	56.8	57.6	1140
ON27	59.3	57.6	1170
Q85	65.2	57.9	1180
BOLT	69.5	57.5	1120
ON47	79.6	57.4	1250
MONT	91.0	57.3	1250



Figure 3.6 A graph of  $^{27}\text{Al}$  peak width plotted against melonite content (Sherriff, et al., 1987a)



this decreases towards the marialite end of the solid solution series.

The discontinuity in the plot of  $^{27}\text{Al}$  peakwidth against meionite content (Fig 3.6), at about 45% Me, can be related to the introduction of Al sites with 3Si and 1Al next nearest neighbours due to the higher content of Al. The continued increase in peakwidth from 45% Me to 91.3% Me is caused by the Al(3Si|Al) peaks increasing in relative intensity. This portion of the plot has a different slope to that below 45% Me indicating a different mechanism controlling the slope.

The specimens from amphibolite-facies metamorphic rocks of the Grenville Province lie on two linear trends (Fig. 3.6). Specimens from other environments deviate from this trend, indicating a different degree of Al-Si order.

#### 3.4.3 SODIUM-23 MAS NMR

In the scapolite structure, sodium is in asymmetric eight-fold co-ordination with seven oxygen atoms from the tetrahedral framework and one chlorine or one oxygen atom from a carbonate or sulphate group (Fig. 3.7). Sodium-anion distances in the polyhedra vary from 2.35 to 3.02 Å (Lin & Burley 1973a) (Fig. 3.8).

$^{23}\text{Na}$  MAS nmr spectra of scapolite all consist of very broad lines with little discernable fine structure

Figure 3.7 Configuration of the Na-O polyhedron  
(Sherriff et al. 1987a)

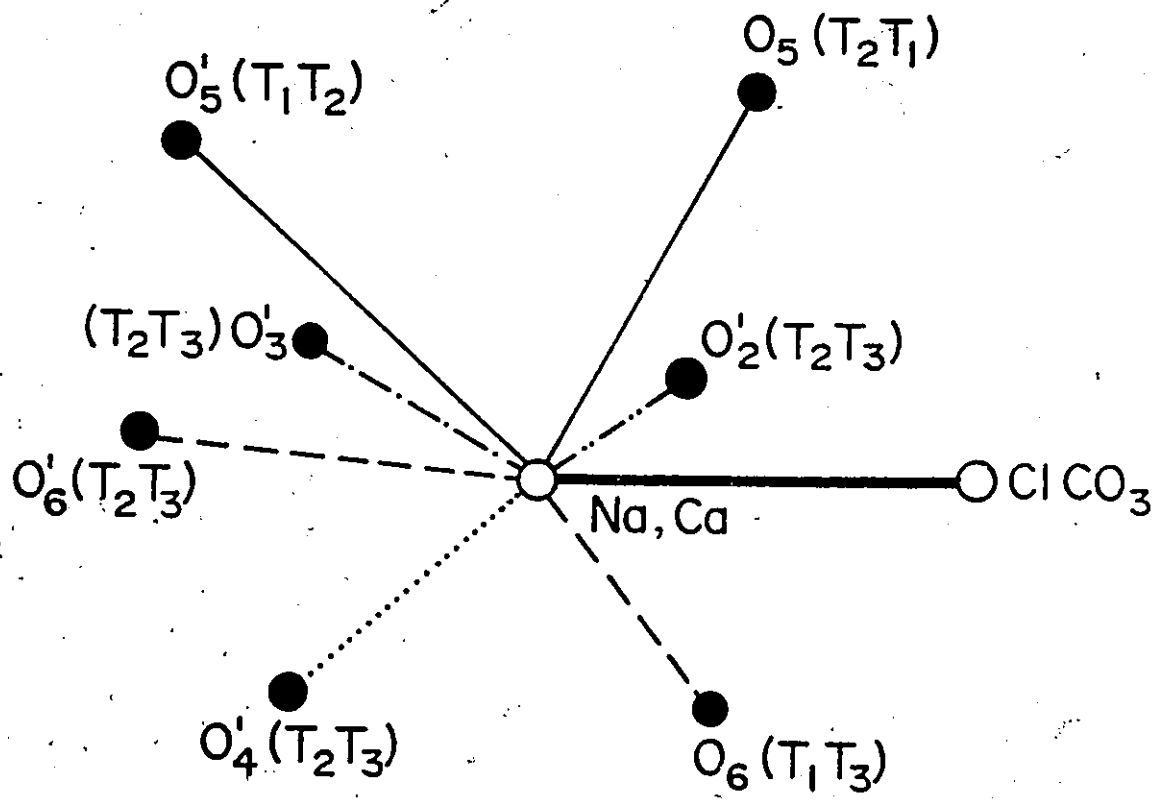
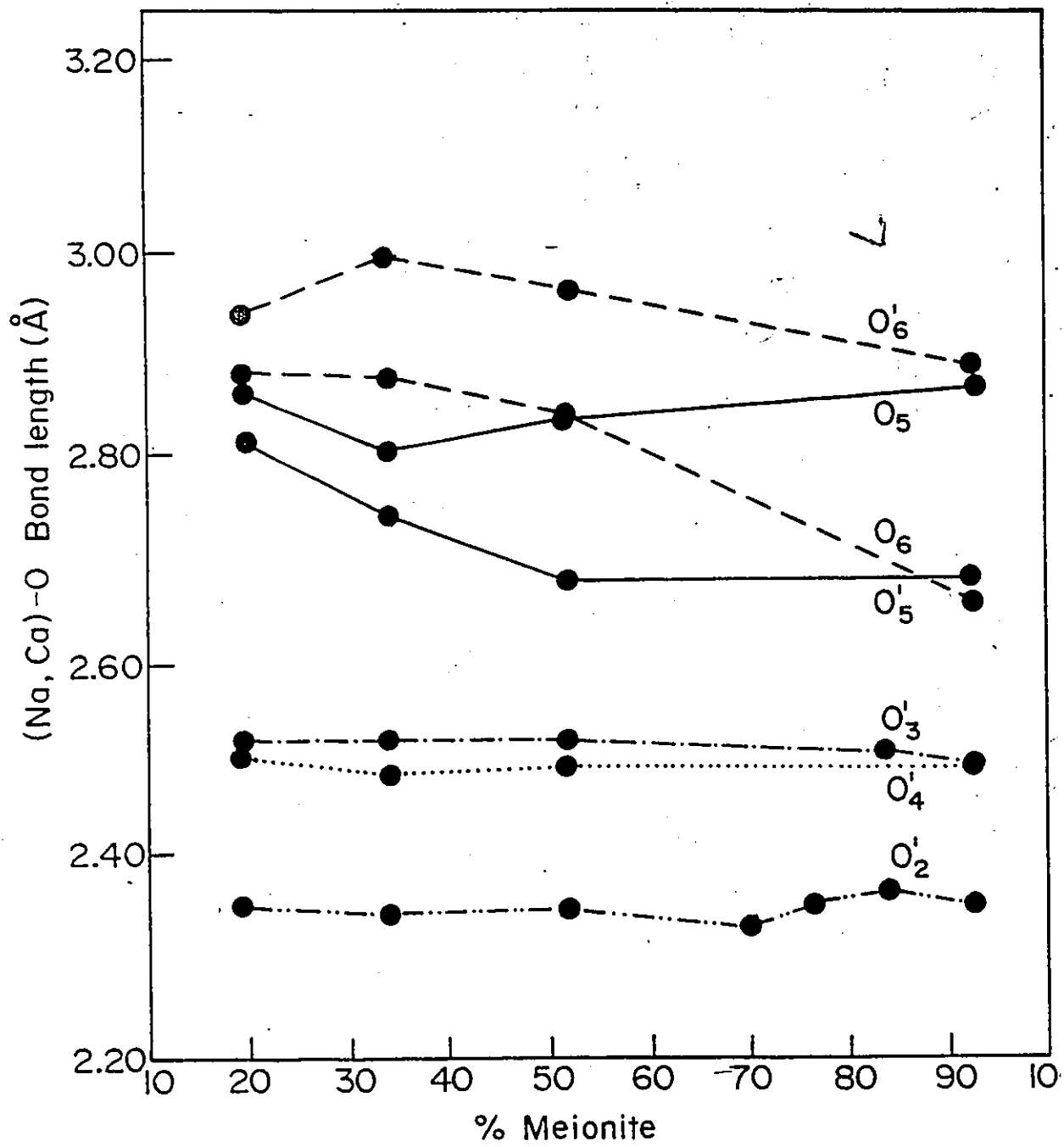


Figure 3.8 A plot of (Na,Ca)-O distances as a function of melonite content (Sherriff et al. 1987a)



(Fig. 3.9; Table 3.9). The spectra of ON7 (33.3% Me), GL (34.1% Me; Fig 3.9b), CA63A (44.5% Me) and MAD (45.2% Me) all have a shoulder at approximately 21 ppm. This is present but not as pronounced in the spectra of ON70 (39.5% Me), Q26 (48.2% Me) and BOLT (69.5% Me).

The relatively symmetrical peak at -14.7 ppm of the  $^{23}\text{Na}$  spectrum of ON8 (21.3% Me) (Fig. 3.9c) is due to sodium adjacent to chlorine and the peak at -15.7 ppm from MONT (91.0% Me) to sodium adjacent to a carbonate group. The shoulder at approximately -21 ppm in the spectra of scapolite containing between 33.3 and 45.2% Me (Fig. 3.9b; Table 3.9) is in the wrong position to be a direct overlap of peaks from Na atoms close to Cl or  $\text{CO}_3$ .

One possible explanation for the shoulder at 21 ppm is that the increased asymmetry of the sodium sites in this compositional range produces additional quadrupolar distortion or shift in some of the  $^{23}\text{Na}$  peaks. This asymmetry can be seen from a plot of (Ca,Na)-O distance against melonite content (Fig. 3.8). Bond distances between alkali cations and O2, O3 and O4 do not vary significantly across the series. (Na,Ca)-O5 and (Ca,Na)-O6 diverge by up to 0.20 Å between 33% and 50% Me but converge toward both end member compositions.

The composition of scapolite at which the shoulder at 21 ppm vanishes, 45% Me, corresponds to the composition at which there is a sudden increase in the  $^{27}\text{Al}$  MAS nmr



Figure 3.9  $^{23}\text{Na}$  MAS nmr spectra of scapolite

samples:

(a) ON47 (79.6% Me)

(b) GL (34.1% Me)

(c) ON8 (21.3% Me)

(Sherriff et al. 1987a)

$^{23}\text{Na}$

a)  
79.6% Me

b)  
34.1% Me

c)  
21.3% Me

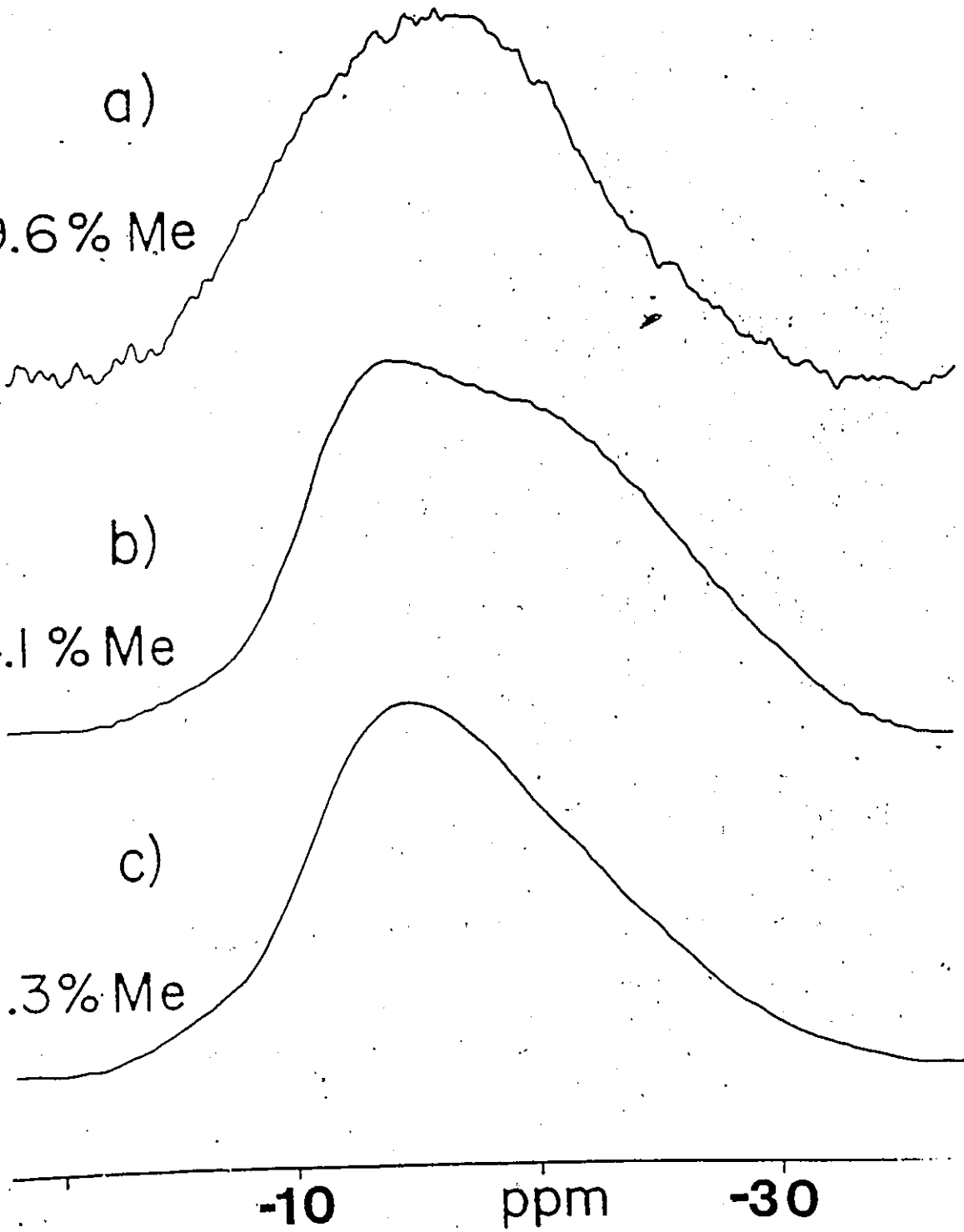


TABLE 3.9

<sup>23</sup>Na MAS nmr parameters

Sample	%Meionite	Peak Position (ppm)	Peakwidth at half height(Hz)
ON8	21.3	-14.7	1460
TANZ	29.5	-14.7	1480
ON7	33.3	-13.8 -19.7	1680
GL	34.1	-13.4 -19.4	1760
ON70	39.5	-13.5 -20.6	1680
CA63A	44.5	-13.8 -21.7	1590
MAD	45.2	-14.7 -21.0	1630
Q26	48.2	-14.7	1590
Q13	51.3	-14.8	1570
MIN	56.8	-15.3	1620
Q85	65.2	-15.4	1540
BOLT	69.5	-14.4 -22.0	2260
ON47	79.6	-15.8	1600
MONT	91.0	-15.7	2300

peak width.

#### 3.4.4 CARBON-13 MAS NMR

The carbonate group in scapolite is planar, tilted less than  $3^{\circ}$  out of the (001) plane (Levien & Papike 1976) and occupies one of eight equivalent sites (Aitkin et al. 1984).

Scapolite gives a very weak  $^{13}\text{C}$  spectrum, consisting of one broad peak at  $165 \pm 1$  ppm, which is about 5 ppm to the high field of other carbonate minerals (Table 3.10). Aragonite resonates at 169.9 ppm, calcite at 167.5 ppm and magnesite at 169.1 ppm. The large error in  $^{13}\text{C}$  chemical shift for scapolites is due to the overlapping peak from the "Delrin" rotor (Fig. 3.10).

There is a suggestion of a slight peak shift across the series, but at the level of instrumental resolution available this cannot be definitely assigned to different carbonate environments.

#### 3.4.5 A MODEL FOR CATION ORDERING

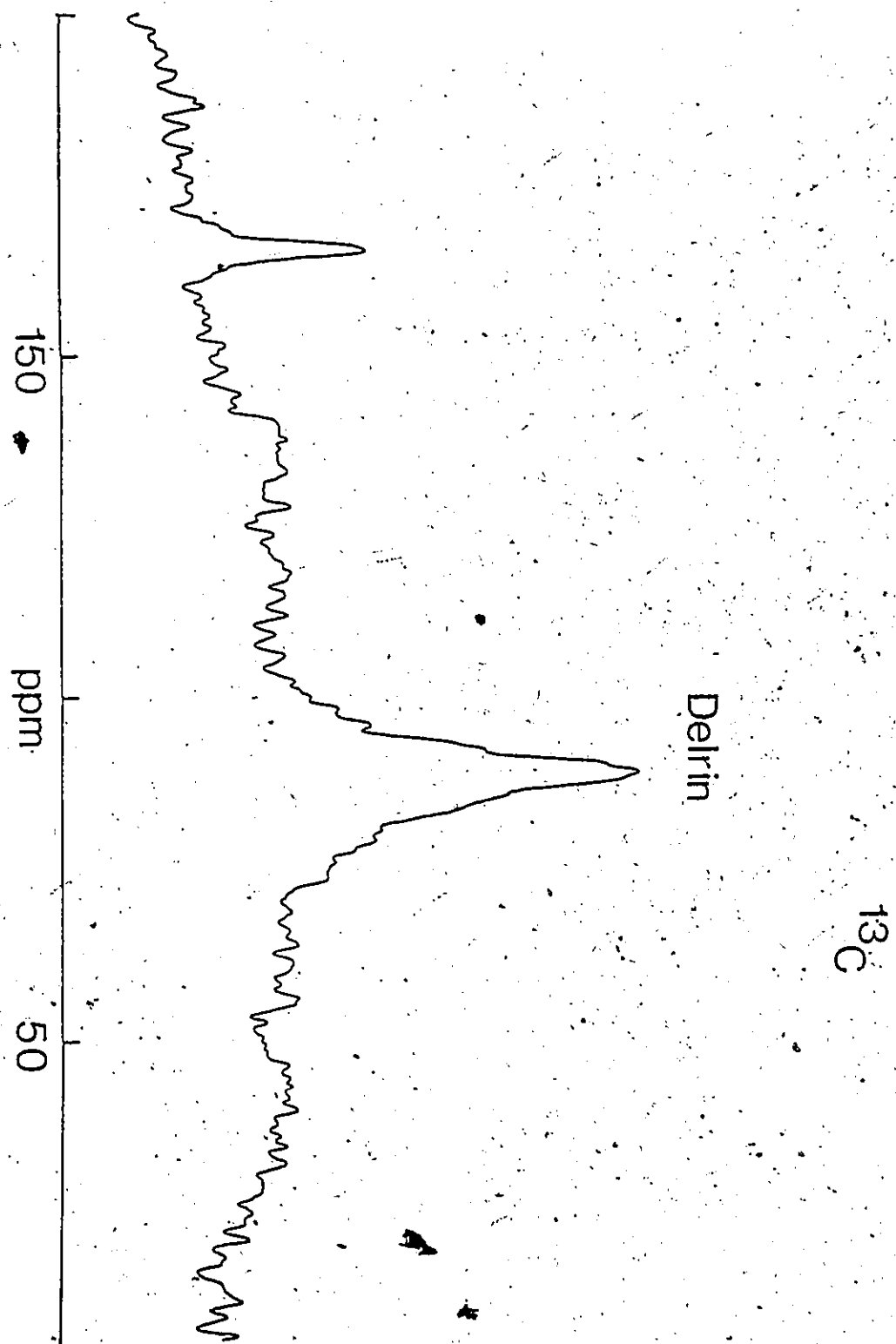
One source of variability in degree of order in scapolite relates to occupancy of the voids. Chamberlain et al. (1985) estimated from energy calculations that the most stable arrangement is one with a maximum number of sodium

TABLE 3.10

<sup>13</sup>C Parameters of Scapolites

Sample	% Meionite	Peak Position (ppm)
ON8	21.3	-
ON7	33.3	-
GL	34.1	165.2
ON70	39.5	165.0
CA63A	44.5	163.8
Q26	48.2	165.9
Q13	52.0	165.1
ON27	59.3	165.8
Q85	65.2	166.3
ON47	79.6	166.4
calcite		167.5
magnesite		169.1
aragonite		169.9
dolomite		167.7

Figure 3.10  $^{13}\text{C}$  MAS nmr spectrum of scapolite sample Q13 (51.3% Me). The large peak at 90 ppm is due to the sample holder which is made of 'Delrin' polymer (Sherriff et al. 1987a).



Delrin

$^{13}\text{C}$

ions around chloride and of calcium ions around carbonate. This arrangement would give predominantly  $\text{Na}_4\text{Cl}$  and  $\text{Ca}_4\text{CO}_3$  configurations, with excess charges of +3 and +6, respectively. However, the clusters of cations and anions in the voids should be related to Si-Al ordering of the framework in order that excess charge can be balanced locally.

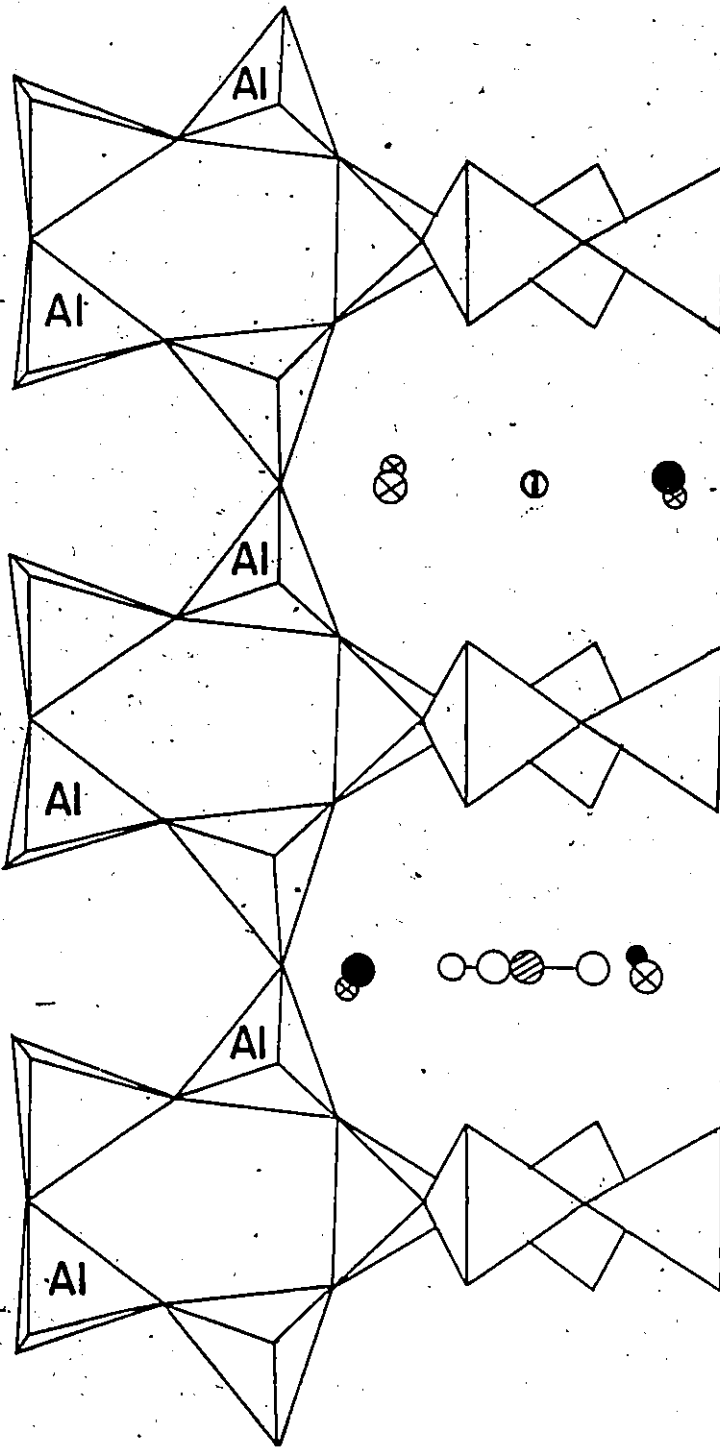
In the theoretically ordered framework of 37% Me, there are four aluminum ions in the T2 sites around each cavity, each contributing a negative charge. Therefore, to obtain a charge balance, the configurations of  $\text{Na}_3\text{CaCl}$  and  $\text{Na}_2\text{Ca}_2\text{CO}_3$  are considered to be the most favourable as both of these have an excess charge of +4 (Fig 3.11). This structure, with all of the Al in the T2 site and only Si in the T1 and T3 sites, contains two silicon configurations, T1(3Si1Al) and T3(1Si3Al), which give  $^{29}\text{Si}$  nmr peaks at -106 and -92 ppm. The T2-T3 chains of four-membered rings are comprised of alternating aluminum T2 sites and silicon T3 sites.

Alkali cation and anion configurations were calculated for scapolite samples from 21.3% to 91.0% Me from chemical analyses and also for stoichiometric compositions for 0, 37, 50, 75 and 100% Me. In these calculations the configurations with +4 charge are assumed to be the most favourable (Table 3.11).

Below 33% Me, the T1 sites theoretically contain



Figure 3,11 Model of cation ordering in 37% Me  
scapolite (Sherriff et al. 1987a).



- Ca
- ⊗ Na
- ⊙ C
- ⊖ Cl
- O

TABLE 3.11

Calculated cation populations of scapolite cavities

Sample (charge)	%Me	Na <sub>4</sub> Cl +3	Na <sub>3</sub> CaCl +4	Na <sub>2</sub> Ca <sub>2</sub> CO <sub>3</sub> +4	Na <sub>2</sub> Ca <sub>2</sub> SO <sub>4</sub> +4	Ca <sub>4</sub> CO <sub>3</sub> +6	Ca <sub>4</sub> SO <sub>4</sub> +6
*	0	1.00	-	-	-	-	-
ON8	21.3	0.35	0.37	0.22	-	-	-
TANZ	29.5	0.20	0.50	0.23	0.07	-	-
ON7	33.3	-	0.61	0.30	0.02	-	-
GL	34.1	-	0.58	0.38	-	-	-
*	37.0	-	0.50	0.50	-	-	-
ON70	39.5	-	0.46	0.44	0.06	-	0.021
CA63A	44.5	-	0.41	0.40	-	-	0.093
MAD	45.2	-	0.46	0.20	-	0.05	0.060
Q26	48.2	-	0.38	0.46	-	0.12	0.026
*	50.0	-	0.33	0.50	-	0.16	-
Q13	51.3	-	0.36	0.41	-	0.20	0.10
MIN	56.8	-	0.30	0.44	-	0.12	0.13
ON27	59.3	-	0.26	0.41	-	0.32	-
Q85	65.2	-	0.21	0.37	-	0.18	0.16
BOLT	69.5	-	0.12	0.44	-	0.44	-
*	75.0	-	-	0.33	-	0.67	-
ON47	79.6	-	0.08	0.39	-	0.28	0.24
MONT	91.0	-	0.04	0.28	-	0.78	0.02
*	100.0	-	-	-	-	1.00	-

\* Calculated from theoretical models described in section 3.4.5

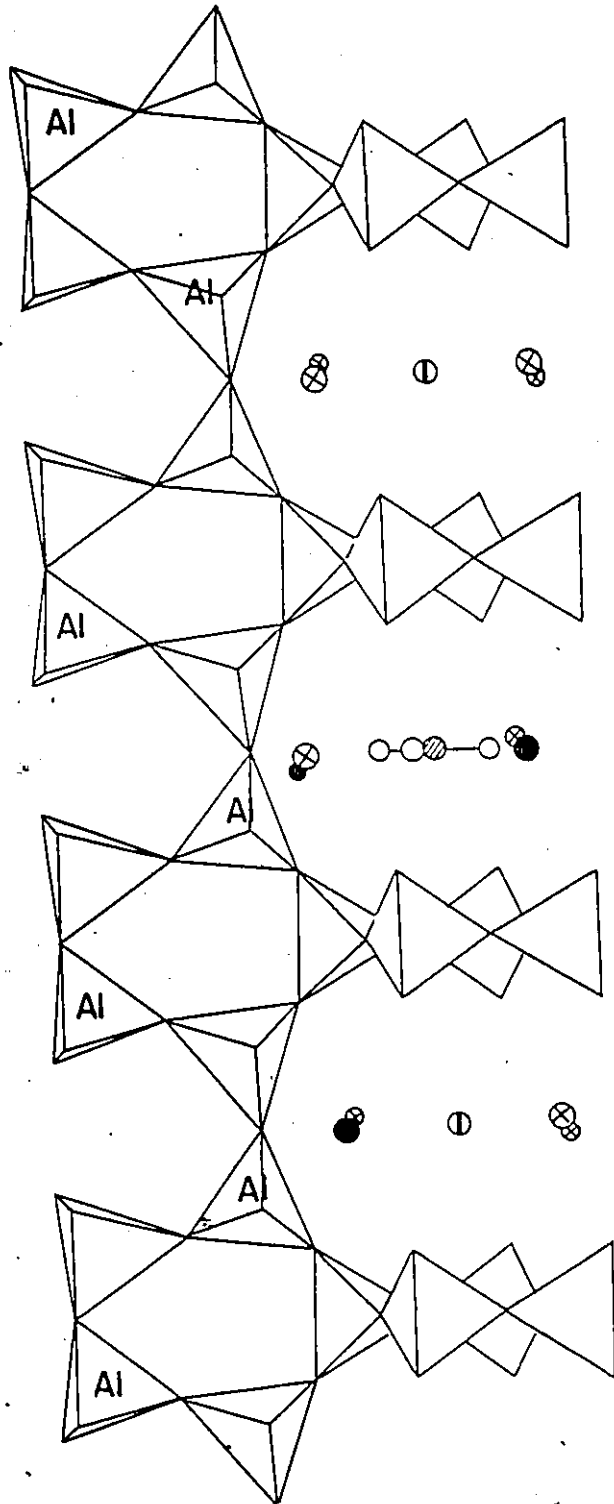
only silicon, with excess Si entering the T2 site. The X-ray data shows Al becoming progressively more evenly distributed between T2 and T3 sites. The increase in sodium requires some  $\text{Na}_4\text{Cl}$  clusters, with a charge of +3 (Fig. 3.12). This is balanced by three rather than four neighbouring  $\text{AlO}_4$  tetrahedra. The extra silicon introduces flexibility in the ordering of the T2-T3 chains, which allows for the distribution of aluminum between T2 and T3 sites, without the necessity of Al-O-Al bonds or more than two Al in any four membered ring.

The  $^{29}\text{Si}$  nmr spectrum of 21.3% Me shows the two peaks as in the 34.1% Me spectrum and also extra peaks due to T1(4Si) at -111 ppm, T2/T3(2Si2AlNa) at -99 ppm and T2/T3(2Si2AlCa) at -101 ppm (Fig. 3.3e). These small peaks are not resolved in this spectrum and show as a raise in the baseline.

In scapolites with meionite contents greater than 37% Me, some  $(\text{Ca}_4\text{CO}_3)^{+6}$  configurations are necessary to use up the excess Ca and  $\text{CO}_3$  ions, with the extra positive charge being balanced by aluminum in the T1 sites. The change of one next-nearest-neighbour T1 from Si to Al produces a progressive decrease in the  $^{29}\text{Si}$  peak due to T1(3Si1Al) at -106 ppm and a corresponding increase in the T1(2Si2Al) peak at -101 ppm. There is also an increase in the intensity of the T2/3(4Al) peak at -88 ppm.

In the structure of 70% Me scapolite each T1 ring

Figure 3.12 Model of cation ordering in 20% Me scapolite (Sherriff et al. 1987a).



- Ca
- ⊗ Na
- ⊘ C
- ⊖ Cl
- O

can have one Al and three Si tetrahedra, but in compositions more aluminous than 70% Me it is necessary to put two aluminum atoms into some T1 rings (Fig. 3.13). This produces T1(1Si3Al) peaks at -93 ppm and T1(4Al) peak at -90 ppm at the expense of the other T1 peaks. There is also a steady increase in the size of the T2/T3(4Al) peaks. The tetrahedral framework of all cavities now have a -5 or -6 charge, which cannot be balanced by Cl containing clusters. Therefore there is virtually no Cl in the structure above 70% Me.

The number of silicon atoms in each tetrahedral configuration were calculated from this model for 20, 37, 50, 70 and 90% Me and compared with those estimated from the measured relative intensities of the peaks fitted to  $^{29}\text{Si}$  spectra (Table 3.12). For the samples ON8, ON7, Q13, BOLT the comparison was quite good. However there are discrepancies between the calculated silicon contents of the lower field peaks relating to the more aluminous sites for the sample of 91.0% Me (MONT). In this spectrum the resolution of the lower field peaks is poor due to many overlapping peaks which increases the experimental error in the peak fitting procedure.

This ordering scheme is ideal. Divergence from the ideal is the rule rather than the exception in the case of minerals. The anomolous presence of Al in the T1 sites of scapolites with meionite contents less than 37% is

Figure 3.13 Model of cation ordering in 75% Me  
scapolite (Sherriff et al. 1987a).



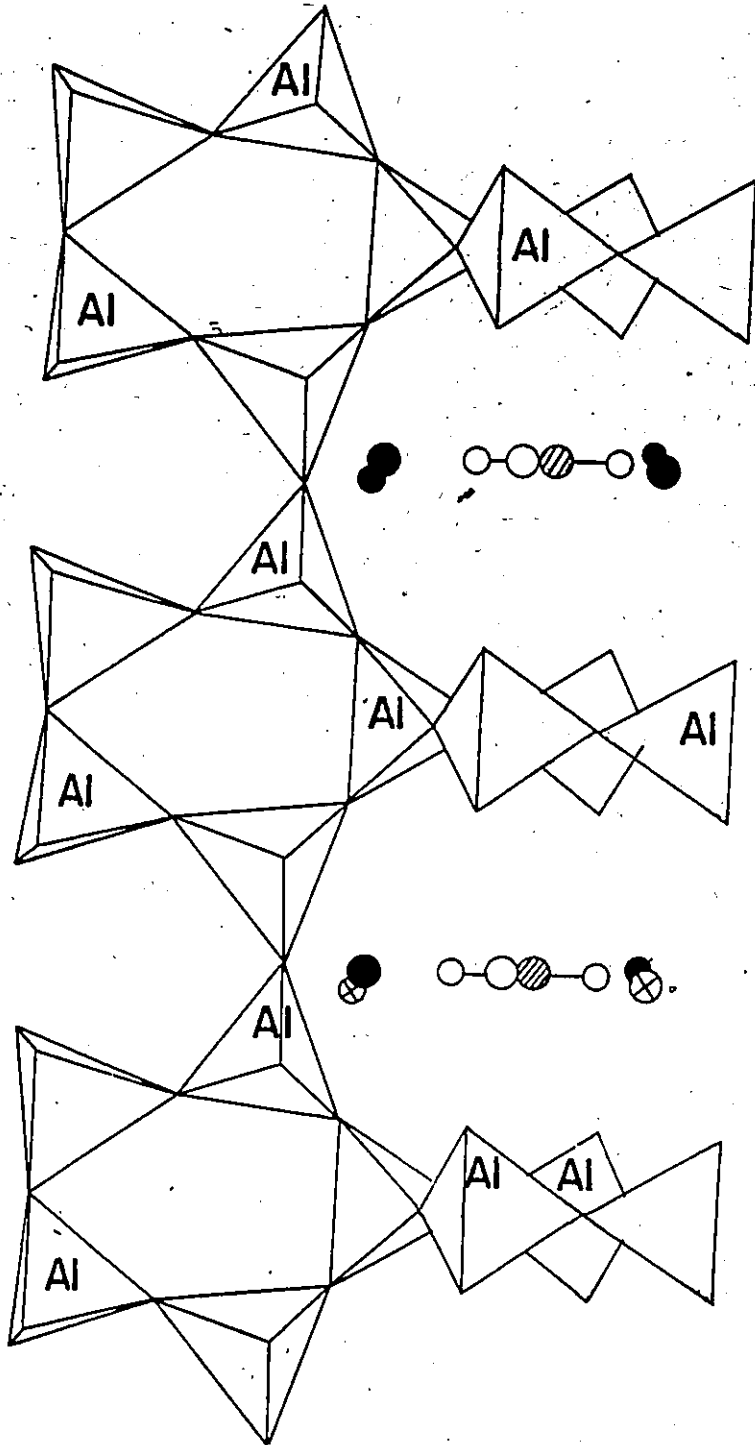


TABLE 3.12

Numbers of Silicon atoms in T Configurations

Sample		T1	T2/T3	T2/T3	T1	T2/T3	T1	T2/T3	T1	T1
		(4A1)	(4A1)	(3A1)	(3A1)	(2A1)	(2A1)	(1A1)	(1A1)	(0A1)
ON8	(a)	-	0.2	2.3	-	1.3	-	0.5	3.4	0.8
	(b)	-	-	2.8	-	1.7	-	-	3.3	0.5
	(c)	-	-	2.9	-	0.8	-	0.7	3.3	0.8
ON7	(a)	-	-	3.8	-	-	0.2	-	4.0	-
	(b)	-	1.0	3.0	-	-	-	-	4.0	-
	(c)	-	-	4.0	-	-	-	-	4.0	-
Q13	(a)	-	0.9	2.9	-	0.2	1.1	-	2.4	-
	(b)	-	1.1	2.9	-	0.2	0.8	-	2.5	-
	(c)	-	0.5	3.5	-	-	0.8	-	2.9	-
BOLT	(a)	-	0.2	3.9	-	-	1.5	-	1.5	-
	(b)	-	0.8	2.4	0.5	0.4	1.6	-	1.6	-
	(c)	-	1.1	2.9	-	-	1.8	-	1.4	-
MONT	(a)	-	0.7	3.1	-	1.0	1.1	-	0.4	-
	(b)	0.7	2.3	1.3	0.6	0.7	0.4	-	0.3	-
	(c)	-	1.8	2.2	-	1.5	0.5	-	0.3	-

(a) Integrals measured by weighing cut out peaks

(b) Integrals measured by fitting peaks to the spectra

(c) Calculated values from model in section 3.4.6

indicated by both  $^{29}\text{Si}$ , and  $^{27}\text{Al}$  nmr spectra and also by detailed examination of the T-O bond distances from X-ray data. Domains within the scapolite structure found by transmission electron microscopy (Hassan and Busek 1987), could contain differing types of order.

The discrepancy between the calculated and measured Si site occupancies for scapolite from the volcanic environment of Monte Somma (MONTE) may indicate that the ordering in scapolite is sensitive to the conditions of temperature and pressure under which it formed. The plot of  $^{27}\text{Al}$  peakwidth against melonite content (Fig. 3.3) also indicates a difference between the ordering of scapolites from the Grenville province (Shaw et al. 1963; 1965) and those formed under other conditions.

### 3.5 CONCLUSION

This study of the scapolite series of minerals shows the potential of MAS nmr to investigate ordering in partially disordered material.

$^{29}\text{Si}$  chemical shifts, calculated from diffraction data using equations 3 and 4 in chapter 2, were used to interpret the broad overlapping peaks of the MAS nmr spectra of scapolite. This was combined with information available from  $^{27}\text{Al}$  and  $^{23}\text{Na}$  MAS nmr and X-ray diffraction data to produce a model for cation ordering throughout the

solid solution series, in which the charge on the cavities is balanced locally by the requisite number of  $AlO_4$  tetrahedra.

In this model there is a maximum of two aluminum atoms in any four membered ring and in these aluminum atoms alternate with silicon atoms. However the five membered rings do contain Al-O-Al bonds at high concentrations of the meionite component. T2/T3 chains remain internally ordered, with the apparent disorder of Al between T2 and T3 sites in compositions greater than 33% Me, indicated by X-ray data, explained by the rotation by  $180^\circ$  of individual T2/T3 chains relative to one another (i.e., interchange of Al from T2 to T3). With less than 33% Me, the excess silicon in the T2/T3 chains allows for a change of Al occupancy from the T2 to T3 site to occur along a chain.

Most of the T1 sites are occupied by silicon below 33% Me. With increasing aluminum content beyond 33% Me, first one Al enters each T1 ring and then, beyond 70% Me a second Al enters the T1 rings. At this point it is impossible to balance the charges of Cl containing cavities by the surrounding tetrahedral framework and Cl is eliminated from the structure.

The difference in ordering between samples of scapolites from different environments shown by both  $^{27}Al$  and  $^{29}Si$  nmr results indicate that scapolite could be used as a geothermometer and geobarometer.

## CHAPTER 4

### A MULTINUCLEAR NMR STUDY OF BERYLS

#### 4.1 INTRODUCTION

Beryls are hexagonal minerals, usually found as barrel shaped crystals, which can grow to large sizes in pegmatite; e.g. a 27 ft tapering crystal weighing 25 tons from Albany, Maine. Gem quality beryls have a variety of names depending on the colours induced by trace elements; aquamarine is pale greenish blue, morganite rose pink, emerald deep green, aquamarine blue and golden beryl clear golden yellow.

In this study  $^{29}\text{Si}$ ,  $^{27}\text{Al}$ ,  $^{23}\text{Na}$ ,  $^7\text{Li}$  and  $^9\text{Be}$  MAS nmr spectroscopy is used to investigate the difference in atomic sites between beryls with slightly different chemical compositions.

Beryl is included with the tectosilicates in Appendix VIII in accordance with the classification of Zoltai (1960) that all tetrahedrally coordinated cations (Si, Al, Be etc.) should be considered as part of the tetrahedral framework. The  $^{29}\text{Si}$  MAS nmr chemical shift for beryl at -102 ppm is in the middle of the range of chemical shifts for tectosilicates (Fig. 1.1).

## 4.2 STRUCTURE OF BERYL

The structure of beryl ( $\text{Be}_3\text{Al}_2\text{Si}_6\text{O}_{18}$ ) consists of six membered rings of  $\text{SiO}_4$  tetrahedra lying parallel to (0001) linked by  $\text{BeO}_4$  tetrahedra and distorted  $\text{AlO}_6$  octahedra (Fig 4.1).

In lithian-cesian beryls sodium and cesium atoms and water molecules occupy the channels, parallel to the c-axis, formed by the silicate rings (Hawthorne and Cerny 1977). There is a controversy as to whether lithium replaces beryllium in the tetrahedral sites or is involved in a coupled exchange of lithium for aluminum which then enters the tetrahedral sites. In the emerald structure trace amounts of Cr replacing Al in octahedral configuration (Gibbs *et al.* 1968) increase the average size of the octahedra over that for the other beryls.

There are differences in atomic positions, shown by diffraction data, between the structures of low alkali beryl, and Li-Cs beryl. These could be either evenly distributed throughout the two structures or there could be domains of low alkali beryl and Li-Cs beryl type structures in the crystals, with the diffraction data recording average atomic positions. Nmr, as a site specific technique, is here used to determine between these possibilities.

Figure 4.1a A photograph of a computer simulated model of the structure of Li-Cs beryl viewed along the c-axis.

Figure 4.1b A photograph of a computer simulated model of the structure of Li-Cs beryl viewed along the a-axis.

Light Blue = beryllium

Yellow = silicon

Dark Blue = sodium

Green = cesium

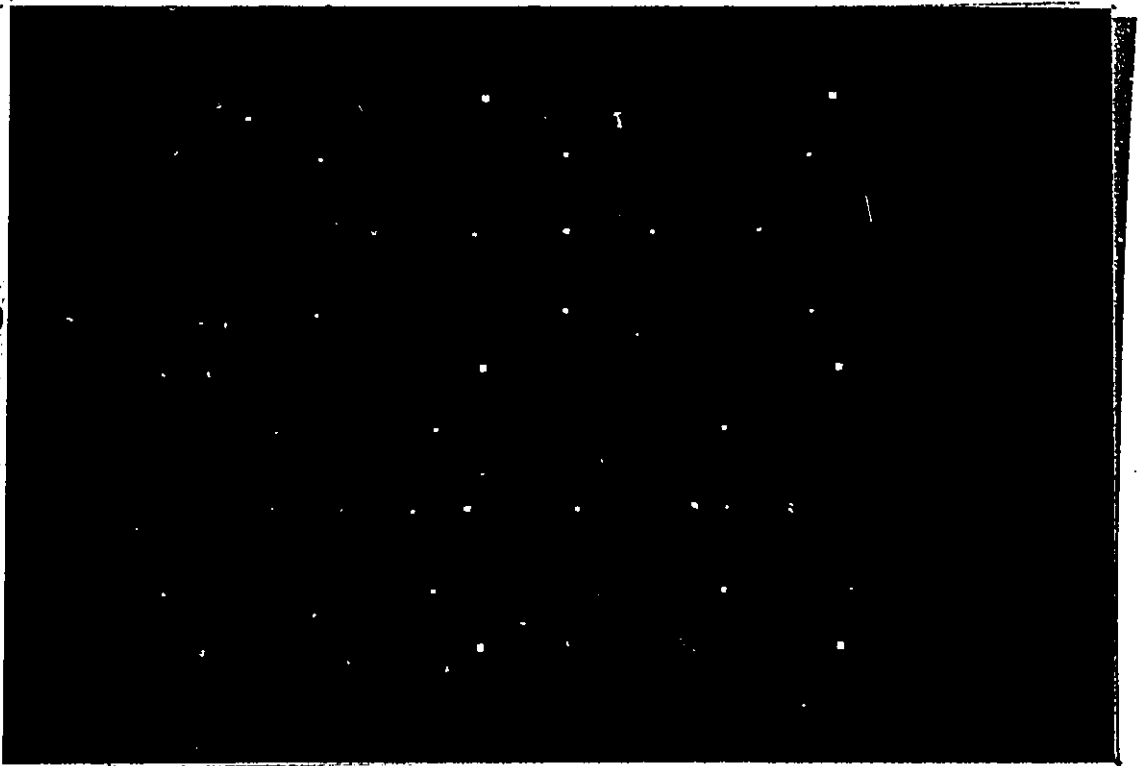
Red = oxygen

Dark Red = aluminum

a



b





### 4.3 EXPERIMENTAL

Four samples of alkali beryls; SHEE-1-6, EEE-10, BLM503, and T-24, from Shatford Lake and the Tanco pegmatite deposit, with differing alkali contents, were obtained for study from Professor F. C. Hawthorne, University of Manitoba, and three samples of emeralds from Brazil, New South Wales and Colombia (Ottaway et al. 1986) from T. Ottaway of the Royal Ontario Museum (Appendix II). Analyses of the alkali beryls were provided by Professor P. Cerny, University of Manitoba (Table 4.1).

The alkali beryl samples were crushed to a powder for packing into nmr rotors. Some of the poorer quality emeralds were crushed but the gem quality emeralds from Columbia were left intact, by request of the owner, and packed into the rotor as chips. This resulted a relative enhancement of one of the peaks of the  $^{27}\text{Al}$  quadrupolar spectra but otherwise the resolution of the spectra from the chips of emeralds is comparable to that from powder samples.

The nmr instruments, parameters and standards for  $^{29}\text{Si}$ ,  $^{27}\text{Al}$ , and  $^{23}\text{Na}$  are as described in Chapter 3.  $^7\text{Li}$  and  $^9\text{Be}$  were measured at 155.5 and 56.2 MHz respectively on the Bruker WH400 using the MAS probe and spinning parameters as previously described, and their chemical shifts measured

TABLE 4.1

Analyses of alkali beryls (weight percent).

	SHEE-1-6	EEE-10	BLM503	T-24
Li <sub>2</sub> O	0.03	[0.36]	[0.42]	1.25
Na <sub>2</sub> O	0.29	0.96	1.14	1.50
K <sub>2</sub> O	0.03	[0.03]	[0.03]	0.06
Rb <sub>2</sub> O	0.006	0.077	0.105	0.08
Cs <sub>2</sub> O	0.17	1.41	2.46	3.68
Total Fe as				
Fe <sub>2</sub> O <sub>3</sub>	0.54	0.025	0.06	n.d.
CaO	0.003	n.d.	0.006	0.01
MgO	0.005	0.004	0.013	n.d.
MnO	n.d.	0.003	0.002	n.d.
H <sub>2</sub> O	n.d.	1.78	1.70	n.d.

n.d. = not determined

[ ] = weight percent of element not oxide

Analyses provided by Professor P. Cerny, University of Manitoba.

with reference to aqueous solutions of LiBr and  $\text{Be}(\text{NO}_3)_2$  respectively.

Values of  $^{29}\text{Si}$  chemical shift were calculated from structures of Li-Cs beryl (Hawthorne & Cerny 1977), gem quality beryl (Morosin 1972) and anhydrous synthetic emerald (Gibbs *et al.* 1968) using equations 3 and 4 and the method described in Chapter 2.

#### 4.4 RESULTS AND DISCUSSION

##### 4.4.1 SILICON-29

The silicon site in beryl is adjacent to two silicon and two beryllium tetrahedra. In lithian-cesian beryls one of the two beryllium atoms could be replaced by either lithium or aluminum depending on which substitution scheme is correct (Hawthorne & Cerny 1977).

The chemical shift of the single peak in the  $^{29}\text{Si}$  MAS nmr spectrum varies from -102.3 to -100.9 ppm with increasing alkali content (Table 4.2). The  $^{29}\text{Si}$  nmr peak of the high alkali beryls is 100Hz wider than that for SHEE-1-6 the low alkali beryl (Fig 4.2) and of the better quality Columbian and Australian emeralds (Table 4.2).

The difference of 1.4 ppm in experimental peak position between the spectra of SHEE-1-6 low alkali beryl and T-24 Li-Cs beryl, is reflected in the 1.7 ppm

Figure 4.2  $^{29}\text{Si}$  MAS nmr spectra of (a) T-24 Li-Cs beryl (b) SHEE-1-6 low alkali beryl

$^{29}\text{Si}$

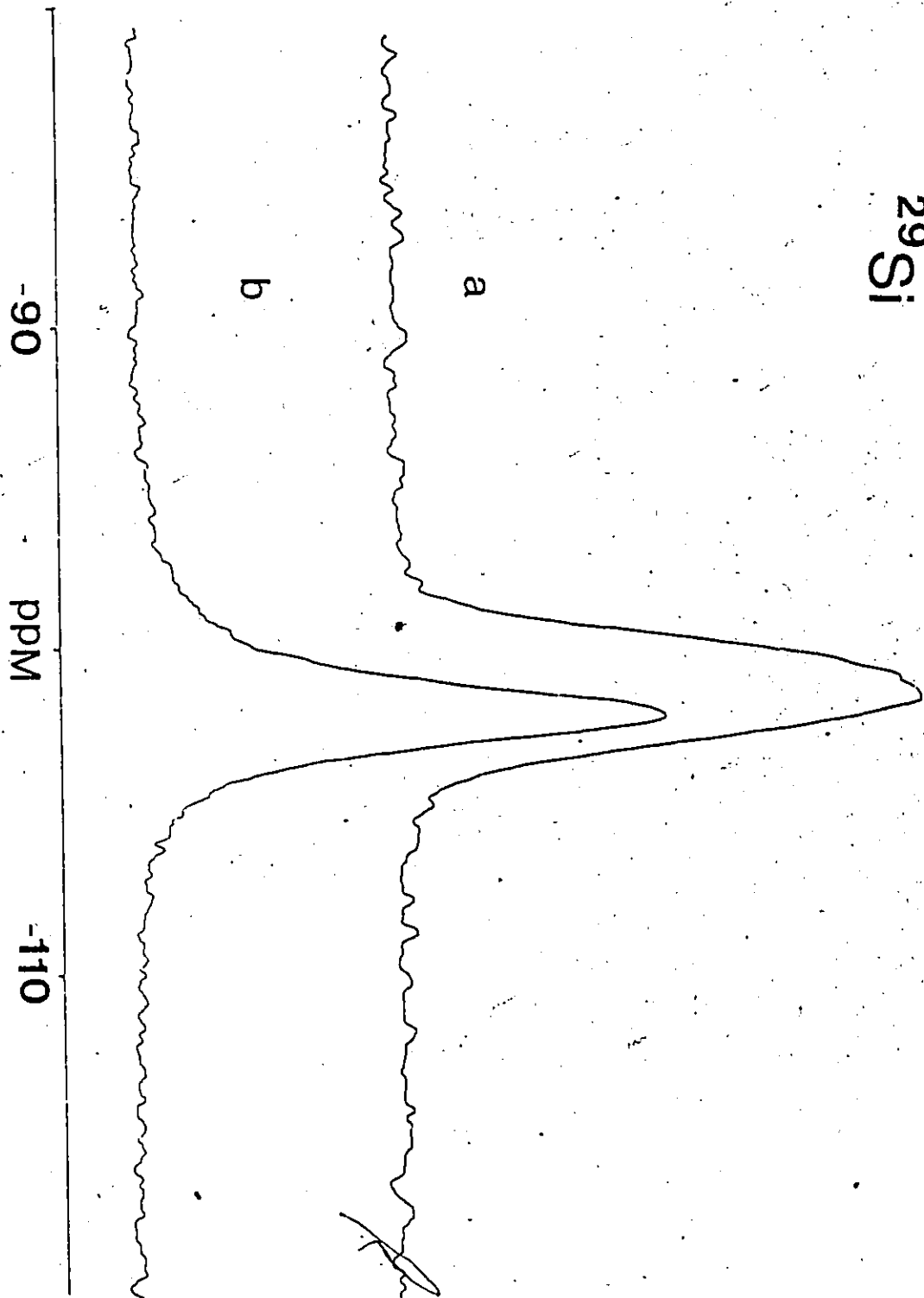


TABLE 4.2

 $^{29}\text{Si}$  MAS nmr parameters of beryl

Sample	Peak width at half height (Hz)	Chemical shift (ppm)	
		Experimental	Calculated*
<u>Low alkali beryl</u>			
SHEE-1-6	190	-102.3	-103.7
<u>Lithian-cesian beryls</u>			
EEE-10	287	-101.9	
BLM-503	290	-101.3	
T-24	289	-100.9	-102.0
T-24			-103.1**
<u>Emeralds</u>			
Brazilian	342	-102.3	
Columbian			
(gem quality)	164	-102.5	-104.0
Australian	110	-102.4	

\* Calculated from equations 3 &amp; 4 in chapter 2.

\*\* Calculated with next nearest neighbour configuration

Si(2Si1Be1Li)

difference between values of chemical shift calculated from equations 3 and 4, using structures of low alkali beryl (Morosin 1972) and high Li-Cs beryl (Hawthorne and Cerny 1977) (Table 4.2). The lower field chemical shift, calculated for the Li-Cs beryl, is due to Be-O tetrahedral distances being 0.02 Å longer in this structure than in that of the low-alkali beryl.

The broad peak for the higher alkali beryls appears to contain at least two unresolved peaks (spectrum (a) Fig. 4.2). These two peaks could be due to Si being both in domains of the alkali beryl crystal with alkalis in the channels, and also in domains of the mineral with empty channel sites. The apparent shift to low field with increasing alkali content is then due to the lower field peak increasing in intensity with respect to the higher field peak.

There is also a possibility, in  $^{29}\text{Si}$  nmr spectra of Li-Cs beryls, of overlapping peaks due to Si with either 2Be or else 1Be and 1Li next nearest neighbours. Unfortunately the calculated chemical shift of the latter environment at -103.1 ppm (Table 4.2) lies midway between the calculated chemical shifts for Si(2Be) site in the low alkali beryl at -103.7 ppm and in the Li-Cs beryl at -102.0 ppm. Therefore such a peak would not be separately resolvable.  $^{29}\text{Si}$  nmr spectra, therefore, give no direct information about the position of Li in Li-Cs beryls.

The chemical shift calculated for anhydrous emerald at  $-104.0$  ppm is  $0.3$  ppm to higher field than for the low alkali beryl structures. This difference is due to the Si-O tetrahedral distance within the silicate ring in emerald being  $1.585$  Å compared to  $1.597$  Å for anhydrous beryl.

The difference of  $1.0$  to  $1.5$  ppm between all the calculated values of chemical shift and the corresponding experimental values could be resolved by allowing for some Si atoms in the  $\text{BeO}_4$  tetrahedra. This would mean that the Be-O distances were actually slightly longer than found by the diffraction data. Increasing the Be-O distances in this way would give calculated values of chemical shift to lower field for all types of beryl and fit with the experimental data.

#### 4.4.2 ALUMINUM-27

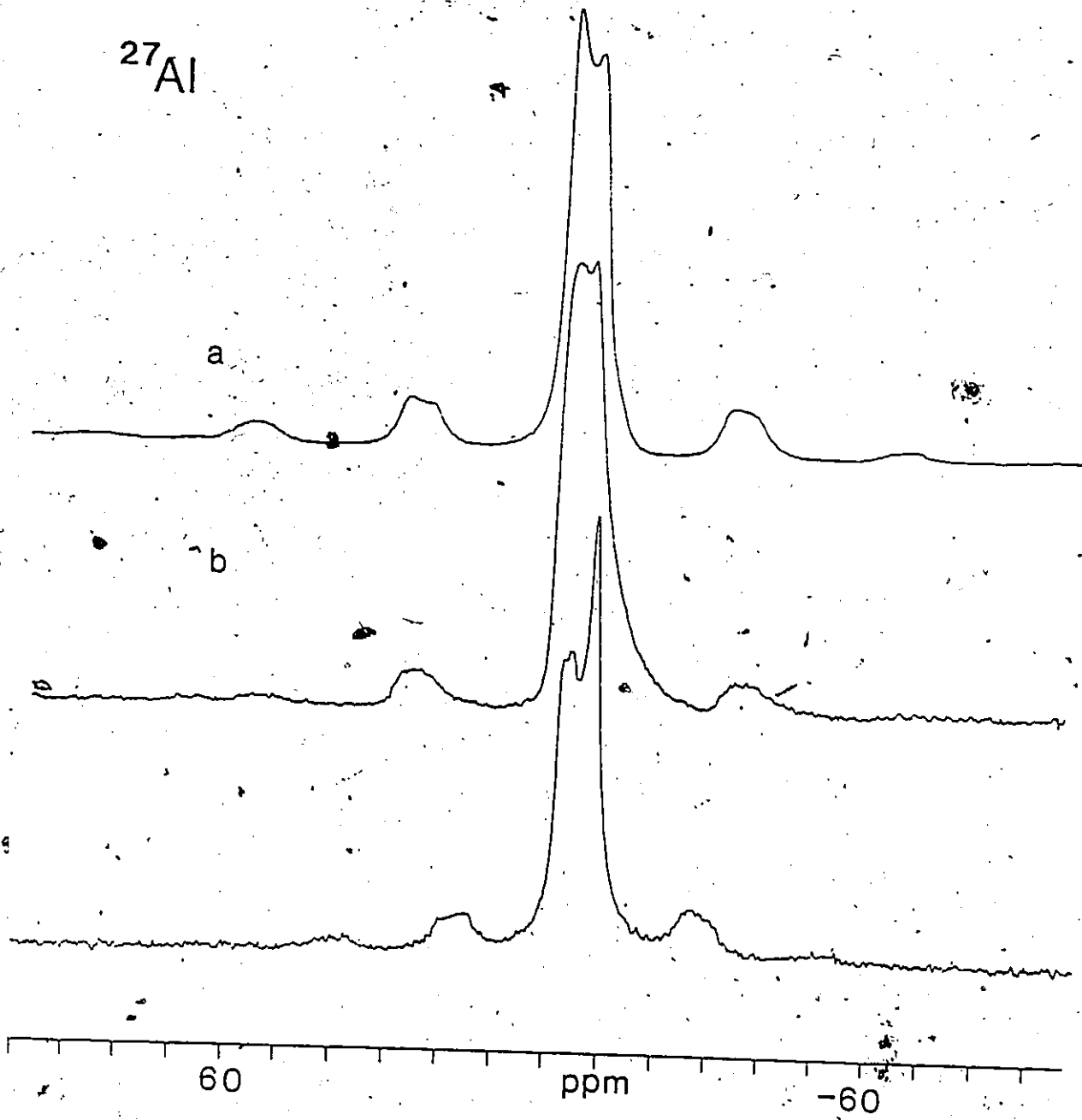
Aluminum is in a distorted octahedral site surrounded by three silicon tetrahedra and three tetrahedra which usually contain beryllium but in lithian-cesian beryls could contain beryllium, lithium or aluminum.

$^{27}\text{Al}$  MAS nmr spectra of all samples of beryl consist of one resonance with two maxima at  $-3.2$  and  $-7.7$  ppm (Fig. 4.3). The shape and broadness of the peak is due to the large quadrupolar moment of the asymmetric octahedral environment. The peak width at half height of



Figure 4.3  $^{27}\text{Al}$  MAS nmr spectra of  
(a) SHEE-1-6 low alkali beryl  
(b) T-24 Li-Cs beryl  
(c) chips of emeralds from Columbia

$^{27}\text{Al}$



the broad resonance increases with alkali content from 840 Hz for SHEE-1-6, low alkali beryl to 974 Hz for T-24, Li-Cs beryl (Table 4.3). This suggests overlapping peaks from aluminum atoms with differing next nearest neighbours in the spectra of the high alkali beryls.

If aluminum replaces beryllium in the tetrahedral site there would be a  $^{27}\text{Al}$  peak at about 60 ppm due to tetrahedral  $^{27}\text{Al}$  which would increase with alkali content. This peak is not visible in any  $^{27}\text{Al}$  MAS nmr spectra of alkali beryls. Therefore the  $^{27}\text{Al}$  MAS nmr spectra do not support the idea of a coupled replacement of lithium for aluminum and aluminum for beryllium in Li-Cs beryls.

$^{27}\text{Al}$  spectra of emeralds are similar to those for the other samples of beryls. The difference in the relative intensity in the two peaks and the possibility of an extra peak at -4.4 ppm in the spectrum of Columbian emeralds (spectrum (c) Fig. 4.3) could be produced by preferential orientation as the chips of emeralds did not have the random orientation of powdered minerals.  $^{27}\text{Al}$  spectra of powdered samples of other emeralds have two peaks of approximately equal intensity as for the other samples of beryl.

#### 4.4.3 SODIUM-23

Sodium is in the 2b channel site coordinated with

TABLE 4.3

<sup>27</sup>Al MAS nmr parameters of beryl

Sample	Peak Position (ppm)	Peak Width at half height (Hz)
<u>Low-alkali beryl</u>		
SHEE-1-6	-3.0, -7.5	840
<u>Lithium-cesian beryl</u>		
EEE-10	-3.2, -7.7	870
BLM-503	-3.7, -7.7	940
T-24	-4.0, -7.7	974
<u>Emeralds</u>		
Brazilian	-3.8, -7.9	945
Columbian		
(chips)	-3.1, -4.4, -8.6	809
Australian	-2.9, -8.0	778

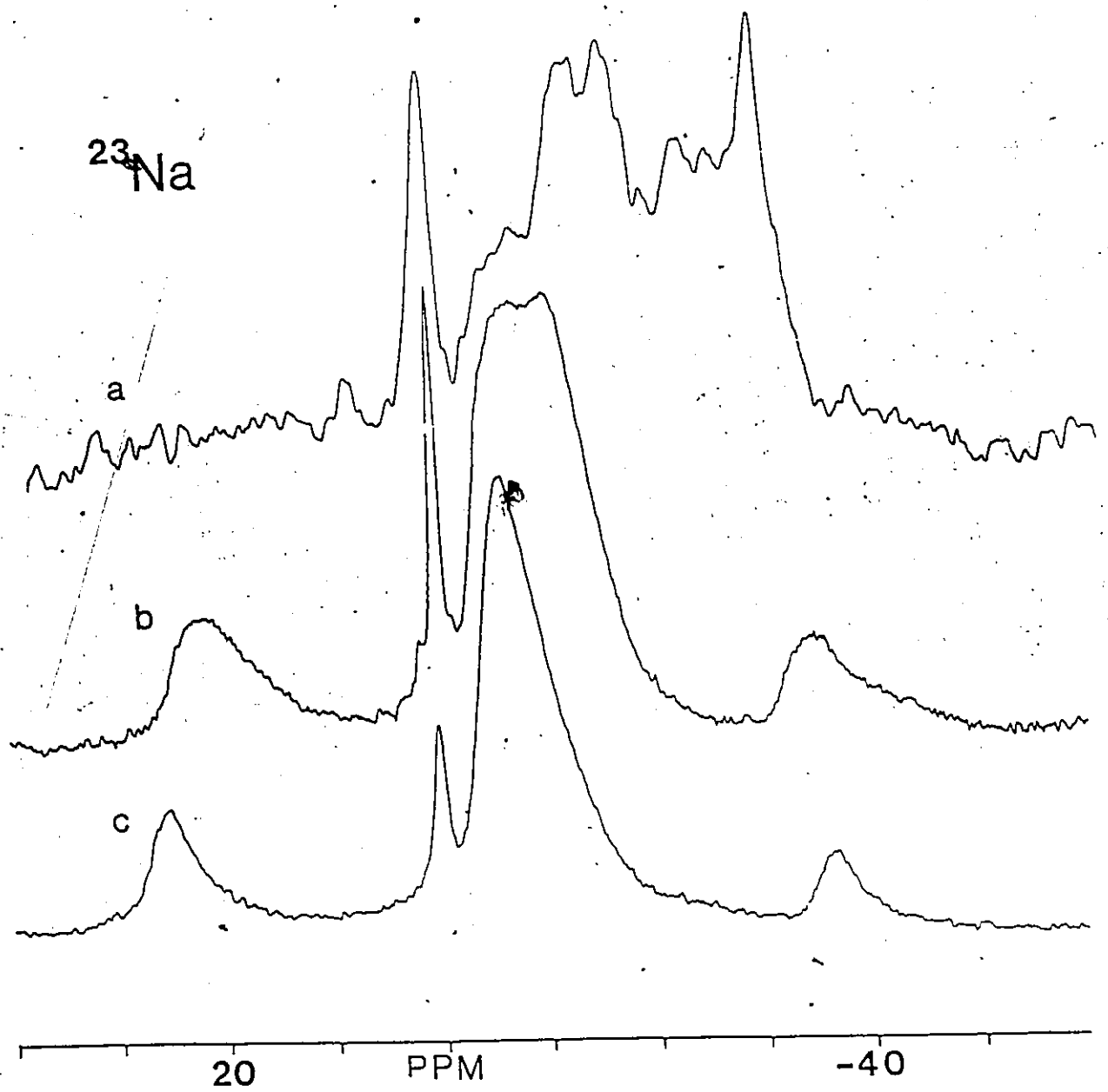
six silicate oxygens and with one or two water molecules (Hawthorne & Cerny 1977). This asymmetric site produces a broad quadrupolar doublet at about 10 ppm in the  $^{23}\text{Na}$  MAS nmr spectrum (Fig 4.4a). The spectrum of SHEE-1-6, which has the lowest concentration of sodium, had additional poorly resolved peaks between -5 and -35 ppm which are possibly due to sodium in defects and along grain boundaries in this sample (Fig 4.4b). These peaks would not be obvious in the spectra of more sodic samples because the very strong peak due to sodium in the channel sites would cause minor peaks to vanish into the baseline.

Quadrupolar effects can be reduced by spinning the sample at different angles to the magnetic field other than the magic angle as explained in Appendix I section I.5. As the angle between the rotational axis of the sample and the applied magnetic field  $H_0$  is progressively increased the quadrupolar doublet, from  $^{23}\text{Na}$  in the channel site of beryl, collapses to a singlet and becomes narrower (Fig 4.4c).

A narrow peak at 0 ppm (Fig 4.4) was present in most of the spectra. It varied in intensity relative to the quadrupolar doublet not only between samples but also between different aliquots of the same sample. There is an increase in the size of the peak at 0 ppm relative to the broad doublet when shorter time intervals are left between pulses, thus indicating that the site causing the narrow

Figure 4.4  $^{23}\text{Na}$  MAS nmr spectra of

- (a) SHEE-1-6 low alkali beryl
- (b) T-24 Li-Cs beryl
- (c) T-24 Li-Cs beryl spinning at an angle of approximately  $65^\circ$  to the applied magnetic field



peak has a faster relaxation rate than the quadrupolar doublet.

This narrow peak was also present in a static  $^{23}\text{Na}$  spectrum of sample T-24 whereas the peak centred at -10 ppm became a broad absorption curve (Fig 4.5). It also became progressively broader as the angle of rotation was moved away from the Magic Angle (Fig. 4.4c) and dipolar interactions were no longer removed (Eckert et al. 1988), indicating that the Na site responsible for this narrow peak, is sufficiently symmetrical for the chemical shift effects to be dominant over quadrupolar effects.

The possibility that the narrow peak could be due to contamination or to sodium loosely bound in fractures in the crystal was investigated by washing the beryl samples and rerunning the spectra. No reduction of signal was observed.

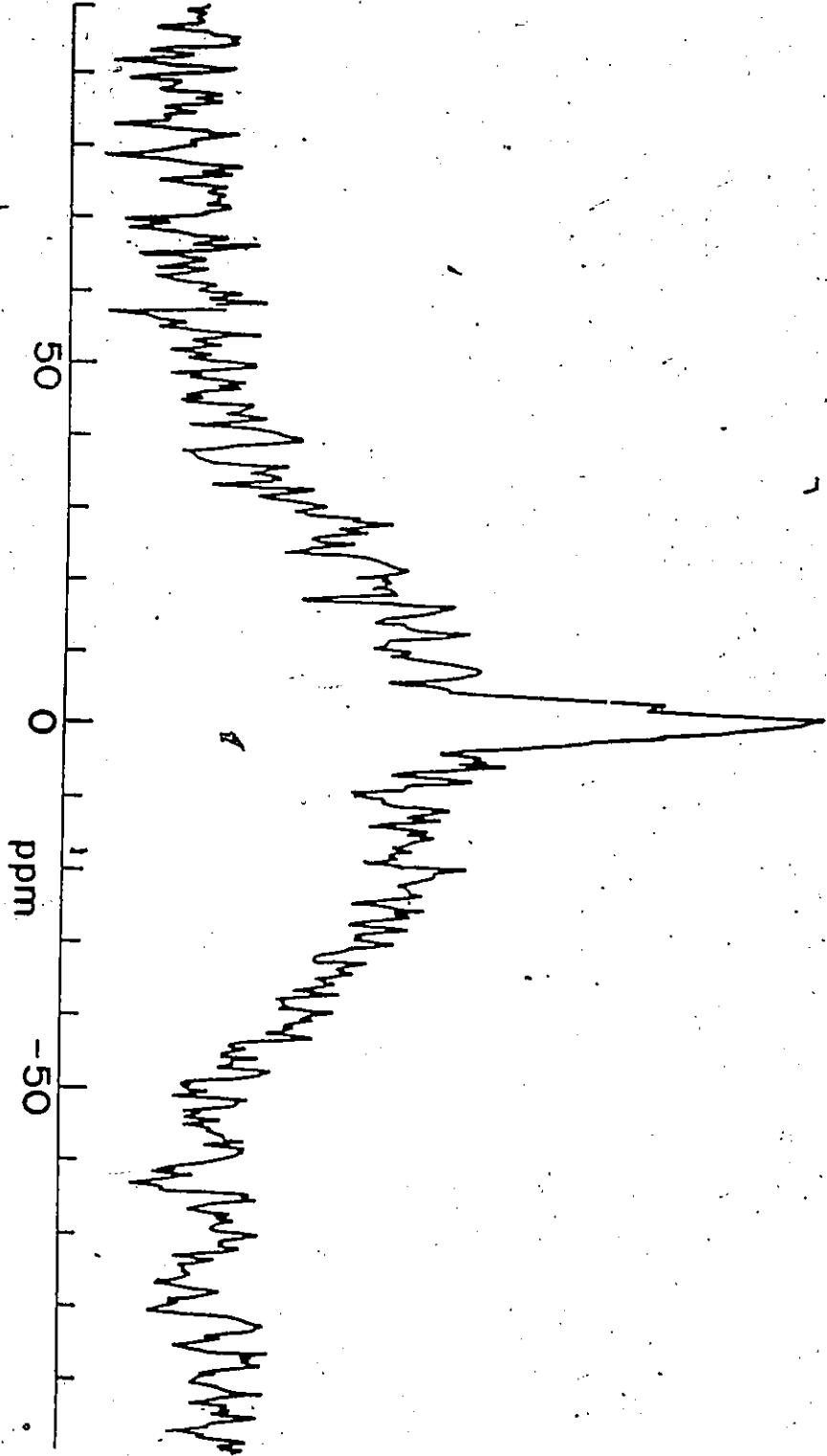
Solid NaCl resonates at +6.5 ppm (Fig. 4.6b) and becomes a broad absorption curve when spinning is stopped. NaCl in aqueous solution, has exactly the same chemical shift as the narrow peak in the spectra of beryls. This is shown by a comparison of spectra (a) and (c) in figure 4.6.

Microscopic examination of the samples of alkali beryls reveals abundant fluid inclusions. It is concluded that the peak at 0 ppm was due to  $\text{Na}^+$  in solution in these fluid inclusions (Sherriff et al. 1987b). The narrow peak is not present in the  $^{23}\text{Na}$  nmr spectra of minerals which



Figure 4.5  $^{23}\text{Na}$  static nmr spectrum of T-24 Li-Cs  
beryl. (Sherriff et al. 1987b)

$^{23}\text{Nd}$



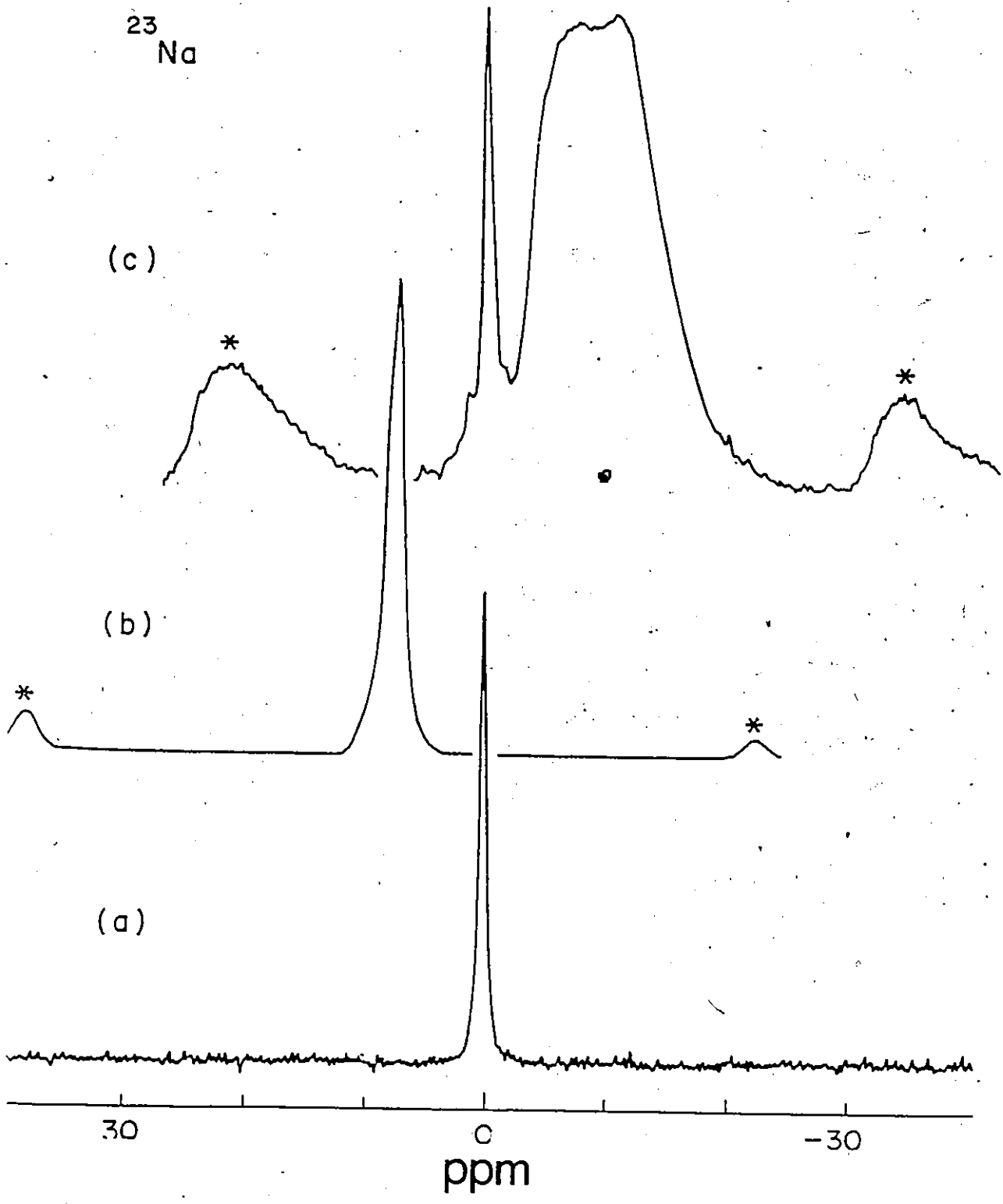
- Figure 4.6 (a)  $^{23}\text{Na}$  nmr spectrum of 1 molar aqueous solution of NaCl
- (b)  $^{23}\text{Na}$  MAS nmr spectrum of solid NaCl
- (c)  $^{23}\text{Na}$  MAS nmr spectrum of T-24 Li-Cs beryl

<sup>23</sup>Na

(c)

(b)

(a)



did not contain such abundant fluid inclusions.  $^{23}\text{Na}$  nmr signals have also been observed from halite rich fluid inclusions in quartz (Sherriff et al. 1987b).

#### 4.4.4 BERYLLIUM-9

Beryllium is in a distorted tetrahedral site linked to four silicate tetrahedra. All four Be-O distances are the same but the O-Be-O angles have values between 90 and  $131^\circ$ .

$^9\text{Be}$  MAS nmr spectra of low alkali beryls and the Columbian emerald all have one broad symmetric peak at about -2.4 ppm (Table 4.4; Fig. 4.7a). In the spectra of Li-Cs beryls the peak is narrower with a maximum at -1.6 and a shoulder at -2.6 ppm (Table 4.4, Fig 4.7b). This could be due to two overlapping peaks; one at about -2.4 ppm due to Be in low alkali type domains and one at -1.6 ppm from alkali rich domains. It could also be due to different second order quadrupolar effects for beryllium in the structures of Li-Cs and low alkali beryl.

There are three conflicting effects to consider in explaining the reason that the  $^9\text{Be}$  peak position for Li-Cs beryl is 1 ppm to low field of that of low alkali beryl.

Firstly, in studies of  $^{29}\text{Si}$  MAS nmr chemical shift it was discovered that chemical shift was directly affected by, and very sensitive to, changes in cation-oxygen bond

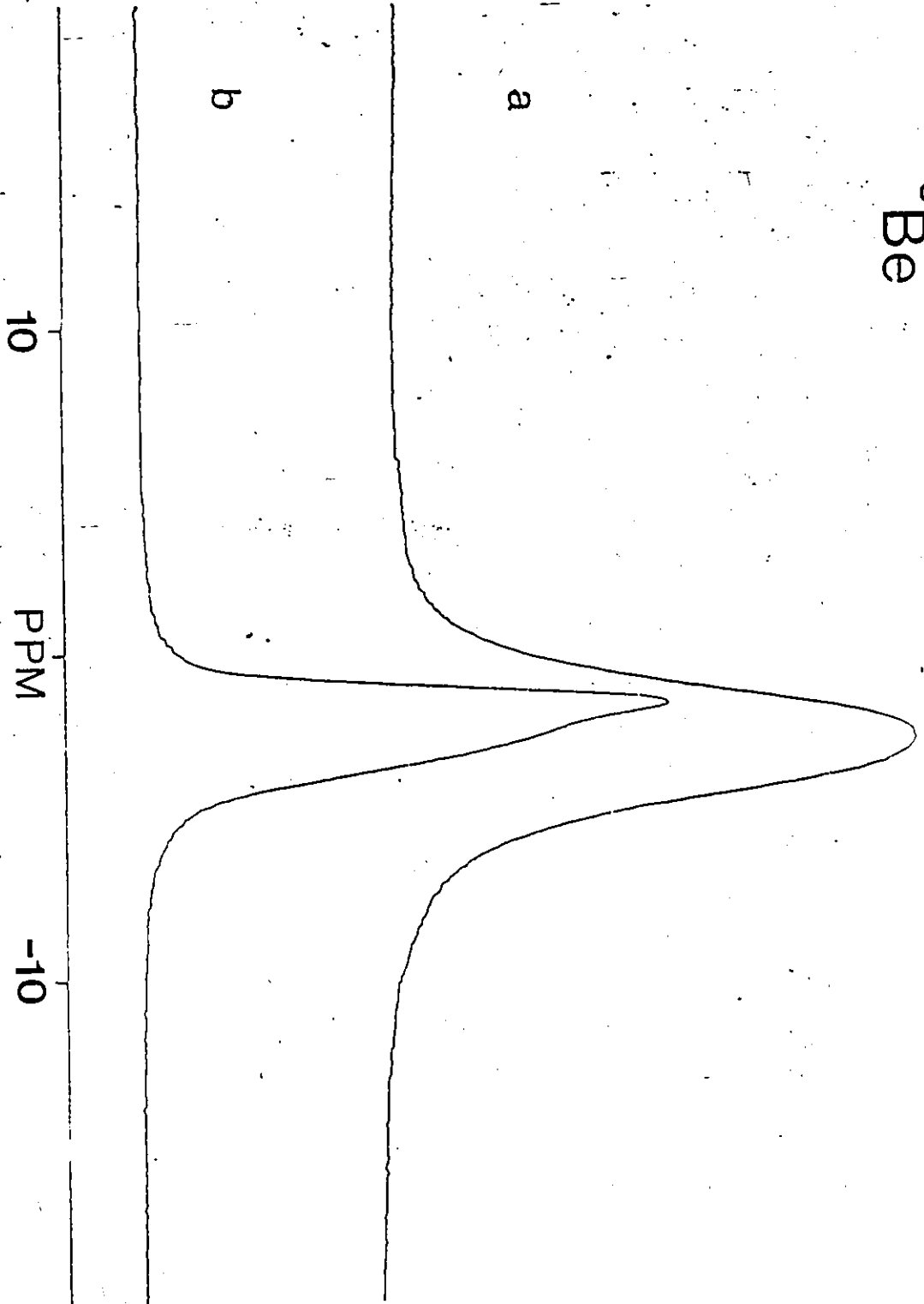
TABLE 4.4

<sup>9</sup>Be MAS nmr parameters for beryls

Sample	Peak Position (ppm)	Peak width at half height (Hz)
Be(NO <sub>3</sub> ) <sub>2</sub> (saturated aqueous solution)	0	130
<u>Low alkali beryl</u>		
SHEE-1-6	-2.5	215
BLS091	-2.4	207
BLS093	-2.4	266
BLS094	-2.5	215
<u>Lithian-cesian beryl</u>		
EEE-10	-1.6 -2.6	132
BLM-503	-1.6 -2.6	136
T-24	-1.6 -2.6	119
<u>Emeralds</u>		
Brazilian	-2.3	244

Figure 4.7  $^9\text{Be}$  MAS nmr spectra of  
(a) SHEE-1-6 low alkali beryl  
(b) T-24 Li-Cs beryl

$^9\text{Be}$





distance (Chapter 5). Increases in distance between the terminal oxygens of the silica tetrahedron and adjacent cations cause a shift to low field. If this idea is applied to  $^9\text{Be}$  MAS nmr spectra, the difference between the adjacent Si-O distances of 1.611 Å for Li-Cs beryl and 1.620 Å for low alkali beryls would cause a shift to high field for the Li-Cs beryl sites.

Secondly the Be-O tetrahedral distance being 0.017Å greater in Li-Cs beryls than in low alkali beryls would cause the opposite effect, i.e. the observed shift to low field.

Thirdly, as  $^9\text{Be}$  is a quadrupolar nuclei with a spin of 3/2, it experiences a quadrupolar shift (Appendix I.5). As the peak at -1.6 ppm appears to be narrower than the peak at -2.6 ppm the Be site in Li-Cs beryls could have a smaller quadrupolar moment than the Be site in low alkali beryls.

The difference between the  $^9\text{Be}$  spectra of low alkali and Li-Cs beryls shows that the Be site is different in the two structures. The difference in Be-O bond distance, shown by the diffraction data, is therefore not necessarily due to there being Li or Al in the  $\text{BeO}_4$  site but could be due to beryllium being in different environments in the two structures.

#### 4.4.5 LITHIUM-7

Lithium is postulated to replace either beryllium in tetrahedral configuration or aluminum in octahedral configuration in alkali beryls. Excess lithium can also occupy the 2b channel sites coordinated with six oxygens and one or two water molecules (Hawthorne & Cerny 1977). Another possible site for lithium is as lithium tetraborate in the abundant fluid inclusions (London 1987).

The beryl samples with a high lithium content give two  $^7\text{Li}$  MAS nmr peaks: a strong narrow peak at 0.8 ppm and a small peak at -1.6 ppm with respect to LiBr in aqueous solution (Table 4.5, Fig 4.8). The chemical shift range for  $^7\text{Li}$  is very small: only 2 ppm in solution nmr. Therefore the 2.4 ppm difference between these two MAS peaks suggests very different environments. These could be in channel sites, in octahedral or tetrahedral crystallographic sites or in solution in the fluid inclusions.

The large peak at 0.8 ppm is unlikely to come from fluid inclusions as there was no signal observed in a static  $^7\text{Li}$  spectrum. The coupled substitution of Li for Al and Al for Be is eliminated by the lack of a tetrahedral  $^{27}\text{Al}$  nmr peak. Therefore, the most likely interpretation of the  $^7\text{Li}$  spectra is that the peak at 0.8 ppm is due to Li in channel sites and that at -1.6 ppm due to Li replacing Be

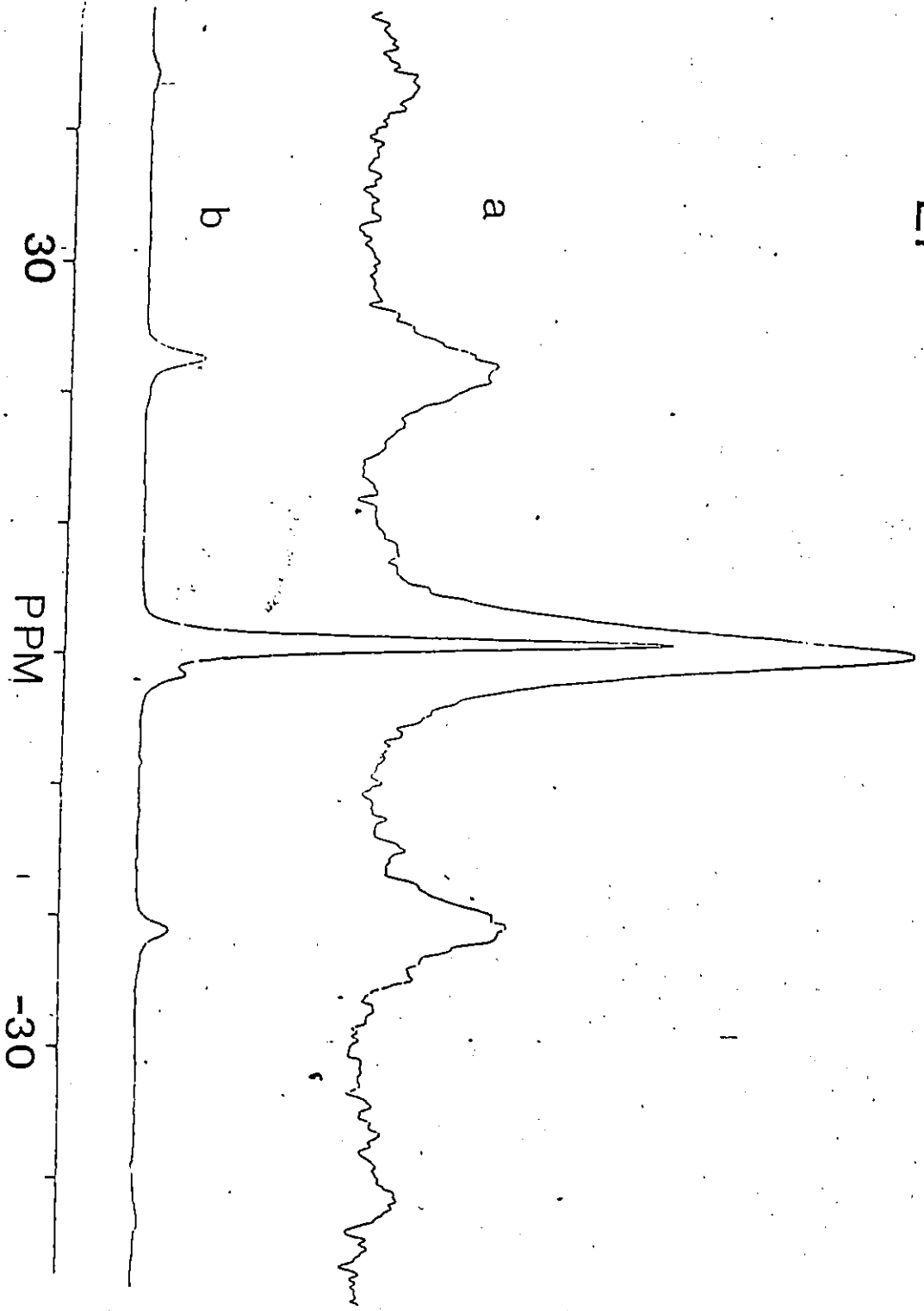
TABLE 4.5

<sup>7</sup>Li MAS nmr parameters for beryls

Sample	Peak Position (ppm)	Peak width at half height (Hz)
LiBr (saturated aqueous solution)	0	140
<u>Low alkali beryl</u>		
SHEE-1-6	0.5	488
<u>Lithian-cesian beryl</u>		
EEE-10	0.7 -1.6	146
BLM-503	0.6 -1.6	156
T-24	0.6 -1.8	150

Figure 4.8  $^7\text{Li}$  MAS nmr spectra of  
(a) SHEE-1-6 low alkali beryl  
(b) T-24 Li-Cs beryl

$^7\text{Li}$



in tetrahedral configuration.

Correct interpretation of MAS nmr spectra requires the ability to simulate the spectra from calculations of chemical shift from mineral structure. Although this can now be done for  $^{29}\text{Si}$  (Sherriff and Grundy 1988), it is not yet possible for other nuclei. Quadrupolar nuclei are especially complex as the quadrupolar shift is superimposed on the chemical shift.

The low alkali sample of beryl, SHEE-1-6, gave a very weak  $^7\text{Li}$  spectrum with a broad peak and large spinning sidebands (Fig 4.8a). This is probably due to small amounts of lithium in a variety of environments, possibly along grain boundaries and in lattice defects as well as in crystal sites and fluid inclusions. As with  $^{23}\text{Na}$  these minor peaks vanish into the baseline when a strong peak in the spectrum overwhelms the minor peaks.

#### 4.5 CONCLUSIONS

This multinuclear MAS nmr study illustrates that useful information about type, environment and symmetry of atomic sites can be obtained even when each spectrum contains only one peak.

Simulation of  $^{29}\text{Si}$  MAS nmr spectra by the technique described in chapter 2, helps in interpreting slight differences between spectra of very similar minerals.

Studies to find relationships between structure and nmr chemical shift for other nuclei would result in a much better understanding of the MAS nmr of these more exotic nuclei.

$^9\text{Be}$  and  $^{29}\text{Si}$  MAS nmr results are in agreement with the presence of domains in the Li-Cs beryls which have structures like low-alkali beryls. The lack of a tetrahedral peak in the  $^{27}\text{Al}$  spectra of Li-Cs beryls eliminates the possibility of a coupled substitution of Li for Al and Al for Be.

The  $^{23}\text{Na}$  peak from NaCl in solution in the fluid inclusions shows the potential of nmr to study the chemistry of fluid inclusions. Also care must be taken in the interpretation of spectra from minerals which contain fluid inclusions.

## CHAPTER 5

### MODELLING THEORETICAL SILICATE STRUCTURES, AND THOUGHTS FOR THE FUTURE

#### 5.1 INTRODUCTION

In this study crystal models have been simulated, from the atomic positions and symmetry elements of mineral structures. In chapter 3 a model of 37% meionite scapolite, with Al-Si ordered in the tetrahedral sites, was used as a starting point to investigate the disordered structure of the rest of the scapolite series of minerals. In this case cation-oxygen bond distances ( $r$ ) were changed to create models representative of the silicon environment seen by  $^{29}\text{Si}$  nmr in contrast to the average environment given by diffraction techniques.

In this chapter models of theoretical structures are based on a symmetrical  $\text{SiO}_4$  tetrahedron with Al or Si atoms added as ligands. These are then used to examine the effect on the calculations of chemical shift of changing the structural parameters, cation-oxygen distance ( $r$ ) and silicon-oxygen-cation angle ( $\alpha$ ) (Fig. 2.1).

The values of  $\chi''$  for the Al-Si tetrahedral framework of all possible silicate structures are



calculated. The effects of other cations, in each silicate group, are taken from the calculations producing values of chemical shift in Appendix VIII. From these two sets of  $\chi''$  values the possible range of chemical shift for each type of silicate is estimated and compared with the original ranges of Lippmaa et al. (1980) (Fig. 1.1).

## 5.2 $\text{SiO}_4$ TETRAHEDRAL MODEL

An  $\text{SiO}_4$  tetrahedron with perfect cubic symmetry, all O-Si-O angles  $109.47^\circ$  and all Si-O distances 1.59 Å, was simulated using Chem-X crystal structure modelling program. Then either one Si or Al atom was added to one of the terminal oxygen.

Distance (r) for the ligand was varied by 0.01 Å increments from 1.67 to 1.75 Å for Al and from 1.55 to 1.67 Å for Si. Three different values of angle  $\alpha$ ;  $180^\circ$ ,  $155^\circ$  and  $130^\circ$ , were used for each distance (r).

Angle ( $\alpha$ ) was also varied from  $125^\circ$  to  $180^\circ$ , by  $5^\circ$  intervals using distances (r) of 1.59 Å for the silicon ligand and of 1.75 Å for the aluminum ligand. Values of  $\chi''$  and hence  $^{29}\text{Si}$  chemical shift were calculated for these models from equations 3 and 4. Calculated values of chemical shift were plotted firstly against (r) for three values of angle ( $\alpha$ ) (Fig. 5.1) and secondly versus angle  $\alpha$  for two values of (r) (Fig. 5.2) to examine the effect on

Figure 5.1 Cation-oxygen distance ( $r$ ) plotted against calculated chemical shift for one Si or Al ligand on a terminal oxygen of a symmetrical  $\text{SiO}_4$  tetrahedron. Angle ( $\alpha$ ) is; (a)  $130^\circ$ , (b)  $155^\circ$ , (c)  $180^\circ$ . Distance ( $r$ ) is 1.55 to 1.67 Å for Si-O and 1.67 to 1.76 Å for Al-O. The discrepancy at 1.67 Å is caused by the change in type of cation from Si to Al.

CATION-OXYGEN DISTANCE (r) (ANGSTROMS)

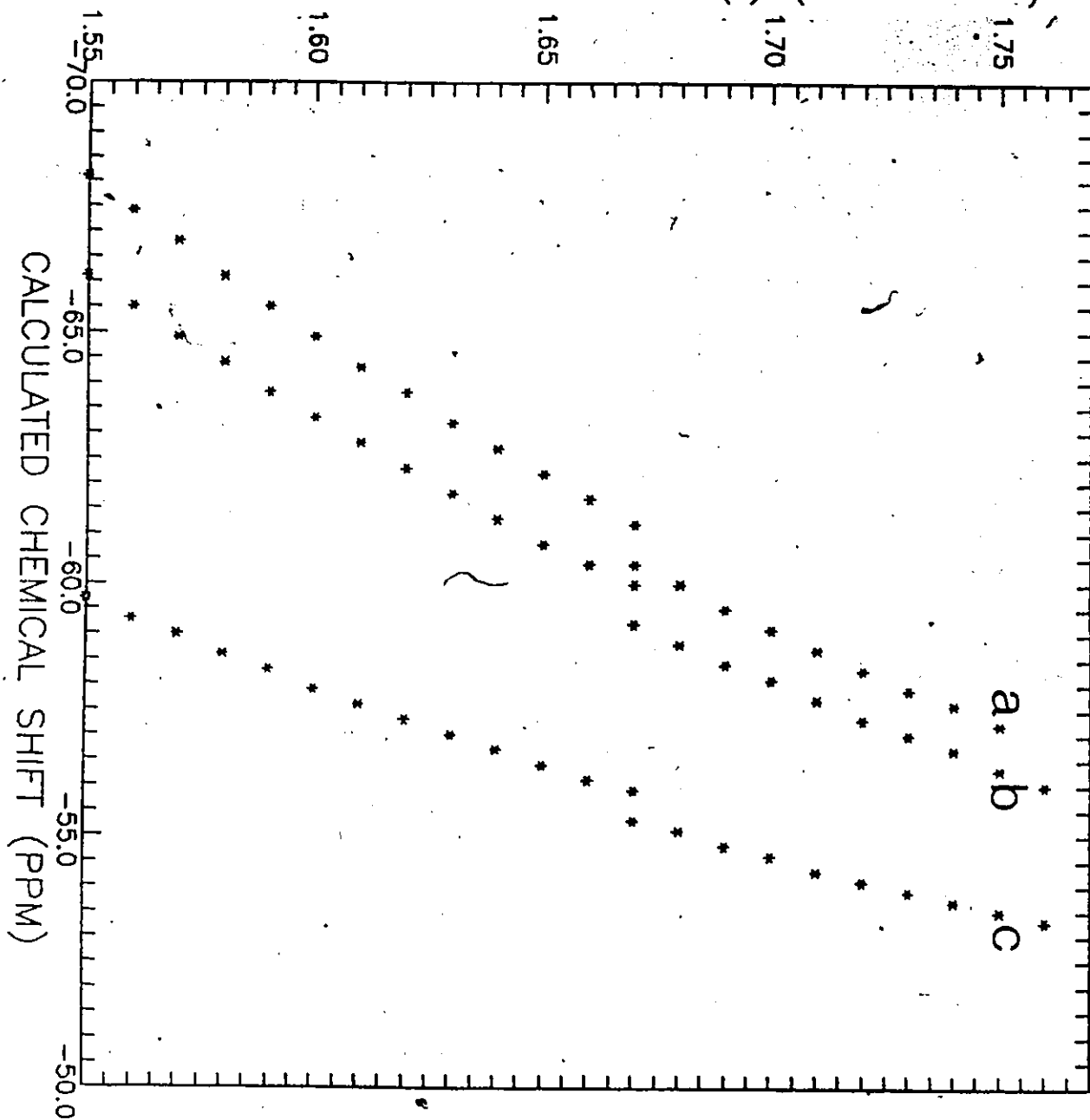
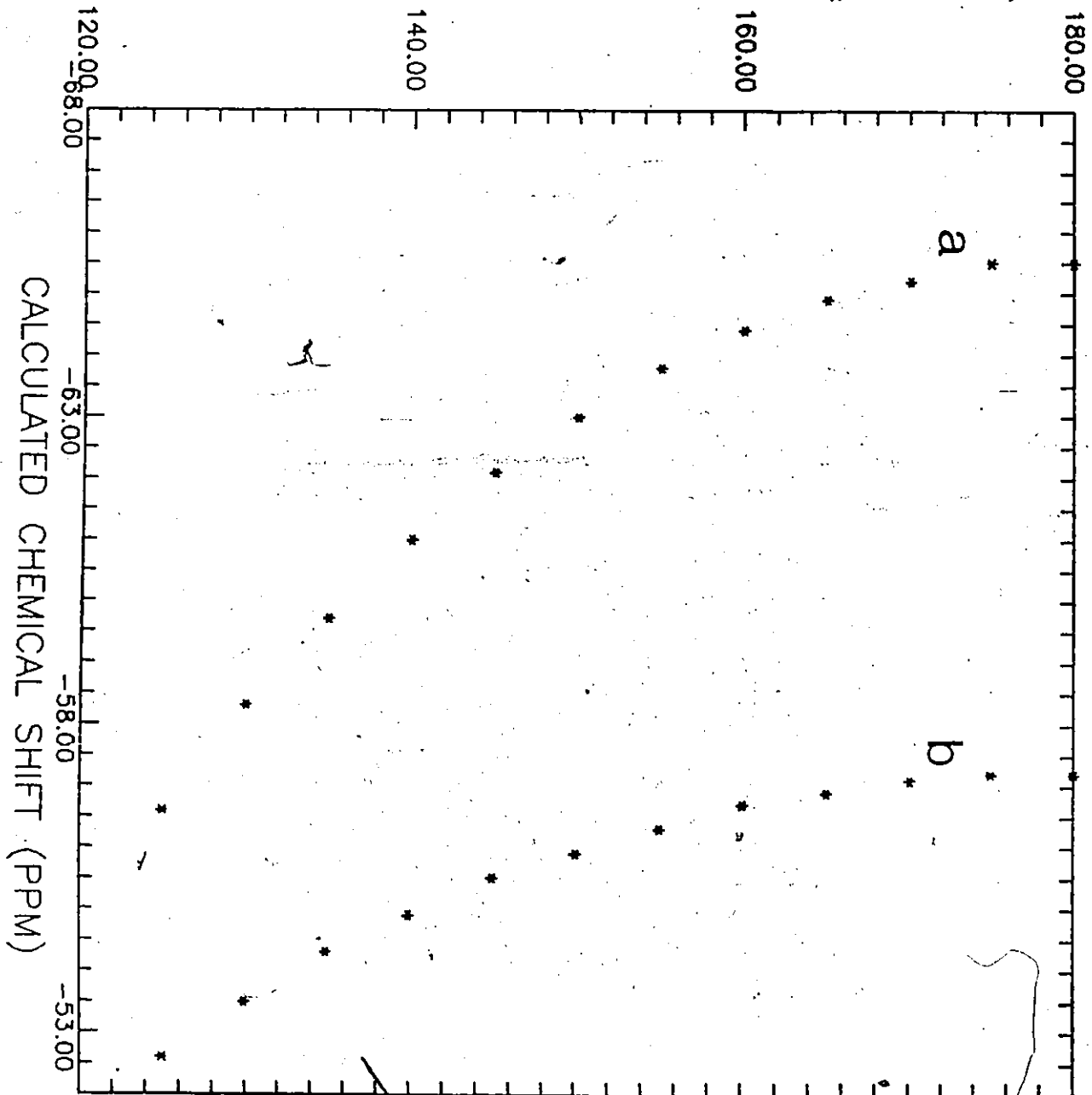


Figure 5.2 A plot of angle ( $\alpha$ ) against calculated chemical shift for; (a) Si-O ( $r = 1.59 \text{ \AA}$ ) and (b) Al-O ( $r = 1.76 \text{ \AA}$ ).

SILICON-OXYGEN-CATION ANGLE (DEGREES)



the calculation of changes in these structural parameters.

The  $\chi''$  values from one Si or Al ligands were multiplied by 2, 3, and 4 to calculate values of  $\chi''$  for ino, phyllo and tectosilicates. The value of  $\chi''$  for the framework of orthosilicates is zero as there are no tetrahedral Si or Al bonds involved in the calculation. All contributions to chemical shift of the orthosilicates come from other cations.

In Table 5.1 the maximum and minimum values of  $\chi''$  are listed for the other cations. These were calculated from the mineral structures, listed in appendix VIII, for each silicate group. These values were then added to the maximum and minimum values of  $\chi''$  for the Al-Si framework calculated from the theoretical model. The results give the ranges of chemical shift possible for each group of silicate minerals (Fig. 5.3).

### 5.3 RESULTS AND DISCUSSION

There is a linear relationship between Si-O or Al-O distance and chemical shift (Fig. 5.1; Appendix IX). Three linear trends are produced by varying cation-O distances, with angle  $\alpha$  set at 180, 155 and 130°. The slopes of the three lines are different because of the effect of changing the angle ( $\alpha$ ) but the correlation coefficient is identical at 0.996 for each line. Realistic values of chemical shift

were produced by changing the ligand cation from Si to Al at distance ( $r$ ) of 1.67 Å, which gives a kink in each line.

The relationship between chemical shift and angle ( $\alpha$ ) is not a straight line but a curve (Fig. 5.2) which is more sensitive to changes of Si-O-T angle at the small values than near  $180^\circ$ . The two trends in Fig. 5.2 are due to the calculations using either Si or Al.

The ranges of chemical shift, for the different types of silicate groups, (Fig. 5.3, Table 5.1) while following the same trend as those of Lippmaa et al. (1981) (Fig. 2.1) show considerably more overlap. These ranges are therefore of limited use for allocating peaks in spectra. As chemical shift is linearly dependant on cation-oxygen distance the shift to high field with increasing condensation can be correlated with an increase in number of short tetrahedral bonds rather than long cation-oxygen bonds from other coordinations of cations.

The shift to low field with replacement of Si next nearest neighbours by Al, found by Lippmaa et al. (1981) can be explained by the larger size of the Al atom compared with Si increasing the distance ( $r$ ) from about 1.59 Å to 1.75 Å. There is also a slight shift due to the different valence value of Si and Al, which is shown by duplicate measurements made at a distance ( $r$ ) of 1.67 Å for Si and Al. The difference between the duplicate measurements varies from 0.82 ppm for angle ( $\alpha$ ) of  $180^\circ$  to 0.53 ppm for

Figure 5.3 Theoretical ranges of  $^{29}\text{Si}$  MAS nmr chemical shift for the five groups of silicates; (a) tectosilicates, (b) phyllosilicates, (c) inosilicates, (d) sorosilicates, (e) orthosilicates.



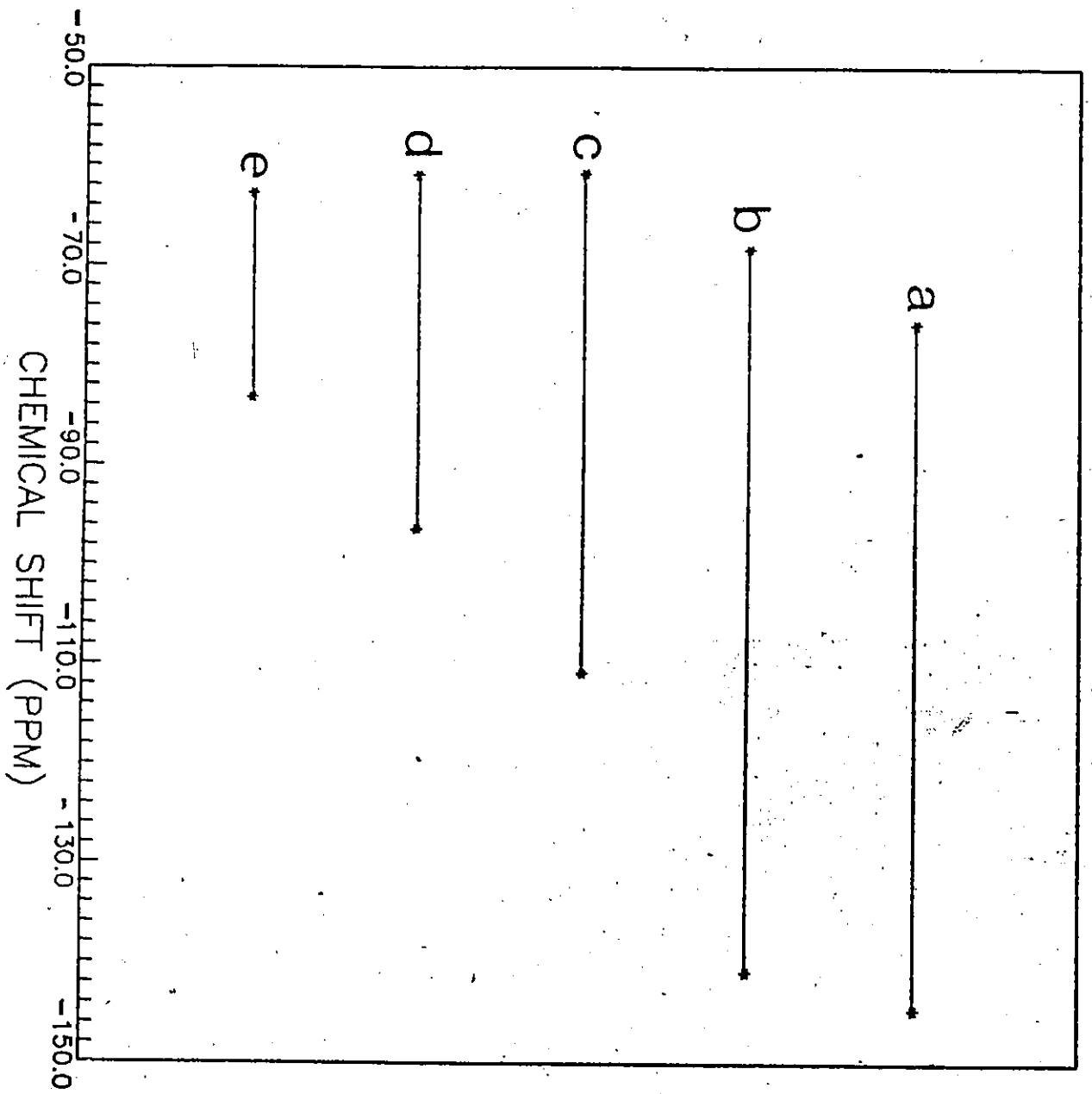


Table 5.1Possible ranges of  $^{29}\text{Si}$  nmr chemical shift

	$\Omega''$ Si-Al framework	$\Omega''$ other cations	$\Omega''$ total	calculated chemical shift (ppm)
orthosilicates				
minimum	-	-0.02243	-0.02443	-62.8
maximum	-	-0.05331	-0.05331	-83.3
sorosilicates				
minimum	-0.01078	-0.01104	-0.02182	-61.0
maximum	-0.03194	-0.04032	-0.07226	-96.4
inosilicates				
minimum	-0.02156	-0.00638	-0.02794	-60.8
maximum	-0.06288	-0.03010	-0.09298	-110.9
phyllosilicates				
minimum	-0.03234	0.00000	-0.03234	-68.4
maximum	-0.09582	-0.04003	-0.13585	-140.9
tectosilicates				
minimum	-0.04312	0.00000	-0.04312	-75.9
maximum	-0.12776	-0.01338	-0.14114	-144.6

Si-O-T angle of  $130^\circ$ .

#### 5.4 PRESENT STATE OF CHEMICAL SHIFT CALCULATIONS

It is now possible to calculate  $^{29}\text{Si}$  chemical shift for ordered silicate structures directly from atomic positions found by diffraction techniques and also to use  $^{29}\text{Si}$  MAS nmr together with theoretical models of structures to study structures with cation disorder.

The zone of influence of atoms on chemical shift has been shown to be very small with only the position of atoms bonded to the terminal oxygens of the  $\text{SiO}_4$  tetrahedron are involved in the calculation of chemical shift.

The relationship developed in this study can explain the chemical shift ranges of Lippmaa et al (1981), relationships between chemical shift and structural parameters such as bond length ( $r$ ), and angle ( $\alpha$ ) including a function for the electronegativity of the cations in the structure.

#### 5.5 Ideas for the Future

$^{29}\text{Si}$  MAS nmr can be used to study reactions on the surface of materials. There have been changes documented in  $^{29}\text{Si}$  MAS nmr spectra of zeolites relating to local changes

in structure when sorbate organic molecules are present (Fyfe et al. 1988). The changes in  $^{29}\text{Si}$  spectra for sorbates in different positions on a silicate surface can be calculated and information about mechanisms of adsorption can be found by relating simulated spectra to experimental results.

The relationship between the  $^{29}\text{Si}$  chemical shift of tetrahedral silicate groups could be extended to octahedrally coordinated silicon, e.g. stishovite. It could also be used to study silicon in structures with different anions such as SiC (Richardson et al. 1988) and  $\text{SiN}_2$  (Carduner et al. 1987). The structural constraints on chemical shift should be the same in all cases but the difference in covalence of the different bonds would probably give different regression equations.

A method similar to that described in chapter 2 could investigate the relationship between structure and chemical shift for other isotopes with spins of  $1/2$ .  $^{31}\text{P}$  in tetrahedral coordination in the  $\text{PO}_4$  group in phosphates should be analogous to  $^{29}\text{Si}$  in silicates. However in this case, the magnetic isotope is 100% abundant there will be dipolar interactions between adjacent  $^{31}\text{P}$  nuclei causing broad, poorly resolved peaks.  $^{13}\text{C}$  nmr of carbonate groups in different environments have a narrow chemical shift range but could be investigated by this method. Other spin  $1/2$  nuclei that would be geologically interesting to study

using MAS nmr include  $^{19}\text{F}$  and  $^{207}\text{Pb}$ .

It is much more difficult to study MAS nmr chemical shift of isotopes with spin greater than  $1/2$  because quadrupolar shift is usually much greater than chemical shift. It is possible to model quadrupolar peak shapes (Fyfe 1983) and deduce the quadrupolar moment of single peaks from static powder patterns. Calculation of chemical shift from model structures of quadrupolar nuclei would require first removing the quadrupole effects from the spectra as has been demonstrated by Lippmaa (1986) for  $^{27}\text{Al}$ . Quadrupolar effects would then be combined with calculated chemical shift to simulate the experimental spectra.

Experimental techniques that can be used to reduce the quadrupolar effect include increasing the magnetic field strength, spinning the sample at a speed of at least 20 KHz, or changing the angle of rotation. 2D nmr in conjunction with pulse techniques such as nutation spectroscopy (DeJong & Veeman 1986) has been used to separate quadrupolar from chemical shift for  $^{23}\text{Na}$ . 2D spectra of less sensitive nuclei are difficult to obtain because of the large amount of instrument time required to obtain the data.

The small selection of possibilities for future nmr studies, discussed above, show that the method of studying  $^{29}\text{Si}$  chemical shift described in this thesis has increased

considerably the potential of solid state nmr.

## REFERENCES

- Abragam, A. (1961): The principles of nuclear magnetism. Oxford University Press, pp 599.
- Alberti, A., Vezzalini, G. & Tazzoli, V. (1981): Thomsonite: a detailed refinement with cross checking by crystal energy calculations. Zeolites 31, 91-97.
- Alexander, C. M. O., Hutchinson, R., Graham, A. L. & Yabuki, H. (1987): Discovery of scapolite in the Bishunpur (LL3) chondritic meteorite. Mineral. Mag. 51, 733-735.
- Altermatt, D., & Brown, I. D., (1985): The automatic searching for chemical bonds in inorganic crystal structures. Acta. Cryst. B41 240-244.
- Aitken, B. G., Evans, H. T. & Konnert, J. A. (1984): The crystal structure of a synthetic meionite, Neues Jahrb. Mineral. (Abhand.), 149, 309-324.
- Barnes, J. R., Clague, A. D. H., Claydon, N. J., Dobson, C. M., Hayes, C. J., Groves, G. W. & Rodger, S. A. (1985): Hydration of Portland cement followed by  $^{29}\text{Si}$  solid state nmr spectroscopy. J. Mat. Sci. Lett. 4, 1293-1295.
- Barron, P. F., Frost, R. L., Skjenstad, J. O. & Koppi, A. J. (1983): Detection of two Si environments in kaolins by solid state  $^{29}\text{Si}$  nmr. Nature 302, 49-50.
- Barron, P. F. & Frost, R. L. (1985): Solid state  $^{29}\text{Si}$  nmr examination of the 2:1 ribbon magnesium silicates sepiolite and palygorskite. Amer. Mineral., 70, 758-766.
- Baur, W. H. & Ohta, T. (1982): The Si<sub>5</sub>O<sub>16</sub> pentamer in zunyite refined and empirical relations for individual silicon-oxygen bonds, Acta. Cryst. B38, 390-401.
- Baur, W. H. (1977): Silicon-oxygen bond lengths, bridging angles Si-O-Si and synthetic low tridymite, Acta. Cryst. B33, 2615-2619.
- Baur, W. H., (1978): Crystal structure refinement of lawsonite. Amer. Mineral., 63, 311-315.

- Becker, E. D. (1980): High resolution nmr, Academic Press, New York, pp 354.
- Bergerhoff, G., Hundt, R., Sievers, R. & Brown, I. D., (1983): The Inorganic Crystal Structure Data Base J. Chem. Inf. Comput. Sci. 23, 66-69.
- Birle, J. D., Gibbs, G.V., Moore, P. B. & Smith, J. V. (1968): Crystal structures of natural olivine, Amer. Mineral. 53, 807-824.
- Börcher, W. & Keidel, J. (1964): Beiträge zur reaktionsfähigkeit der silikate bei niedrigen temperaturen II Mitteilung die strukturen. Beitr. zur Mineral. und Petrol. 10, 132-140.
- Brevard, C. & Granger, P. (1981): Handbook of high resolution multinuclear nmr. John Wiley & Sons, New York.
- Brindley, G. W. & Robinson, K. (1946): The structure of kaolinite. Mineral. Mag. 627, 242-253.
- Brown, B. E. & Bailey, Y. W. (1964): The structure of maximum microcline, Acta Crystallogr., 17, 1391-1400.
- Brown, I. D. (1981): Chapter 14. The bond valence method: An empirical approach to chemical structure and bonding in Structure and Bonding in crystals vol II, Academic Press Inc.
- Brown, I. D. & Altermatt, D. (1985): Bond valence parameters obtained from a systematic analysis of the inorganic crystal structure database. Acta Crystallogr. B41, 244-247.
- Brown, I. D., & Shannon, R. D., (1973): Empirical bond-strength bond length curves for oxides. Acta Cryst. A29, 266-282.
- Bruno, E., Carbonin, S. & Molin, G., (1982): crystal structures of Ca-rich clinopyroxenes on the  $\text{CaMgSi}_2\text{O}_6$ - $\text{Mg}_2\text{Si}_2\text{O}_6$  join. Tschermaks Mineral. Petrogr., 29, 223-240.
- Burnham C.W. (1963b): Refinement of the crystal structure of kyanite. Z. Kristallogr. 118, 337-360.
- Burnham C.W. (1963b): Refinement of the crystal structure of sillimanite, Z. Kristallogr. 118, 127-148.



- Burnham, C. W. & Buerger, M. J. (1961): Refinement of the crystal structure of andalusite, Z. Kristallogr., 115, 269-290.
- Carduner, K. R., Carter, R. O. III, Milberg, M. E. & Crosbie, G. M. (1987): Determination of phase composition of silicon nitride powders by  $^{29}\text{Si}$  MAS nmr spectroscopy. Anal. Chem. 59, 2794-2797.
- Chamberlain, C. P., Docka, J. A., Post, J. E. & Burnham, C. W. (1985): Scapolite: alkali atom configurations, antiphase domains, and compositional variations. Amer. Mineral., 70, 134-140.
- Clark, J. R., Appleman, D. E. & Papike, J. J. (1969): crystal chemical characterization of clinopyroxenes based on eight new structure refinements Mineral. Soc. Amer. Spec. Paper, 2, 31-50.
- De Jong, B. H. W. S., van Hoek, J., Veeman, D. V. & Manson, D. V. (1987): X-ray diffraction and  $^{29}\text{Si}$  MAS nmr of opals; incoherent long and short range order in opal-CT. Amer. Mineral., 72, 1195-1203.
- De Jong, B. H. W. S. & Veeman, W. S. (1986):  $^{29}\text{Si}$  MAS and  $^{23}\text{Na}$  nutation nmr reveal that local sodium environment is the principal difference between sodium silicate gel and glass. Abstracts of the 14th General Meeting of the International Mineral. Assoc. Stanford, California; 87.
- Dollase, W. A., (1965): Reinvestigation of the structure of low-cristobalite, Z. Kristallogr., 121, 369-377.
- Dollase, W. H. (1969): Crystal structure and cation ordering of piemontite, Amer. Mineral., 54, 710-717.
- Dollase W.A. (1970): Least-squares refinement of the structure of a plutonic nepheline, Z. Kristallogr., 132, 27-44.
- Donnay, G. & Buerger, M. J. (1950): Determination of the crystal structure of tourmaline, Acta. Cryst. 3, 379-388.
- Drits, V. A. & Kashaev, A. A. (1960): An X-ray study of a single crystal of kaolinite, Kristallogr., 5, 224-227.
- Dupree, R., Holland, D. & Williams, D. S. (1986): Structure of binary alkali silicate glasses J. Noncryst. Solids, 81, 399-410.

- Dupree E., & Pettifer, R. F., (1984): Determination of the Si-O-Si bond angle distribution in vitreous silica by magic angle spinning nmr. Nature 308, 523-525
- Eckert, H., Yesinowski, J. P., Silver, L. A. & Stolper E. M. (1988): Speciation of water in glasses by high-speed  $^1\text{H}$  MAS-nmr Abstracts 29th Experimental nmr spectroscopy conference, Rochester, New York, abstract number 120, page 159.
- Effenberger, H. (1980): Petalit verfeinerung der kristallstruktur. Tschermaks Mineral. Petrogr. 27, 129-142.
- Engelhardt, G., Magi, M. & Lippmaa, E. (1973):  $^{29}\text{Si}$  nmr spektroskopische untersuchungen an methyl und methyl-phenyl-siloxanen und ihre anwendung in der silikonanalytik, J. Organomet. Chem., 54, 115-122.
- Engelhardt, G., & Radeaglia, R. (1984): A semi-empirical quantum-chemical rationalization of the correlation between SiOSi angles and  $^{29}\text{Si}$  nmr chemical shifts of silica polymorphs and framework aluminosilicates. Chem. Phys. Letters 108, 271-274.
- Ernst, C.A., Spialter, L., Buell, G. R., & Wilhite, D. L., (1974): Silicon-29 nuclear magnetic resonance. Chemical shift substituent effects. J. Amer. Chem. Soc. 96, 5375-5381.
- Evans, B. E., Shaw, D. M. & Haughton, D. R. (1969): Scapolite stoichiometry. Contr. Mineral. and Petrology. 24, 293-305.
- Faelth, L. & Hansen, S. (1979): Structure of scolecite from Poona, India. Acta Crystallogr. 35, 1877-1880.
- Fischer, K. (1969): Verfeinerung der kristallstruktur von Benitoit. Z. Kristallogr. 129, 222-243.
- Foit, F. F. Jr., Phillips, M. W. & Gibbs, G. V., (1973): A refinement of the crystal structure of datolite, Amer. Mineral. 1973, 58, 909-914.
- Fyfe, C. A. (1983): Solid state nmr for chemists. CFC Press, Guelph, Ontario.

- Fyfe, C. A., Gobbi, G. C., Hartman, J. S., Lenkinski, R. E., O'Brien, J. H., Beange, E. R. & Smith, M. A. R. (1982): High resolution solid state MAS spectra of  $^{29}\text{Si}$ ,  $^{27}\text{Al}$ ,  $^{11}\text{B}$  and other nuclei in inorganic systems using a narrow bore 400MHz high resolution nmr spectrometer. J. Magn. Resonance, 47, 168-173.
- Fyfe, C. A., Kennedy, G. J., De Schutter, C. T. & Kokotailo, G. T. (1984): Sorbate-induced structural changes in ZSM-5 (Silicalite) J. Chem. Soc. Chem. Commun. 541-542.
- Fyfe, C. A., O'Brien, J. H. & Strobl, H. (1987): Ultra high resolution  $^{29}\text{Si}$  MAS nmr spectra of highly siliceous zeolites. Nature 326, 281-282.
- Fyfe, C. A., Strobl, H., Kokotailo, G. T., Kennedy, G. T. & Barlow, G. E., (1988): Ultra-high Resolution  $^{29}\text{Si}$  solid-state MAS nmr investigation of sorbate and temperature induced changes in the lattice structure of zeolite ZSM-5, J. Amer. Chem. Soc. 110, 3373-3380.
- Fyfe, C. A., Thomas, J. M., Klinowski, J. & Gobbi, G. C. (1983): Magic Angle Spinning nmr spectroscopy and the structure of zeolites. Angew Chem. Int. Ed. Engl., 22, 259-275.
- Galli, E., Passaglia, E. & Zanazzi, P. F. (1982): Gmelinite: structural refinements of sodium rich and calcium rich natural crystals. Neues Jahrb. Mineral. (Aband) 1145-1155.
- Ganapathy, S., Schramm, S. & Oldfield, E. (1982): VARIable angle sample spinning high resolution nmr of solids, J. Chem Phys. 71, 4360-4368.
- Gibbs, G. V., (1982): Molecules as models for bonding in silicates. Amer. Mineral. 67, 421-450.
- Gibbs, G. V., Breck, D. W. & Meigher, E. P. (1968): Structural refinement of hydrous and anhydrous synthetic beryl  $\text{Al}_2(\text{Be}_3\text{Si}_6)\text{O}_{18}$  and emerald  $\text{Al}_{1.9}\text{Cr}_{0.1}(\text{Be}_3\text{Si}_6)\text{O}_{15}$ . Lithos 1, 275-285.
- Gibbs, G.V., Prewitt, C.T. & Baldwin, K. J. (1977): A study of the structural chemistry of coesite, Z. Kristallogr. 145, 108-123.
- Gibbs, G. V., Ribbe, P. H. & Anderson, C. P. (1970): The crystal structures of humite minerals II chondrodite. Amer. Mineral., 55, 1182-1194.

- Gladdeq, L. F., Carpenter, T. A. & Eliot, S. R. (1986):  $^{29}\text{Si}$  MAS nmr studies of spin-lattice relaxation time and bond angle distribution in vitreous silica. Phil. Mag. 853, L81-L87.
- Grimmer, A. -R., (1985): Correlation between individual Si-O bond lengths and the principal values of the  $^{29}\text{Si}$  chemical shift tensor in solid silicates. Chem. Phys. Letters 119, 416-420.
- Grimmer, A. -R., Peter, R., Echner, E., & Molgedey, G., (1981): High-resolution  $^{29}\text{Si}$  nmr in solid silicates. Correlations between shielding tensor and Si-O bond length. Chem. Phys. Letters 77, 331-335
- Grimmer, A. -R., Radeaglia, R., (1984): Correlation between the isotropic  $^{29}\text{Si}$  chemical shifts and the mean silicon-oxygen bond lengths in silicates. Chem. Phys. Letters 106, 262-265
- Grimmer, A. -R., von Lampe, F., Mägi, M., & Lippmaa, E., (1983): Solid-state high-resolution  $^{29}\text{Si}$  nmr: Si-O-Si bond angle and chemical shift in disilicates. Monatsh. Chemi. 114, 1053-1057.
- Grimmer, A. -R., von Lampe, F., Mägi, M., & Lippmaa, E., (1984): Solid-state high-resolution  $^{29}\text{Si}$  nmr: influence of the Si-O-Si bond angle on the isotropic chemical shift in t- and h- $\text{Y}_2\text{Si}_2\text{O}_7$ . Monatsh. Chemi. 115, 561-564.
- Grobet, P. J., Mortier, W. J. & Van Genechten, K. (1985): Influence of the cation distribution in zeolites on the isotropic  $^{29}\text{Si}$  nmr chemical shift. Chem. Phys. Lett., 119, 361-364.
- Grundy, H. D. & Hassan, I. (1982): The crystal structure of carbonate-rich cancrinite, Can. Mineral. 20, 239-251.
- Gunther, H. (1980): Nmr spectroscopy John Wiley and Sons, New York, pp 436.
- Harlow, G. E. & Brown, G. E. B. Jr., (1980): Low albite, an X-ray and neutron diffraction study, Amer. Mineral., 65, 986-995.
- Hassan, I., & Busek, P. R. (1988): HRTEM characterization of scapolite solid solutions. Amer. Mineral. 73, 119-134.
- Hassan, I. & Grundy, H. D., (1983): Structure of basic sodalite. Acta Crystallogr. 39-45.

- Hassan, I. & Grundy, H. D. (1984): The crystal structure of sodalite group minerals, Acta Crystallogr., 40, 6-13.
- Hawthorne, F. C. & Cerny, P., (1977): The alkali-metal positions in Cs-Li beryl, Can. Mineral., 15, 414-421.
- Hawthorne, F. C. & Grundy, H. D. (1976): The crystal chemistry of the amphiboles: IV. X-ray and neutron refinements of the crystal structure of tremolite, Can. Mineral 14, 334-345.
- Higgins, J.B., & Woessner, D. E., (1982):  $^{29}\text{Si}$ ,  $^{27}\text{Al}$  &  $^{23}\text{Na}$  nmr spectra of framework silicates. EOS, 63, 1139.
- Hill, R. J. & Gibbs, G. V. (1979): Variation in d(T-O), d(T...T) and TOT in silica and silicate minerals, phosphates and aluminates, Acta Cryst. B35, 25-30.
- Hill, R. J., Gibbs, G. V., Craig, J. R., Ross, F. K. & Williams, J. M. (1977): Neutron diffraction study of hemimorphite. Z. Kristallogr. 146, 241-259.
- Hoebbel, D., Garzo, G., Jancke, H., Franke, P., & Wieker W., (1976): Gaschromatographic and  $^{29}\text{Si}$  nmr spectroscopic investigations on silicic acid trimethyl silylestere. Z. Anorg. Allg. Chem. 424, 115-127.
- Janes, N., & Oldfield, E., (1985): Prediction of silicon-29 nuclear magnetic resonance chemical shifts using a group electronegativity approach: Applications to silicate and aluminosilicate structure. J. Amer. Chem. Soc. 107, 6769-6775.
- Janes, N., & Oldfield, E., (1986): Oxygen-17 nmr study of bonding in silicates: The d-orbital controversy. J. Amer. Chem. Soc. 108, 5743-5753.
- Kimata, M. & Li, N., (1981): The crystal structure of synthetic akermanite, Neues. Jahrb. Mineral. (Monatsh), 1-10.
- Kimata, M. & Li, N., (1982): The structural property of synthetic gehlinit. Neues. Jahrb. Mineral. (Abhand.) 143, 254-267.
- Kinsey, R. A., Kirkpatrick, R. J., Haver, J., Smith, K. A. & Oldfield, E. (1985): High resolution aluminum-27 and silicon-29 nuclear magnetic resonance spectroscopy study of layer silicates including clay minerals. Amer. Mineral. 70, 537-548.

- Kirfel, A., Will, G. & Arndt, J. (1979): A new phase of coesite  $\text{SiO}_2$  Z. kristallogr. 149, 315-326.
- Kirfel, A. & Will, G. (1984): Ending the "P21/a coesite" discussion. Z. Kristallogr. 167, 287-291.
- Kirkpatrick, R. J., Carpenter, M. A., Yang, W-H. & Montez B. (1988):  $^{29}\text{Si}$  magic-angle NMR spectroscopy of low-temperature ordered plagioclase feldspars. Nature 325, 236-238.
- Kirkpatrick, R. J., Kinset, R. A., Smith, K. A., Henderson, D. M. & Oldfield, E. (1985): High resolution solid state sodium-23, aluminum-27 and silicon-29 nuclear magnetic resonance spectroscopic reconnaissance of alkali and plagioclase feldspars. Amer. Mineral. 70, 106-123.
- Kirkpatrick, R. J., Oestrike, R., Weiss, C. A., Jr, Smith, K. A. & Oldfield, E. (1986): High resolution  $^{27}\text{Al}$  and  $^{29}\text{Si}$  nmr spectroscopy of glasses and crystals along the join  $\text{CaMgSi}_2\text{O}_6$   $\text{CaAl}_2\text{SiO}_6$  join, Amer. Mineral. 71, 705-711.
- Klinowski, J., (1984): Nuclear magnetic resonance studies of zeolites. Progress in nmr spectroscopy 16, 237-309.
- Lamb, W. E. (1941): Internal diamagnetic fields, Phys. Rev. 60, 817-819.
- Lee, J. H. & Guggenheim, S. (1981): Single crystal x-ray refinement of pyrophyllite-1TC Amer. Mineral., 66, 350-357.
- Le Page, Y. & Donnay, G. (1976): Refinement of the crystal structure of low-quartz, Acta. Crystallogr., 32, 2456-2459.
- Levien, L. & Papike, J. J. (1976): Scapolite crystal chemistry. Aluminum-silicon distributions, carbonate group disorder and thermal expansion. Amer. Mineral., 61, 864-877.
- Lin, S.B. (1971): The crystal structure and crystal chemistry of scapolites, Ph.D. Thesis, McMaster University, Hamilton, Ontario.
- Lin, S. B. & Burley B. J. (1973a): Crystal structure of a sodium and chlorine-rich scapolite. Acta Crystallogr. B29, 1272-1278.

- Lin, S. B. & Burley, B. J. (1973b): The crystal structure of meionite, Acta Crystallogr., B29, 2024-2026.
- Lin, S. B. & Burley, B. J. (1975): The crystal structure of an intermediate scapolite-wernerite, Acta Crystallogr., B31, 1806-1814.
- Lippmaa, E., Alla, M.A., Pehk, T.J., (1978): Solid state high resolution nmr spectroscopy of spin 1/2 nuclei ( $^{13}\text{C}$ ,  $^{29}\text{Si}$ ,  $^{119}\text{Sn}$ ) in organic compounds. J. Amer. Chem. Soc. 100, 1929-1931.
- Lippmaa, E., Mägi, M., Samosan, A., Engelhardt, G., & Grimmer A, -R., (1980): Structural studies of silicates by solid-state high-resolution  $^{29}\text{Si}$  nmr. J. Amer. Chem. Soc. 102, 4889-4893.
- Lippmaa, E., Mägi, M., Samosan, A., Tarmak, M., and Engelhardt, G., (1981): Investigation of the structure of zeolites by solid-state high-resolution  $^{29}\text{Si}$  nmr spectroscopy. J. Amer. Chem. Soc. 103, 4992-4996.
- Lippmaa, E. (1986): High resolution  $^{27}\text{Al}$  nmr of aluminosilicates. J. Amer. Chem. Soc., 108, 1730-1735.
- Liu, S. B., Pines, A., Brandriss, M. & Stebbins, J. F. (1987): Relaxation mechanisms and the effect of motion in albite liquid and glass: A high temperature nmr study. Phys. Chem. Mineral. 15, 155-162.
- London, D., Zolensky, M.E. & Roedder, E (1987): Diomignite: natural  $\text{Li}_2\text{B}_4\text{O}_7$  from the Tanco pegmatite, Bernic Lake, Manitoba. Can. Mineral. 25, 173-180.
- Lowenstein, W. (1954): The distribution of aluminum in the tetrahedra of silicates and aluminosilicates. Amer. Mineral., 39, 92-96.
- Mägi, M., Lippmaa, E. & Samosan, A., (1984): Solid-state high-resolution silicon-29 chemical shifts in silicates. J. Phys. Chem. 88, 1518-1522.
- Matsumoto, T., Tokonami, M. & Morimoto, N. (1975): The crystal structure of omphacite, Amer. Mineral., 60, 634-641.
- McConnell, H., M. (1957): Theory of nuclear magnetic shielding in molecules I Long range dipolar shielding of protons. J. Chem. Phys. 27, 226-229.

- McDonald, W. S. & Cruickshank, D. W. (1967): Refinement of the crystal structure of hemimorphite, Z. Kristallogr., 124, 180-191.
- McGlinchey, M.J., Burns, R. C., Hofer, R., Top, S. & Jaouen, G., (1986): Diamagnetic anisotropy of organometallic moieties: X values for  $M(CO)_3$  (M=Cr, Mo, W) and for ferrocene. Organometallics 5, 104-109.
- Meier, W. M. (1960): The crystal structure of natrolite. Z. Kristallogr. 113, 430-444.
- Merkle, A. B. & Slaughter, M. (1968): Determination and refinement of the structure of heulandite. Amer. Mineral. 53, 1120-1138.
- Merlino, S. (1984): Feldspathoids: their average and real structure, Feldspars and feldspathoids, ed. W. L. Brown NATO ASI series.
- Morosin, B., (1972): Structure and thermal expansion of beryl, Acta Crystallogr., 28, 1899-1903.
- Newsam, J. M., (1985): The influence of second-neighbour aluminums on the isotropic chemical shift of  $^{29}Si$  in a zeolite environment. J. Phys. Chem. 89, 2002-2005.
- Newton R.C. & Goldsmith, J.R. (1975): Stability of the scapolite meionite ( $3CaAl_2Si_2O_2 \cdot CaCO_3$ ) at high pressures and storage of  $CO_2$  in the deep crust. Contrib. Mineral. Petrology., 49, 49-62.
- Novak, G. A. & Gibbs, G. V. (1971): The crystal chemistry of the silicate garnets. Amer Mineral. 56, 791-823.
- Oestrike, R. & Kirkpatrick, R. J. (1987):  $^{27}Al$  and  $^{29}Si$  MASS nmr spectroscopy of glasses in the system anorthite-diopside-forsterite. Amer. Mineral. 73, 534-546.
- Ohashi, Y. (1984): polysynthetically twinned structures of enstatite and wollastonite. Phys. and Chem. of Minerals 10, 217-229.
- Onken, H. (1965): Verfeinerung der Kristallstruktur von Monticellit, Ischermaks Mineral. Petrogr., 10, 34-44.
- Ottaway, T.L., Wicks, F.J., Bryndzia, L.T. & Spooner, E.T.C. (1986): Characteristics and origin of the Muezo emerald deposit, Columbia. Internat. Mineral. Assoc. 14<sup>th</sup> General Meeting Abstracts 193.



- Pannhorst, W. (1984): High temperature crystal structure refinement of low-clinenstatite up to 700C, Neues Jahrb. Mineral. (Abhand.), 150, 209-218.
- Papike, J.J. & Stephenson N.C (1966): The crystal structure of mizzonite, a calcium and carbonate rich scapolite. Amer. Mineral. 51, 1014-1027.
- Papike, J. J. & Zoltai, T. (1965): The crystal structure of a marialite scapolite. Amer. Mineral., 50, 641-655.
- Paudler, W. W. (1987): Nuclear Magnetic Resonance General Concepts and Applications, John Wiley & Sons Inc. pp 292.
- Pauling, L. (1967): The chemical bond Cornell Press, Ithaca, New York, pp 266.
- Perrotta, A. J., Smith, S. M. & Smith, J. V. (1965): The crystal structure of kalsilite Mineral. Mag. 35, 588-617.
- Peterson, R. C., Donnay, G. & LePage, Y. (1979): Sulphate disorder in scapolites, Can. Mineral., 17, 53-61.
- Phillips, M. W., Gibbs, G. V. & Ribbe, P. H. (1974): The crystal structure of danburite. A comparison with anorthite, albite, and reedmergnerite, Amer Mineral., 59, 79-84.
- Prewitt, C. T. (1967): Refinement of the structure of pectolite, Z. Kristallogr., 125, 298-316.
- Prewitt, C. T. & Burnham, C. W. (1966): The crystal structure of jadeite, Amer. Mineral., 51, 956-975.
- Prince, E. (1971): Refinement of the crystal structure of apophyllite. III Determination of hydrogen positions by neutron diffraction, Amer. Mineral., 56, 1243-1251.
- Radeglia, R, & Engelhardt, G., (1985): Correlation of Si-O-T (T=Si or Al) angles and  $^{29}\text{Si}$  nmr chemical shifts in silicates and aluminosilicates. Chem. Phys. Letters 114, 28-30
- Radoslovich, E. W. (1960): The structure of muscovite Acta. Crystallogr. 913, 919-932.
- Ramdas, S., & Klinowski, J., (1984): A simple correlation between isotropic  $^{29}\text{Si}$ -nmr chemical shifts and T-O-T angles in zeolite frameworks. Nature 308, 521-523.

- Rayner, J.H. & Brown, G. (1973): The crystal structure of talc. Clays Clay Mineral. 21, 103-114.
- Ribbe, P. H., Ferguson, R. B. & Traill, R. J., (1969): The albite structures, Acta. Crystallogr., 25, 1503-1517.
- Richardson, M. F., Hartman, J. S. & Guo, D. (1988): Long-range shielding and chemical shift in silicon carbide polytypes. Experimental nmr conference abstracts, 200.
- Robinson, K., Gibbs, G.V. and Ribbe, P.H. (1971): The structure of zircon, a comparison with garnet, Amer. Mineral. 56, 782-789.
- Saburi, S., Kusachi, I., Henmi, C., Kawahara, A., Henmi, K. & Kawada, I. (1976): Refinement of the crystal structure of rankinite Mineral. J. (Tokyo), 8, 240-246.
- Sasaki, S., Chesa, H. K., Prewitt, C. T. & Nakajima, Y. (1983): Reexamination of  $P2_1/a$  coesite Z. Kristallogr. 164, 67-78.
- Sanz J., & Serratosa J.M., (1984):  $^{29}\text{Si}$  and  $^{27}\text{Al}$  high-resolution MAS-nmr spectra of phyllosilicates. J. Amer. Chem. Soc. 106, 4790-4793.
- Schramm, C. M., de Jong, B. H. W. S. & Parziale, V. E. (1984):  $^{29}\text{Si}$  MAS nmr study of local silicon environments in amorphous and crystalline Li silicates. J. Amer. Chem. Soc. 106, 4396-4402.
- Shaw, D.M. (1960a): The geochemistry of scapolites. Part I, Previous work and general mineralogy. J. Petrology 1, 218-260.
- Shaw, D.M. (1960b): The geochemistry of scapolites. Part II, Trace elements, petrology and general geochemistry. J. Petrology, 1, 261-285.
- Shaw, D. M., Moxham, R.L., Filby, R.H. & Lapkowsky, W.W., (1963): The petrology and geochemistry of some Grenville skarns. Part I Geology and petrology. Can. Mineral, 7, 420-442.
- Shaw, D. M., Schwarz, H.P. & Sheppard S.M.F., (1965): The petrology of two zoned scapolite skarns. Can. J. Earth Sci., 2, 577-595.

- Sherriff, B. L. & Grundy, H. D., (1988) Calculations of  $^{29}\text{Si}$  MAS nmr chemical shift from silicate mineral structure. Nature 332, 819-822.
- Sherriff, B.L., Grundy, H.D., and Hartman, J.S. (1987a): Occupancy of T-sites in the scapolite series. A multinuclear nmr study using magic angle spinning. Can. Mineral., 25, 717-730.
- Sherriff, B.L., Grundy, H.D., and Hartman, J.S. (1987b): Analysis of fluid inclusions using nuclear magnetic resonance. Geochimica et Cosmochimica Acta, 51, 2233-2235.
- Sherriff, B. L., & Hartman, J. S. (1985): Solid state high-resolution  $^{29}\text{Si}$  nmr of feldspars Al-Si disorder and the effects of paramagnetic centres. Can. Mineral. 23, 205-212.
- Shirozu, H. & Bailey, S. W. (1966): Crystal structure of two-layer Mg-vermicullite. Amer. Mineral., 51, 1124-1143.
- Simmons, W. B., Peacor, J. R. and Peacor, D. R. (1972): Refinement of the crystal structure of a volcanic nepheline. Amer. Mineral. 57, 1711-1719.
- Smith, J. V., & Blackwell, C. S., (1983): Nuclear magnetic resonance of silica polymorphs. Nature 303, 223-225.
- Smith, J. V. & Rinaldi, F. (1963): Crystal structures with a chabasite framework II hydrated Ca-chabasite at room temperature. Acta Crystallogr. 916, 45-53.
- Smith, K. A., Kirkpatrick, R. J., Oldfield, E., & Henderson, D. M., (1983): High resolution silicon-29 nuclear magnetic resonance spectroscopy of rock-forming silicates. Amer. Mineral. 68, 1206-1215.
- Smolin, Y. I., Shepelev, Y. F. & Titov, A. P. (1972): Refinement of the crystal structure of thorveiteite. Krystallogr. 17, 857-858.
- Speer, J. A. & Gibbs, G.V. (1976) The crystal structure of synthetic titanite and the domain textures of natural titanites Amer. Mineral. 61, 238-247.
- Stebbins, J. F., Murdoch, J. B., Carmichael, I. S. E. & Pines, A. (1986): Defects and short range order in nepheline group minerals a  $^{29}\text{Si}$  nmr study. Phys. Chem. Minerals. 13, 371-381.

Steinfink, H. (1962): Crystal structure of a trioctahedral mica phlogopite. Amer. Mineral. 47, 886-889.

Takeuchi, Y. (1966): Structures of brittle micas, Clays Clay Minerals, 13, 1-25.

Tossell, J. A., (1984): Correlation of  $^{29}\text{Si}$  nuclear magnetic resonance chemical shifts in silicates with orbital energy differences obtained from x-ray spectra. Phys. Chem. Minerals 10, 137-141.

Tossell, J. A., & Lazzeretti (1986): Ab initio calculations of  $^{29}\text{Si}$  nmr chemical shifts for some gas phase and solid state silicon fluorides and oxides. J. Chem. Phys. 84, 369-374.

Tossell, J. A., & Lazzeretti (1987): Ab initio calculations of oxygen nuclear quadrupole coupling constants and oxygen and silicon nmr shielding constants in molecules containing Si-O bonds. Chem. Phys. 112, 205-212.

Ulbrich, H. H. (1973): Structural refinement of the Monte Somma Scapolite a 93% Meionite. Schweizer Mineral. Petrogr. Mitt. 53, 385-393.

Wainwright, J. E. & Starkey, J. (1971): A refinement of the structure of anorthite, Z. Kristallogr., 133, 75-84.

Weiss Jr., C. A., Altaner, S. P. & Kirkpatrick, R. J. (1987): High resolution  $^{29}\text{Si}$  nmr spectroscopy of 2:1 layer silicates: Correlations among chemical shifts, structural distortions and chemical variations. Amer. Mineral., 72, 935-942.

Williams (Sherriff) B. L. (1984): An investigation of the application of  $^{29}\text{Si}$  magic angle spinning nuclear magnetic resonance in geology, M.Sc. thesis, Brock University, St Catharines, Ontario.

Winter, J. K. & Ghose, S., (1979): Thermal expansion and high temperature crystal chemistry of the  $\text{Al}_2\text{O}_5$  polymorphs. Amer. Mineral. 64, 573-586.

Wright, A. F. & Lehman, M. S. (1981): The structure of quartz at 25 and  $590^\circ\text{C}$  determined by neutron diffraction, J. Solid State Chem. 36, 371-380.

Yamanaka, T. & Mori, H. (1981): The structures and polytypes of alpha  $\text{CaSiO}_3$  pseudowollastonite. Acta Crystallogr. 37, 1010-1017.

Zachariasen, W. H. (1971): Refined crystal structure of phenacite, Kristallogr., 16, 1161-1166.

Zobetz E., Zemann, J., Heger, G. & Voellenkle, H. (1979): Strukturbestimmung eines OH-reichen topases, Anz. Osterr. Akad. Wiss. Math-Naturwiss Kl., 116, 145-147.

Zoltai, T. (1960): Classification of silicates and other minerals with tetrahedral structures. Amer. Mineral. 45, 960-973.

## APPENDIX I

### THE THEORY OF NUCLEAR MAGNETIC RESONANCE (NMR)

#### I.1 GENERAL THEORY OF NMR SPECTROSCOPY

A spinning nucleus possesses angular momentum ( $p$ ) which is related to  $I$  the nuclear spin quantum number by

$$p = Ih/2\pi$$

where  $h$  is Planck's constant and  $I$  can be either an integer or a half integer.

For isotopes where the mass number ( $A$ ) and charge number ( $Z$ ) are both even,  $I$  is zero, the nucleus has no angular momentum and therefore gives no nmr signal. This applies to about two thirds of all isotopes.

The magnetic moment ( $\mu$ ) of a nucleus is given by

$$\mu = \gamma p = \gamma Ih/2\pi$$

$\gamma$  is the magnetogyric ratio, which is an inherent property of the nucleus and is different for each isotope.

When a nucleus is placed in a uniform magnetic

field ( $B_0$ ) it attains a series of Zeeman energy levels each with energy

$$E_m = -\gamma m B_0 h/2\pi$$

The quantum number ( $m$ ) may assume the values  $-I, -I+1, \dots, I-1, I$ , thus giving  $2I+1$  energy levels (Fig. 1.1). The separation between energy levels is proportional to the applied magnetic field.

Nuclei with  $I=1/2$  such as  $^{29}\text{Si}$  have two Zeeman energy levels with a small excess of nuclei in the ground ( $I=+1/2$ ) state. The nmr signal results from the excitation, with radio frequency radiation, of this excess of ground state nuclei, from the  $+1/2$  to  $-1/2$  level.

An alternative way of describing this transition is by using Newtonian physics.

When a magnetic field ( $B_0$ ) is applied to a spinning nucleus, it causes the magnetic moment ( $\mu$ ) to precess around  $B_0$  with an angular momentum ( $\omega$ ) given by

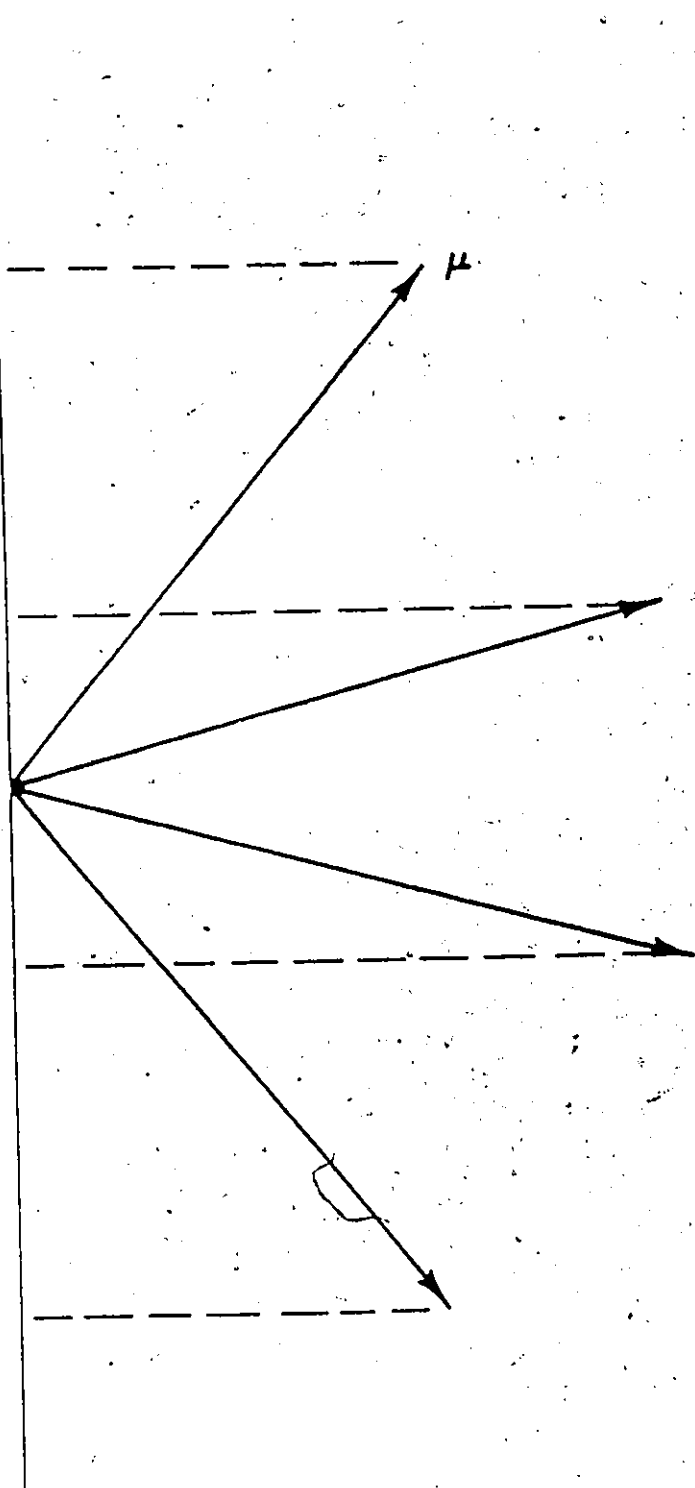
$$\omega_0 = -\gamma B_0 \quad (\text{Fig. 1.2})$$

The frequency of precession ( $\nu_0$ ) (the Larmor frequency) is proportional to the magnetogyric ratio ( $\gamma$ ) and the applied magnetic field  $B_0$ .  $x'$ ,  $y'$  and  $z'$  are Cartesian coordinates in a frame of reference which is

Figure I.1 The  $2l+1$  orientations with respect to  $B_0$  and the quantization of  $\mu$  on  $B_0$ . The case illustrated is  $l=3/2$  (Becker 1980).



$H_0$



$m$

$\frac{3}{2}$

$\frac{1}{2}$

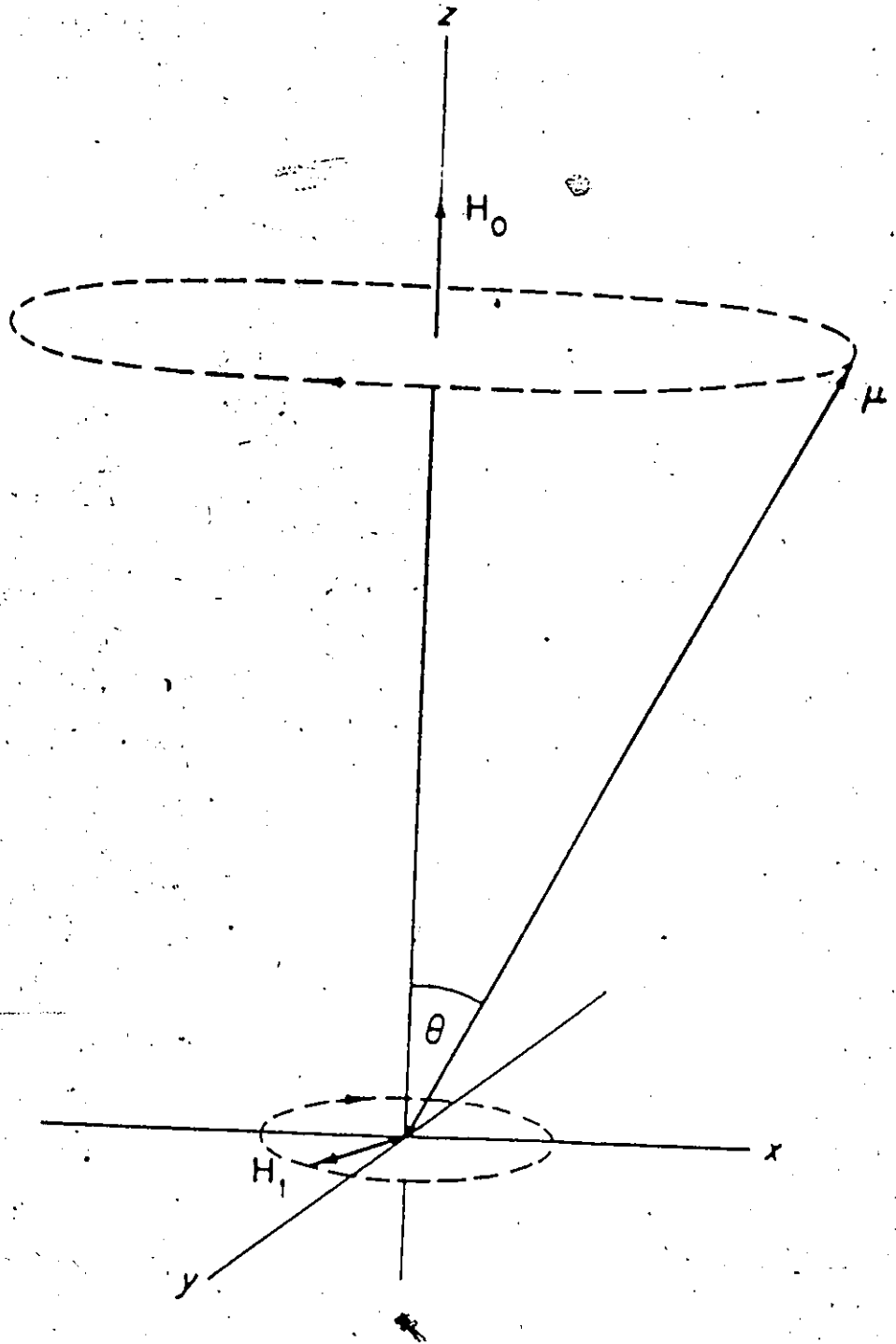
$-\frac{1}{2}$

$-\frac{3}{2}$



Figure I.2 Vectorial representation of Larmor precession (Becker 1980).





rotating around  $B_0$  at the Larmor frequency.

$$\nu_0 = \gamma B_0 / 2\pi$$

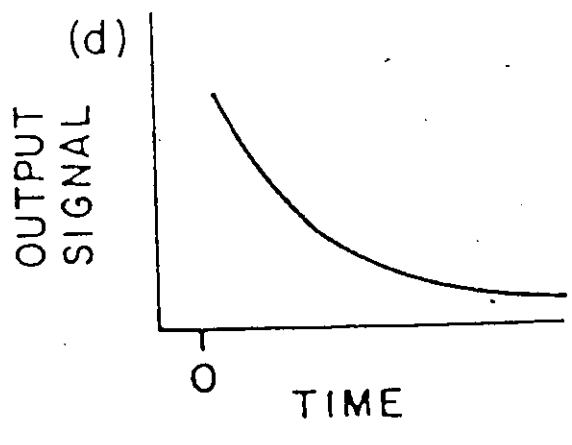
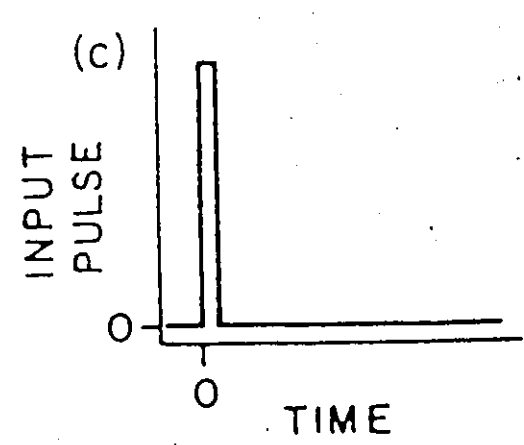
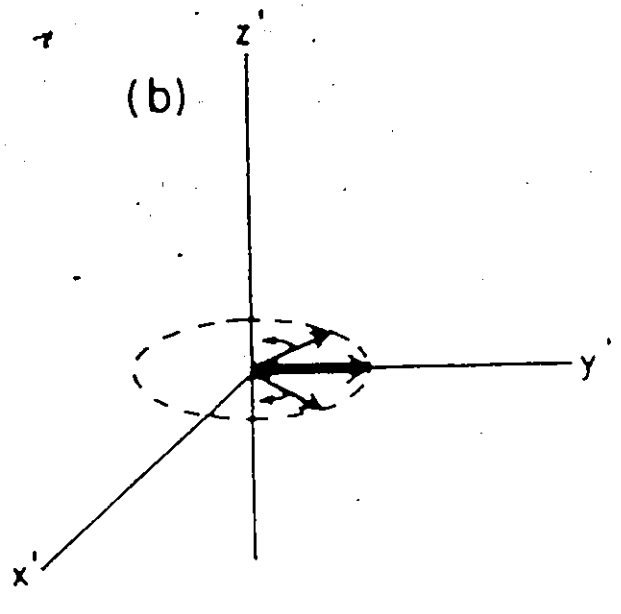
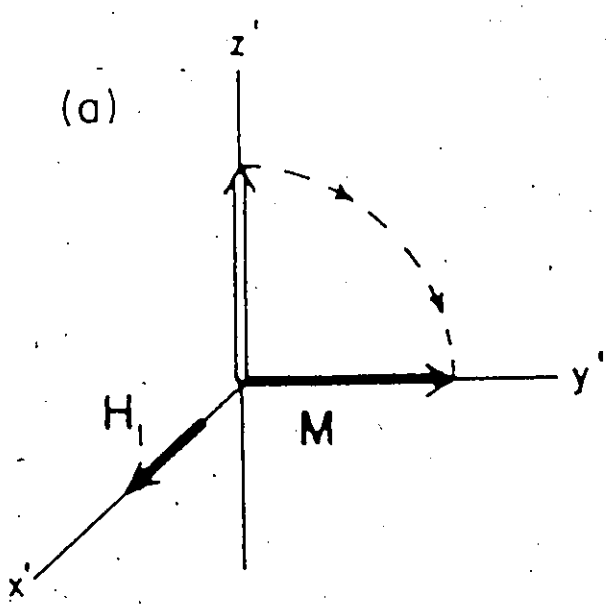
The Larmor frequency can be related to the energy difference between energy levels in the quantum mechanical description of nmr.

A small magnetic field ( $H_1$ ), formed by the passage of an electric current through a coil, which rotates with the Larmor frequency, is placed at right angles to  $B_0$  along  $x'$ . The magnetisation of the nucleus reacts to the resultant field by rotating towards the  $x'$ - $y'$  plane (Fig. 1.3a; 1.3b). The  $y'$  vector of magnetization is then measured.

## 1.2 PULSE FOURIER TRANSFORM

In the pulse Fourier Transform nmr experiment a very short radiofrequency (rf) pulse containing a wide range of frequencies is applied along the  $x'$  axis (Fig. 1.3a, 1.3c). This excites all nuclei with Larmor frequencies within this range and results in an interference pattern of sine waves (Fig. 1.3b, 1.3d). This free induction decay (FID) (Fig. 1.3d) is then Fourier Transformed from the time domain to the frequency domain to give the nmr spectrum.

Figure I.3 (a) A  $90^\circ$  pulse along  $x'$  rotates the magnetization from the equilibrium position to the  $y'$  axis.  
(b) The magnetization decreases as the magnetic moments dephase  
(c) The input signal, a  $90^\circ$  pulse  
(d) Exponential free induction decay (FID) output signal  
(Becker 1980)



### 1.3 CHEMICAL SHIFT

The electrons surrounding the nucleus, both those belonging to the nucleus being studied and to adjacent atoms, are moving charged particles which respond to magnetic fields. These fields effectively shield the nucleus from the effect of the applied magnetic field. The field seen by the nucleus is given by

$$H_{(\text{effective})} = B_0 - \sigma B_0$$

where  $\sigma$  is the shielding factor and depends on the chemical environment of the atom. Each nucleus with a different magnetic environment will have a different shielding factor and hence a different chemical shift. The term chemical shift comes from the fact that to obtain a resonance condition for a shielded nucleus either the frequency is held constant and the magnetic field is shifted to a higher value or the field is held constant and the frequency is shifted to a lower value.

The shielding factor  $\sigma$  is made up of four components; a paramagnetic term,  $\sigma_p$ , and a diamagnetic term  $\sigma_D$  both due to the electrons of the atom being studied, and also screening contributions caused by neighbouring atoms

and by interatomic electrons.

$\sigma_D$  refers to the shielding due to electron density of s electrons. It is always greater than zero because, by Lenz's Law, the magnetic field created by the motion of the diamagnetic electrons always opposes the applied magnetic field.  $\sigma_D$  can be calculated for a theoretical single free atom in a spherically symmetrical s electronic configuration from the equation of Lamb (1941)

$$\sigma = 4e^2/3mc^2 \int_0^{\infty} r \rho(r) dr$$

where  $\rho(r)$  is the density of electrons as a function of radial distance from the nucleus. The numerical size of the shielding component is related to atomic number and varies from  $1.8 \times 10^{-5}$  for hydrogen to  $8.82 \times 10^{-3}$  for thallium (Paudler 1987).

$\sigma_p$ , which is always negative, allows for asymmetry in electronic orbitals around the nucleus being observed. Thus p electrons contribute towards the paramagnetic component of shift. The paramagnetic effect is dominant for all nuclei other than hydrogen and causes chemical shift ranges of several hundred ppm for large atoms such as lead. The mathematical expression for  $\sigma_p$  includes terms for the energies of excitation of the electronic states. The computation of  $\sigma_p$  is therefore extremely complex so that with the opposing terms for  $\sigma_p$  and  $\sigma_D$  the calculation of



chemical shift from first principles is extremely difficult for any system other than a bare proton.

The screening effect of other electrons and interatomic currents causes the difference in chemical shift between atoms in similar electronic configurations, e.g.  $^{29}\text{Si}$  chemical shift of  $\text{SiO}_4$  groups. This is again extremely complex to calculate and can be studied best by empirical types of correlations.

Because of the difficulty of absolute calculations, chemical shift is always measured with respect to a reference, which for  $^{29}\text{Si}$  nmr is tetramethylsilane (TMS).

$$\delta = (\sigma_{\text{REFERENCE}} - \sigma_{\text{SAMPLE}}) \times 10^6$$

Chemical shift is actually measured in frequency units (Hz) but as the frequency is proportional to the applied magnetic field, the shift is usually reported as parts per million of the magnetic field. Thus chemical shift is independent of field strength and the results from different instruments are easily comparable.

#### 1.4 HIGH RESOLUTION NMR OF SOLIDS

In solids, nmr peaks are broadened due to dipolar interaction between adjacent nuclei and also chemical shift anisotropy which is caused by differing orientations of the

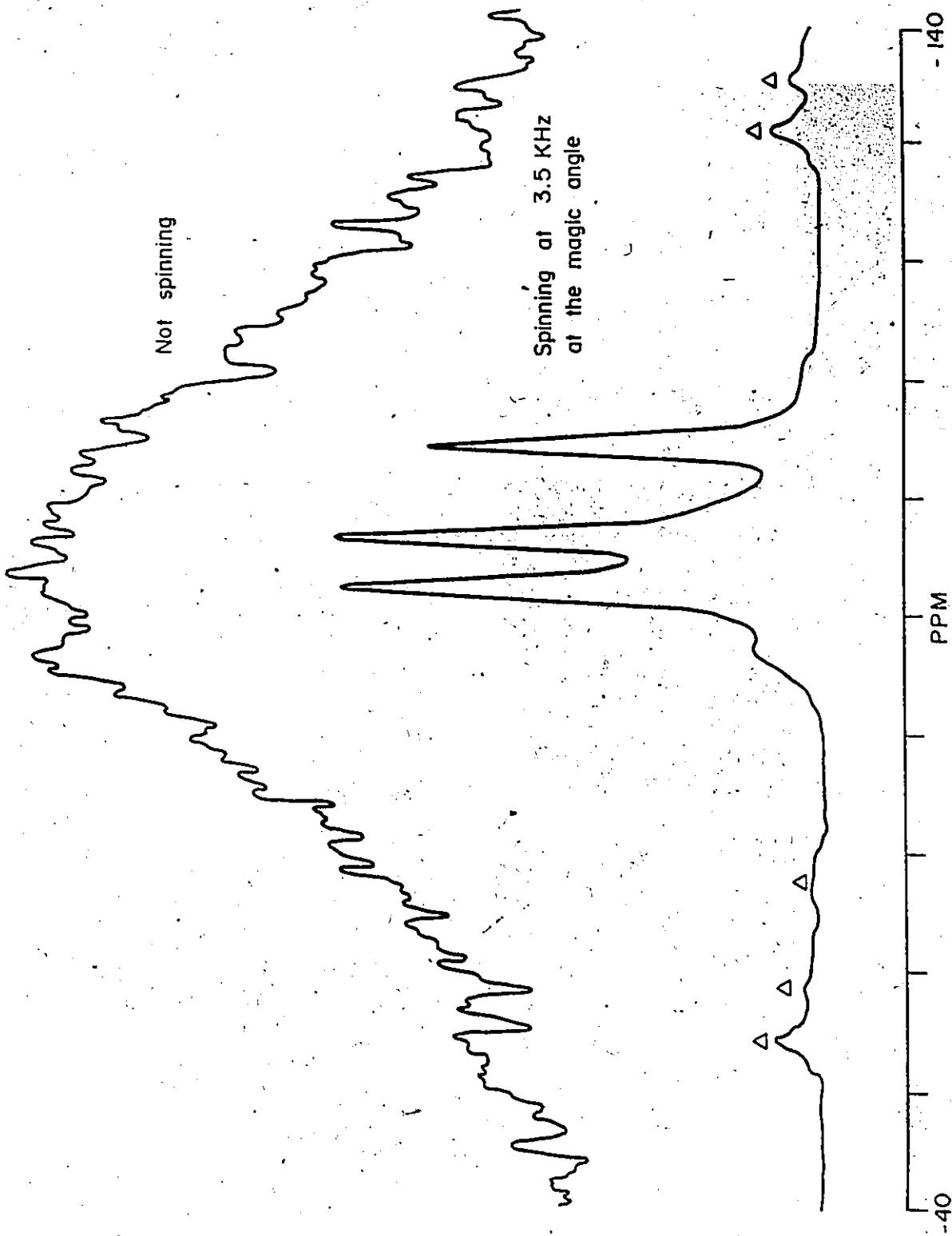
magnetic dipole with respect to the applied magnetic field.

Dipole-dipole interaction is the perturbation of the magnetic field at one nucleus due to other magnetic nuclei producing dipolar fields in the vicinity. In solids, these interactions produce a range of magnetic environments and hence overlapping peaks. This problem can be reduced or eliminated by studying only dilute spin systems.  $^{29}\text{Si}$  is only 4.6% abundant so that the chances of adjacent Si atoms having magnetic dipoles for interaction are remote. The sole magnetic nucleus of oxygen,  $^{17}\text{O}$ , is 0.037% abundant, and therefore does not cause dipolar interactions in silicate minerals.

Different orientations of the magnetic dipole with respect to the applied magnetic field cause differing values of the effective field at the nucleus. The isotropic value is obtained in solution due to rapid motion. In the case of nonspinning solids, the result is many overlapping resonances leading to broad envelopes of peaks with very little fine structure (Fig. 1.4a). Chemical shift anisotropy (CSA) refers to the width of the spread of chemical shifts between the extreme cases of having the dipole either parallel or perpendicular to the magnetic field.

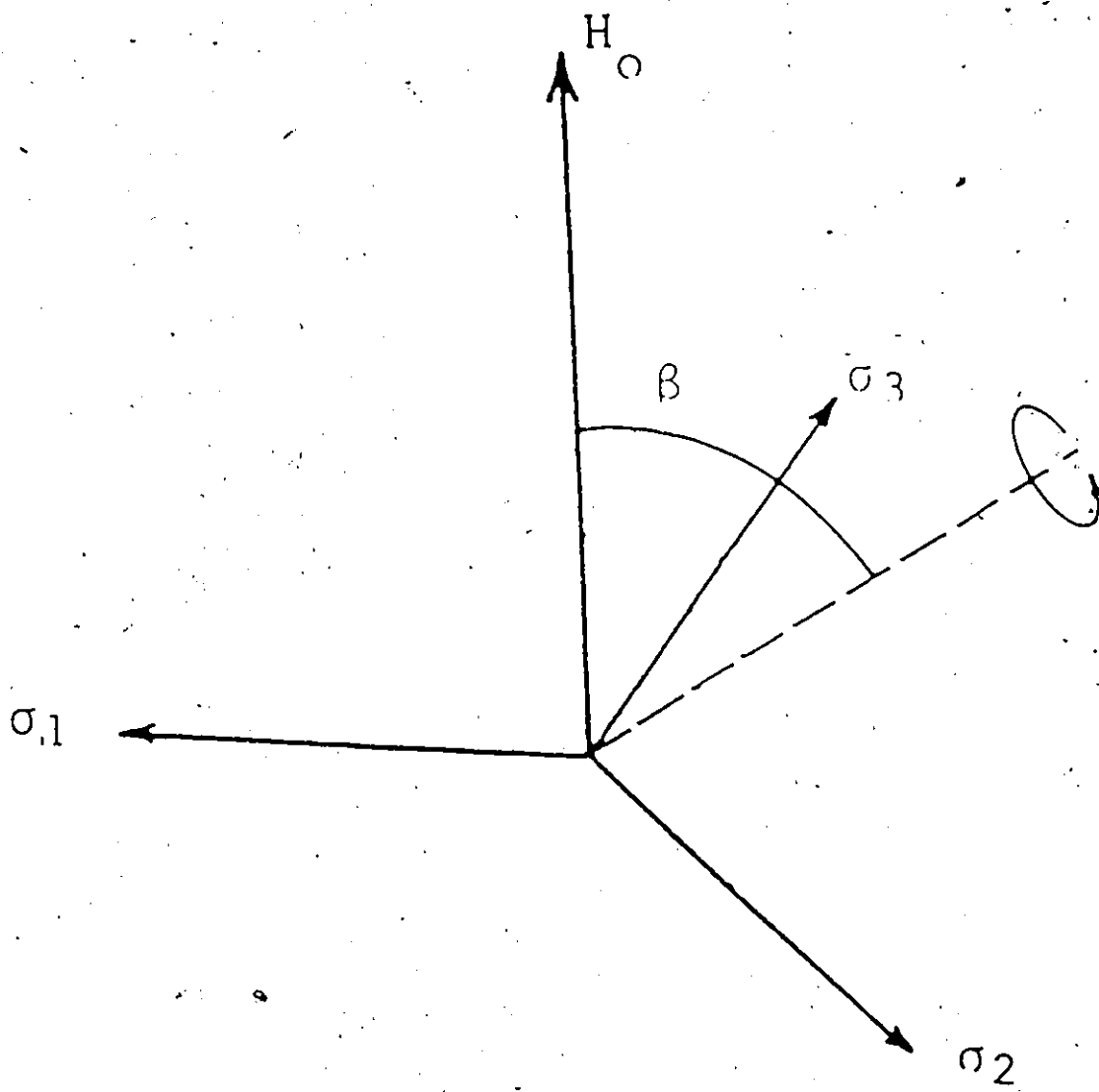
The chemical shift anisotropy Hamiltonian contains a term  $(3\cos^2\theta-1)$  which becomes zero if  $\theta$  is  $54.7^\circ$ . By spinning the sample at a speed greater than the value of

Figure 1.4  $^{29}\text{Si}$  nmr spectra of BLS036 oligoclase feldspar: (a) static sample  
(b) sample spinning at the magic angle of  $54.7^\circ$  to the applied magnetic field at a speed of approximately 3200 Hz  
(Williams (Sherriff) 1984)



OLIGOCLASE  $^{29}\text{Si}$  nmr spectrum  $\Delta$  spinning sidebands

Figure I.5 Magic Angle Spinning vectors (Paudler  
1987)



CSA at an angle of  $54.7^\circ$  (Fig. 1.5) the anisotropic term becomes zero and the isotropic chemical shift is observed.

The spectra in this study were obtained at spinning speeds between 3.2 and 3.5 KHz and often show a residual of the CSA as spinning sidebands either side of the isotropic peak at a distance equal to the spinning speed (Fig. 1.4b). Faster spinning can help to reduce these spinning sidebands and speeds of up to 20 KHz are now available.

### 1.5 MAS NMR SPECTRA OF QUADRUPOLEAR NUCLEI

Spectra of nuclei with spin quantum number  $I$  greater than  $1/2$  are dominated by quadrupolar interaction, which is the interaction of the nuclear quadrupolar moment ( $eQ$ ) with non spherically symmetrical electric field gradients (Klinowski 1984; Fyfe 1983; Fyfe *et al.* 1983). This has the effect of causing broad odd shaped peaks which can be extremely difficult to interpret (Fig. 1.6).

The first order quadrupolar effects can be calculated from

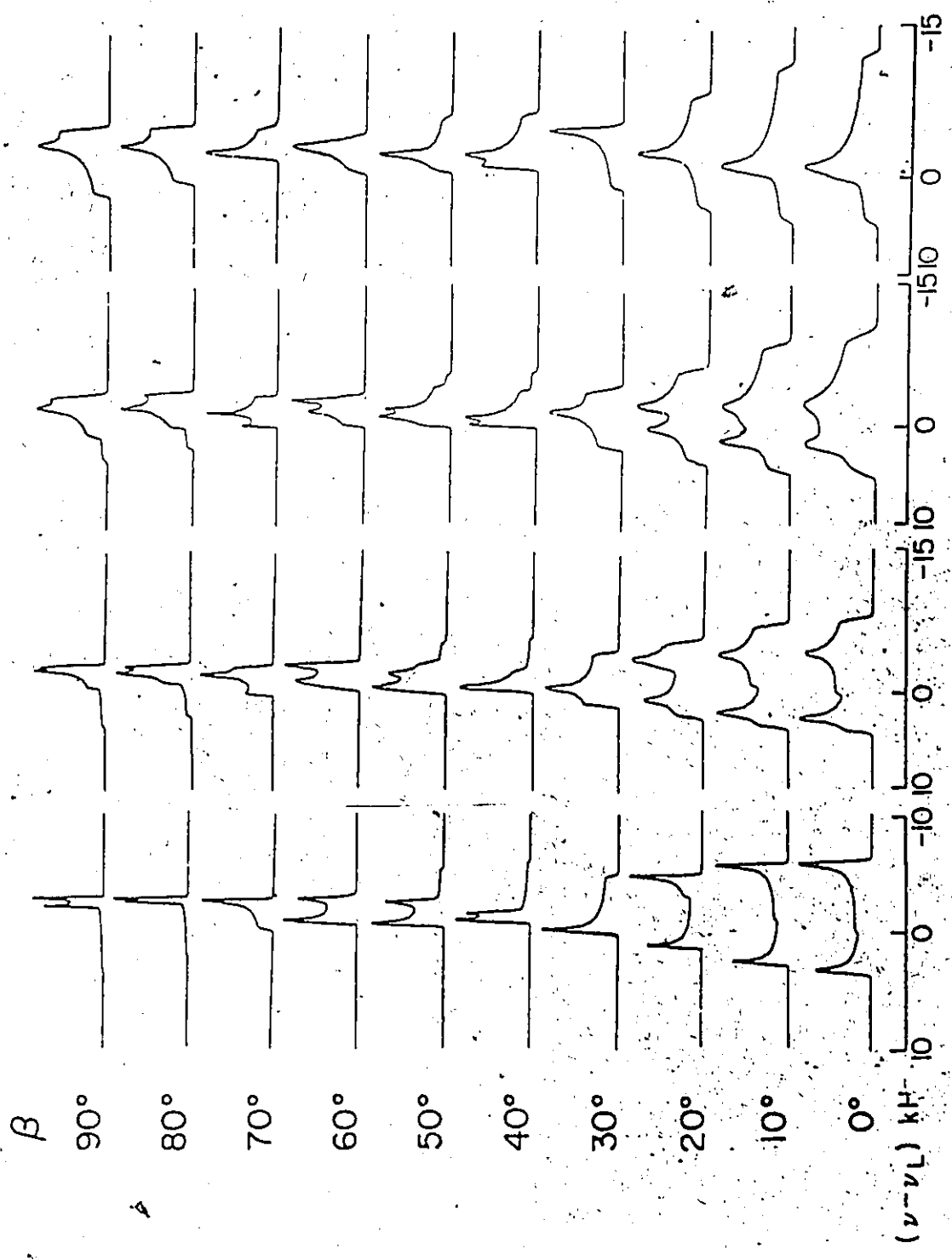
$$\nu_m = 1/2 \nu_Q (m-1/2)(3\cos^2\theta-1)$$

(Klinowski 1984) where  $\nu_m$  is the frequency of transition for a particular value of  $m$  and  $\nu_Q$  the quadrupole resonance frequency is given by

Figure I.6 Computer simulated variable angle sample spinning lineshapes for the central ( $m = 1/2$ ) to ( $m = -1/2$ ) transition of  $^{23}\text{Na}$  ( $i = 3/2$ ) broadened by second order quadrupole effects (Ganapathy et al. 1982).



A  $\eta = 0.0$     B  $\eta = 0.3$     C  $\eta = 0.6$     D  $\eta = 1.0$



$$[\nu_Q = 3e^2qQ/2hI(2I-1)]$$

From these equations it can be seen that in the case of non-integer spin nuclei such as  $^{27}\text{Al}$  and  $^{23}\text{Na}$ , the first order term for  $m=1/2$  transition is zero and in fact the  $+1/2$  to  $-1/2$  transition is unchanged by first order quadrupolar effects (Fig. 1.7). All other first order effects can be reduced by spinning the sample at the magic angle and reducing the term  $(3\cos^2\theta-1)$  to zero. In most spectra of non integer nuclei obtained at high field only the central transition is observed as the other transitions are shifted to higher or lower field.

The equation for the second order frequency shift is more complex

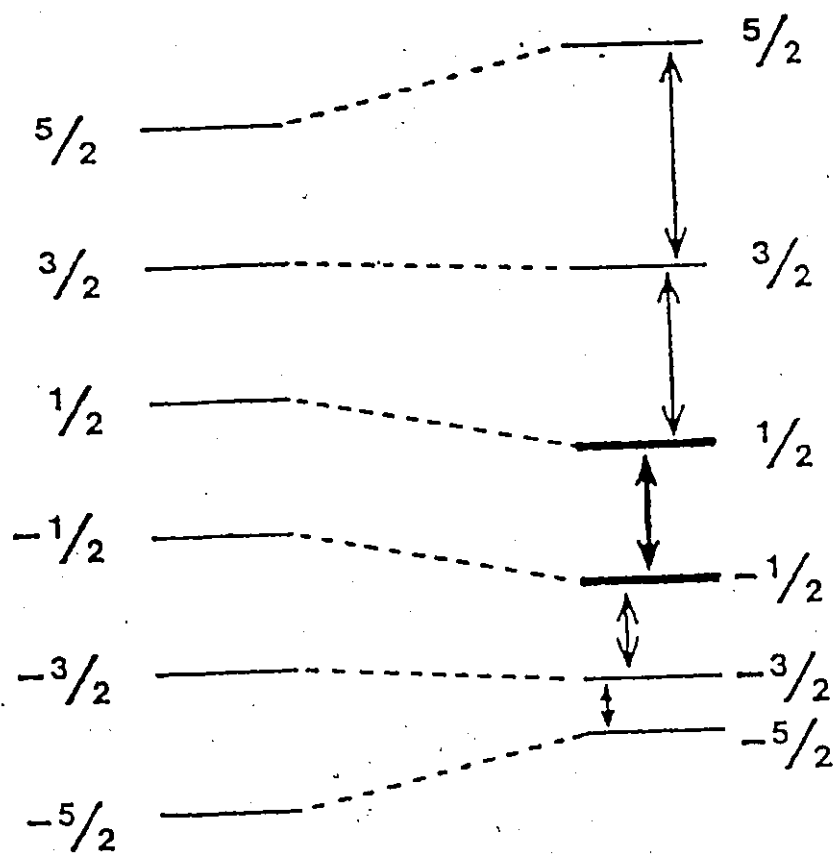
$$\nu_{1/2} = -\nu_Q^2/16\nu_L(a-3/4)(1-\cos^2\theta)(9\cos^2\theta-1)$$

$$[\nu_L = \gamma B_0(1-\sigma)/2\pi]$$

The second order effect is therefore not reduced by spinning at the magic angle although it can be reduced by spinning at other angles (Ganapathy *et al.* 1982). It is however inversely proportional to applied magnetic field whereas chemical shift is proportional to magnetic field. Thus the chemical shift component can be increased and the quadrupolar shift component decreased by obtaining the

7

Figure I.7 Energy level diagram for a spin  $5/2$  nucleus showing the effect of first order quadrupolar interaction on Zeeman energy levels. (Fyfe et al. 1983).



spectra at as high a field as possible.

## 1.6 RELAXATION TIMES

There are two relaxation times:  $T_1$  the spin lattice or longitudinal relaxation time and  $T_2$  the spin-spin or transverse relaxation time. Both are related to the time during which the nuclei regain their state of equilibrium.

$T_1$  is the time in which the nuclear spins return to the  $z'$  axis from being perturbed. In quantum theory it is expressed as the rate at which the populations of the spin energy levels return to equilibrium and can be expressed as

$$dn/dt = -2W(n-n_{eq})$$

where  $W$  is the mean of the probabilities of upward or downward transition and  $n$  is the number of nuclei in the different spin states (Paudley 1987).

For spin lattice relaxation to occur a specific quantum of energy must be given up to the surrounding lattice. In liquids this is accomplished by molecular rotational or translational motions causing fluctuating magnetic fields that provide the mechanism for energy transfer. In solids these motions do not exist and spin lattice relaxation occurs by the often very inefficient method of spin diffusion through the lattice (Abragam

1961). Unpaired electrons of paramagnetic ions and  $^1\text{H}$  nuclei in water molecules (Gladden *et al.* 1986) can provide an efficient relaxation mechanism and shorten  $T_1$  relaxation times.

Spin-spin relaxation ( $T_2$ ) is due to the nuclear spins becoming out of phase in the  $x'-y'$  plane.  $T_2$  is an internal function but it is affected by inhomogeneities in the magnetic field which can be caused by the unpaired electrons of paramagnetic species. Nuclei with short  $T_2$  times give broad peaks due to the out of phase spins having slightly different frequencies.

The electric quadrupole moment  $Q$  of quadrupolar nuclei can interact with the electric field gradient of the nucleus and contribute towards  $T_1$  relaxation. Therefore quadrupolar nuclei, even in solids usually have extremely fast relaxation rates and the FID can be accumulated with a minimum of delay between pulses. For some quadrupolar nuclei, such as  $^{35}\text{Cl}$  in an asymmetric electronic environment the quadrupolar relaxation rate can be faster than the nmr time scale and the spectra cannot be recorded.

APPENDIX II

Mineral samples

Mineral	Number	Locality	Donor
Beryl	SHEE-1-6	Shatford Lake, Manitoba.	F.C.Hawthorne
Beryl	EEE-10	Tanco pegmatite, Manitoba.	F.C.Hawthorne
Beryl	BLM-503	Tanco pegmatite, Manitoba.	F.C.Hawthorne
Beryl	T-24	Tanco pegmatite, Manitoba.	F.C.Hawthorne
Emerald		Columbia	T. Ottaway
Emerald		Emmaville, New South Wales	T. Ottaway
Emerald		Brazil	T. Ottaway
Lepidolite	T-38	Tanco pegmatite, Manitoba.	F.C.Hawthorne
Muscovite	TL-48	Tanco pegmatite, Manitoba.	F.C.Hawthorne
Heulandite	8407	Stodvarfiordur, S-Mulasyslu, Iceland	Icelandic Museum of Natural History Reykjavik
Chabasite	7924	Mjoidalur, Isafjordur, N-Isafjordarsysla, Iceland	Iceland Museum of Natural History Reykjavik
Thomsonite	1580	Runna, Berufjordur, S-Mulasyslu, Iceland	Icelandic Museum of Natural History Reykjavik
Scolesite	1112	Teighorn, Berufjordur, S-Mulasyslu, Iceland	Icelandic Museum of Natural History Reykjavik
Sphene	BLS396	(synthetic)	M. Crowe, McMaster University

APPENDIX III

---

DUM.FOR Fortran program for emplacement of dummy atoms  
at midpoints of all cation-oxygen bonds.

---

```
CHARACTER*85 LINE
DIMENSION LA(10000), B(3,10000)
INTEGER C(8,10000),P
OPEN(UNIT=1,FILE='TEMP.DAT',TYPE='OLD')
OPEN(UNIT=2,FILE='DUM.DAT',TYPE='NEW')

DO 2 I=1,2
100 READ(1,100)LINE
2   FORMAT(A85)
   CONTINUE

READ(1,106)NUM, LINE
106 FORMAT(I4,A81)
   READ(1,100)LINE

DO 98 I=1,NUM
101 READ(1,101)LA(I), (B(K,I),K=1,3), (C(J,I),J=1,8)
98  FORMAT(5X,A1,5X,3F10.5,8I4,12X)
   CONTINUE

N=NUM
DO 97 I=1,NUM
   IF(LA(I).NE.'O')GO TO 97

DO 96 J=1,8
   IF(C(J,I).EQ.0)GO TO 96
   IF(LA(C(J,I)).NE.'S') GO TO 96

N=N+1
DO 95 K=1,3
95  B(K,N)=B(K,I)-((B(K,I))-B(K,(C(J,I))))/2.
   CONTINUE
96  CONTINUE
97  CONTINUE

REWIND 1

M=N
DO 77 I=1,NUM
   IF(LA(I).NE.'O')GO TO 77
```



```

DO 76 J=1,8
IF(C(J,I).EQ.0)GO TO 76

IF(LA(C(J,I)).NE.'A') GO TO 76

M=M+1
DO 75 K=1,3

B(K,M)=B(K,I)-((B(K,I))-B(K,(C(J,I))))/2.

75 CONTINUE
76 CONTINUE
77 CONTINUE

REWIND 1
P=M
DO 67 I=1,NUM
IF(LA(I).NE.'O')GO TO 67

DO 66 J=1,8
IF(C(J,I).EQ.0)GO TO 66

IF(LA(C(J,I)).EQ.'A') GO TO 66
IF(LA(C(J,I)).EQ.'S') GO TO 66

P=P+1
DO 65 K=1,3

B(K,P)=B(K,I)-((B(K,I))-B(K,(C(J,I))))/2.

65 CONTINUE
66 CONTINUE
67 CONTINUE

REWIND 1

DO 3 I=1,2
READ(1,100)LINE
WRITE(2,100)LINE

3 CONTINUE

READ(1,106)NUM, LINE
WRITE(2,106)P,LINE

L=NUM+1

DO 4 I=1,L
READ(1,100)LINE
WRITE(2,100)LINE

```

```
4      CONTINUE
      DO 6 I=L,N
      WRITE(2,104)(B(K,I),K=1,3)
104    FORMAT(5X,'D',4X,3F10.5,4X,'0',7(3X,'0'),
           3X,'0.000',3X,'1')
6      CONTINUE
      N=N+1
      DO 7 I=N,M
      WRITE(2,105)(B(K,I),K=1,3)
105    FORMAT(5X,'E',4X,3F10.5,4X,'0',7(3X,'0'),
           3X,'0.000',3X,'1')
7      CONTINUE
      M=M+1
      DO 8 I=M,P
      WRITE(2,107)(B(K,I),K=1,3)
107    FORMAT(5X,'G',4X,3F10.5,4X,'0',7(3X,'0'),
           3X,'0.000',3X,'1')
8      CONTINUE
      CLOSE(1)
      CLOSE(2)
      END
```

APPENDIX IV

LEN.FOR A Fortran program to calculate atomic distances and angles from the atomic coordinates from Chem-X

```

CHARACTER*85 LINE
DIMENSION
LA(9000),B(3,9000),ANG(100),LO(100),OANG(9000)
DIMENSION SI(9000)
INTEGER C(10000), O(10000)
REAL LN(3,10000), COSA(10000), COSO(10000)
CHARACTER*1 LSYM(100)
IARR=10000

OPEN(UNIT=1,FILE='DUM.DAT',TYPE='OLD')
OPEN(UNIT=2,FILE='D2:[8426701.ZX003.GEOM]CO.DAT',
      TYPE='NEW')

DO 2 I=1,2
100 READ(1,100)LINE
2   FORMAT(A85)
   CONTINUE

   READ(1,106)NUM, LINE
106 FORMAT(I4,A81)
   IF(NUM.LE.IARR)GOTO 1112
   WRITE(6,1113)NUM,IARR
1113 FORMAT(IX,' ERROR NUM GT IARR NUM=',I5,' IARR=',I5)
1112 READ(1,100)LINE

   DO 98 I=1,NUM
101 READ(1,101)LA(I),O(I),(B(K,I),K=1,3),C(I)
   FORMAT(5X,A1,A2,3X,3F10.5,2I4,36X)

98   CONTINUE
   M=0
   DO 97 I=1,NUM
   IF(LA(I).NE.'D')GO TO 97
   X=0
   DO 95 K=1,3
   X=X+((B(K,I)-B(K,1))**2)
95   CONTINUE
   M=M+1
   LN(1,M)=SQRT(X)

   Y=0
   DO 81 K=1,3

```

```

81      Y=Y+((B(K,(C(I))))-B(K,I))**2)
      CONTINUE
      LN(2,M)=SQRT(Y)

      Z=0
      DO 82 K=1,3
82      Z=Z+((B(K,(C(I))))-B(K,I))**2)
      CONTINUE
      LN(3,M)=SQRT(Z)

      COSA(M)=(X+Z-Y)/(2*(SQRT(X))*(SQRT(Z)))
      COSO(M)=(Y+Z-X)/(2*(SQRT(Y))*(SQRT(Z)))
      SI(M)=(SQRT(Z+X+(COSA(M)*2*(SQRT(Z))*(SQRT(X))))))
97      CONTINUE
      DO 74 I=1,M

      WRITE (2,105)(LN(K,I),K=1,3),COSA(I),COSO(I),SI(I)
105     FORMAT(6(X,F9.5))

      74      CONTINUE
      WRITE(2,116)
116     FORMAT('E')

      M=0
      DO 67 I=1,NUM
      IF(LA(I).NE.'E')GO TO 67

      X=0
      DO 65 K=1,3
65      X=X+((B(K,I))-B(K,1))**2)
      CONTINUE
      M=M+1
      LN(1,M)=SQRT(X)

      Y=0
      DO 61 K=1,3
61      Y=Y+((B(K,(C(I))))-B(K,1))**2)
      CONTINUE
      LN(2,M)=SQRT(Y)

      Z=0
      DO 62 K=1,3
62      Z=Z+((B(K,(C(I))))-B(K,1))**2)
      CONTINUE
      LN(3,M)=SQRT(Z)

      COSA(M)=(X+Z-Y)/(2*(SQRT(X))*(SQRT(Z)))
      COSO(M)=(Y+Z-X)/(2*(SQRT(Y))*(SQRT(Z)))
      SI(M)=SQRT(Z+X+(COSA(M)*2*(SQRT(Z))*(SQRT(X))))

67      CONTINUE
      DO 64 I=1,M

```

```

64 WRITE (2,105) (LN(K,I),K=1,3), COSA(I), COSO(I), SI(I)
CONTINUE
WRITE(2,116)
M=0
DO 57 I=1,NUM
IF (LA(I).NE.'G') GO TO 57

X=0
DO 55 K=1,3
55 X=X+((B(K,I)-B(K,1))**2)
CONTINUE
M=M+1
LN(1,M)=SQRT(X)

Y=0
DO 51 K=1,3
51 Y=Y+((B(K,(C(I)))-B(K,1))**2)
CONTINUE
LN(2,M)=SQRT(Y)

Z=0
DO 52 K=1,3
52 Z=Z+((B(K,(C(I)))-B(K,1))**2)
CONTINUE
LN(3,M)=SQRT(Z)

COSA(M)=(X+Z-Y)/(2*(SQRT(X))*(SQRT(Z)))
COSO(M)=(Y+Z-X)/(2*(SQRT(Y))*(SQRT(Z)))
SI(M)=SQRT(Z+X+(COSA(M)*2*(SQRT(Z))*(SQRT(X))))

57 CONTINUE
DO 54 I=1,M

54 WRITE (2,105) (LN(K,I),K=1,3), COSA(I), COSO(I), SI(I)
CONTINUE

WRITE(2,116)
CLOSE(1)
CLOSE(2)
END

```

APPENDIX V

---

CHISI-FOR A fortran program which calculates  $x''$  and hence  $^{29}\text{Si}$  nmr chemical shift from

$$x'' = \sum (\exp[(r_0 - r_i)/0.37]) ((1 - 3\cos^2\theta_i)/3R_i^3) (\log(\text{Si} - X_i))$$

$$\delta = 701.6 x'' - 45.7$$

---

```
CHARACTER*85 LINE
CHARACTER*20 MIN
CHARACTER*1 E
DIMENSION B(5,10000)

OPEN(UNIT=1,FILE='CO.DAT',TYPE='OLD')
OPEN(UNIT=2,FILE='SUM1.DAT',TYPE='NEW')
OPEN(UNIT=3,FILE='SUM2.DAT',TYPE='NEW')
OPEN(UNIT=4,FILE='CHISI4.DAT',TYPE='OLD')

WRITE(6,80)
80  FORMAT(2X,'WHAT IS CATION?')
READ(5,81)CAT
81  FORMAT(A2)

WRITE(6,180)
180  FORMAT(2X,'WHAT IS MINERAL?')
READ(5,181)MIN
181  FORMAT(A20)
WRITE(6,181)MIN

1111  M=0
      I=1

10    READ(1,100)E,TEMP1,TEMP2,TEMP3,TEMP4
100   FORMAT(A1,F9.5,11X,3(F9.5,1X))

      IF(E.EQ.'E') GO TO 20

      B(1,I)=TEMP1
      B(2,I)=TEMP2
      B(3,I)=TEMP3
      B(4,I)=TEMP4

      I=I+1
      M=M+1
```

```
I=I+1
M=M+1
GO TO 10

20  SUMSI=0
    DO 9 I=1,M

    X=0
    S=0
    Z=0
    Y=0

    R=B(1,I)
    T=B(2,I)
    A=B(3,I)
    C=B(4,I)

108  WRITE(2,108)R,T,A,C
    FORMAT(1X,F9.5,3(2X,F9.5))

    X=(1-(3*((A)**2)))/(3*((R)**3))
    S=EXP((1.64-(2*T))/0.37)
    Y=LOG10(C)
    Z=X*S*Y
    SUMSI=SUMSI+Z

    WRITE(2,104)X,S,Y,Z
104  FORMAT(4(2X,F9.5))
9    CONTINUE

    WRITE(2,105)SUMSI
105  FORMAT(' SUMSI=',F9.5)
    WRITE(6,105)SUMSI

    WRITE(3,106)SUMSI
106  FORMAT(2X,'SUMSI=',F9.5)

    M=0
    I=1

101  READ(1,100)E,TEMP1,TEMP2,TEMP3,TEMP4

    IF(E.EQ.'E') GO TO 201
    B(1,I)=TEMP1
    B(2,I)=TEMP2
    B(3,I)=TEMP3
    B(4,I)=TEMP4

    I=I+1
    M=M+1
    GO TO 101
```

```

DO 91 I=1,M

X=0
S=0
Z=0
Y=0

R=B(1,I)
T=B(2,I)
A=B(3,I)
C=B(4,I)

WRITE(2,108)R,T,A,C

X=(1-(3*((A)**2)))/(3*((R)**3))
S=EXP((1.62-(2*T))/0.37)
Y=LOG10(C)
Z=X*S*Y
SUMAL=SUMAL+Z

WRITE(2,104)X,S,Y,Z
91 CONTINUE

WRITE(2,1051)SUMAL
1051 FORMAT('SUMAL=',F9.5)
WRITE(6,1051)SUMAL

WRITE(3,1061)SUMAL
1061 FORMAT(2X,'SUMAL=',F9.5)

M=0
I=1

111 READ(1,100)E,TEMP1,TEMP2,TEMP3,TEMP4

IF(E.EQ.'E') GO TO 211

B(1,I)=TEMP1
B(2,I)=TEMP2
B(3,I)=TEMP3
B(4,I)=TEMP4

I=I+1
M=M+1
GO TO 111

211 SUMCAT=0

DO 911 I=1,M
X=0
S=0
Z=0

```



Y=0

R=B(1,I)  
T=B(2,I)  
A=B(3,I)  
C=B(4,I)

WRITE(2,108)R,T,A,C

$X = (1 - (3 * ((A) ** 2))) / (3 * ((R) ** 3))$   
Y=LOG10(C)

IF(CAT.EQ.'C')GO TO 70  
IF(CAT.EQ.'H')GO TO 71  
IF(CAT.EQ.'K')GO TO 72  
IF(CAT.EQ.'NA')GO TO 73  
IF(CAT.EQ.'CA')GO TO 74  
IF(CAT.EQ.'MG')GO TO 75  
IF(CAT.EQ.'BE')GO TO 76  
IF(CAT.EQ.'ZR')GO TO 77  
IF(CAT.EQ.'TI')GO TO 78  
IF(CAT.EQ.'FE')GO TO 69  
IF(CAT.EQ.'ZN')GO TO 68  
IF(CAT.EQ.'SC')GO TO 67  
IF(CAT.EQ.'MN')GO TO 66  
IF(CAT.EQ.'BA')GO TO 65  
IF(CAT.EQ.'LI')GO TO 64  
IF(CAT.EQ.'B')GO TO 63  
IF(CAT.EQ.'CS')GO TO 62  
IF(CAT.EQ.'P')GO TO 61

WRITE(6,83)

83       FORMAT(2X,'BEWARE, CATION NOT LISTED!!!!')

61       S=EXP((1.617-(2\*T))/0.37)  
          GO TO 79

62       S=EXP((2.417-(2\*T))/0.37)  
          GO TO 79

63       S=EXP((1.371-(2\*T))/0.37)  
          GO TO 79

64       S=EXP((1.466-(2\*T))/0.37)  
          GO TO 79

65       S=EXP((2.285-(2\*T))/0.37)  
          GO TO 79

66       S=EXP((1.753-(2\*T))/0.37)  
          GO TO 79

67       S=EXP((1.849-(2\*T))/0.37)  
          GO TO 79

68       S=EXP((1.704-(2\*T))/0.37)  
          GO TO 79

69       S=EXP((1.734-(2\*T))/0.37)  
          GO TO 79

```
70      S=EXP((1.390-(2*T))/0.37)
        GO TO 79
71      S=EXP((0.882-(2*T))/0.37)
        GO TO 79
72      S=EXP((2.132-(2*T))/0.37)
        GO TO 79
73      S=EXP((1.803-(2*T))/0.37)
        GO TO 79
74      S=EXP((1.967-(2*T))/0.37)
        GO TO 79
75      S=EXP((1.693-(2*T))/0.37)
        GO TO 79
76      S=EXP((1.381-(2*T))/0.37)
        GO TO 79
77      S=EXP((1.928-(2*T))/0.37)
        GO TO 79
78      S=EXP((1.815-(2*T))/0.37)
        GO TO 79

79      Z=X*S*Y

        SUMCAT=SUMCAT+Z
        WRITE(2,104)X,S,Y,Z
911     CONTINUE

        WRITE(2,1151)SUMCAT
1151    FORMAT(' SUMCAT=',F9.5)
        WRITE(6,1151)SUMCAT

        WRITE(3,1161)SUMCAT
1161    FORMAT(2X,'SUMCAT=',F9.5)

        SUM=SUMSI+SUMAL+SUMCAT
        DEL=701.6*SUM-45.7

        WRITE(6,1171)SUM,DEL
        WRITE(3,1171)SUM,DEL
1171    FORMAT(2X,'SUMCHI=',F9.5,'CHEM SHIFT=',F11.5)

1191    READ(4,1181,END=999)LINE
        GO TO 1191

999     CONTINUE

1192    WRITE(4,1181)MIN,SUMSI,SUMAL,SUMCAT,SUM,DEL
1181    FORMAT(A20,5(2X,F11.5))

        CLOSE(1)
        CLOSE(2)
        CLOSE(3)
        CLOSE(4)
        END
```

APPENDIX VI

Values of  $\Omega$  for  $\text{SiO}_2$  polymorphs summed at  
1/2 Å intervals to 10 Å

Distance from Si (Å)	Quartz		Cristo- balite		Value of $\Omega$ Coesite		Tridymite			
	T1	T2	T1	T2	T1	T2	T1	T2	T3	T4
2.0	-5.121	-5.160	-5.113	-5.093	-5.229	-5.196	-5.189	-5.219		
3.0	-5.283	-5.328	-5.281	-5.253	-5.401	-5.371	-5.359	-5.396		
3.5	-5.252	-5.298	-5.255	-5.218	-5.370	-5.344	-5.328	-5.368		
4.0	-5.256	-5.310	-5.210	-5.185	-5.383	-5.354	-5.340	-5.378		
4.5	-5.217	-5.310	-5.179	-5.130	-5.394	-5.372	-5.364	-5.399		
5.0	-5.211	-5.296	-5.220	-5.180	-5.376	-5.355	-5.341	-5.371		
5.5	-5.226	-5.290	-5.228	-5.192	-5.371	-5.325	-5.317	-5.352		
6.0	-5.239	-5.284	-5.227	-5.182	-5.366	-5.331	-5.314	-5.356		
6.5	-5.239	-5.286	-5.236	-5.192	-5.358	-5.340	-5.325	-5.359		
7.0	-5.252	-5.295	-5.220	-5.186	-5.369	-5.344	-5.337	-5.365		
7.5	-5.228	-5.300	-5.213	-5.167	-5.376	-5.345	-5.334	-5.370		
8.0	-5.226	-5.305	-5.221	-5.183	-5.378	-5.351	-5.337	-5.375		
8.5	-5.231	-5.300	-5.217	-5.183	-5.378	-5.350	-5.335	-5.371		
9.0	-5.231	-5.294	-5.224	-5.185	-5.377	-5.345	-5.329	-5.366		
9.5	-5.238	-5.293	-5.224	-5.177	-5.371	-5.338	-5.329	-5.365		
10.0	-5.231	-5.288	-5.213	-5.172	-5.365	-5.334	-5.322	-5.358		

	Quartz		Cristo- balite		Value of $\Omega$ Coesite		Tridymite					
	T5	T6	T7	T8	T9	T10	T11	T12	T13	T14	T15	
2.0	-5.313	-5.263	-5.368	-5.219	-5.253	-5.215	-5.155	-5.262				
3.0	-5.494	-5.433	-5.550	-5.388	-5.425	-5.386	-5.327	-5.435				
3.5	-5.470	-5.400	-5.526	-5.354	-5.393	-5.354	-5.298	-5.406				
4.0	-5.477	-5.415	-5.533	-5.370	-5.406	-5.367	-5.310	-5.418				
4.5	-5.490	-5.422	-5.548	-5.388	-5.419	-5.388	-5.312	-5.437				
5.0	-5.468	-5.406	-5.522	-5.359	-5.398	-5.370	-5.292	-5.412				
5.5	-5.454	-5.390	-5.510	-5.339	-5.378	-5.355	-5.290	-5.391				
6.0	-5.462	-5.398	-5.509	-5.348	-5.383	-5.352	-5.292	-5.391				
6.5	-5.460	-5.393	-5.514	-5.355	-5.393	-5.348	-5.287	-5.398				
7.0	-5.463	-5.405	-5.522	-5.363	-5.400	-5.357	-5.297	-5.414				
7.5	-5.468	-5.408	-5.523	-5.359	-5.397	-5.359	-5.299	-5.412				
8.0	-5.474	-5.404	-5.531	-5.362	-5.400	-5.362	-5.300	-5.412				
8.5	-5.471	-5.407	-5.527	-5.362	-5.402	-5.362	-5.299	-5.413				
9.0	-5.466	-5.404	-5.519	-5.358	-5.391	-5.359	-5.297	-5.407				
9.5	-5.465	-5.400	-5.519	-5.353	-5.389	-5.354	-5.294	-5.402				
10.0	-5.459	-5.393	-5.512	-5.348	-5.384	-5.349	-5.286	-5.398				

APPENDIX VII

Summations of geometric terms for SiO<sub>2</sub> polymorphs  
averaged from 6 to 10 Å

Mineral site	<sup>29</sup> Si nmr shift (ppm)	Chemical	Geometric terms*		
			1	2	3
quartz	-107.1		-5.235	2.332	-6.478
crystalite	-108.5		-5.294	2.415	-6.312
coesite T2	-108.1		-5.181	2.300	-6.469
coesite T1	-113.9		-5.222	2.395	-6.174
tridymite T1	-111.5		-5.371	2.472	-6.311
tridymite T2	-111.0		-5.342	2.491	-6.117
tridymite T3	-109.3		-5.329	2.437	-6.322
tridymite T4	-111.0		-5.365	2.512	-6.093
tridymite T5	-113.5		-5.465	2.580	-6.122
tridymite T6	-113.0		-5.401	2.462	-6.443
tridymite T7	-114.0		-5.520	2.609	-6.173
tridymite T8	-111.0		-5.356	2.434	-6.420
tridymite T9	-112.0		-5.393	2.476	-6.366
tridymite T10	-111.0		-5.356	2.458	-6.329
tridymite T11	-109.3		-5.295	2.446	-6.164
tridymite T12	-113.0		-5.405	2.490	-6.331

\*Geometric term (1)       $\Sigma((1-3\cos^2\theta_i)/3R_i^3)$

\*Geometric term (2)       $\Sigma((1-3\cos^2\theta_i)/3R_i^3)(\cos\alpha/\cos\alpha-1)$

\*Geometric term (3)       $\Sigma((1-3\cos^2\theta_i)/3R_i^3)(1/\cos\alpha)$

APPENDIX VIII

<sup>29</sup>Si chemical shift of silicate minerals, experimental values and values calculated from equations 3 and 4

Mineral sites	<sup>29</sup> Si nmr chemical shift			References	
	Measured	Calculated	Difference	nmr	structure
<b>ORTHOSILICATES</b>					
topaz	-85.6	-83.1	-2.5	4	14
andalusite	-79.8	-79.7	-0.1	1,3,4	15
kyanite T1	-83.2	-83.1	-0.1	1	16
kyanite T2	-82.3	-83.0	-0.7	1	16
sillimanite	-86.4	-86.2	-0.2	1,3,4	17
datolite	-83.0	-81.2	-1.8	5	18
zircon	-81.6	-80.2	-1.4	4	19
sphene	-79.6	-80.9	1.3	2	20
phenacite	-74.2	-75.5	1.3	4	21
monticellite	-66.3	-64.7	-1.6	3	22
olivine	-62.0	-62.8	0.8	4	23
chondrodite	-60.0	-63.5	3.5	4	24
garnet*	-83.4	-77.1	-6.3	4	25
<b>SOROSILICATES</b>					
akermanite	-73.7	-76.7	3.0	3	26
gehlenite	-72.5	-74.3	1.8	3	27
rankinite T1	-74.5	-74.0	-0.5	3,4	28
rankinite T2	-76.0	-78.7	2.7	3,4	28
thorveiteite	-95.3	-92.6	-2.7	4	29
lawsonite	-81.0	-80.4	-0.6	5	30
piemontite T1	-86.4	-85.6	-0.8	1	31
piemontite T2	-90.4	-89.4	-1.0	1	31
piemontite T3	-81.9	-78.3	-3.6	1	31
hemimorphite*	-77.1	-85.8	7.9	5	32
<b>INOSILICATES</b>					
clinoenstatite T1	-84.2	-84.6	0.5	3	33
clinoenstatite T2	-81.8	-82.2	0.4	3	33
orthenstatite T1	-82.0	-85.2	3.2	4	34
orthenstatite T2	-82.0	-82.5	0.5	4	34
pseudowollastonite T1	-83.5	-83.3	-0.2	3,4	35
pseudowollastonite T2	-83.5	-83.3	-0.2	3,4	35

Mineral sites	$^{29}\text{Si}$ nmr chemical shift			References	
	Measured	Calculated	Difference	nmr structure	
pseudowollastonite T3	-83.5	-82.6	-0.9	3,4	35
pseudowollastonite T4	-83.5	-82.5	-1.0	3,4	35
pseudowollastonite T5	-83.5	-83.1	-0.4	3,4	35
pseudowollastonite T6	-83.5	-82.0	-1.5	3,4	35
diopside	-84.8	-84.6	-0.2	1	36
jadeite	-91.8	-89.9	-1.9	3	37
wollastonite T1	-91.7	-91.0	-0.7	1	34
wollastonite T2	-91.7	-91.5	-0.2	1	34
wollastonite T3	-87.6	-84.6	-3.0	1	34
spodumene	-91.4	-89.4	-2.0	1,3,4	38
tremolite T1	-91.2	-91.0	-0.2	1,3,4	39
tremolite T2	-87.2	-86.6	-0.6	1,3,4	39
omphacite T1	-85.4	-86.3	0.9	1	40
omphacite T2	-85.4	-86.9	1.5	1	40
pectolite T1	-86.3	-84.4	-1.9	1,3	41
pectolite T2	-86.3	-85.9	-0.4	1,3	41
pectolite T3	-86.3	-89.2	2.9	1,3	41
benitoite*	-94.2	-88.9	-5.3	4	42
PHYLLOSILICATES					
talc T1	-97.2	-96.9	-0.3	1,4	43
talc T2	-97.2	-96.8	-0.4	1,4	43
apophyllite	-92.0	-92.0	0.0	4	44
kaolinite T1	-91.5	-92.4	0.9	1,4,7	45
kaolinite T2	-91.5	-92.4	0.9	1,4,7	45
kaolinite T3	-91.5	-92.2	0.7	1,4,7	45
kaolinite T4	-91.5	-92.2	0.7	1,4,7	45
danburite	-89.0	-88.3	-0.7	1	46
lepidolite	-89.6	-91.5	1.9	2,4	47
vermiculite T1	-88.0	-88.3	0.3	8	48
vermiculite T2	-88.0	-87.3	-0.7	8	48
phlogopite	-86.0	-84.9	-1.1	4,8	49
muscovite T1	-89.0	-89.9	0.9	2,4,8	50
muscovite T2	-85.5	-86.1	0.6	2,4,8	50
margarite T1	-76.0	-78.0	2.	4,7	51
margarite T2	-76.0	-77.3	1.3	4,7	51
pyrophyllite T1	-94.0	-93.0	-1.0	1,4	52
pyrophyllite T2	-94.0	-93.1	-0.9	1,4	52
TECTOSILICATES					
quartz	-107.1	-105.5	-1.6	1,9	53
coesite T1	-113.9	-110.1	-3.8	9	54

Mineral sites	$^{29}\text{Si}$ nmr chemical shift			References	
	Measured	Calculated	Difference	nmr	structure
coesite T2	-108.1	-105.9	-2.2	9	54
anorthite T1	-82.7	-81.9	-0.8	10	55
anorthite T2	-82.7	-81.9	-0.8	10	55
anorthite T3	-89.3	-89.0	-0.3	10	55
anorthite T4	-84.7	-86.8	2.1	10	55
anorthite T5	-84.7	-83.6	-0.9	10	55
anorthite T6	-84.7	-86.4	1.7	10	55
anorthite T7	-84.7	-86.1	1.4	10	55
anorthite T8	-84.7	-86.5	1.8	10	55
tridymite T1	-111.0	-111.8	0.8	9	56
tridymite T2	-113.0	-115.1	2.1	9	56
tridymite T3	-111.0	-111.3	0.3	9	56
tridymite T4	-113.0	-115.2	2.2	9	56
tridymite T5	-114.0	-116.6	2.6	9	56
tridymite T6	-109.3	-109.5	0.2	9	56
tridymite T7	-114.0	-116.0	2.0	9	56
tridymite T8	-109.3	-109.6	0.3	9	56
tridymite T9	-111.0	-111.1	0.1	9	56
tridymite T10	-111.0	-111.4	0.4	9	56
tridymite T11	-112.0	-113.2	1.2	9	56
tridymite T12	-111.0	-111.0	0.0	9	56
petalite T1	-110.9	-109.5	-1.4	3	57
petalite T2	-109.5	-108.1	-1.4	3	57
crystalite	-108.5	-108.8	0.3	9	58
scapolite T1	-106.2	-104.0	-2.2	11	59
scapolite T3	-92.6	-92.6	0.0	11	59
Amelia albite T2	-104.9	-102.8	-2.1	10	60
Amelia albite T3	-97.1	-97.3	0.2	10	60
Amelia albite T4	-92.8	-93.5	0.7	10	60
sodalite	-84.9	-87.6	2.7	1	61
gmelilite	-97.2	-99.0	1.8	3,12	62
canerinite	-86.3	-88.8	2.5	1,3	63
oligoclase T2	-104.6	-102.6	-2.0	10	64
oligoclase T3	-97.1	-98.1	1.0	10	64
oligoclase T4	-92.8	-93.5	0.7	10	64
microcline T2	-100.2	-100.2	0.0	10	65
microcline T3	-97.1	-97.6	0.5	10	65
microcline T4	-94.7	-96.3	1.6	10	65
nepheline T1	-85.1	-88.5	3.4	1,13	66
nepheline T2	-85.1	-88.5	3.4	1,13	66
chabazite	-98.7	-96.2	-2.5	2,3,12	67
thomsonite T1	-89.0	-85.4	-3.6	2,3,12	68
thomsonite T2	-86.4	-83.3	-3.1	2,3,12	68
thomsonite T3	-91.7	-86.8	-4.9	2,3,12	68

Mineral sites	$^{29}\text{Si}$ nmr chemical shift			References	
	Measured	Calculated	Difference	nmr	structure
scolecite T1	-95.7	-90.4	-5.3	2,3	69
scolecite T2	-86.4	-84.6	-1.8	2,3	69
scolecite T3	-88.8	-89.1	0.3	2,3	69
natrolite T1	-95.4	-92.6	-2.8	3,6	70
natrolite T2	-87.7	-88.5	0.8	3,6	70
heulandite T1	-95.0	-95.7	0.7	2,12	71
heulandite T3	-105.0	-104.4	-0.6	2,12	71
heulandite T4	-108.0	-109.4	1.4	2,12	71
heulandite T5	-100.0	-99.0	-1.0	2,12	71
heulandite T6	-105.0	-103.6	-1.4	2,12	71
heulandite T7	-95.0	-96.6	1.6	2,12	71
heulandite T8	-102.0	-100.2	-1.8	2,12	71
kalsilite	-88.8	-88.9	0.1	13	72
tourmaline	-88.1	-89.8	1.7	1	73
beryl	-102.3	-103.8	1.5	2	74
beryl Cs Na	-101.0	-102.0	1.0	2	75
carnegeite*	-82.2	-93.6	11.4	13	76
zunyite T1*	-128.5	-114.4	14.1	3	77
zunyite T2*	-96.7	-89.2	7.5	3	77

\* not used in calculation of correlation

#### REFERENCES

- |                                  |                                 |
|----------------------------------|---------------------------------|
| 1 Williams (Sherriff) 1984       | 2 Listed in Appendix II         |
| 3 Janes & Oldfield 1984          | 4 Magi <u>et al.</u> 1984       |
| 5 Smith <u>et al.</u> 1983       | 6 Lippmaa <u>et al.</u> 1980    |
| 7 Kinsey <u>et al.</u> 1985      | 8 Sanz & Seratoza 1984          |
| 9 Smith & Blackwell 1983         | 10 Sherriff <u>et al.</u> 1984  |
| 11 Sherriff <u>et al.</u> 1987   | 12 Lippmaa <u>et al.</u> 1981   |
| 13 Stebbins <u>et al.</u> 1986   | 14 Zobetz <u>et al.</u> 1979    |
| 15 Burnham & Buerger 1961        | 16 Burham 1963a                 |
| 17 Burham 1963b                  | 18 Foit Phillips & Gibbs 1973   |
| 19 Robinson, Gibbs & Ribbe 1971  | 20 Speer & Gibbs 1976           |
| 21 Zachariasen 1971              | 22 Onken 1965                   |
| 23 Birlle <u>et al.</u> 1965     | 24 Gibbs, Ribbe & Anderson 1970 |
| 25 Novak & Gibbs 1971            | 26 Kimata & Li 1981             |
| 27 Kimata & Li 1982              | 28 Saburi <u>et al.</u> 1976    |
| 29 Smolin, Shepelev & Titov 1972 | 30 Baur 1978                    |
| 31 Dollase 1969                  | 32 Hill <u>et al.</u> 1977      |
| 33 Pannhorst 1984                | 34 Ohashi 1984                  |



- 35 Yamanaka & Mori 1981  
37 Prewitt & Burnham 1966  
39 Hawthorne & Grundy 1976  
41 Prewitt 1967  
43 Raynor & Brown 1973  
45 Brindley & Robinson 1946  
47 Guggenheim 1981  
49 Steinfink 1962  
51 Takeuchi 1966  
53 LePage & Donnay 1976  
55 Wainwright & Starkey 1971  
57 Effenberger 1980  
59 Levién & Papike 1976  
61 Hassan & Grundy 1983  
63 Grundy and Hassan 1982  
65 Brown & Bailey 1964  
67 Smith & Rinaldi 1963  
69 Faelth & Hansen 1979  
71 Merkle & Slaughter 1968  
73 Donnay & Buerger 1950  
75 Hawthorne & Cerney 1977  
77 Baur & Ohta 1982
- 36 Bruno Carboni & Molin 1982  
38 Clarke Appleman Papike 1969  
40 Matsumoto et al. 1975  
42 Fischer 1969  
44 Prince 1971  
46 Phillips Gibbs & Ribbe 1974  
48 Shirozu & Bailey 1966  
50 Radoslovich 1960  
52 Lee & Guggenheim 1981  
54 Kirfel & Will 1984  
56 Baur 1977  
58 Dollase 1965  
60 Harlow & Brown 1980  
62 Galli Passaglia Zanazzi 1982  
64 Ribbe et al. 1969  
66 Simmons Peacor & Peacor 1972  
68 Albert et al. 1981  
70 Meier 1960  
72 Perrotta et al. 1965  
74 Morosin 1972  
76 Borchert & Keidel 1964

APPENDIX IX

Calculated chemical shifts from theoretical models  
(angle  $\alpha$  varied between 125 and 180°)

$\alpha$	r	$\Omega''^*$	soro	ino	phyllo	tecto
T=Si						
180	1.59	-0.02826	-65.5	-85.4	-105.2	-125.0
175	1.59	-0.02817	-65.5	-85.2	-105.0	-124.8
170	1.59	-0.02788	-65.2	-84.8	-104.4	-124.0
165	1.59	-0.02740	-65.9	-84.2	-103.4	-122.6
160	1.59	-0.02672	-64.4	-83.2	-102.0	-120.7
155	1.59	-0.02583	-63.8	-82.0	-100.1	-118.2
150	1.59	-0.02473	-63.0	-80.4	-97.8	-115.1
145	1.59	-0.02340	-62.1	-78.5	-95.0	-111.4
140	1.59	-0.02184	-61.0	-76.4	-91.7	-107.0
135	1.59	-0.02002	-59.7	-73.8	-87.9	-101.9
130	1.59	-0.01793	-58.3	-70.9	-83.5	-96.0
125	1.59	-0.01556	-56.6	-67.5	-78.5	-89.4
T=Al						
125	1.75	-0.00982	-52.6	-59.5	-66.4	-73.3
130	1.75	-0.01107	-53.5	-61.3	-69.0	-76.8
135	1.75	-0.01217	-54.3	-62.8	-71.3	-79.8
140	1.75	-0.01312	-54.9	-64.1	-73.3	-82.5
145	1.75	-0.01393	-55.5	-65.3	-75.0	-84.8
150	1.75	-0.01461	-55.9	-66.2	-76.5	-86.7
155	1.75	-0.01517	-56.3	-67.0	-77.6	-88.3
160	1.75	-0.01562	-56.7	-67.6	-78.6	-89.6
165	1.75	-0.01597	-56.9	-68.1	-79.3	-90.5
170	1.75	-0.01621	-57.1	-68.5	-79.8	-91.2
175	1.75	-0.01636	-57.2	-68.7	-80.1	-91.6
180	1.75	-0.01641	-57.2	-68.7	-80.3	-91.8

\*  $\Omega''$  calculated for one Si or Al bonded to SiO<sub>4</sub> tetrahedron.

APPENDIX X

Calculated chemical shifts from theoretical models  
(distance r varied between 1.75 and 1.55 Å)

$\alpha$	r	$\Omega''''$	soro	ino	phyllo	tecto
T' = Al						
180	1.75	-0.01641	-57.2	-68.7	-80.3	-91.8
180	1.74	-0.01692	-57.6	-69.5	-81.3	-93.2
180	1.73	-0.01744	-57.9	-70.2	-82.4	-94.7
180	1.72	-0.01798	-58.3	-70.9	-83.5	-96.2
180	1.71	-0.01854	-58.7	-71.7	-84.7	-97.8
180	1.70	-0.01912	-59.1	-72.5	-86.0	-99.4
180	1.69	-0.01971	-59.5	-73.4	-87.2	-101.0
180	1.68	-0.02033	-60.0	-74.2	-88.5	-102.8
180	1.67	-0.02096	-60.4	-75.1	-89.8	-104.5
T = Si						
180	1.67	-0.02212	-61.2	-76.8	-92.3	-107.8
180	1.66	-0.02281	-61.7	-77.7	-93.7	-109.7
180	1.65	-0.02352	-62.2	-78.7	-95.2	-111.7
180	1.64	-0.02425	-62.7	-79.7	-96.8	-113.9
180	1.63	-0.02501	-63.2	-80.8	-98.4	-115.9
180	1.62	-0.02578	-63.8	-81.9	-100.0	-118.1
180	1.61	-0.02658	-64.3	-83.0	-101.7	-120.3
180	1.60	-0.02741	-64.9	-84.2	-103.4	-122.7
180	1.59	-0.02826	-65.5	-85.4	-105.2	-125.0
180	1.58	-0.02914	-66.1	-86.6	-107.1	-127.5
180	1.57	-0.03005	-66.8	-87.9	-109.0	-130.7
180	1.56	-0.03098	-67.4	-89.2	-110.9	-132.7
180	1.55	-0.03194	-68.1	-90.5	-113.0	-135.4
155	1.55	-0.02911	-66.1	-86.6	-107.0	-127.4
155	1.56	-0.02825	-65.5	-85.4	-105.2	-125.0
155	1.57	-0.02742	-64.9	-84.2	-103.4	-122.7
155	1.58	-0.02662	-64.4	-83.1	-101.8	-120.4
155	1.59	-0.02583	-63.8	-82.0	-100.1	-118.2
155	1.60	-0.02508	-63.3	-80.9	-98.5	-116.1
155	1.61	-0.02434	-62.8	-79.9	-97.0	-114.0
155	1.62	-0.02362	-62.6	-78.9	-95.4	-112.0

$\alpha$	r	$\Omega''''$	soro	ino	phyllo	tecto
155	1.63	-0.02293	-61.8	-77.9	-94.0	-110.1
155	1.64	-0.02225	-61.3	-76.9	-92.6	-108.2
155	1.65	-0.02160	-60.8	-76.0	-91.2	-106.3
155	1.66	-0.02096	-60.4	-75.1	-89.8	-104.5
155	1.67	-0.02035	-60.0	-74.3	-88.6	-102.8

T = Al

155	1.67	-0.01928	-59.2	-72.8	-86.3	-99.8
155	1.68	-0.01871	-58.8	-72.0	-85.1	-98.2
155	1.69	-0.01816	-58.4	-71.2	-83.9	-96.7
155	1.70	-0.01762	-58.1	-70.4	-82.8	-95.2
155	1.71	-0.01710	-57.7	-69.7	-81.7	-93.7
155	1.72	-0.01660	-57.3	-69.0	-80.7	-92.3
155	1.73	-0.01611	-57.0	-68.3	-79.6	-90.9
155	1.74	-0.01563	-56.7	-67.6	-78.6	-89.6
155	1.75	-0.01517	-56.3	-67.0	-77.6	-88.3
155	1.76	-0.01473	-56.0	-66.4	-76.7	-87.1
130	1.76	-0.01078	-53.3	-60.8	-68.4	-76.0
130	1.75	-0.01107	-53.5	-61.2	-69.0	-76.8
130	1.74	-0.01138	-53.7	-61.7	-69.7	-77.7
130	1.73	-0.01169	-53.9	-62.1	-70.3	-78.5
130	1.72	-0.01201	-54.1	-62.6	-71.0	-79.4
130	1.71	-0.01233	-54.3	-63.0	-71.7	-80.3
130	1.70	-0.01267	-54.6	-63.5	-72.4	-81.3
130	1.69	-0.01301	-54.8	-64.0	-73.1	-82.2
130	1.68	-0.01337	-55.1	-64.5	-73.9	-83.2
130	1.67	-0.01373	-55.3	-65.0	-74.6	-84.2

T = Si

130	1.67	-0.01449	-55.9	-66.0	-76.2	-86.4
130	1.66	-0.01488	-56.1	-66.6	-77.0	-87.5
130	1.65	-0.01528	-56.4	-67.2	-77.9	-88.6
130	1.64	-0.01570	-56.7	-67.7	-78.8	-89.8
130	1.63	-0.01612	-57.0	-68.3	-79.6	-91.6
130	1.62	-0.01656	-57.3	-68.9	-80.6	-92.2
130	1.61	-0.01700	-57.6	-69.6	-81.5	-93.4
130	1.60	-0.01746	-57.9	-70.2	-82.5	-94.7
130	1.59	-0.01793	-58.3	-70.9	-83.5	-96.0
130	1.58	-0.01841	-58.6	-71.5	-84.5	-97.4
130	1.57	-0.01890	-59.0	-72.2	-85.5	-98.8
130	1.56	-0.01941	-59.3	-72.9	-86.6	-100.2
130	1.55	-0.01992	-59.7	-73.7	-87.6	-101.6

\*  $\Omega''''$  calculated for one Si or Al atom bonded to the  $\text{SiO}_4$  tetrahedron

## APPENDIX XI

The relationship between the McConnell equation  
and equations 3 and 4

When a bond is placed in a magnetic field the magnetic susceptibility anisotropy ( $\chi$ ) of a bond creates a magnetic dipole. The term  $((1-3\cos^2\theta)/3R^3)$  (McConnell 1957) describes the interaction between magnetic dipoles. The effect on the nmr shielding tensor  $\sigma_N^G$  of  $\Delta\chi^G$  the magnetic susceptibility anisotropy of a group G is given by:

$$\sigma_N^G = \Delta\chi^G (1-3\cos^2\theta)/(3R^3 L_O)$$

where  $L_O$  is Avogadro's number and  $\theta$  and  $R$  are as defined in Figure 2.1.

$$\Delta\chi^G = \chi_{\text{parallel}}^G - \chi_{\text{perpendicular}}^G$$

McGlinchey et al. (1985) used the McConnell equation and defined  $\chi$  as the difference between the longitudinal magnetic susceptibility ( $\chi_{\text{parallel}}$ ) and the transverse magnetic susceptibility ( $\chi_{\text{perpendicular}}$ ) of a bond with cylindrical symmetry.

$$\sigma = (X/N)((1-3\cos^2\theta)/3R^3)$$

In section 2.3.1  $\Omega$  is used in equation (1) as a geometric term for a summation of magnetic dipole moments for Si-O bonds around an  $\text{SiO}_4^{-2}$  group.

$$\Omega = \sum((1-3\cos^2\theta_i)/3R_i^3) \quad (1)$$

In section 2.3.2 equation (1) was modified to include a term allowing for variations in types of cations and length of cation-oxygen bonds.

$$\Omega' = \sum(\exp[(r_0-r_i)/0.37])((1-3\cos^2\theta_i)/3R_i^3) \quad (2)$$

Equation (3) in section 2.3.4 includes a term to allow for the effect of tight rings on chemical shift.

$$\Omega'' = \sum[(((1-3\cos^2\theta_i)/3R_i^3)(\exp[(r_0-r_i)/0.37])(\log(\text{Si-X}_i)))] \quad (3)$$

$\Omega''$  is a geometrical term for the summation of modified magnetic moments from all type of bonds surrounding an  $\text{SiO}_4$  tetrahedron. If the summation for all bonds between cations and the terminal oxygens of the  $\text{SiO}_4$  tetrahedron is plotted against chemical shift the regression

equation of the resultant straight line is:

$$\delta = 701.6 \Omega'' - 45.7 \quad (4)$$

The slope of the line 701.6 is a mean value for magnetic susceptibility for all bonds involved in the calculation and the intercept -45.7 ppm is the chemical shift of an isolated  $\text{SiO}_4$  tetrahedon.

$\delta$  can then be calculated from equation (4) using the values of  $\Omega''$  calculated from the structure of the silicate minerals.

Figure 2.4 is a plot of calculated against measured chemical shift.  $\xi$  is the difference between calculated and measured chemical shift.